The lost maps: Two-Photon Investigations of the Fine Scale Organization of Auditory Cortex



Mariangela Panniello

Lincoln College, University of Oxford

A thesis submitted in partial fulfilment of the requirements for the degree of

Doctor of Philosophy

Trinity Term 2016

Ai miei genitori

To my parents

Acknowledgements

A long journey is only worth when there are people to remember.

My DPhil adventure would not have been possible without my supervisors, Dr Kerry Walker and Prof Andrew King.

Kerry, your patience, your suggestions, your kind words and smiles in my many bad days (and your Matlab wizardry!) have been invaluable. I will keep them with me, together with the hope to continue learning from you in the future.

Andy, thanks for the freedom of trying, making mistakes and succeeding that you give to your graduate students. Being part of your team has changed me both as a scientist and as a person.

The inspiring ideas and precious suggestions from Dr Nicol Harper and Prof Jan Schnupp have also been fundamental for my research, thank you both.

A mandatory mention goes to my best lab-buddies: Quentin Gaucher, thank you for the patient answers to my questions and for all the chocolate and coffee we had together. Sebastian Vasquez - Lopez, thanks for our chats and for your support in the last months of my DPhil.

Dr Michael Kohl and his lab members have reminded me, throughout this jouney, how beautiful science is when done as a team. Thanks for adopting me in your group!

Although he was not directly involved in my DPhil, I will never be grateful enough to my first supervisor, Dr Gian Michele Ratto. Thanks Gimmi, because having seen your eyes ecstatic in front of a bunch of fluorecent neurons twinkling on a screen, five years ago, still inspires me every day in what I do.

I am highly grateful to Lincoln College for giving me the honor of being among its students, to the Newton Abraham Studentship for generously funding my graduate studies for eleven terms, and to the Goodger and Schorstein Scholarship for supporting me in the last term.

Finally, thanks to all the people in Oxford with whom I have shared my life outside the lab, you know who you are!

A special place in my heart belongs to Emma. I am so lucky to know you and be your friend, thanks for being such a wonderful young woman.

Thanks to Shakespeare, my canine brother and buddy of mischiefs.

To Roberto, my most effective painkiller, my source of patience, and faithful companion of smiles and sorrows. The most joyful life is awaiting me thanks to you, our bunch of super - real - imaginary friends, and our many books to put in a huge bookshelf.

To my mother, for being my home.

To my father, whose protective hug I keep feeling timelessly.

The lost maps: Two-Photon Investigations of the Fine Scale Organization of Auditory Cortex

Mariangela Panniello

Lincoln College, University of Oxford

A thesis submitted in partial fulfilment of the requirements for the degree of Doctor of Philosophy

Trinity Term 2016

The spatial arrangement of neuronal responses in primary auditory cortex (A1) has so far been investigated by using microelectrode recording techniques or imaging of the intrinsic signal, which led to controversial results, at present still discussed.

On the other hand, two-photon calcium imaging allows us to investigate the cortical functions at an unprecedented level of spatial detail, and has recently offered new insight into the fine-scale organization of frequency responses in A1.

In this thesis, I used two-photon calcium imaging to compare, for the first time, the fine-scale cortical representation of sound frequency to that of two other sound features, crucial for survival and communication in all mammals: differences in intensity between the two ears (interaural level differences; ILDs), and frequency modulation (FM).

I found that most neurons in layers II-III of the mouse A1 were tuned to ILDs favouring the contralateral ear, but midline and ipsilateral tuning were present too. Binaural preferences were heterogeneously distributed in space, both on the fine scale (within ~ 200 μm) and on the global one (up to ~ 1 mm).

Moreover, A1 neurons were mostly tuned to slow FM sweeps within the range of those used in species-specific calls. Cells activated by similar rates tended to be spatially proximal, indicating a level of local organization similar to the one I found for frequency tuning, and higher than that of ILD responses.

Finally, I set the groundwork for two-photon studies of the A1 of the ferret, by presenting the first evidence of the microscopic organization of the tonotopic map in this species.

My results shed light on some long-held questions about the response properties of A1, and confirm two-photon imaging as a powerful tool for investigating the processing of sensory signals in the cortex of both small and large mammals.

List of Abreviations

2D	Two Dimensional
3D	Three Dimensional
A1	Primary auditory cortex
A2	Secondary auditory cortex
a.u.	Arbitrary Units
AAF	Anterior Auditory Field
AAV	Adeno-Associated Virus
ABL	Average Binaural Level
ADI	Aural Dominance Index
AM	Amplitude Modulated
AN	Auditory Nerve
ANOVA	ANalysis Of VAriance
AVCN	Anteroventral division of the Cochlear Nucleus
BF	Best Frequency
C	Caudal
CF	Characteristic Frequency
CN	Cochlear Nucleus
CNIC	Central Nucleus of the Inferior Colliculus
D	Dorsal
dB	deciBel
DCIC	Dorsal Cortex of the Inferior Colliculus
DCN	Dorsal division of the Cochlear Nucleus
DP	Dorsal Posterior
DV	Dorsoventral
F	Frontal
FM	Frequency Modulated
FRA	Frequency Response Area

HRTF	Head-Related Transfer Function
IC	Inferior Colliculus
ILD	Interaural Level Difference
ITD	Interaural Time Difference
LSO	Lateral Superior Olive
M	Medial
MGBd	dorsal division of the Medial Geniculate Body
MGBm	medial division of the Medial Geniculate Body
MGBv	ventral division of the Medial Geniculate Body
MSO	Medial Superior Olive
NC	Noise Correlation
NMDA	N-methyl-D-aspartate
PC	Principal Component
PCA	Principal Component Analysis
PVCN	Posteroventral division of the Cochlear Nucleus
R	Rostral
RC	Rostrocaudal
SC	Signal Correlation
sd	standard deviation
se	standard error
SPL	Sound Pressure Level
SSG	Suprasylvian Gyrus
UF	Ultrasonic Field
V	Ventral
V1	Primary visual cortex

Contents

1 General Introduction **2**

1.1 The multitasking auditory cortex 3

1.2 The choice of the sound features 5

1.2.1 Interaural Level Differences 5

1.2.2 Frequency Modulated sweeps 8

1.3 Subcortical processing of sounds 10

1.3.1 The cochlea and the auditory nerve 10

1.3.2 The Cochlear Nucleus 11

1.3.3 The Superior Olive 12

1.3.4 The Inferior Colliculus 12

1.3.5 The Superior Colliculus 15

1.3.6 The Medial Geniculate Body 16

1.4 Cortical processing of sounds 17

1.4.1 ILD processing 17

1.4.2 FM sweep processing 19

1.5 Spatial organization of auditory cortex 20

1.5.1 Functional architecture across cortical fields 20

1.5.2 Functional architecture within A1 21

1.5.3 The organization of responses to binaural stimuli and FM sweeps . 21

1.5.4 Other sound features systematically represented in A1 23

1.5.5 Cortical maps are plastic 24

1.6 The cortex at high definition: two-photon calcium imaging 25

1.7 Scope and organization of the thesis 28

2 Methods **31**

2.1 Experimental procedures 31

2.1.1 Animals 31

2.1.2 Viral vector injections 32

2.1.3 Retrobead injections 34

2.1.4 Terminal surgery for *in vivo* two-photon calcium imaging 34

2.1.5 *In vivo* two-photon calcium imaging 36

2.1.6 Sound presentation 36

2.1.7 Histology 37

2.2 Data analysis 37

2.2.1 Isolating responses from individual neurons 37

2.2.2 Identifying responsive neurons 39

2.2.3 Determining stimulus sensitivity in responsive neurons 39

2.2.4 Inferring spikes from calcium transients 40

2.2.5 Principal components analysis 40

2.2.6 Estimating pairwise correlations 41

2.2.7 Cluster analysis 42

3 The question of tonotopy **44**

3.1 Introduction 44

3.1.1 Aims 46

3.2 Methods 47

3.2.1 Pure tone stimulation 47

3.2.2 Identifying responsive neurons 47

3.3 Results 48

3.3.1 Frequency responses in the mouse auditory cortex 48

3.3.2 Anatomical confirmation of imaging location in mice 50

3.3.3 Functional confirmation of imaging location 52

3.3.4 Tonotopy: fine-scale organization 56

3.3.5 Evidence for local subnetworks: pairwise correlations 57

3.3.6 Tonotopy: large-scale organization 59

3.3.7 Two-photon imaging in ferrets: an ongoing challenge 62

3.3.8 Frequency tuning in the ferret auditory cortex 64
3.4 Discussion 70
3.4.1 Results overview 70
3.4.2 Contrasting results from low and high spatial resolution techniques 70
3.4.3 Contrasting results across two-photon imaging studies 72
3.4.4 Rodents and carnivores: possible species differences 74
3.4.5 Conclusions 77

4 The representation of ILDs in A1 80
4.1 Introduction 80
4.1.1 Aims 82
4.2 Methods 83
4.2.1 ILD noise burst presentation 83
4.2.2 Identifying responsive neurons 84
4.2.3 Determining ILD sensitivity in responsive neurons 84
4.2.4 Categorizing the binaural properties of neurons 84
4.2.5 Aural Dominance Index 86
4.2.6 Principal components analysis 86
4.3 Results 87
4.3.1 Calcium transients in response to binaural noise bursts 87
4.3.2 Testing the neuronal sensitivity to binaural stimuli 88
4.3.3 Sharpness of ILD sensitivity 91
4.3.4 Looking for common response patterns: PCA 93
4.3.5 Local arrangement of binaural preferences 95
4.3.6 The generation of ILDs at low sound frequencies 98
4.3.7 ILD tuning in low BF neurons 100
4.3.8 Evidence for subcortical networks: pairwise correlations 101
4.3.9 Binaural and frequency preferences within the local microcircuit . 102
4.3.10 Global arrangement of ILD preferences 104
4.3.11 Global arrangement of binaural categories 105
4.4 Discussion 106
4.4.1 Results overview 106

4.4.2 ILD sensitivity . . . 107
4.4.3 The ethological relevance of tuning to large ILDs . . . 108
4.4.4 Spatial organization of binaural preferences . . . 110
4.4.5 Methodological considerations . . . 111

5 The representation of FM sweeps in A1 115

5.1 Introduction . . . 115
5.1.1 Aims . . . 117
5.2 Methods . . . 118
5.2.1 FM sweep presentation . . . 118
5.2.2 Identifying responsive neurons . . . 119
5.2.3 Determining FM preferences of responsive neurons . . . 120
5.2.4 Principal components analysis . . . 121
5.2.5 Direction selectivity index . . . 121
5.3 Results . . . 121
5.3.1 Neuronal sensitivity to FM sweeps . . . 122
5.3.2 Rate sensitivity is invariant to FM bandwidth . . . 123
5.3.3 Rate sensitivity is invariant to FM direction . . . 127
5.3.4 The effect of starting frequency on FM sensitivity . . . 128
5.3.5 Local organization of rate preferences . . . 130
5.3.6 Global organization of rate preferences . . . 132
5.3.7 Evidence for local subnetworks: signal correlations . . . 134
5.3.8 Evidence for local subnetworks: noise correlations . . . 139
5.3.9 Correlation between FM direction sensitivity and BFs . . . 139
5.3.10 Correlation between best FM rates and BFs . . . 140
5.4 Discussion . . . 141
5.4.1 Results overview . . . 141
5.4.2 FM Rate sensitivity: main features . . . 142
5.4.3 FM Rate sensitivity: comparison with rates of species-specific calls 143
5.4.4 FM Rate sensitivity: relationship with frequency tuning . . . 145
5.4.5 Direction selectivity: relationship with frequency tuning . . . 145
5.4.6 Prevalence of tuning to upward sweeps . . . 147

5.4.7 Spatial distribution of FM rate preferences 147
5.4.8 Methodological considerations 148

6 General Discussion **153**
6.1 Summary of findings 153
6.2 Evidence for local networks in auditory cortex 155
6.3 What is the functional relevance of local heterogeneity? 156
6.4 The spatial variability of ILD responses 158
6.5 Unresponsive neurons and the search for the optimal auditory stimulus . . 160
6.6 General methodological considerations 162
6.6.1 The use of anaesthesia 162
6.6.2 The choice of the calcium indicator 163
6.7 In conclusion 165

References **167**

List of Figures

1.1 Sound pressure transformation curves 7
1.2 Mouse vocalizations 9
1.3 Inhibitory sidebands 14
1.4 Overlapping stimulus feature maps in A1 22

3.1 Calcium transients in response to pure tones 49
3.2 Best frequencies in injected mice 50
3.3 Retrobead injections 53
3.4 Comparison between primary and secondary fields 55
3.5 The mouse auditory cortex 56
3.6 Local organization of BFs 58
3.7 Pairwise correlations during tones 59
3.8 Best frequencies in transgenic mice 60
3.9 Global organization of BFs 61
3.10 GCaMP6 injections in the ferret A1 64
3.11 Calcium transients in the ferret A1 65
3.12 FRAs of neurons in the A1 of the ferret 66
3.13 Spatial organization of BFs in the ferret cortex 68
3.14 Pairwise correlations in the ferret A1 69

4.1 Calcium transients in response to ILD noise bursts 88
4.2 Spike trains inferred from GCaMP6 calcium transients 89
4.3 Neuronal sensitivity to binaural modulations 90
4.4 Distributions of ILD preferences 92

4.5 Sharpness of ILD sensitivity 93
4.6 Principal component analysis 94
4.7 Local organization of ILD preferences 96
4.8 Distribution of neuronal binaural types 97
4.9 Local organization of binaural classes 99
4.10 The relationship between frequency and ILD sensitivity 101
4.11 Pairwise correlations during ILD noise bursts 102
4.12 How pairwise correlations change with neuronal distance 103
4.13 Global organization of ILD preferences 104
4.14 GLobal organization of binaural classes 106

5.1 Calcium transients in response to FM sweeps 122
5.2 Distrbutions of FM preferences 124
5.3 Fm rate tuning: invariance to FM bandwidth 125
5.4 The effect of bandwidth and rate 127
5.5 The effect of FM direction and duration 128
5.6 The effect of starting frequency 129
5.7 Local organization of best FM rates 131
5.8 Local organization of best FM durations 133
5.9 Global organization of FM preferences 135
5.10 Signal correlations: FM sweeps and pure tones 136
5.11 Signal correlations: FM sweeps and ILD noise bursts 137
5.12 Evidence for local subnetwroks 138
5.13 DSI values versus BFs 140
5.14 Best FM rates versus BFs 141
5.15 FM rates tuning across species 143

List of Tables

3.1 Responsive neurons in the ferret A1 66

5.1 FM rates in mice expressing GCaMP6m 118
5.2 FM rates in mice expressing GCaMP6f 119
5.3 Local clusters of preferences 134

Chapter 1

General Introduction

Possibly more than any other sense, audition establishes the possibility for humans and many other species to be social beings. Seeing someone involved in a conversation with us is not enough for interaction without being able to hear and understand what she or he is saying. Similarly, locating a car by hearing it dangerously approaching from a hidden corner of the street, may be more useful for our survival than noticing it when it becomes visible or, even worse, when it touches us! However, sounds encountered in natural environments are a complicated spectro-temporal tangle of simple sounds, and the auditory system has the challenge of encoding their basic components, as well as integrating them, to form comprehensive "auditory objects".

In order to accurately represent the external world, the auditory system (as well as other sensory systems) relies on spatially ordered projections connecting the peripheral receptors of the cochlea in the inner ear to a number of subcortical stations, and eventually to the auditory cortex. To start with, sound frequency is represented according to a high-to-low gradient going from the base to the apex of the cochlear surface: an arrangement defining the primary topographic organization of the auditory system, that is, the ordered spatial representation of sensory information within a brain area. For frequency preferences, this arrangement is known as tonotopicity.

If the spatial distribution of sound features within the most peripheral auditory regions is fairly systematic and, probably for this reason, well understood (Nelken, 2008), the same cannot be said for the cortex. Why is this? Part of the reason stems from the general nature of cortical regions, and part from the specific characteristics of the

auditory system.

1.1 The multitasking auditory cortex

The cortex is an extremely complicated environment. Dozens of neuronal sub-types with different morphological and functional features establish thousands of cortico-cortical and cortico-subcortical connections, so that the information flow is more entangled than earlier in the pathway (Harris and Shepherd, 2015). Furthermore, along its journey, auditory information goes through at least four synapses before entering the cortex, while, for example, only one station separates the bottom from the top of the visual system (i.e. the lateral geniculate body of the thalamus, where inputs from the retina are processed before being transmitted to the primary visual cortex).

The presence of so many obligatory relays implies that the processing of many sound features other than frequency is accomplished subcortically. To have an idea, consider that the inferior colliculus, two processing steps away from the primary auditory cortex (A1), has been compared to the primary visual cortex (V1), given the many different acoustic attributes its neurons are sensitive for (Nelken *et al.*, 2003). In this scenario, it is not trivial to define the functions of auditory cortex (King and Nelken, 2009), and it is hard to imagine that the spatial representation of sound features is as rigorous here as in lower regions.

The columnar organization is perhaps the best established model of spatial arrangement of cortical areas (Mountcastle, 1997), but the presence of columns seems less clear in auditory (Chechik *et al.*, 2006; Hromádka *et al.*, 2008), compared to other sensory cortices (Linden and Schreiner, 2003; Panzeri *et al.*, 2003). On the other hand, it has been proposed that the auditory cortex (particularly deep layer III and layer IV) might contain overlapping topographic maps of numerous sound features, such as sound intensity, or binaural responses, extending perpendicular to the tonotopic map (for a comprehensive review, see Schreiner and Winer (2007)). For instance, bands of neurons with different binaural properties have been described (Imig *et al.*, 1977; Kelly and Judge, 1994; Middlebrooks *et al.*, 1980). These are shaped by cells preferring sounds that are more intense in the contralateral hemifield, alternating with those driven mostly by sounds that are equally intense at the two ears.

These findings emerged from microelectrode recordings examining the large-scale organization of auditory cortex and lacking enough spatial resolution to reveal details about the fine-grain functional architecture of brain regions. We therefore know very little about the organization of local cortical networks and the relationships between the receptive fields of neighbouring neurons. A deeper comprehension could be greatly informative about cortical computations, by revealing to what extent topography is respected and functionally necessary.

The opportunity to advance our knowledge in this field depends on the technology available. In the last decade, a single-cell resolution, high spatial sampling microscopy technique, namely two-photon imaging (Denk *et al.*, 1990), has started to revolutionize our understanding of the functional organization of cortical circuits. To explain it with an artistic metaphor: if we look at a Paul Signac' pointillist painting from afar, our eyes will average the colours on the canvas, and the sky will look locally fairly uniform in its shades of blue or pink. But if we get closer, than the variety of colours used for drawing neighbouring points resulting in an overall blue sky, will be revealed. Similarly, with *in vivo* two-photon imaging, we can measure the activity of hundreds of neighbouring neurons simultaneously (the points of the painting) and understand if, and to what degree, sensory responses are locally variable. In contrast, some microelectrode techniques average neuronal responses across the cortical space, possibly returning a spatial organization smoother than the actual one. Even when single neuron recordings have been used, they inevitably sample cells more sparsely and potentially more selectively than is the case with two-photon imaging. Indeed, six years ago, when two-photon microscopy was introduced to the study of auditory cortex, tonotopy, which was thought to be the best established functional principle of this area, was found to be surprisingly fractured at the fine spatial scale, within 200 μm (Bandyopadhyay *et al.*, 2010; Rothschild *et al.*, 2010). Nothing is currently known about the organization of other sound features.

For my D.Phil. project, I compared the fine-scale cortical representation of sound frequency to that of two other features of the sound: interaural level differences and frequency modulation.

The main reason of my choice is that these sound parameters are crucial for survival and communication in all mammals, and constitute the basis of many natural stimuli, as

I shall explain in sections 1.2.1 and 1.2.2. Equally important is that there are many open questions about the spatial representation of these features in auditory cortex, which I shall review in sections 1.4.1, 1.4.2, 4.1 and 5.1.

My primary animal model will be the mouse (*Mus musculus*). Although it relies heavily on hearing for communication purposes (Nyby, 2001), this species has not been traditionally very much used in auditory neuroscience, but is rapidly gaining in popularity thanks to the genetic engineering methods that can be applied to it (Chen *et al.*, 2013; Kumar *et al.*, 2009).

In addition, I shall present some preliminary data from *in vivo* two-photon experiments in the ferret (*Mustela putorius furo*), examining the spatial organization of frequency responses in A1. Although hearing in this species has been extensively studied, two-photon imaging of its auditory system has never been performed before, and nothing is known about the fine-scale arrangement of auditory cortical responses.

1.2 The choice of the sound features

1.2.1 Interaural Level Differences

Being able to localize sounds is essential for the ability of all mammals to interact with the surrounding world. It is crucial for survival and reproductive success in many species, and aids communication in humans: from distinguishing voices in noisy environments (the so called "cocktail party problem") (Eramudugolla *et al.*, 2008; O'Connor and Sutter, 2000), to judging the content and the size of enclosed spaces.

In contrast to the visual and somatosensory systems, the stimulus dimension encoded by the receptors cells of the auditory epithelium is frequency, and not location. Thus, information about the spatial coordinates of a sound source must be extracted from cues that are not explicitly represented in the cochlea. These cues are generated by the interaction of the sound waves with the head and the external ears, as reviewed in Grothe *et al.* (2010).

To localize on the vertical plane (in "elevation"), mammals use mainly monaural spectral cues. Each external ear filters incoming sounds according to their frequency and their angle of incidence. Consequently, each frequency will be amplified or weakened

depending on its elevation from the interaural axis, following a pattern established by the interaction with the head and known as the Head Related Transfer Function (HRTF). In the horizontal plane ("azimuth"), mammals use similar spectral cues for front-back distinction, and can also learn to use these cues for general sound localization (Keating *et al.*, 2016; Kumpik *et al.*, 2010). Normally, however, binaural cues provide the principal basis for localization in the horizontal plane (King *et al.*, 2001).

Unless a sound is coming from exactly in front or exactly behind our head (that is, at 0° or 180° on the azimuth), it will naturally reach the ear closer to its source before the further one. This creates a cue known as the Interaural Time Difference (ITD) (extensive reviews of the neural basis of ITD processing can be found in Grothe *et al.* (2010) and McAlpine (2005)). Interaural time difference on the interaural axis increase with the dimension of the head, which determines the distance between the ears. For example, their maximum value is about 700 μs in humans (Middlebrooks, 1999) for sound sources located 90° lateral to the head, but 500 μs in the cat (Calford *et al.*, 1986). Because of the shadow cast by the listener's head on the path of the sound waves, acoustic signals may also reach the further ear attenuated in intensity. This effect is known as the Interaural Level Difference (ILD).

According to the Duplex Theory, formulated by Lord Relaygh in 1907 and confirmed by successive experimental studies (Mills, 1958), ITDs are maximally informative for locating low frequency sounds, while ILDs are mainly used for high frequency signals (but see Shinn-Cunningham *et al.* (2000), where authors demonstrate deviations from the Duplex Theory, as significant ILDs can occur at low frequencies for close by sounds). ILDs are minimal at low frequencies because of the little interference that the sound waves encounter when propagating in the space, receiving only a weak shadowing effect by the head, especially when this is particularly small. To the contrary, high frequency waves produce much larger ILDs due to their interaction with the head and external ears, and for this reason auditory neurons activated by high frequencies are also sensitive to ILDs. For example, in mice, whose interaural distance is $\sim$2 cm, the limit for using ILDs is very low, about 1 kHz.

Thus, if mammals with large enough heads can rely on ITDs for localizing frequencies below 4 kHz (Lauer *et al.*, 2011), smaller animals whose heads produce only negligible

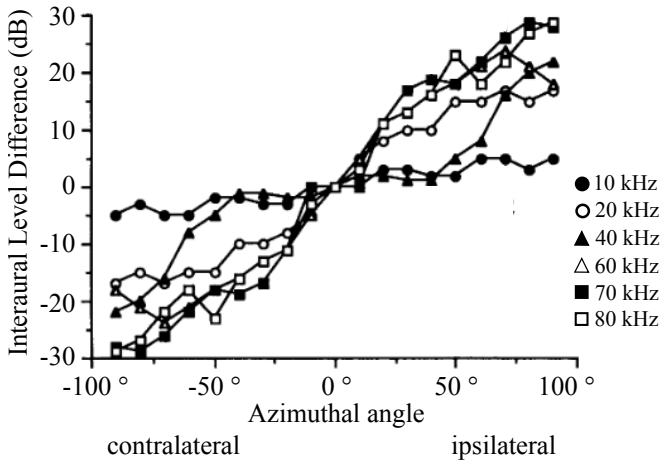

Figure 1.1: The ILDs generated by tones at six different frequencies were measured by Chen *et al.* (1995) through a microphone inserted in one ear of a mouse, to assess the shadowing effects of the head and the external ears. The ILDs are shown in the plot as a function of azimuthal angles. Each tone frequency is indicated by a different symbol on the corresponding curve.

ITDs have adopted a different strategy, specializing for high-frequency hearing, and thus for ILD detection. One case is that of the mouse, which can hear frequencies between 1 - 80 kHz (Ehret (1974); for comparison, humans hear frequencies between approximately 0.02 and 20 kHz). Poor sensitivity for low-frequencies, together with small head size, constrains ITD processing in this species. In fact, the localization abilities of mice are significantly impaired when tested with band-pass noise bursts including frequencies lower than 10 kHz (Allen and Ison, 2010; Heffner *et al.*, 2001; Radziwon *et al.*, 2009). Unable to rely on ITDs, small rodents must take advantage of ILDs, if they rely at all on binaural cues for locating sound sources. This has been demonstrated in experiments in which binaural cues have been compromised by depriving, either temporarily or permanently, the input to one ear. Such procedure impairs mice localization performances (Lauer *et al.*, 2011) and broadens auditory midbrain (Drager and Hubel, 1975) and cortical spatial receptive fields in rats (Popescu and Polley, 2010) and mice (Polley *et al.*, 2013).

Behaviourally relevant ILD values in mice can reach up to ∼30 dB for 90° lateral sounds, depending on the frequency of the stimulus Chen *et al.* (1995) (Figure 1.1).

1.2.2 Frequency Modulated sweeps

Frequency modulated (FM) sweeps are sequences of tones changing continuously over time. As such, they are characterized by a certain degree of spectro-temporal complexity, which is explained by the combination of some parameters:

- direction: whether sound frequency increases (upward sweeps) or decreases (downward sweeps) over time;
- duration;
- bandwidth: the range of frequencies crossed by a FM sweep, determined by its starting and ending frequencies;
- rate (or slope): the speed of frequency modulation over time, given by the ratio between bandwidth and duration.

Frequency modulated sweeps constitute simple acoustic patterns in the communication sounds used by many animals and by humans, providing part of the basis for their spectro-temporal complexity and richness.

These modulations are greatly represented in mouse communication calls produced at all ages and in different contexts (Portfors, 2007). Figure 1.2A represents the spectrogram of a call emitted by an adult male mouse during exposure to female pheromones prior to mating. The vocalization in Figure 1.2B comes from a mother deprived of her litter before the normal weaning time. In turn, wriggling calls from the pups, shown in Figure 1.2C, can trigger a "search-and-rescue" behaviour in the mother. Frequency modulated sequences are present in all cases, as indicated by the red arrows, highlighting both upward and downward sweeps, which are sometime combined to form chevrons.

Similar sweeps have been found in the vocalizations of all other animals studied (bats: Kanwal *et al.* (1994); ferrets: Nelken and Versnel (2000); cats: Pick (1979); Yeon *et al.* (2011); non-human primates: Weiss *et al.* (2001); Rendall *et al.* (1996)) as well as in human speech (Zeng *et al.*, 2005).

To understand the importance of this type of sound, consider that altering the structure of a speech signal by filtering out certain frequency modulations impairs its comprehension (Drullman *et al.*, 1994; Elliott and Theunissen, 2009). Moreover, it has been

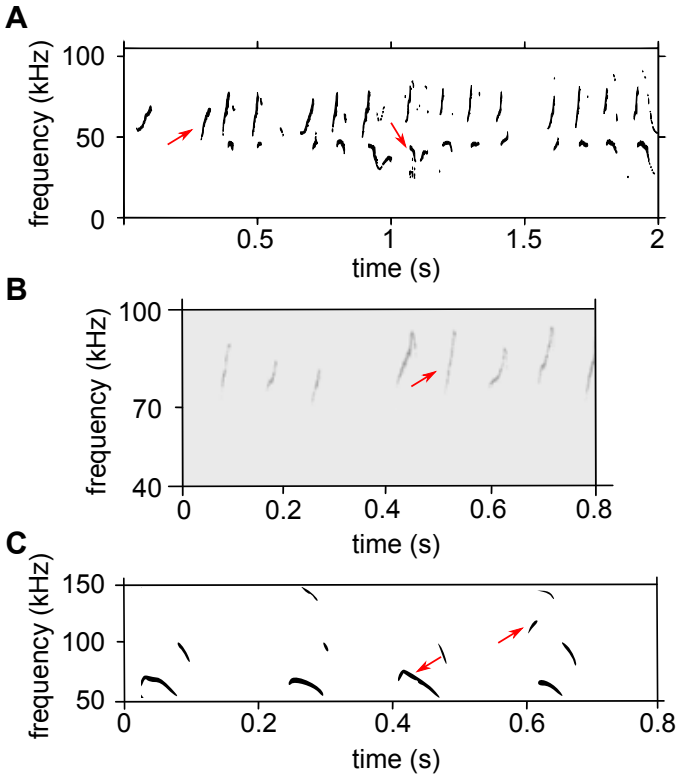

Figure 1.2: Spectrograms of various mouse communication calls: adult male (A), adult female (B) and pup (C). Red arrows indicate the occurrance of upward and downward FM sweeps. Modified respectively from Holy and Guo (2005), Portfors (2007), Grimsley *et al.* (2011).

proposed that the impairment in language learning seen in children suffering from developmental aphasia may originate from the inability of the auditory system to correctly process temporal information, which in turn prevents the patients from identifying features of speech, including FM sweeps (Tallal and Piercy, 1973). Indeed, cognitive training programs that utilize a range of FM sweeps crucial for speech perception, have been effective in improving the ability of language-learning impaired children to recognize sequences of speech sounds (Merzenich *et al.*, 1996). Finally, experiments in the auditory cortex of rats have demonstrated an age-related decrease in the processing of fast FM sweeps, which may be the cause of difficulties in speech discrimination in the elderly (Mendelson and Ricketts, 2001).

1.3 Subcortical processing of sounds

According to the textbook description of the auditory system, acoustic signals travel on a unique track, defined by projections that connect consecutive processing stations leading to the auditory cortex (Winer and Schreiner, 2005). Although this is a practical oversimplification, it is useful at this point to give a similarly synthetic overview of sound processing at the subcortical level, focusing in particular on the functions and the functional architecture of the nuclei involved in frequency, ILD and FM sweep coding. This section will help orient the reader before introducing the topic of study in this thesis, the auditory cortex.

1.3.1 The cochlea and the auditory nerve

The cochlea is a spiral-shaped structure in the inner ear, and the surface of its basilar membrane is home of the auditory peripheral sensory receptors.

When sound-induced vibrations of the oval window occur, they are decomposed along the cochlea according to the frequency of the acoustical energy they contain, with an effect similar to that of a Fourier transformation. High frequencies make the base of the basilar membrane resonate while, in a logarithmic progression, lower frequencies cause vibrations of the apex. This arrangement gives rise to the first of the auditory maps: the "tonotopic" or "cochleotopic" one, which will be preserved along the core regions of the auditory pathway.

Hair cells along the basilar membrane are activated by the local mechanical displacement of the cochlear surface, and are responsible for translating this into changes in membrane potential. The release of glutamate from the base of the hair cells activates neurons in the spiral ganglia, whose axons constitute the fibers of the auditory nerve (AN; VIIIth cranial nerve): different fibers will be activated depending on their position, so that the tonotopic principle can be maintained.

Beside this "place code" used to encode sound frequency, the eighth nerve fibers also use a "rate code", which provides the basis for the processing of sound intensity in the auditory system. As the level of a sound increases, the fibers of the AN fire a higher number of spikes per time unit, up to an intensity which will cause the firing rate to saturate. Different groups of fibers have different intensity thresholds, sensitivity and

dynamic ranges, resulting in a specific pattern of nerve action potentials (a population code) that will be transmitted to the next auditory station.

The combination of different frequencies and intensities that each AN fibre responds to can be represented by its Frequency Response Areas (FRA). The FRA allows the identification of two properties of the AN fibers: (1) the characteristic frequency (CF), the pure tone frequency eliciting a response at the lowest sound level the fibre is responsive to (threshold level); (2) the best frequency (BF), the frequency eliciting the maximum response across sound levels.

Auditory nerve fibers can also exhibit a third coding strategy, based on their ability to phase lock to sound frequencies up to a limit of ∼1.5 kHz to ∼4 kHz depending on the species (Kettner *et al.*, 1985; Köppl, 1997; Palmer and Russell, 1986). This means that each fibre fires at a particular phase of the sine wave. Thus, groups of AN fibers can faithfully capture the fine temporal structure of complex sounds and be informative about behaviourally relevant sound features such as periodicity, the main cue for pitch (Cariani, 1999). On the other hand, they are not sensitive to FM parameters, nor to interaural differences, as the information flow at this level is still unilateral.

1.3.2 The Cochlear Nucleus

The first station of the central auditory system is the cochlear nucleus (CN), located in the brainstem. The ascending AN branch enters the anteroventral division (AVCN) of the cochlear nucleus, while the discending one synapses in the posteroventral region (PVCN) and then proceeds onto the dorsal division (DCN). All these divisions are tonotopically organized, with neurons inheriting their BFs from the fibers innervating them.

A number of morphologically and physiologically distinct cell types have been described in the CN, which initiate the parallel processing of several sound features. A full description of the functions of this nucleus is beyond the scope of this Chapter, and I shall focus here on binaural and FM sensitivity.

Although binaural processing does not happen yet at this level, neuronal sensitivity to FM sweeps has been occasionally reported. Cochlear nucleus neurons in rats and bats do not show preferences for upward or downward FM sweeps (Kuo and Wu, 2012; Moller, 1969; Suga, 1965b), whereas stronger direction, as well as rate selectivity, have

been found in the cat, depending on the cell type (Britt and Starr, 1976; Erulkar *et al.*, 1968). A topographic organization of FM direction or rate preferences in the CN has never been reported.

The axons originating in the CN can take two different pathways: entering the superior olivary complex, where binaural sensitivity is first established, or bypass it and travel to the Inferior Colliculus (IC), where FM sensitivity becomes a prominent neuronal feature.

1.3.3 The Superior Olive

The superior olive is the first structure in the auditory pathway to integrate binaural signals. The medial superior olive (MSO) is dedicated to the processing of ITDs, while ILDs are encoded by neurons in the lateral superior olive (LSO). The difference in the size of the two divisions in mice may be a further demonstration of the use of ILDs as a localization cue in these rodents. Indeed, while the mouse LSO contains approximately 1200 projection neurons (about 2000 less than the cat), the MSO only has 210 (one order of magnitude less than the cat) (Irving and Harrison, 1967).

The LSO in each hemisphere receives direct excitatory inputs from the ipsilateral AVCN and indirect (via the trapezoid body) inhibitory inputs from the contralateral CN (Sanes, 1990): a pattern of innervation that determines the sensitivity of LSO neurons to sounds that favour the ipsilateral ear. Neuronal ILD response functions here are generally sigmoid in shape, and it has occasionally been reported that cells with similar slopes of their ILD function are spatially clustered (Boudreau and Tsuchitani, 1968; Reed and Blum, 1990).

1.3.4 The Inferior Colliculus

Most ascending projections from the brainstem and descending ones from the auditory cortex reach the IC. This comprises a central nucleus (CNIC) surrounded by a cortex, which is divided into two regions: the dorsal cortex (DCIC) and the external nucleus.

The convenient, superficial location of the DCIC in the mouse has allowed *in vivo* two-photon calcium imaging experiments to be performed, which highlighted the boundary between this area and the CNIC (Barnstedt *et al.*, 2015) better than previous microelec-

trode recordings (Portfors *et al.*, 2011), and confirmed the tonotopic organization of the CNIC, which can be divided into iso-frequency laminae defining a low-to-high, dorsal-to-ventral gradient of BFs (Merzenich and Reid, 1974; Portfors *et al.*, 2011). On the other hand, tonotopy in the DCIC appeared to be less clear in both electrophysiological and imaging studies (Barnstedt *et al.*, 2015; Ito and Oliver, 2014; Winer and Schreiner, 2005).

Responses to other sound features have been described as systematically organized too (best modulation rate for AM tones: Schreiner and Langner (1988); tone threshold: Stiebler and Ehret (1985); sharpness of frequency tuning; Stiebler (1987)).

The IC is innervated by several lower nuclei (Park *et al.*, 2004). Sites lacking binaural sensitivity receive direct projections from the CN, the ipsilateral MSO innervates primarily areas containing low frequency, ITD-sensitive neurons and, finally, high-frequency binaural areas receive multiple inputs, bringing both ITD and ILD information. These inputs are excitatory from the contralateral LSO, inhibitory from the ipsilateral LSO, and excitatory from the ipsilateral MSO (Loftus *et al.*, 2010, 2004).

Because of this partial overlap of projections, IC neurons can represent multiple binaural cues, using more than one coding strategy (Chase and Young, 2005, 2006). A prevalence of tuning to contralateral or midline locations has been found in the external nucleus (Binns *et al.*, 1992), as well as in the CNIC (Aitkin and Martin, 1987). Neurons with similar binaural properties were found to be spatially proximal in both these areas (Schreiner and Langner, 1988).

Sensitivity for FM sweeps becomes prominent in IC neurons compared to lower auditory stations (Gittelman *et al.*, 2009; Kuo and Wu, 2012; Lee *et al.*, 2002; Poon *et al.*, 1992) and is largely determined by the cell's frequency tuning. Two mechanisms have been proposed to explain the emergence of FM direction and rate sensitivity in the auditory system: these were described initially in bats (Fuzessery, 1994; Suga, 1965a).

In the "inhibitory sideband" model, neurons tuned to high frequencies, with FRAs dominated by inhibition at frequencies lower than BF, respond preferentially to downward sweeps, as these reach the excitatory frequencies in the neuron's receptive field earlier than the inhibitory ones (Figure 1.3). Conversely, low frequency neurons are activated by upward frequency sweeps preferentially. The two sidebands may not only be

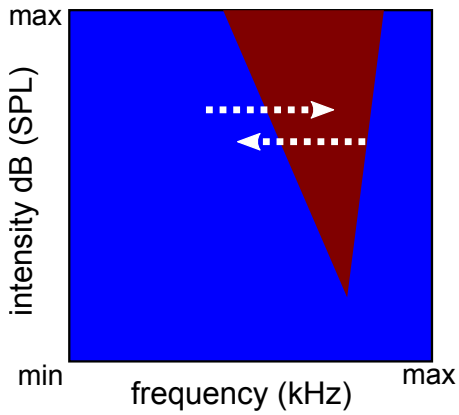

Figure 1.3: The schematic drawing shows a Frequency Response Area plot of a hypothetic auditory cortical neuron. The red area shows the combinations of sound frequencies and intensities eliciting a response in the neuron. The blue area indicates the combinations that do not activate the neuron, or activate it only weakly. The two white arrows of the same length indicate two FM sweeps of the same bandwidth, crossing the same range of frequencies, but in opposite directions: one upward, the other downward. The FM sweep represented by the arrow above starts at frequencies that constitute the "inhibitory sidebands" of the neuron's receptive field. This sweep is unlikely to elicit a response. In contrast, the FM sweep defined by the arrow below encompasses the neuron's frequency receptve field in a direction that will likely activate the neuron.

.

asymmetric across frequency, but also in their temporal properties: for example, low-frequency inhibition may arrive earlier than high-frequency inhibition. According to this model, rate tuning is shaped by the arrival time of the sideband inhibition: the earlier inhibition arrives when the sweep crosses the inhibitory sidebands, the more likely it will cause suppression of responses when the sweep enters the excitatory frequency band (Fuzessery *et al.*, 2006; Zhang *et al.*, 2003). If the low and high frequency sidebands in the neuron's FRA have similar properties, the neuron should not be sensitive to FM sweep direction or rate.

The "facilitation model" relies on the temporal coincidence in the arrival of synaptic inputs: only FM sweeps crossing frequencies in the right sequence, and with the right speed, activate enough excitatory inputs coincidentally to elicit a response from the neuron. The null direction instead activates more inhibitory inputs together (Razak and Fuzessery, 2008).

A third mechanism, that of "duration tuning to tones", has been proposed to explain

rate selectivity, mainly in subcortical regions (Fuzessery *et al.*, 2006). This depends on an early inhibition occurring at the neuron's BF, and lasting the duration of the sound. The later, fixed-latency excitation will then be unable to elicit a response, if the sound is long enough for the inhibition to overlap with the excitation. In this scenario, the optimal rate will be that of sweeps that remain within the excitatory band for a duration that matches the best one.

As we have seen, FM sensitivity has been only occasionally described in the CN and several studies have indicated that FM direction selectivity may be created *de novo* in the IC. The first finding supporting this hypothesis is that blockade of local inhibition can reduce or even eliminate it (Andoni *et al.*, 2007; Fuzessery and Hall, 1996; Koch and Grothe, 1998). This result was ultimately confirmed in an elegant *in vivo* experiment in which individual IC neurons were recorded in both voltage and current-clamp regimes, in order to dissect both their inputs and their outputs (Kuo and Wu, 2012). In terms of spatial organization, neurons showing fast best FM rates and preference for downward sweeps have been found peripherically within one CNIC lamina, while neurons preferring slow downward sweeps are located more centrally, defining a roughly concentric organization (Hage and Ehret, 2003; Kuo and Wu, 2012; Poon *et al.*, 1992).

1.3.5 The Superior Colliculus

Located dorso-frontally to the IC within the midbrain, the Superior Colliculus (SC) deserves a special mention when talking about topographic organization of auditory responses, although it is not involved only in auditory processing.

It is a laminated structure, with superficial layers receiving almost exclusively visual inputs and deeper layers processing visual, auditory and somatosensory signals, which makes it an important centre for multisensory integration. The deep layers of the SC are the only nervous structure to contain a point-to-point map of auditory space (King and Palmer, 1983). This is registered with space maps defined by visual and tactile inputs. Specifically, neurons in the rostral region of the SC respond to frontal visual and auditory stimuli, while caudal neurons are selective to progressively more contralateral locations (King *et al.*, 1998).

In mammals, the auditory map is defined by the sensitivity of SC neurons to ILDs

(Middlebrooks, 1987; Palmer and King, 1985) and spectral cues (King *et al.*, 1994; Palmer and King, 1985), while ITDs do not contribute to the representation of the space in this nucleus (Campbell *et al.*, 2006). The alignment of multiple space maps in the SC facilitates its role in coordinating eye, head, and body movements in response to multisensory stimuli, as reviewed by King (2004).

1.3.6 The Medial Geniculate Body

In contrast with the textbook description as a simple "gateway" for information flow en route to the cortex, the thalamus was defined as a "funhouse mirror" in a recent report (Bartlett, 2013), because of the filtering and distortion that incoming inputs undergo here to facilitate the representation of relevant sensory features in the cortical areas (Sherman and Guillery, 2002).

The auditory thalamus is known as the Medial Geniculate Body (MGB), which is divided into a dorsal (MGBd), a medial (MGBm), and a ventral subdivision (MGBv). Recent high-density multielectrode recordings in the mouse have described an ordered increase in BFs going from latero-caudal to medio-rostral areas of the MGBv (Hackett *et al.*, 2011). This is a confirmation of the presence of tonotopy in this area, which is also the basis of the tonotopically ordered projections originating in the MGBv and arriving in A1 (Budinger and Scheich, 2009; Lee *et al.*, 2004; Winer *et al.*, 1999). The MGBv provides about 3/4 of the thalamic projections reaching A1, the remaining 1/4 come from the MGMm (Hackett *et al.*, 2011).

Published studies focusing on FM processing in the MGBv of mammals other than bats described a prevalence of tuning for medium to fast FM sweep rates and a higher degree of direction selectivity than in lower nuclei (Creutzfeldt *et al.*, 1980; Lui and Mendelson, 2003). As in the IC, FM preferences are predicted by frequency tuning, so that their topographic organization proceeds in parallel to that of neurons' BFs (Kuo and Wu, 2012).

1.4 Cortical processing of sounds

The previous section has highlighted the considerable amount of subcortical processing that takes place for ILDs and FM sweeps. These are just two of the many features that are encoded along the auditory pathway. Neurons at the top of this hierarchy, in the auditory cortex, have therefore multidimensional receptive fields defined by several parameters, such as best frequency, spectral excitatory bandwidth around BF, degree of symmetry around BF of such bandwidth, sensitivity to sound source location, and tuning to temporal modulations of sound envelope. Such complexity is key in order to ultimately achieve a comprehensive representation of acoustic stimuli as auditory objects (King and Nelken, 2009; Nelken and Bar-Yosef, 2008).

How do cortical neurons respond to relatively basic sound attributes such as ILDs and frequency modulation? Does the neuronal sensitivity to these sound attributes follow a systematic spatial organization in the complex cortical environment? I shall review the answers we have to these questions in the next sections of this chapter and further in sections 3.1, 4.1 and 5.1, highlighting the limited amount of data currently available from the mouse cortex, my experimental model. The mouse is nonetheless a species holding great potential in auditory neuroscience, thanks to its suitability for the application of modern techniques that may help clarify old questions and answer new ones.

1.4.1 ILD processing

Cortical neurons show different degrees of sensitivity to binaural cues (Brugge *et al.*, 1994; Imig *et al.*, 1990; Mrsic-Flogel *et al.*, 2001; Recanzone *et al.*, 2000). Spatial receptive fields generally expand with increasing sound level (Middlebrooks and Pettigrew, 1981; Mrsic-Flogel *et al.*, 2005; Rajan *et al.*, 1990) and are broader than the localization abilities of the animals, suggesting the presence of a population code underlying the perception of space (Fitzpatrick *et al.*, 1997; Furukawa *et al.*, 2000; Recanzone *et al.*, 2000). At the single neuron level, Chadderton *et al.* (2009) have described an "iceberg effect" underlying spatial tuning: pyramidal neurons receive inputs from a large range of locations along the azimuth, all generating at least subthreshold membrane potentials, while spiking response profiles are more sharply tuned. A similar mechanism shapes spatial responses in somatosensory (Margrie *et al.*, 2002) and visual (Carandini and Ferster, 2000) cortex.

Studies in a range of species have shown that the majority of A1 neurons prefer stimuli favouring the contralateral ear, although some respond best to ipsilateral locations or to ILDs close to zero, which indicate sounds around the midline, and some are omnidirectional (i.e. lack spatial selectivity) (Campbell *et al.*, 2006; Irvine *et al.*, 1996; Middlebrooks and Pettigrew, 1981; Mrsic-Flogel *et al.*, 2005; Rajan *et al.*, 1990; Razak, 2011; Zhou and Wang, 2012). In contrast, neurons in rat A1 exhibit almost exclusively contralateral hemifield spatial preferences (Higgins *et al.*, 2010; Kyweriga *et al.*, 2014; Yao *et al.*, 2013), raising the question of whether A1 in mice is similarly organized.

As mentioned earlier, disrupting hearing monaurally in mice broadens cortical ILD receptive fields, as reported from the only published study investigating cortical sensitivity to ILDs in mice (Polley *et al.*, 2013). Nonetheless, it is not clear whether auditory cortex in this species is necessary for localizing sounds, or if localization performances can be accounted for by processing in the brainstem. In fact, the extensive subcortical involvement in ILD coding, and the presence of an auditory space map in the SC cast doubts about the contribution of auditory cortex to sound localization in all mammals. However, both carnivores and primates show deficits in sound localization abilities after surgical removal (Heffner and Heffner, 1990; Jenkins and Merzenich, 1984; Kavanagh and Kelly, 1987), cryogenic (Malhotra *et al.*, 2004; Malhotra and Lomber, 2007) or pharmacological inactivation (Bizley *et al.*, 2007; Nodal *et al.*, 2010; Smith *et al.*, 2004) of auditory cortex. Naturally, the magnitude of these deficits depends on the extent of the damage. For example, unilateral lesions impair localization in the contralateral hemifield, while bilateral lesions can disrupt performance for all locations, barely preserving the ability of the animal to lateralize a sound (Nodal *et al.*, 2010).

Different outcomes come instead from the few, early published studies in rats. Here, even bilateral ablation of the auditory cortex has only negligible effects on localization abilities (Kelly, 1980; Kelly and Kavanagh, 1986), suggesting again a possible difference between rodents and other mammals. Similar experiments in mice have yet to be carried out. Thus, we are at a point where, despite many years of investigations, the cortical processing of such a relevant acoustic attribute as ILDs still needs clarification.

1.4.2 FM sweep processing

Neurons sensitive to the rate and direction of FM sweeps have been found in the auditory cortex of all species studied so far (chinchilla: Brown and Harrison (2009); squirrel monkey: Godey *et al.* (2005); cat: Heil *et al.* (1992), Mendelson and Cynader (1985); ferret: Shamma *et al.* (1993), Nelken and Versnel (2000); bat: Razak and Fuzessery (2006); rhesus monkey: Tian and Rauschecker (2004); rat: Zhang *et al.* (2003); mouse: Trujillo *et al.* (2011), Honma *et al.* (2013)).

In contrast to what is seen for binaural cues, the auditory cortex of rodents seems to be actively involved in the processing of FM sweeps. Mongolian gerbils trained to discriminate sweep direction in an avoidance go/no-go task showed a drop in their performance following both unilateral and bilateral lesion of the auditory cortex (Wetzel *et al.*, 2008). Interestingly, researchers from the same group found no discrimination impairment when gerbils where trained to discriminate pure tones after bilateral damage (Ohl *et al.*, 1999). While it is true that gerbils differ from other rodents because of their human-like low frequency hearing range, similar results have been found also in mice: in this case, the auditory cortex proved to be necessary for negative memory formation in a fear conditioning experiment in which FM sweeps were paired with foot-shocks (Letzkus *et al.*, 2011). Finally, in a behavioural study from Rybalko *et al.* (2006), rats with a lesion to the auditory cortex (either bilateral or unilateral to the right hemisphere, which is also the side I have tested in my experiments) performed significantly worse than controls when trained to discriminate upward from downward sweeps in order to receive water rewards.

From these findings, it seems that encoding FM sweep direction may be an important function of auditory cortex, and perhaps particularly of A1. Supporting evidence comes from studies where pharmacological blockade of inhibition in A1 reduces direction and also rate selectivity, suggesting that these properties are locally shaped (Razak and Fuzessery, 2009; Zhang *et al.*, 2003). Specifically, auditory cortical neurons do not inherit duration tuning from midbrain nuclei, and rate selectivity can be created here through the asymmetry of sideband inhibition (Fuzessery *et al.*, 2011).

Since auditory cortical neurons act as "integrators", being sensitive to specific spectro-temporal modulations of the sound rather than to steady tones, then FM rate, reflecting

the spectro-temporal dynamics of FM sweeps, may be a prime candidate for features that cortical neurons extract from the incoming sounds. Evidence for FM rate sensitivity in the mouse A1 neurons is limited to two studies (Trujillo *et al.*, 2011; Trujillo and Razak, 2013) and, in general, cortical specialization for any complex sound feature in this species has not been comprehensively studied yet (Linden *et al.*, 2003). Sensitivity to FM rate will receive particular attention in Chapter 5, alongside the fine-scale organization of FM responses in A1.

1.5 Spatial organization of auditory cortex

1.5.1 Functional architecture across cortical fields

Organizing brain regions in a map-like fashion can optimize computational power by avoiding costly wiring of neurons in distant areas (Chklovskii and Koulakov, 2004; Kaas, 1997). However, neuroscientists do not have a clear picture yet of what auditory cortex does or how (King and Nelken, 2009; Nelken, 2008) and, unsurprisingly, its functional architecture, both on the large and on the fine scale, is still a hugely debated topic (recent reviews are in: Kanold *et al.* (2014); Rothschild and Mizrahi (2015); Schreiner and Winer (2007)).

On the large scale, the validity of the "what" and "where" independent streams hypothesis, assigning sound identification ("what") to ventral cortical fields, and sound localization ("where") to more dorsal areas is unconfirmed (Rauschecker, 1998; Recanzone and Cohen, 2010; Romanski *et al.*, 1999). While dorsal regions do seem to be specialized for "where" (Lomber and Malhotra, 2008; Woods *et al.*, 2006), the existence of specific areas dedicated to auditory object identification remains more elusive (Recanzone, 2008; Tian *et al.*, 2001). In fact, a recent study testing the same cortical neurons on both "sound patterns" (such as pitch or timbre) and sound localization cues, described a distributed representation of these acoustic features across several regions (Bizley *et al.*, 2009).

Another controversy is specific to the mouse. In this species, five different auditory cortical regions were first identified on the basis of differences in response profiles to sound frequency and other sound features: two primary areas (A1 and AAF, the anterior au-

ditory field), a secondary field (A2), the dorsal posterior (DP), and the ultrasonic fields (UF) (Stiebler *et al.*, 1997). However, a later study denied the existence of the UF and considered it part of the primary regions (Guo *et al.*, 2012), and a recent dispute dealing with a possible subdivision of A1 into two different fields is still open (Issa *et al.*, 2014; Tsukano *et al.*, 2015, 2013). Last, in an unpublished report, Issa and colleagues identified, in a stripe of cortex between A1 and AAF, a separate field that may be specialized for FM processing (Issa *et al.*, 2016).

1.5.2 Functional architecture within A1

If we focus on the organization of A1 only, things are just as complicated. In fact, this region has traditionally been described as a multi-layered territory defined by the overlapping representations of multiple sound features. The existence of a large-scale tonotopic gradient of frequency responses is undoubtedly its best established topographic arrangement (monkeys: Merzenich *et al.* (1973); cats: Merzenich *et al.* (1975); ferrets: Kelly *et al.* (1986); humans: Talavage *et al.* (2000); guines pigs: Hellweg *et al.* (1977); gerbils: Ryan *et al.* (1982); rats: Sally and Kelly (1988); mice: Stiebler *et al.* (1997)). However, the precision of such organization is still a controversial issue and it often depends on the recording technique used to identify it, as we will see more in detail in sections 3.1 and 3.4.

Beside frequency, other sound features, not isomorphic to the sensory receptor surface, have been described as systematically organized across the surface of A1, defining so-called "computational maps" (Knudsen *et al.*, 1987). These are interleaved with tonotopy similarly to how the orientation, ocular dominance, and spatial frequency preferences vary within the retinotopic map in V1 (Hübener *et al.*, 1997): a schematic representation of this arrangement can be seen in Figure 1.4.

1.5.3 The organization of responses to binaural stimuli and FM sweeps

Some computational maps co-vary globally with the tonotopic gradient. Preferences for FM sweep direction change progressively from upward to downward in rats (Zhang *et al.*, 2003) and squirrel monkeys (Godey *et al.*, 2005). According to the asymmetric influence of the inhibitory sidebands, low frequency neurons prefer upsweeps and high frequency

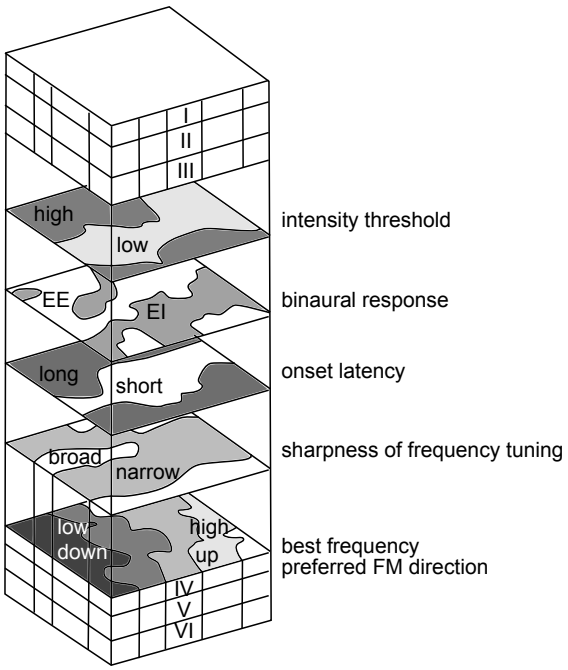

Figure 1.4: The schematic image shows the overlapping maps of responses to several sound features in the A1 of the cat. The systematic progression of neuronal CFs defines the tonotopic cortical map. Other response properties, including onset latency, binaural interactions, and intensity threshold, vary along a dimension perpendicular to that of the tonotopic gradient. Modified from Linden and Schreiner (2003)

.

neurons prefer downsweeps. Experiments in mice (Trujillo *et al.*, 2011) and owl monkeys (Atencio *et al.*, 2007), however, failed to reproduce such an arrangement. Tuning to the speed of FM sweeps was found to be similarly poorly organized in the A1 of the mouse, as preferences for slow modulations prevail here (Trujillo *et al.*, 2011). However, in the dorsal areas of cats A1, FM rates are organized following a roughly concentric organization (Mendelson *et al.*, 1993), possibly inherited from the IC (Hage and Ehret, 2003).

The representation of some sound features extends perpendicular to the tonotopic gradient, along isofrequency bands, corresponding to the local A1 areas where neighbouring neurons have identical, or very similar BFs. The most studied case, which is nonetheless still controversial, is that of binaural properties. Early studies described bands of neurons belonging to different categories defined according to their responses to binaural sounds. Categories were identified with a two-letters code, in which the first

letter indicated the neuronal response to sounds in the contralateral ear, and the second one the response to stimuli in the ipsilateral ear. The letters used were "E" and "I" (sometime replaced by "O"), respectively indicating excitation and inhibition (or occlusion). Within isofrequency areas, neurons preferring stimuli favouring the contralateral ear, belonging to the EI category, were found flanking groups of cells excited by stimulation of either ear, named EE cells (Imig *et al.*, 1977; Kelly and Judge, 1994; Middlebrooks *et al.*, 1980). The identification of this arrangement was usually based on a qualitative approach, where authors did not adopt empirical methods to quantify the actual degree of local response similarity, but simply relied on visual inspection of the cortical maps they produced.

Later reports, using more complex acoustic stimuli, only found spatial clusters of cells with similar properties, again relying mainly on a visual criterion to define them (Kelly and Sally, 1988; Nakamoto *et al.*, 2004; Reale and Kettner, 1986; Recanzone *et al.*, 1999; Reser *et al.*, 2000; Rutkowski *et al.*, 2000). On the other hand, a precise point-to-point description of the space, similar to that of the superior colliculus, has never been found in auditory cortical regions.

A case that stands apart is that of the pallid bat. In the A1 of this species, two binaural clusters have been identified, and occupy the area tuned to frequencies between 5 - 30 kHz (Razak and Fuzessery, 2000, 2002). In contrast to any other mammal, a systematic spread in neuronal activity associated to the presentation of sounds on the horizontal plane was found within each of these two regions (Razak, 2011). In particular, in the cluster preferring the contralateral hemifield, neuronal activation spread progressively as sound sources were moved to more contralateral positions. In the second cluster, dedicated to the processing of near-midline stimuli, activity dropped as sound sources were moved laterally. Appealing as it may be, however, this model may apply to the pallid bat only, given its rather specific use of auditory cues: passive hearing of frequencies up to ∼30 kHz to localize preys, and echolocation for obstacle avoidance (Razak, 2011).

1.5.4 Other sound features systematically represented in A1

Embedded within A1 isofrequency bands, there are also groups of neurons more or less sharply tuned to frequency, as described in cats (Schreiner and Mendelson, 1990) and

primates (Cheung *et al.*, 2001; Philibert *et al.*, 2005). Although both these groups systematically recur within each band, suggesting a representation independent from the tonotopic gradient, narrowly tuned neurons are particularly numerous in the midfrequency band in cats, where BFs are between 5 - 20 kHz (Imaizumi *et al.*, 2004; Schreiner and Mendelson, 1990). In this species, local areas dominated by shallow or steep frequency gradients also exist, and it was shown that the areas where local BF changes are less pronounced are also characterized by sharp frequency tuning (Imaizumi and Schreiner, 2007).

A topographic correlation between sharpness of tuning and intensity threshold has also been described (Brosch and Schreiner, 1999). Specifically, low threshold neurons should be the most sharply tuned; these cells also have peaked intensity response curves, meaning that they are preferentially activated by a specific sound level and exhibit weaker responses to higher or lower intensities. It has been argued that cortical areas containing neurons with such receptive field properties might be involved in signal detection close to background noise level (Sutter and Schreiner, 1995). It is worth noting though, that "peaked" neurons occupy only a limited area and are a small minority of A1 neurons, as these mostly respond monotonically with respect to sound pressure level, that is, their firing rates increase with increasing intensities, until reaching a plateau level (for an example in rodents see Polley *et al.* (2007)). The organization of both sharpness of tuning and intensity sensitivity differed slightly, in the same species, when analysed with single rather than multi-units recordings (Schreiner and Sutter, 1992; Sutter and Schreiner, 1995).

Finally, neurons with short or long response latencies to tones alternate orthogonally to the tonotopic gradient in the A1 of the cat (Mendelson *et al.*, 1997), while their organization is more "patchy" and independent from that of frequency tuning in the A1 of the rat (Polley *et al.*, 2007).

1.5.5 Cortical maps are plastic

Technical differences are only some of the reasons why cortical maps may appear different across studies. For instance, the tonotopic gradient is much less clear if measured based on responses to tones well above neuronal threshold, because at such levels neurons can

exhibit responses to a range of frequencies spanning several octaves (Schreiner and Winer, 2007).

Moreover, topographic arrangements are intrinsically labile because they reflect the lability of the receptive fields of cortical neurons. Response profiles of single neurons are naturally plastic, as reviewed in Froemke and Martins (2011), and can change with the level of wakefulness (Hackett *et al.*, 2011) and attentional state (Fritz *et al.*, 2003), or based on experience (Bakin and Weinberger, 1990; Bao *et al.*, 2001; Recanzone *et al.*, 1993; Rutkowski *et al.*, 2000).

Finally, obvious species differences should be taken into consideration when judging cortical spatial organization. For instance, neurons selective for pitch have been found in a low-frequency region in the A1 of marmoset monkeys (Bendor and Wang, 2005), but they were not organized topographically, in contrast with the existence of a gradient of sensitivity to sound periodicity in a corresponding area in gerbils (Schulze *et al.*, 2002).

Despite all the factors that can influence the identification of topographies, their existence on the large-scale in A1 is a recurring theme in many studies and cannot therefore be easily dismissed. On the other hand, the precision of such topographies at the fine scale, together with other issues like the general relevance of cortical maps for the emergence of perception, is more controversial (Thivierge and Marcus, 2007). Modern neuroscience techniques can certainly help clarify this matter.

1.6 The cortex at high definition: two-photon calcium imaging

In order to obtain information about the functions of auditory cortex from its structure, we must look into the building blocks of the cortical architecture: the individual neurons and the relationships between their sensory responses and those of the surrounding cells.

The aforementioned evidence describing auditory response properties as represented systematically across the cortical surface is mostly based on microelectrode recordings of single or multi-unit activity. Multi-unit recordings suffer from a spatial resolution limitation. They collect signals from dozens, if not hundreds of neurons present in a cortical patch, and return these as a unique value, corresponding to the neurons' average

response. Naturally, this value mostly mirrors the activity of the local "leading actors", that is, it underrepresents small neurons, neurons with low basal activity and unresponsive or weakly tuned neurons, making the sampled area look more homogeneous than it might actually be.

The consequences of this limitation have been highlighted already in auditory cortex. When recoding multi-unit activity in the mouse A1, Guo *et al.* (2012) found a remarkably precise tonotopy. However, a more scattered organization of BFs emerged in the same study from single-unit responses (see also Sutter and Schreiner (1995)). Thus, single-unit recordings are better suited for capturing the richness of response profiles in mapping experiments. However they tend to have a low yield and may still be biased by the presence of large neurons, which are physically easier to record from.

The minimum technical requirements to obtain detailed fine-scale functional maps of the brain are currently met better by *in vivo* two-photon calcium imaging. This technique reports an indirect sign of neuronal activity, corresponding to the fluctuations in the intracellular calcium concentration, which are measured through the changes in fluorescence of a calcium probe (Grienberger and Konnerth, 2012). *In vivo*, it takes advantage of pulsed laser light of wavelengths compatible with biological tissues, and of the rarity of two-photon excitation, to avoid heat-related damage, bleaching, and out-of-focus contamination (Svoboda *et al.*, 1997). By rapidly scanning the cerebral tissue with a spatial resolution of $\sim$1 μm, it records the activity of all local neurons in a given area and allows the production of fine-grained maps of sensory responses.

The first *in vivo* two-photon mapping studies were published about 10 years ago (Ohki *et al.*, 2005, 2006; Van Hooser *et al.*, 2006) and examined orientation selectivity in V1. This feature was initially studied by Hubel and Wiesel, who described it as organized in bands running along the cortical surface (Braitenberg and Braitenberg, 1979; Hubel and Wiesel, 1963). Later, the well-known "pinwheel organisation" was reported, and experiments combining low-resolution imaging and single-unit recordings highlighted possible tuning differences between neighbouring neurons, although a more precise picture was hampered by the low resolution of the imaging techniques used (Bonhoeffer *et al.*, 1991; Maldonado *et al.*, 1997). With two-photon imaging, a systematic, smoothly progressing representation of orientation preferences was confirmed by recording an unprecedented

number of neighbouring single neurons in the cat (Ohki *et al.*, 2006). To the contrary, local disorder dominated in the V1 of the rat, where nearby cells even exhibited selectivity for opposing orientations (Ohki *et al.*, 2005).

Since these first reports, the vast majority of two-photon mapping studies have been carried out in the mouse and to a less extent in the rat. From these experiments, local heterogeneity of neuronal responses emerged like a rule shared among sensory cortices. Indeed, similar results have been reported when studying several characteristics of neuronal receptive fields in V1 (Bonin *et al.*, 2011; Mrsic-Flogel *et al.*, 2007; Smith and Häusser, 2010), as well as whisker selectivity in barrel cortex (Sato *et al.*, 2007). Nonetheless, in the motor cortex of awake mice, neurons showing similar patterns of activity during running or grooming were found to be located significantly more closely than less correlated neurons, forming local functional clusters (Dombeck *et al.*, 2009). Although this is not exactly a study mapping sensory responses, the fact that it was performed in awake rather than anaesthetized animals may again highlight possible differences between the two states in the functional relationships of neighbouring neurons. In contrast, in an elegant and technically challenging experiment in the V1 of awake mice, Andermann *et al.* (2013) chronically imaged neuronal activity across layers and cortical columns, finding a striking disorder of orientation preferences both locally and across layers and columns. A coarse retinotopy was instead present.

The first two-photon calcium imaging experiments in the auditory system were published recently (Bandyopadhyay *et al.*, 2010; Rothschild *et al.*, 2010), and brought to light the unexpected randomness of A1 local frequency responses in a species, the mouse, in which precise tonotopy was thought to be the governing functional principle as in all other mammals (Horie *et al.*, 2013; Kubota *et al.*, 2008; Stiebler *et al.*, 1997; Zhang *et al.*, 2005). Sensitivity to sound intensity and sharpness of frequency tuning were also described as locally variable (Bandyopadhyay *et al.*, 2010).

In the wake of a newly ignited debate around a matter that seemed to be settled before the introduction of two-photon imaging, further two-photon and electrophysiological investigations sought to re-investigate the existence of local ordered tonotopy in rodents, but with inconclusive outcomes (Guo *et al.*, 2012; Hackett *et al.*, 2011; Issa *et al.*, 2014).

Frequency preferences remain so far the only functional feature of auditory cortex

studied with two-photon imaging, despite the variety of response-evoking inputs defining its many overlaid maps. It is therefore a great time to challenge our views on the spatial representation of other acoustic parameters in the cortex.

1.7 Scope and organization of the thesis

Inspired by the new controversies raised by two-photon imaging experiments, and by the many outstanding questions regarding the representation of acoustic parameters in auditory cortex, I have explored how the A1 of the mouse represents two sound features particularly relevant for survival purposes and for intra-specific communication: interaural level differences and frequency modulation. Neuronal responses to such stimuli have previously been described as being systematically organized in the A1 of higher species of mammals using microelectrode recordings. In this thesis, *in vivo* two-photon calcium imaging allowed me to shed light on this matter at an unprecedented level of spatial resolution and without the technical biases typical of electrophysiological techniques.

Although my main focus was on the study of ILD and FM sweeps responses, the very first objective of my DPhil was to characterize the frequency responses of neurons in the mouse auditory cortex. Indeed, the start of my graduate studies in Prof King's group coincided with the commencement of two-photon imaging experiments in the lab, at a time, October 2012, when only three groups in the world were using this techniques to study the auditory system. For this reason, it was important to start my research by exploring what is possibly the most basic property of auditory neurons: frequency tuning. I have studied neuronal responses to frequency tones both in mice and, because of the possibility that the rodent sensory cortex may be organized differently from that of higher mammals, also by carrying out preliminary experiments in ferrets.

Thus, this thesis sets out to meet the following aims:

1. Describe the fine and large-scale organization of frequency responses in the A1 of the mouse (Chapter 3),

2. provide preliminary data about the fine-scale organization of frequency preferences in the ferret A1, in order to explore possible species differences (Chapter 3),

3. characterize the binaural (Chapter 4) and FM responses (Chapter 5) of neurons in the mouse auditory cortex,

4. describe the cortical organization of such responses at the microcircuit level and provide evidence about the coding principles underlying the processing of ILD and FM stimuli in local populations of neurons (Chapters 4 and 5),

5. compare the cortical organization of frequency preferences with that of binaural responses (Chapter 4) at both local (within 250 μm) and global (up to 1 mm) scales, and with that of FM sweep preferences at the local scale in the mouse A1 (Chapter 5).

Chapter 2

Methods

In the present Chapter I will describe experimental and data analysis procedures applying to all the experiments I performed during my DPhil I will then provide details of the experimental and analytical procedures that are specific to some of the experiments in Chapters 3, 4 and 5.

2.1 Experimental procedures

2.1.1 Animals

All animal procedures were approved by the Central Animal Care and Ethical Review Committee at the University of Oxford and performed under license from the UK Home Office. A total of 89 female mice was used in my imaging experiments, but I report here results from 24 animals. The reason for this difference lies in the low yield of two-photon calcium imaging experiments (about one out of three experiments are successful; Dr Patrick Kanold, personal communication). Most of the mice did not report a successful expression of the calcium indicator, while some others died during the experimental procedure. Of the mice yielding data, 18 were C57BL/6J (Harlan Laboratories): all 18 received pure tone stimulation; 15 of them were presented with ILD noise bursts and 11 received FM sweeps.

A further six mice were a GCaMP6f reporter line obtained by mating the floxed Ai95 (RCL-GCaMP6f)-D line (Jackson Laboratories; stock number 024105) with the CaMKIIalpha-Cre T29-1 line (Jackson Laboratories; stock number: 005359): three of

these were tested with pure tones and ILD stimuli, and three others with pure tones and FM sweeps.

Six further mice were used for tracer injection only (see section 2.1.3).

Thirteen adult female pigmented ferrets were used for calcium imaging experiments (Marshall, UK). Results are reported for two ferrets, the reasons for this difference are extensively explained in section 3.3.7.

2.1.2 Viral vector injections

GCaMP6m expression was induced through viral vector injection. I will now describe the injection procedures separately for mice and ferrets.

Mouse injections: at age 5-6 weeks, mice were premedicated with dexamethasone (4 μg s.c.) to reduce cerebral oedema, atropine sulfate (1 μg s.c.) to reduce bronchial secretion, and with the antinflammatory drug carprofen (0.15 μg s.c.). The animals were then put under general anesthesia with fentanyl (0.05 mg/kg i.p.), midazolam (5 mg/kg i.p.) and medetomidine hydrochloride (0.5 mg/kg i.p.).

Ferret injections: ferrets aged 12 weeks were put under general anaesthesia with an intramuscular injection of ketamine (5 mg/kg) and medetomidine (0.02 mg/kg). Isofluorane was then delivered throughout the surgery to maintain anaesthesia (flow rate 0.5 - 2%). The right radial vein was cannulated and a solution containing sodium chloride (0.9%) and glucose (5%) was continuously delivered intravenously to avoid loss of physiological fluids due to dehydration during surgery. Ferrets were medicated, prior to and during surgery, with atropine sulfate (0.06mg/kg), dexamethasone (0.5mg/kg), buprenorphine (0.03 kg/mg) and meloxicam (0.2 mg/kg). Respiratory rate, end-tidal CO_2 end electrocardiogram (ECG) were continuously monitored.

Once anaesthetized, both mice and ferrets were placed in a stereotaxic frame (Model 900LS, David Kopf Instruments). Body temperature was kept at 36-38°C through the use of a DC Temperature Controller (FHC) with a rectal thermometer input and a heating mat output. Eyes were covered with eye ointment (Maxitrol, Alcon) to prevent corneal desiccation. The skin over the injection site was shaved, cleaned with betadine and injected with bupivacaine (40 μg s.c.). A scalp incision was then made. The right temporal muscle was cut along the superior temporal line and then retracted to reveal

the right squamosal bone of the skull. The location of A1 was estimated as follows:

In mice, I referred to stereotaxic coordinates (70% of the distance from Bregma to Lambda, and ∼4.5 mm lateral from the midline) and vascular landmarks (Stiebler *et al.*, 1997). I then drilled two small holes into the skull, separated rostro-caudally by ∼0.7 mm, as the diameter of the drill bit used was 0.5 mm.

In ferrets, the irregularities of the skull surface and the gyrification of the cortex facilitate the localization of A1. Nonetheless, we have proceeded with the aid of stereotaxic coordinates (1.2 cm ventral to the midline and 0.8 cm frontal of Lambda) to carry out an approximately squared craniotomy of about 0.5 mm^2 above the ectosylvian gyrus, which is the area containing A1 in its middle part (Kelly and Kavanagh, 1986). Following the removal of the *dura mater* in this region, we idenitifed six to eight locations suitable for stereotaxic injection.

Approximately 200 nl of the viral construct AAV1.Syn.GCaMP6m.WPRE.SV40 (Penn Vector Core), diluted (1:2) in phosphate-buffered saline (PBS, Sigma Aldrich), were injected via each craniotomy in mice, whereas the volume injected in ferrets was about 500 nl. I chose to reduce the viral titer of the vector through dilution in order to avoid excessive transfection of the neurons, which would have compromised their function. The injections were performed at four depths spanning 50-400 μm below the pial surface in mice and at 10 depths between 50-800μm below the surface in ferrets. Injections were made using a pulled glass pipette (20-30 μm inner tip diameter) and a custom-made air pressure injection system.

Following injection, the skin was sutured together and the intravenous delivery of anaesthetic drugs was suspended in ferrets, while general anaesthesia was reversed in mice with flumazenil (0.5 mg/kg i.p.) and atipamezol (2.5 mg/kg i.p.). Postoperative buprenorphine (1 ml/kg s.c.) and enrofloxacine (2 ml/kg s.c.) were administered to mice immediately after surgery and again 24 hours later. Ferrets were medicated with buprenorphine (0.01 mg/kg) in the 48 hours after surgery, and with amoxycillin (20 mg/kg) and meloxicam (0.1 mg/kg) for five days after surgery.

2.1.3 Retrobead injections

To confirm injection of the viral vector into the auditory cortex, I injected red fluorescent retrobeads (Lumafluor Inc, 2 μl undiluted) into six mice of the same age (5 - 6 weeks), following the same surgical procedure and the same injection coordinates. Retrograde labeling of thalamocortical neurons in the medial geniculate body (MGB), which is the main thalamic relay sending feed-forward inputs to auditory cortex, was later assessed (see section 2.1.7).

2.1.4 Terminal surgery for *in vivo* two-photon calcium imaging

In vivo two-photon imaging sessions were performed 3 - 6 weeks after the injection in both mice and ferrets. I imaged all mice at <12 weeks of age, before the development of any high frequency hearing loss (Ison *et al.*, 2007).

Mouse anaesthesia: mice were premedicated as above with dexamethasone and atropine. I induced general anaesthesia with an intraperitoneal injection of 100 mg/kg ketamine, a N-methyl-D-aspartate (NMDA) antagonist, and 0.14 mg/kg medetomidine hydrochloride, an alpha2 adrenoceptor agonist. Anaesthesia was maintained with hourly subcutaneous injections of ketamine (50 mg/kg/h) and medetomidine (0.07 mg/kg/h).

Ferret anaesthesia: general anaesthesia was induced with an intramuscular injection of ketamine (5 mg/kg/h) and medetomidine (0.02 mg/kg/h), and was maintained through continuous intravenous infusion (4 ml/h) of the same drugs in sodium chloride (0.9%) and glucose (5%) solution.

My choice of the anaesthetic regime was made primarily for ease of comparison with past studies of auditory cortical responses in the mouse, which used a mix of ketamine and medetomidine (Linden *et al.*, 2003; Rothschild *et al.*, 2010; Stiebler *et al.*, 1997). However, I am aware that the choice of anaesthesia can affect both sound-evoked responses and spontaneous activity of auditory neurons. In particular, ketamine caused a reduction in the amplitude of auditory responses and an increase of selectivity for pure tones in the cat A1 compared to low doses of nitrous oxide (Zurita *et al.*, 1994). On the other hand, ketamine provoked an increase in both spontaneous and tone-evoked activity in a study in the A1 of the rat, compared to a mix of medetomidine and midazolam (Osanai and Tateno, 2016). In the same study, the temporal response patterns of auditory

neurons were also affected, in a layer-specific manner. In particular, layer V neurons showed fast-onset, single increases in activity in response to tones in the presence of ketamine, and double peaks of activity under medetomidine and midazolam. The temporal response profiles of neurons in layers II-III did not differ between the two anaesthetic regimes. In the mouse A1, medium levels of ketamine anaesthesia increased the trial-to-trial variability of multi-unit responses (Kisley and Gerstein, 1999). To partly avoid these effects, I used a mix of ketamine and medetomidine in my experiments, which allowed me to reduce the concentration of the NMDA antagonist compared to previous studies. Further discussion of the specific effects of anaesthesia on the spatial organization of auditory responses can be found in sections 3.4.3 and 6.6.1.

Ferrets also received a subcutaneous dose of 0.06 mg/kg/h atropine sulfate repeated every four hours and a dose of 0.5 mg/kg dexamethasone. The animals were intubated, connected to a ventilator and supplemented with oxygen. Body temperature, end-tidal CO_2 and ECG were monitored throughout the experiments, which lasted between 30 and 34 hours.

After shaving the scalp and applying bupivacaine (40 μg s.c.), the skin was incised and the temporal muscle retracted in mice and then removed in ferrets, to expose the viral vector injection sites, or simply the right auditory cortex in the transgenic mice. A circular craniotomy $\sim$2.5 mm in diameter in mice, and 1 cm in ferrets, was performed following the same stereotaxic coordinates and vasculature landmarks for all animals.

I placed a cover glass (Thermo Fisher Scientific) on top of the exposed area. In ferrets, this was attached to a plastic ring of the same diameter, and of a thickness similar to that of the skull, in order to optimize stability. I then secured the implant to the skull edge with cyanoacrylate adhesive (UltraGel, Pattex). I used dental cement (UniFast Trad, GC Dental Products Corporation) to secure a steel holding bar onto the left side of the skull and to create a fluid basin around the craniotomy, in order to immerse the objective in artificial cerebro-spinal fluid (ACSF) during imaging experiments in mice. In ferrets, as the head of the microscope was rotated to ensure access to auditory cortex, ACSF was replaced by the denser agarose gel. The animals were then head-fixed to the stage and placed under the microscope.

2.1.5 *In vivo* two-photon calcium imaging

I performed imaging of calcium transients using a ThorLabs B-Scope two-photon microscope controlled by ScanImage 4.1 software (`http://scanimage.org`). Excitation light was emitted by a Mai-Tai eHP laser (SpectraPhysics; 70 fs pulse width, 80 MHz repetition rate) tuned to 930 nm. The beam was directed into a Conoptics modulator (laser power, as measured under the objective, varied from 15 to 30 mW) and scanned through an 8 kHz resonant scanner in the x-plane and a galvanometric scanning mirror in the y-plane. I used the resonant scanner in bidirectional mode, at a resolution of 512 x 512 pixels, allowing frames to be acquired at a rate of ∼30 Hz. I used a 16X/0.80W LWD immersion objective (Nikon) and emitted photons were guided through a 525/50 filter onto GaAsP photomultipliers (Hamamatsu). All neuronal fields were 250 x 250 μm in size and were imaged 200 - 350 μm below the pial surface in mice, and not deeper than 250 μm in ferrets.

2.1.6 Sound presentation

I presented all stimuli binaurally via a closed acoustic delivery system comprising two EC1 electrostatic speakers (Tucker-Davis Technologies), each coupled to a 12-cm-long silicone tube leading into the ear canals. Delivery of the sounds directly into the ear canals provided precise control over ILDs and prevented acoustic cross-talk between the two ears. Nonetheless, I made cross-talk measurements between the speaker inputs to the two ears by inserting the calibration microphone in one ear canal and presenting a 95 dB SPL, 500-ms-long broadband noise burst to the contralateral ear. The intensity of the noise burst measured at the ear contralateral to stimulation was barely (<1 dB) above ambient room noise level.

Sound stimuli were generated using a RZ6 multiprocessor (Tucker-Davis Technologies) and controlled via customized MATLAB (MathWorks) software. The output response of the speakers was measured using a Brüel & Kjær calibration system with a GRAS 40DP microphone coupled to the end of the silicone tube. The speaker output was then filtered to produce a flat spectral response (±3 dB) from 1 - 80 kHz at the desired sound levels.

The microscope and the animals were enclosed within a sound- and light-attenuating

box. Ambient room noise was <42 dB SPL inside this box, and primarily consisted of energy <200 Hz, which is outside the hearing range of the mouse and at the lower edge of that of the ferret (Heffner and Heffner, 2007). The resonant scanner generated a constant acoustical tone of 8 kHz during imaging that was <30 dB SPL near the animal's head.

During my experiments I have presented either pure tones, or ILD noise bursts or FM sweeps. To briefly introduce the stimuli here: pure tones were presented at 18 different frequencies and at four sound levels. Noise bursts were presented at seven different ILDs and three average binaural sound levels (ABLs). Frequency modulated sounds were sweeps of four different durations and three different bandwidths, presented in two directions, both upwards and downwards. More specific details about the characteristics of the stimuli I have used can be found in section 3.2.1 for pure tones, section 4.2.1 for noise bursts and section 5.2.1 for FM sweeps.

2.1.7 Histology

At the end of each imaging session, or three days after the injection of fluorescent retrobeads in mice, the experimental animal was overdosed (100 mg/kg ketamine and 0.14 mg/kg medetomidine, i.p.) and perfused transcardially, first with PBS and then with 4% paraformaldehyde in PBS. After two days in fixative, the brain was sectioned in the coronal plane at a thickness of 100 μm on a vibratome, or immersed in 20% sucrose solution and then sectioned at a thickness of 60 μm on a freezing stage microtome. I then mounted the sections on glass slides and examined them with a Leica DMR upright fluorescence microscope or with the two-photon microscope. Excitation wavelength was 480 nm for visualizing eGFP and 530 nm for rhodamine retrobeads (930 nm at the two-photon microscope). Images were processed offline using ImageJ (NIH).

2.2 Data analysis

2.2.1 Isolating responses from individual neurons

Image analysis was performed offline using customized MATLAB software and was similar for ferrets and mice experiments.

Mechanical drift in the x-y imaging plane was corrected using efficient subpixel reg-

istration methods (Guizar-Sicairos *et al.*, 2008), and a time-averaged image was then generated from all recorded frames in the given field.

I identified neurons by visually inspecting this time-averaged stack and videos of frame-by-frame changes in fluorescence. I manually circled regions of interest (ROIs) corresponding to cell bodies, as in Barnstedt *et al.* (2015). For each cell, the signal at each time frame was calculated as the average fluorescence across all pixels inside the ROI ($F(t)$).

A high pass filter with a cut-off of 0.02 Hz was applied to this time series to eliminate slow fluctuations in the signal.

A correction for neuropil signal contamination was applied to each neuron's fluorescence trace as described previously (Chen *et al.*, 2013), so that the somatic fluorescent signal at each timepoint ($F_{cellfinal}(t)$) corresponded to:

$$F_{cellfinal}(t) = F(t) - (F_{neuropil}(t) \times r) \tag{2.1}$$

where $F_{neuropil}(t)$ is the neuropil signal surrounding each cell, measured by averaging the signal of all pixels within a 20 μm region from the cell centre (excluding all selected cells), and r is the contamination ratio. This is an empirical constant whose value depends on the objective used and on the depth of imaging, and is calculated as $F_{bloodvessel}(t)/F_{neuropil}(t)$ on the time-averaged stack image of a neuronal field (Kerlin *et al.*, 2010). I used an r of 0.7, corresponding to the mean value obtained from 20 imaging fields at depths between 200 - 300 μm below the cortical surface.

The baseline fluorescence (F_0) for a given ROI was calculated as the median of the 10th - 70th percentiles of fluorescence values across all frames. The highest 30% of fluorescence values was not included in the baseline calculation in order to exclude the transient increases in calcium concentration due to action potentials.

The fluorescence time series for the neuron was then corrected for the baseline using the formula: $(F(t) - F_0)/F_0$, which is commonly denoted as $\Delta F/F_0$. This normalizes the differences in overall florescence across cells that can occur due to differences in GCaMP6 expression.

2.2.2 Identifying responsive neurons

I determined whether each neuron was significantly responsive to sounds as follows. The response to each presentation of a stimulus (pure tones, or noise bursts, or FM sweeps) was examined in two time windows: the pre-stimulation period (comprised of the 14 frames immediately prior to stimulus onset; ∼500 ms), and the stimulation period (14 frames from the onset of the stimulus). When analysing responses to ILD noise bursts and pure tones these two windows had the same length, while I used windows of different lengths for the analysis of responses to FM sweeps (reasoning and details are provided in section 5.2.2).

The neuron's activity in each of these two windows was expressed as the maximum $\Delta F/F_0$ value across all the 14 frames included in the two time-periods when analysing responses to pure tones and ILD stimuli. When presenting FM sweeps, I have expressed neural responses as the averages of the $\Delta F/F_0$ values in the two time windows. By using alternatively the two methods on the responses to each of the stimuli presented, I obtained similar results.

Paired t-tests (one-tailed, alpha = 0.01) were carried out on the maximum (or average) $\Delta F/F_0$ values in the pre and post-stimulus windows across repeated presentations of any one sound, as detailed for each stimulus type in the following Chapters.

2.2.3 Determining stimulus sensitivity in responsive neurons

To assess the ILD, frequency, and FM sweep sensitivity of responsive neurons, I represented the response of each neuron to each stimulus as the difference between the neuron's maximum (or average) $\Delta F/F_0$ in the stimulation and pre-stimulation period. By estimating the response as a difference between the values obtained in these time periods, I controlled for any temporally local fluctuations in fluorescence signals. To test if a neuron was sensitive to the parameters of the sound stimulation (e.g. ILD, tone frequency, FM speed), the sound responses were compared across the values of each parameter examined (for instance, the seven ILDs) using ANOVA tests (alpha = 0.05). All the details of this procedure are provided separately for each stimulus type in the following Chapters.

2.2.4 Inferring spikes from calcium transients

The calcium indicators belonging to the GCaMP6 family should detect increases in intracellular calcium concentration due to spiking activity, but not subthreshold fluctuations of the membrane potential (Chen *et al.*, 2013). Nonetheless, in order to confirm that the calcium transients that were considered to be sensory responses according to the previously described analysis corresponded to real action potentials, I inferred, in a subset of my data, spikes trains from neuronal calcium traces using a compressive sensing technique described in Dyer *et al.* (2010) and available on github.

Put simply, spike extraction is achieved by deconvolving the calcium signal. This procedure is adopted because calcium signals can be considered as the convolution of an original signal (corresponding to the action potentials fired by the cell) with a template. This template depends on the biophysical properties of the calcium indicator and, in particular, on its binding kinetics. These ultimately indicate the time that it will take for the fluorescent transient to peak and then return to baseline. Thus, the occurrence of an action potential can be detected by using a filter to correlate a known template with a measured transient. Action potentials are detected when the correlation exceeds a certain threshold value.

In order to optimize the algorithm's performances, I adapted some input parameters to the biophysical properties of GCaMP6m and GCaMP6f separately (Chen *et al.*, 2013), and to the characteristics of the calcium traces I obtained experimentally. These included number of algorithm iterations needed to deconvolve the calcium transient, length of the calcium signal to deconvolve, and the thresholding value for the identification of spikes.

It is worth noting though, that this procedure was used exclusively as a validation method, while the results described throughout this thesis are based on the analysis of calcium transients only.

2.2.5 Principal components analysis

Throughout the thesis, I used principal components analysis (PCA) to identify common patterns emerging in response to sound stimuli resulting from the combination of particular stimulus parameters (for instance, noise bursts at different ILDs, or FM sweeps at different rates or directions). The large number of neurons recorded in two-photon imag-

ing experiments makes PCA a useful tool for population analysis, because it captures common trends emerging in the whole set of sound responsive neurons, in a way that is independent from any preconceived expectations. Details of the procedure are provided separately for each stimulus type.

2.2.6 Estimating pairwise correlations

Signal correlation was estimated to determine the degree to which a pair of neurons showed similar tuning to sound properties. A related metric, noise correlation, was also calculated for each neuronal pair to estimate the correlation between the activity of the two neurons that is unrelated to the type of sound presented, but which may instead arise due to network dynamics and connectivity between the neurons. Signal and noise correlations were calculated separately from responses to pure tones (Chapter 3), ILD noise stimuli (Chapter 4), and FM sweeps (Chapter 5). In each case, only neurons showing a significantly driven response and sensitivity to the stimulus parameter of interest (according to the results of the ANOVA tests) were included in the correlation analyses.

I followed the procedures for calculating noise and signal correlations previously described by Rothschild *et al.* (2010). We can think of each presentation of a sound as a single "trial" in our experiment. To calculate noise correlations, each trial-by-trial response of a neuron was normalized for stimulus effects by subtracting the neuron's average response to a given stimulus type across multiple presentations (for instance, a given ILD at a given ABL). The noise correlation between a pair of neurons was then estimated as the correlation between the normalized trial-by-trial responses of the two neurons. Signal correlations were estimated as the correlation between the mean responses (averaged across repeated presentations) of any two neurons, minus the noise correlation estimate for the neuronal pair.

A bootstrapping approach was used to estimate the significance of the noise and signal correlations. During noise correlation bootstrapping, the trial-to-trial responses were randomly drawn with replacement from the neuron's responses to all repetitions of the given stimulus. During signal correlation bootstrapping, responses on each trial were randomly drawn (with replacement) from responses to all stimuli. The average noise and signal correlations across 1000 iterations of this shuffling procedure produced

a distribution of noise and signal correlations that were compared to the signal and noise distributions from our non-shuffled dataset, in order to assess their significance (paired t-test). Repeating the bootstrapping for 500 and 2000 iterations produced similar results (data not shown).

2.2.7 Cluster analysis

I used a bootstrapping approach to test if the response preferences of neurons were clustered in 3-dimensional (3D) cortical space. Specifically, I tested whether neurons having either similar BF, or preferred ILD, or preferred FM duration, or preferred FM rate were located close to one another.

It is important to comment here on the use of the word "cluster" throughout this thesis. Cluster analysis is usually intended as a statistical method using established algorithms to classify data into groups (the clusters). However, in this thesis, the word "cluster" will be exclusively used in relation to the results of this analysis, that is, to indicate neurons that are located proximally in cortical space and have similar preferences for the values of the sound features I have studied.

To test, for instance, for BFs clusters, I calculated the absolute difference between the BFs ("BF similarity") of all pairs of neurons that were separated by no more than 150 μm in 3D cortical space. A similar metric was calculated according to preferred ILD, preferred FM duration and preferred FM rate. I then used bootstrapping (1000 repetitions) to estimate the BF similarity of the same number of randomly chosen pairs of neurons that were located >150 μm apart, as in Schnupp *et al.* (2015) and Rothschild *et al.* (2010). In each iteration, I saved the average BF similarity (or ILD similarity and so on) of the randomly chosen distant neuron pairs, in order to build a distribution for statistical comparison with the local pairs. If the average BF difference between the local pairs of neurons was below the lower 5th percentile of the bootstrapped BF differences of distant pairs, this indicated a spatial clustering of BFs in the mouse in question.

I repeated this analysis at several spatial bin sizes (100, 150, 200, and 250 μm), and found the greatest amount of clustering for all stimulus parameters at 150 μm in mice. Therefore, only the results of 150 μm binning are reported in the results.

Chapter 3

The question of tonotopy

3.1 Introduction

A systematic spatial arrangement of sensitivity to the stimulus feature represented by the peripheral receptors characterizes the primary sensory areas of the cerebral cortex.

In the auditory system, a logarithmic gradient of best frequencies (BFs) emerged in early investigations as the defining characteristic of the primary auditory cortex (A1) of all species studied (monkeys: Merzenich *et al.* (1973); cats: Hind (1953); ferrets: Kelly *et al.* (1986); humans: Talavage *et al.* (2000); guinea pigs: Hellweg *et al.* (1977); gerbils: Ryan *et al.* (1982); rats: Sally and Kelly (1988); mice: Stiebler *et al.* (1997)). Such organization is known as tonotopic, or cochleotopic, from the name of the auditory structure where it originates, the cochlea. However, neurons throughout the auditory pathway progressively integrate spectral and temporal features of the sound and therefore cortical neurons, at the top of this hierarchy, have multidimensional receptive fields which are poorly predicted by frequency preferences alone (Ahrens *et al.*, 2008; Bar-Yosef *et al.*, 2002; Nelken *et al.*, 2005; Sadagopan and Wang, 2009). For this reason, tonotopy may not be rigorously represented in the cortex.

Perhaps in light of this complexity of the neuronal receptive fields, auditory scientists have continued to investigate the cortical representation of sound frequency over many decades (Woolsey and Walzl, 1942). Some aspects of this matter are still under debate.

Recent multi-electrode recordings and large-scale imaging experiments have confirmed the presence of a smooth tonotopy over large areas of primary auditory cortex

(Imaizumi *et al.*, 2004; Nelken *et al.*, 2004; Recanzone *et al.*, 1999), while single-unit acquisitions reported both strong (Bendor and Wang, 2008) and weak tonotopic arrangements (Evans and Whitfield, 1964; Goldstein Jr and Abeles, 1975).

In the late years of the 20th century, the introduction of the mouse as an experimental model provided further controversial evidence on the nature of the tonotopic map. The first extensive mapping of auditory cortex in this species was carried out by Stiebler and collegues (1997) by recording multi-unit activity in layer IV. The authors described two tonotopically organized fields, namely A1 and AAF (anterior auditory field), containing gradients running along the rostrocaudal axis and reversing at the high-frequency boarder between the two areas. Successive low-resolution optical imaging experiments (Horie *et al.*, 2013; Kubota *et al.*, 2008) and electrophysiological reports, which carefully dissected the response properties of cortical neurons (Linden *et al.*, 2003; Zhang *et al.*, 2005), did not question the smooth tonotopy previously described. Its existence was only challenged following the introduction of *in vivo* two-photon calcium imaging in auditory neuroscience (Bandyopadhyay *et al.*, 2010; Rothschild *et al.*, 2010). In these imaging experiments, the authors recorded an unprecedented number of neurons simultaneously in a local region of the A1 of the anesthetised mouse and revealed a considerable fine-scale variability of frequency responses in layers II-III, even though a smoother tonotopic gradient was present on the global scale.

One of the key differences between these studies and Stiebler et al. lies in the spatial resolution: if the latter obtained one measurement every 200 μm in A1, the former examined separately the responses of about 30 individual neurons in areas of the same size. These results reignited the debate around cortical tonotopy. Since then, several groups tried to clarify the ambiguities on the fine-scale representation of tone frequency, obtaining divided outcomes.

A compelling result came from experiments measuring the frequency responses of single dendritic spines in the mouse A1. Here, even neighbouring spines on the same dendrite were found to be tuned to different frequencies, supporting the newly proposed "salt and pepper" organization of this area of the brain (Chen *et al.*, 2011). However, a consistent tonotopy and a more homogenous local arrangement of frequency preferences (within 100 μm) emerged in a two-photon study of somatic responses a few years later

(Issa *et al.*, 2014). Robust tonotopy with few local variations was also found, this time by means of electrophysiological techniques, by Hackett *et al.* (2011), and in a comprehensive study by Guo *et al.* (2012), which dissected auditory cortex responses across "fields, laminae, anaesthetic state and neurophysiological signal types".

One potentially important issue that Guo *et al.* (2012) did not tackle, but that emerged in two-photon investigations of the micro-organization of other sensory cortical regions, is that of species differences. Sensory responses in rodent V1 have been reported as being less precisely organized compared to their counterparts in larger species (Lee *et al.*, 2016; Li *et al.*, 2008; Ohki *et al.*, 2005, 2006).

These results have sometimes raised doubts about the validity of the mouse as a model for sensory research. While a direct comparison of the organization of visual cortex between lower and higher mammals has been carried out by analysing both systems through fine-scale imaging techniques, there is a complete lack of two-photon data from the auditory cortex of large species. In this respect, the ferret would be of particular interest, as it is a popular animal model in auditory research.

Ferret auditory cortex has been well characterized electrophysiologically, with recent data suggesting the presence of a tonotopic map that is composed of local variability in frequency preferences (Bizley *et al.*, 2005). Understanding whether the global dorsoventral tonotopic gradient described with microelectrode recordings in this species (Kelly *et al.*, 1986; Phillips *et al.*, 1988) is supported by an ordered local representation of sound frequency would set a milestone in auditory research and would directly address the controversy about species differences in the spatial organisation of A1.

3.1.1 Aims

The principal aim of this Chapter is to investigate both the local and the global distribution of responses in the A1 of the mouse.

If the functional micro-architecture of rodents' sensory areas is dominated by local variability, I should be able to confirm this by injecting a genetically encoded calcium indicator (GCaMP6) in small regions of A1 and then testing the neuronal responses to pure tones in anaesthetized mice. Moreover, by imaging calcium transients in a reporter line widely expressing GCaMP6 in layers II-III, I should also see the presence of tonotopy

on larger scales. These experiments will serve two purposes.

First, they represent a new contribution to the ongoing and still controversial debate about the local organization of frequency responses in the mouse auditory cortex. Second, they form the necessary background to answer two questions examined later on in this dissertation, when the organization of responses to the most basic of sound properties, tone frequency, will be compared with that of responses to two behaviourally relevant sound features: interaural level differences and frequency modulation.

A second important target of this Chapter is to provide preliminary data about the spatial organization of frequency responses in the primary auditory cortex of a higher mammalian species: the ferret. Here, if two-photon results from the visual cortex of other carnivores can be generalized to the ferret auditory cortex (Ohki *et al.*, 2005, 2006; Van Hooser *et al.*, 2006), I expect to detect a rather tight tonotopy, even within local imaging fields.

3.2 Methods

Surgical procedures and image analysis are described in detail in section 2.1 and 2.2.1.

3.2.1 Pure tone stimulation

All stimuli used in the experiments described in this Chapter were 100 ms in duration (∼3 imaging frames) with 5 ms cosine onset and offset ramps, and were presented at a rate of 0.65 Hz at four intensity levels (40, 60, 80 and 100 dB SPL). In the mouse experiments, pure tones were presented at 18 frequencies between 1.9 and 50 kHz (0.27 octave spacing). In the ferret experiments, 20 frequencies between 1.2 and 41 kHz were delivered (0.27 octave spacing). Ten repetitions of each tone were presented in pseudorandom order for both mice and ferrets.

3.2.2 Identifying responsive neurons

Neurons found to be responsive to pure tones (details in section 2.2.2) were tested for their selectivity for tone frequency. First, I represented the responses to each pure tone as the difference between the maximal response during the pre-stimulation and stimulation

periods. I used a two-way ANOVA to determine if the neuronal response was significantly modulated by sound frequency or intensity (alpha = 0.05). If the ANOVA showed an effect of frequency, best frequency (BF) was then determined as the frequency eliciting the highest mean response, averaged across all intensity levels (Barnstedt *et al.*, 2015; Guo *et al.*, 2012). If the neuron's response at BF was <3 standard deviations above the pre-stimulus response, I classified it as having no clear BF. Another way of identifying the BFs of auditory neurons is by visually inspecting the plots of the their Frequency Response Areas (FRAs) (Rothschild *et al.*, 2010). These represent the neuron's response to each combination of frequency and intensity of the pure tones presented, and their inspection yielded BFs similar to those found with the method I have described above (data not shown).

To identify the orientation of the BF gradient in transgenic mice and in ferrets, I correlated the BF of all neurons with their position on the x-axis, corresponding to the anatomical rostrocaudal plane in mice and dorsoventral plane in ferrets. This correlation was recalculated 360 times, while rotating the x-axis in 1° intervals throughout 360°. The axis rotation producing the strongest correlation was taken as the orientation of the tonotopic gradient.

3.3 Results

3.3.1 Frequency responses in the mouse auditory cortex

To investigate the micro-organization of frequency tuning in layers II-III of the mouse A1, I performed *in vivo* two-photon calcium imaging in 18 animals in which the calcium indicator GCaMP6m had been expressed by AAV injection.

I imaged 1857 neurons in 69 imaging fields with an area of 250 x 250 μm (neurons from one example area are shown in Figure 3.1A, B). While imaging, I presented 18 pure tones spanning ∼4.5 of the 6 octaves audible to mice (Stiebler *et al.*, 1997) (Figure 3.1C). Among all imaged neurons, 50.3% (934 neurons) were responsive to tones (paired t-test, $p < 0.01$) and of these neurons, 75.8% were sensitive to sound frequency (708 neurons; two-way ANOVA, $p < 0.05$).

In keeping with electrophysiological recording studies of mouse auditory cortex (Joachim-

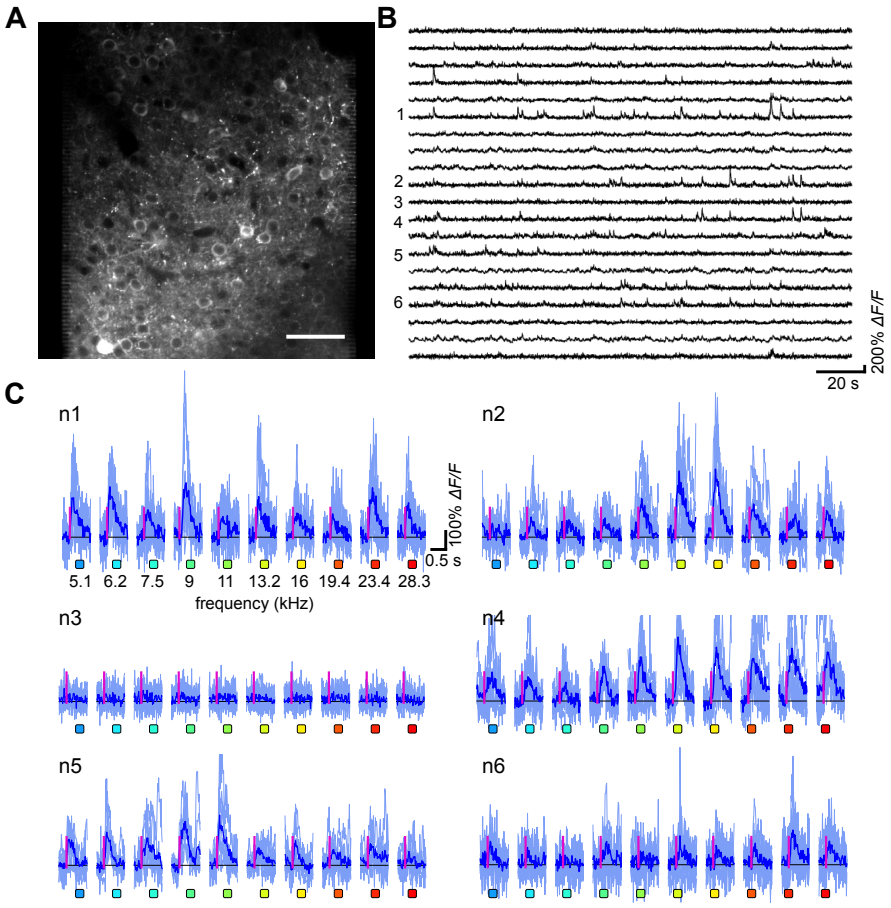

Figure 3.1: (A) An *in vivo* two-photon image of an optical plane at 270 μm below the pial surface. Scale bar is 50 μm. (B) Relative changes in fluorescence of 20 neurons from the field in A during presentation of pure tones. (C) Trial wise (light blue) and mean (dark blue) responses of the six neurons indicated in B to tones of 10 different frequencies (between 5.1 and 28.3 kHz; coloured squares) presented at 80 dB SPL. Magenta bars indicate stimulus onset and duration.

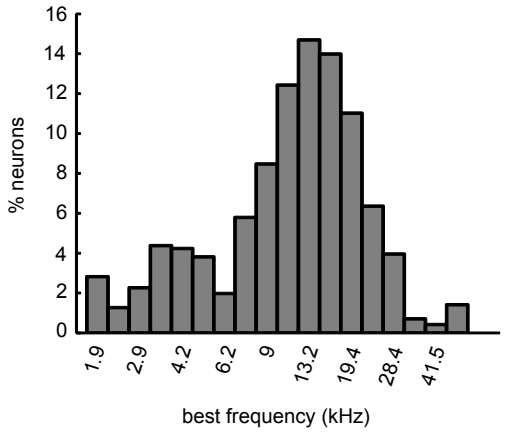

Figure 3.2: Percentage histogram of best frequencies from all neurons in the 18 mice injected with GCaMP6m showing sensitivity for sound frequency (n = 708 neurons).

sthaler *et al.*, 2014; Linden *et al.*, 2003), I observed an over-representation of BFs from ∼9 to 23 kHz (Figure 3.2). Previous two-photon calcium imaging studies of A1 (Issa *et al.*, 2014; Rothschild *et al.*, 2010) and of auditory cortico-collicular terminals (Barnstedt *et al.*, 2015) have also reported a similar BF distribution.

3.3.2 Anatomical confirmation of imaging location in mice

As my research focused specifically on studying sensory responses in the core region of the auditory cortex, corresponding to areas A1 and AAF in the mouse, it was important to determine if my calcium indicator injections and imaging experiments accurately targeted these areas.

The cerebral cortex of most mammalian species is characterized by different degrees of gyrification, which constitute a convenient anatomical reference to target specific areas of the cortex. The mouse brain is lissencephalic, but the presence of certain blood vessels on the surface of the auditory cortex is reliably recognizable across individuals, and is therefore often used to target A1. In particular, the area extending between two major V-shaped vessels running ventrodorsally has been described as corresponding to the core auditory region (Tsukano *et al.*, 2016) (Figure 3.3A left). Consequently, when injecting the viral vector expressing GCaMP6m, besides relying on published stereotaxic coordinates (70% of the distance from Bregma to Lambda, and ∼4.5 mm lateral from

the midline), I followed these vascular landmarks, which resulted in labelling of the area just mentioned, putatively corresponding to A1 and AAF (Figure 3.3A right).

As adeno-associated viral vectors can be transported trans-synaptically throughout the brain, cortical injections of my construct should result in GCaMP labelling of areas upstream from the auditory cortex. The two tonotopically organized regions of the mouse auditory cortex, A1 and AAF, receive inputs primarily from a tonotopically organized region of the thalamus, the ventral subdivision of the medial geniculate body (75%; MGBv) and, to a less extent, from the medial (24%; MGBm) and dorsal (1%; MGBd) subdivisions of the same nucleus (Caviness and Frost, 1980; Hackett *et al.*, 2011; Wong *et al.*, 2008). Thus, an injection targeting the primary auditory areas should result in the labelling of these thalamic regions. Figure 3.3B shows a fluorescent image from a coronal section in which GCaMP6 clearly labelled MGBv, which can be recognized as a small, elliptical structure protruding from the mesencephalic block of the section. This section corresponds to the number 92 of the online Allen Brain Coronal Atlas, which may be used as a reference to confirm the location of my injection `http//:mouse.brain-map.org/static/atlas`.

Assessing the coordinates of a cortical injection through retrograde transportation of fluorescent molecules is common practice, and beads specifically designed to serve this purpose exist. Thus, I injected retrograde red fluorescent microbeads in the cortex of six mice, following the same stereotaxic coordinates and vascular markers used for the calcium indicator injection in the 18 mice injected with GCaMP6m. The resulting pattern of retrograde labelling in the MGB confirmed that my injections had targeted auditory cortex in two mice (Figure 3.3C; one mouse shown), while my injections failed in the other four, resulting in the absence of labelling. Nonetheless, even after a successful injection such as the one shown in Figure 3.3C, labelling was not confined to the MGBv and was in fact stronger in the MGBm, suggesting that both primary and non primary areas were targeted by the injection. Indeed, if my injections had targeted exclusively A1 and AAF, at least 3/4 of the beads should have reached the MGBv (Hackett *et al.*, 2011). On the other hand, discriminating the thalamic projections targeting each of the two primary regions would have been possible only using two retrograde tracers of different colors.

This result may occur because the fluorescent beads spread on the cortical surface over an area of about 1.5 mm dorsoventrally, corresponding not only to primary cortex, but also to other auditory fields. If the beads were in direct contact with the cortical surface, they may have entered the axonal projections in layer I originating in the MGBm. Indeed, this nucleus sends non-topographic projections to most auditory cortical areas, terminating in both layer I and IV (Mitani *et al.*, 1987; Schofield *et al.*, 2014).

In follow-up experiments, I injected a less concentrated and smaller volume of fluorescent retrobeads. However, this did not result in a more confined labelling of the MGBv and again the beads reached the MGBm as well (data not shown). Such an outcome is difficult to explain, but I suggest that my injections were still not accurate enough to reliably target A1 only. Injecting fluorescent retrobeads was more technically challenging than injecting GCaMP6m, primarily due to the high viscosity of the beads. These could only be injected through a glass pipette with a tip of a considerably large diamater ($\sim$50 μm, while $\sim$20-30 μm for GCaMP6 injections), which often caused the beads injected into the cortical parenchima to quickly return to the pial surface.

As my tracer injections were not reliable enough, I decided to adopt a more functional approach to confirm imaging location.

3.3.3 Functional confirmation of imaging location

A well established feature of neurons in A1 is that they are more finely tuned to sound frequencies compared to cells in secondary auditory cortical areas. Thus, this difference may be a good parameter for discriminating auditory cortical regions, and therefore for providing further validation of injection sites.

For this reason, in six mice I injected GCaMP6m in a more dorsal and posterior area than the one I targeted to obtain labelling in A1 or AAF. I then compared the Frequency Response Areas (FRAs) of neurons between these two regions. The FRAs were constructed according to the maximal response of the each neuron to each frequency-intensity combination. The plots were smoothed with a three-point running average across frequencies, for visualisation purposes. Figure 3.4 shows 56 example neurons from the two populations. The FRAs of neurons in the primary areas of auditory cortex have been often described as V-shaped; they show narrow frequency tuning in response to

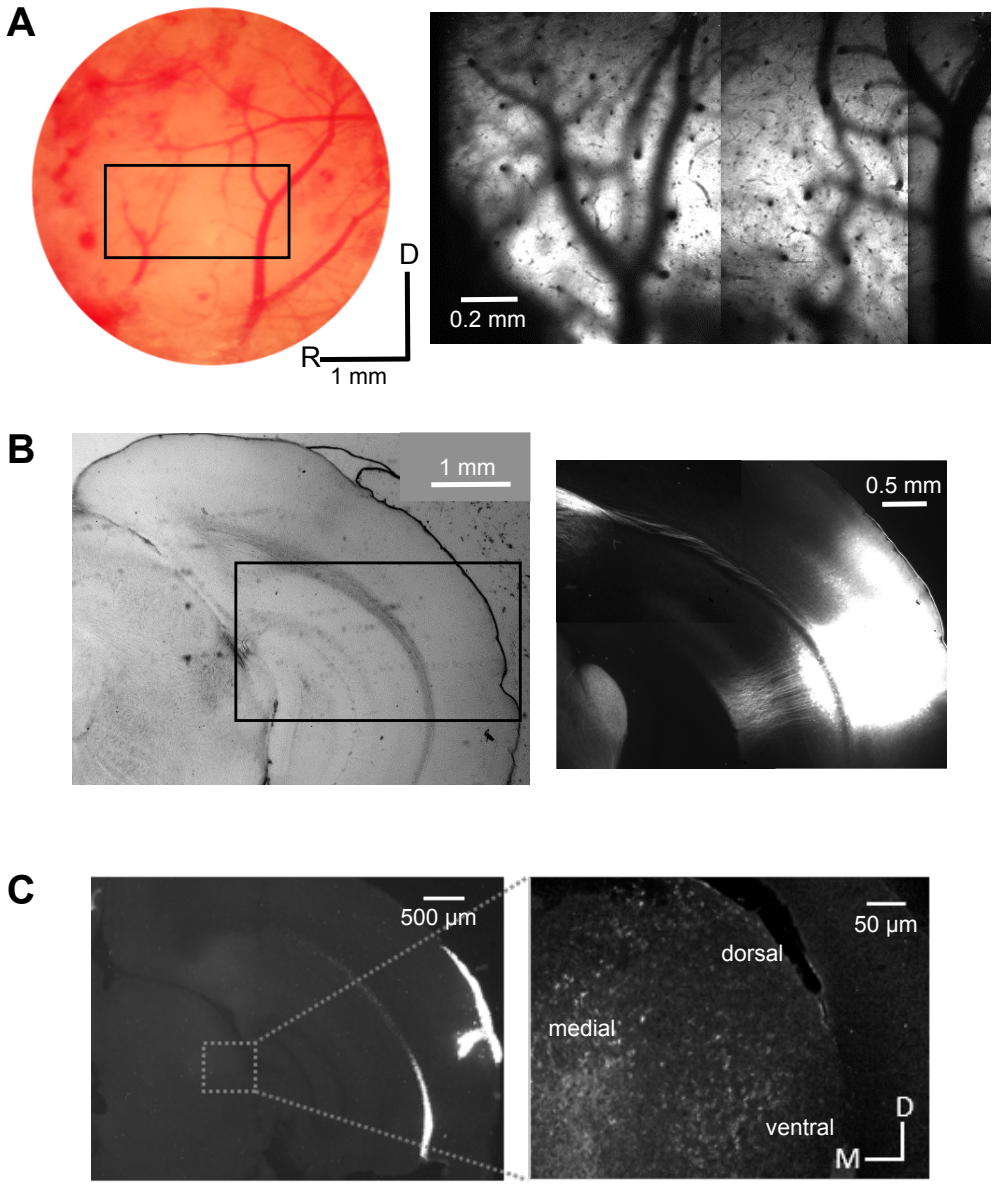

Figure 3.3: (A) A picture of the cortical surface of one mouse, showing the areas were A1 and AAF are located. The detail shows a wide field two-photon image of the same area, labelled with GCaMP6m. (B) The right hemisphere of one mouse in a coronal section. The inset on the right shows labelling of GCaMP6m, extending from the cortex to the MGBv of the thalamus. (C) A coronal section from a mouse in which red fluorescent retrobeads were injected into the auditory cortex following the same coordinates used for GCaMP6m injections. The inset shows labelling in the MGB at higher magnification.

quiet pure tones, which broadens at higher sound intensities. Neurons in A1 and AAF may also show narrow frequency tuning regardless of sound intensity (I-shaped FRAs) or non monotonic tuning to intensity (O-shaped FRAs) (Moshitch *et al.*, 2006; Rothschild *et al.*, 2010). All these frequency-intensity tuning types were present in the imaged fields from putative areas A1-AAF (Figure 3.4A; V-shape: neurons 3, 4, 6, 8, 16, 20, 25, 27; I-shape: neurons 7, 23; O-shape: neurons 13, 21, 28). Regardless of the shape of their FRAs, these neurons generally showed a clear preference for one frequency or a narrow frequency range. Although neurons in the two primary auditory areas of the rodent cortex are both narrowly tuned for sound frequency, differences between their pure tone response profiles exist, and are mainly temporal. In particular, first spike latencies and response duration are much shorter in AAF compared to A1 Hackett *et al.* (2011); Linden *et al.* (2003); Polley *et al.* (2007). However, the limited temporal resolution of two-photon imaging did not allow me to reveal these properties. On the other hand, neurons outside primary regions (Figure 3.4B) usually have "multipeaked" or "patchy" FRAs and, consequently, no single BF. When injecting GCaMP6m in putative secondary areas, the majority of the labelled neurons showed broad or multipeaked tuning to pure tones. Typical examples are the FRAs of cells 30, 46, 48 and 50 in Figure 3.4B.

A frontocaudal gradient of frequency preferences characterizes A1 and AAF in the mouse, so that neighbouring neurons in these areas have more similar best frequencies than neighbouring cells in secondary, non-tonotopic regions (Guo *et al.*, 2012; Hackett *et al.*, 2011; Issa *et al.*, 2014). This feature may be useful to further confirm imaging locations in A1. I calculated the standard deviation of BF across neurons within the same imaging field, in order to quantify neuronal "cotuning" in 56 putative A1-AAF imaging fields and 15 fields in putative secondary areas (Issa *et al.*, 2014). The comparison between the two areas is shown in the plot in Figure 3.4C. The median value was 0.78 $\pm$ 0.04 octaves (mean $\pm$ se) for primary imaging fields containing at least 10 frequency-sensitive neurons, and 1.03 $\pm$ 0.12 octaves for imaging fields in the putative secondary cortical areas (two-sample t-test; $p = 0.028$).

While I cannot rule out the possibility that my imaging fields extended beyond A1, it is likely that the majority of the data presented from the original 18 animals with GCaMP6m injections were from primary auditory fields (i.e. A1 and AAF). In partic-

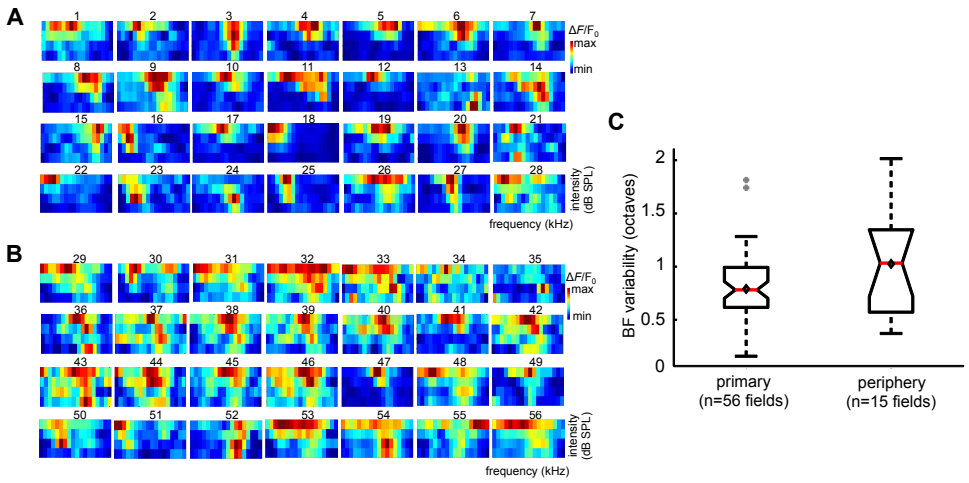

Figure 3.4: (A) shows the FRA plots of 28 neurons imaged in the core region of auditory cortex (A1 or AAF), while (B) represents FRAs from 28 neurons located in the periphery of auditory cortex. (C) Box plot visualizing the variability of BFs in imaging fields from primary (left) and peripheral (right) regions of auditory cortex. Red line represents median, while black diamond is mean value. Dotted lines are 95% confidence intervals. Grey dots are outliers.

ular, based on the coordinates of the two injections performed in each mouse and the distribution of BFs shown in Figure 3.2, I expect my two-photon imaging data to come from the central isofrequency bands of A1 and, occasionally, AAF (Figure 3.5).

Data from the six mice expressing GCaMP6m in secondary areas were used here exclusively for the purpose of confirming the accuracy of my injections in A1, and they will not be analysed further in this dissertation.

The higher similarity of tuning within primary regions compared to peripheral ones is an established and common functional principle across auditory cortical areas, even in rodents (Guo *et al.*, 2012; Hackett *et al.*, 2011; Stiebler *et al.*, 1997). But to what extent is frequency tuning in A1 homogeneous? Is it possible to reproduce the results recently obtained in calcium imaging experiments, reporting a high degree of local variability in these responses? For the first time, I used a genetically encoded calcium probe, GCaMP6, to answer these questions in anesthetized animals, and to compare the fine and global scale organization of A1 frequency tuning. My results are presented in the following sections of this Chapter.

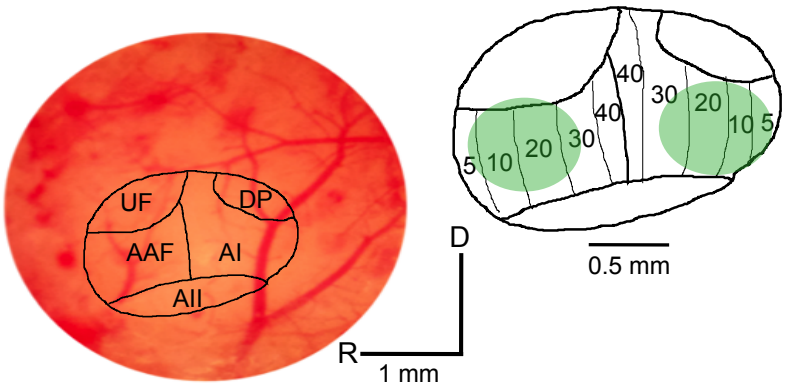

Figure 3.5: A schematic representation of the mouse auditory cortex adapted from Linden *et al.* (2003). On the left, the model is projected on the same picture of the cortical surface shown in Figure 3.3. Numbers indicate the most common best frequency of neurons in each isofrequency band (kHz). The two green areas indicate the locations where most of the labelled neurons were found.

3.3.4 Tonotopy: fine-scale organization

The spatial location of cortical neurons with different frequency preferences was examined by producing two-dimensional (2D) maps of neuronal BFs along the rostrocaudal and dorsoventral axes of the cortex. Figure 3.6 shows BF maps obtained from 12 mice, in which every square (dotted lines) identifies an area of 100 x 100 μm. In many cases, the imaged region extended over ~300 μm both rostrocaudally and dorsoventrally (mice 1, 2, 3, 4 and 9).

Visual inspection of the maps revealed that within a local region of A1, neurons were often tuned to a common frequency range. Some imaged areas contained predominantly high-frequency neurons (mouse 3 and 9), whereas others were dominated by lower frequency tuning (mouse 1 and 10). Occasionally, the region transfected by the AAV vector was larger, allowing me to examine BF organization in areas extending up to ~700 μm rostrocaudally (mouse 5, 7, 8, 11, and 12), enough to demonstrate the presence of a tonotopic gradient. This was particularly evident in mouse 5, presumably imaged in AAF, as frequency preferences progressed from high to low rostrocaudally, and in mice 8 and 12, in which the spatial progression of preferences matches the one expected in A1. On the other hand, neuronal BFs in mouse 7 did not seem to be organized tonotopically. Imaged neurons in mice 3, 6 and possibly 10 may have been located at the boarders

between two isofrequency bands in A1, as there is an appreciable increase in BFs going from more caudal to more rostral positions. The bootstrapped cluster analysis (described in section 2.2.7) indicated that the BFs of neurons located up to 150 μm apart in 3D cortical space were significantly spatially clustered in 9 out of 18 mice. The maps of BFs for six of these mice are shown in Figure 3.5. These are mice 2, 5, 6, 8, 11 and 12. The absence of significant clustering in the other animals may be linked to the particularly limited cortical area in which neuronal BFs were measured. This is the case, for example, in mice 1, 9 and 10, were frequency sensitive neurons occupied an area approximately corresponding to one imaging field ($\sim$200 x 200 μm).

3.3.5 Evidence for local subnetworks: pairwise correlations

A homogeneous local representation of BFs may arise because neighbouring neurons are connected together in a local network in which cells fire together. To investigate the extent to which this was the case in my recordings, I calculated the "signal" correlations (SCs) between pairs of simultaneously recorded neurons (within a 250 μm distance), which quantifies the degree of similarity between the receptive fields of the two cells (see Methods, section 2.2.6). On the other hand, "noise" correlations (NCs) are independent from the response profiles of the neurons and give an indication of the degree to which the two neurons fire together regardless of the sound being presented. Noise correlations are therefore argued to represent the connectivity in the neuronal network, and mirror the general cortical state during the recordings (Kohn and Smith, 2005). Pairwise signal and noise correlations were carried out on those neurons whose responses were significantly modulated by tone frequency. It is important to note that neurons were reused between pairs, which increased the number of neuronal pairs included in the analysis, and may have led to higher signal and noise correlation values compared to a scenario in which each neuron is used in one pair only.

The mean signal correlation in my dataset, after removing the effects of trial-to-trial noise correlations, was 0.47 $\pm$ 0.22 (mean $\pm$ sd; n = 6586 neuron pairs) (in Figure 3.7A). Noise correlations were lower than signal correlations, and mainly ranged between 0 and 0.4, with a mean value of 0.25 $\pm$ 0.16 (Figure 3.7B). Shuffling the data across trials in a bootstrapping analysis demonstrated that both the signal and noise correlations I

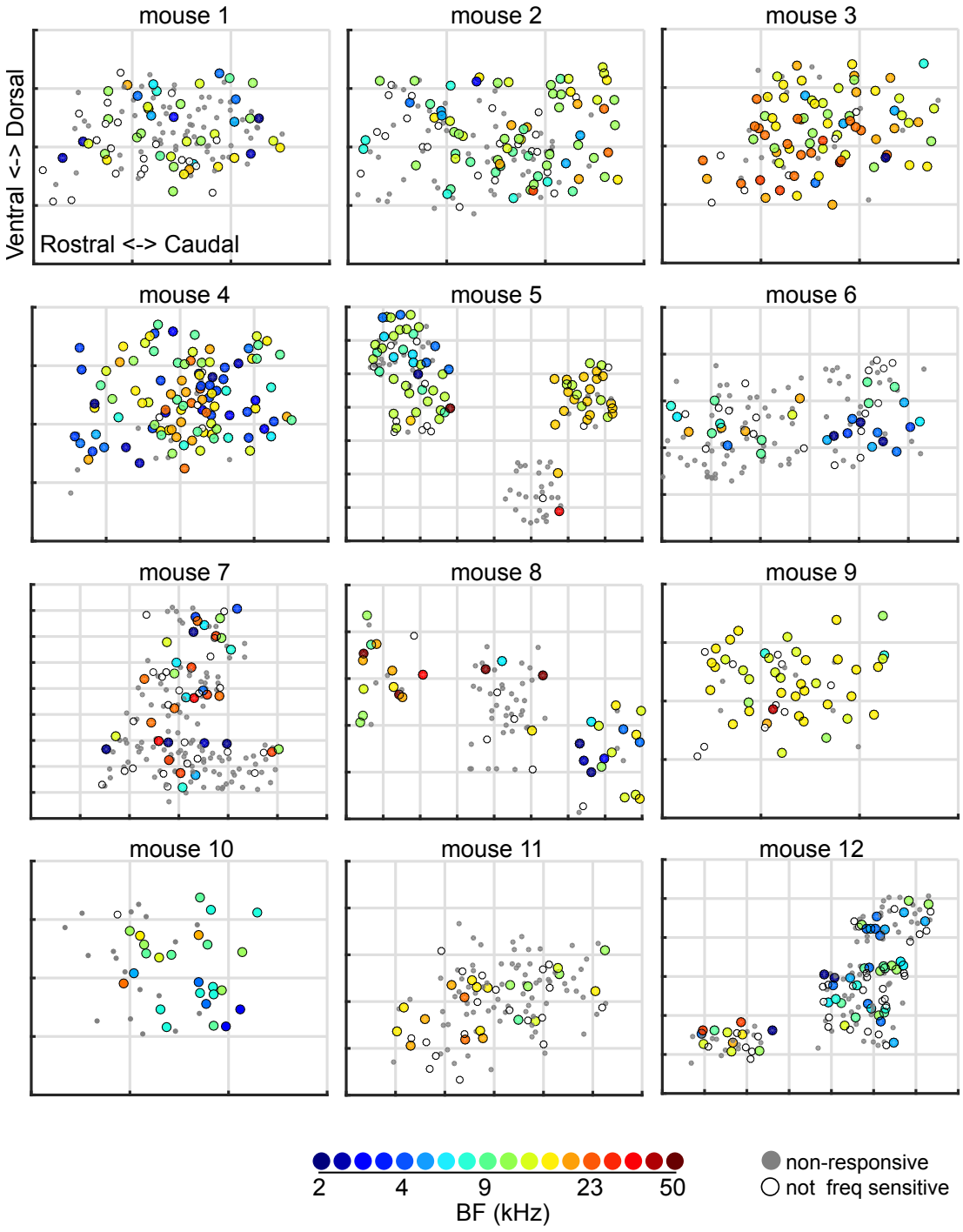

Figure 3.6: Neurons from 12 mice injected with GCaMP6m are plotted according to their position along the rostrocaudal and dorsoventral axes, with z-dimension collapsed. Non-responsive neurons are represented by grey dots, while responsive neurons that are not sensitive to frequency are represented by white dots. Frequency-sensitive neurons are colour coded according to their best frequency. Dotted grids represent areas of 100 x 100 μm.

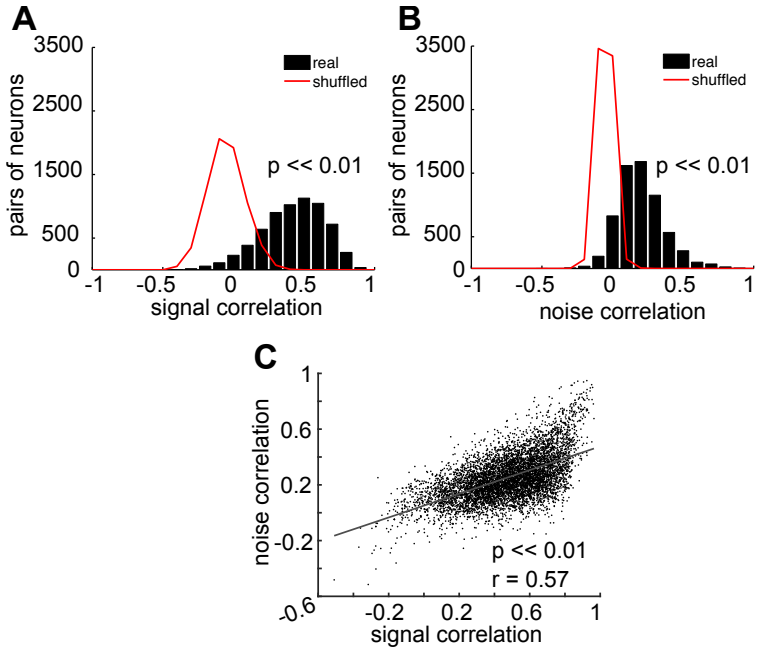

Figure 3.7: (A) Histogram of the pairwise signal correlations between sound-responsive neurons in the GCaMP6m injected animals (black bars). The distribution of signal correlations among a randomly shuffled version of the dataset is also shown (red line). P-values are given for a paired t-test on the real and shuffled data. (B) Noise correlation distributions, plotted as in A. (C) Scatter plot of noise correlations plotted as a function of signal correlations in the same neuronal pairs. The line indicates the best linear fit to the data. The Pearson correlation values for these fits are displayed as text.

observed were significantly larger than chance (t-test; $p \ll 0.001$).

When the signal and noise correlations of each neuronal pair were compared across the entire neural population, these were found to be highly correlated (Figure 3.7C; $r = 0.57$; $p \ll 0.001$). This result, together with the high signal correlation values, may be an indication that proximal auditory cortical neurons that tend to be active together (i.e. have a high noise correlation) are also similarly tuned to frequency (i.e. have a high signal correlation).

3.3.6 Tonotopy: large-scale organization

In order to have a more complete picture of the spatial organization of frequency preferences in mouse A1, I have used a reporter line expressing GCaMP6f in cortical neurons constitutionally expressing the excitatory marker CaMKII-alpha. Excitatory neurons

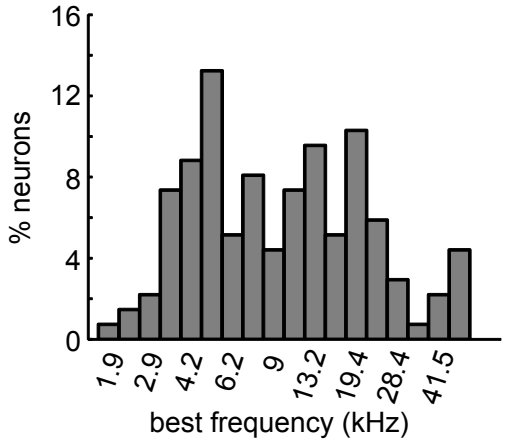

Figure 3.8: Percentage histogram of best frequencies from all neurons in three transgenic mice exprressing GCaMP6f showing sensitivity for sound frequency (n = 136 neurons).

are the majority of neocortical cells (∼80%) (White, 1989), and the availability of a GCaMP6f line enabled me to examine the representation of their best frequencies over an area of up to ∼1.2 x 1.2 mm in three mice.

Out of a total of 992 imaged cells, 26.4% (262 neurons) of the imaged neurons were found to be responsive to tones (t-test, $p < 0.01$) and of these, 51.9% (136 neurons) were sensitive to the tone frequency (two-way ANOVA, $p < 0.05$). This decrease in tone responsive and frequency sensitive neurons in the transgenic mice compared to the injected ones is expected due to the weaker calcium sensitivity of GCaMP6f compared to GCaMP6m (Chen *et al.*, 2013). The distribution of BFs across all sensitive neurons in the three transgenic mice covers a larger range than in the GCaMP6m-injected ones, possibly because of the larger region of the cortex sampled (Figure 3.8).

When 2D maps of BFs were produced, a gradient of low to high frequency preferences emerged in the three mice, proceeding from the most caudal to the most rostral imaging fields, as expected for mouse A1 (Figure 3.9A). For each mouse, the orientation of the tonotopic gradient was identified empirically by correlating the BF of all neurons with their position on the x-axis, corresponding to the anatomical rostrocaudal plane. This correlation was recalculated 360 times, while rotating the x-axis in 1° intervals. The axis rotation producing the strongest correlation was taken as the orientation of the tonotopic gradient and is indicated by the arrows in the plots (Figure 3.9A). Plotting the BF of

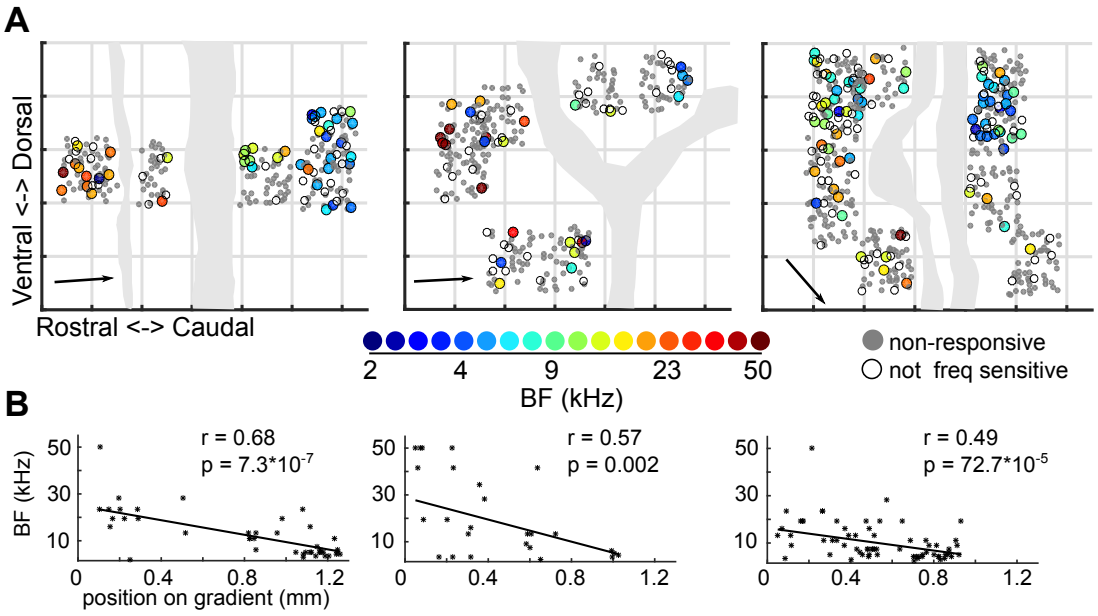

Figure 3.9: Data from three different mice expressing GCaMP6f are plotted in each column. (A) In each plot, neurons are positioned along the rostrocaudal and dorsoventral axes, and are colour coded according to their BF. Dotted grids indicate areas of 200 x 200μm. Grey areas illustrate the position of blood vessels. (B) BFs of imaged neurons in each mouse are plotted against their position on the axis producing the strongest correlation between the two measures (the tonotopic gradient). The corresponding lines of best fit for each mouse are shown. Pearson correlation values are displayed as text.

each neuron as a function of its position along this axis confirmed the existance of a smooth tonotopic gradient in all animals, as indicated by the best fit line in Figure 3.9B. The bootstrapped cluster analysis confirmed the presence of clusters of neurons with similar BFs in all three transgenic animals ($p < 0.05$). Since I imaged neuronal calcium transients following the same stereotaxic coordinates and vascular landmarks in all 21 animals in this study, the presence of this tonotopic gradient is a further confirmation that primary auditory fields (A1 or AAF) were targeted in the three transgenic mice as well as in the 18 GCaMP6-injected mice.

I calculated the standard deviation of BF distribution within an imaging field in transgenic mice in order to quantify the cotuning of local neurons. Across the three mice in my dataset, the median value for imaging fields containing at least 10 frequency-sensitive neurons was 0.79 $\pm$ 0.1 octaves. This value is, as expected, very similar to

the one observed above in GCaMP6-injected mice (section 3.3.3). It is on the other hand slightly higher than that obtained using GCaMP6m in the central nucleus of the IC of anesthetized mice, where local BFs are more uniformly distributed (0.727 ± 0.43; Barnstedt *et al.* (2015)).

Together, these results indicate that despite a certain degree of local heterogeneity, neurons in local areas of A1 of the mouse have more similar responses than distant neurons: a signature which delineates, on a larger scale, the tonotopic organization of this region of the cortex.

3.3.7 Two-photon imaging in ferrets: an ongoing challenge

The mouse is the common model for two-photon imaging studies of the neocortex. The benefits in using mice include the availability of genetically modified strains, allowing functional dissection of the many circuits involved in cortical processing. Moreover, the small size of this rodent species minimizes the possibility of movement artefacts during imaging, which is instead a major issue when imaging larger mammals. These factors have significantly limited the employment of non-rodent species in two-photon experiments.

One way scientists working on non-rodent mammals have tried to overcome the problem is by performing imaging on juvenile individuals: these provide the advantages of studying high mammals but are nonetheless smaller than adults, thereby facilitating imaging (Li *et al.*, 2008; Wilson *et al.*, 2016; Yu *et al.*, 2011). However, the brains of these animals are under-developed and so assessing the reproducibility of tonotopic maps in the A1 of adult, non-rodent mammals is critical to validating the unexpected "salt and pepper" organization demonstrated in the mouse (Bandyopadhyay *et al.*, 2010; Rothschild *et al.*, 2010). For this reason, we have developed a two-photon calcium imaging protocol to study layers II-III of the A1 of adult ferrets, in order to elucidate the fine scale organization of frequency responses. I conducted these experiments with Dr Kerry Walker and Dr Quentin Gaucher.

Two ferrets produced reliable data out of 13 injected with GCaMP6m. This apparently low yield is mainly due to the long process of "trial and error" characterizing the set up of a new, challenging experiment. Moreover, as I mentioned before, calcium

imaging yields data in about one out of three experiments even when performed in mice, the best-suited species for this type of protocol (personal information from Dr Patrick Kanold, but see also my experiments in mice). Our biggest technical challenges were linked to the presence of major movement artefacts while imaging, and to the lack of GCaMP6 labelling in some animals.

We first carried out viral vector injections without performing an incision of the *dura mater* over the injection site (four ferrets). *Dura mater* is the most superficial, strongest and thickest of the cerebral meninges and it likely prevented the viral vector from diffusing throughout the cerebral parenchima. A durotomy was performed in the subsequent animals, which provided more reliable neuronal labelling, although not consistently in all animals.

In some cases, we injected an AAV vector carrying GCaMP6f instead of GCaMP6m (three animals). It was in these ferrets that we observed particularly weak neuronal labelling. Given the low calcium sensitivity of this indicator, labelled cells are reliably visible only when their intracellular calcium concentration increases considerably, that is, mainly when they are strongly responding to sensory stimulation. This effect, together with the poor quality of the imaging in some animals, may have prevented us from recording calcium transients large enough to produce useful evidence for our investigation of frequency tuning.

The clarity of the cranial window is a major issue in ferret two-photon experiments, because of the necessity of a durotomy prior to imaging. The *dura mater* is a highly innervated structure and a small amount of bleeding from it can compromize cortical imaging even at very superficial depths. During our last experiments we were able to carry out more accurate durotomies than in the past, and we optimized our protocol with several expedients that proved to be key to increasing the yield from our experiments. After performing the durotomy, we introduced inside the craniotomy a cover-glass attached to a plastic ring of the same diamater as the craniotomy, and of the same thickness as that of the skull (about 1 mm). The superior edge of the plastic ring was then glued to the skull along its whole perimeter, so to obtain a "sealed configuration". This procedure helped to minimize brain movements during imaging and partly prevented the diffusion of bleeding too.

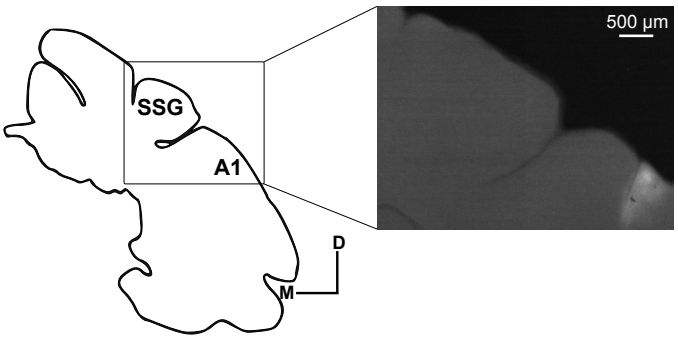

Figure 3.10: A schematic outline of a coronal section showing the right auditory cortex in the ferret (modified from Bajo *et al.* (2010). SSG is suprasylvyan gyrus). The inset shows the site of one GCaMP6m injection in one section from ferret F1606, and confirms labelling in A1.

Moreover, in order to optimize stability, we tried to control the breathing of the experimental animal. First, we made sure that the head of the ferret was raised relative to its body. Second, we intubated the ferrets and connected them to a ventilator. Pumping oxygen artificially into the respiratory system of the animals guaranteed a constant and controlled respiration rate throughout the experiment.

Carrying out two-photon imaging experiments in adult ferrets has therefore been a demanding and stimulating challenge. We were only able to observe auditory-evoked responses to tones in the final few months of my doctoral work and it is for this reason that this dissertation contains preliminary results obtained from only two animals. Nonetheless, I am aware that more experiments are necessary in order to obtain a reliable and comprehensive view of the fine-scale organization of frequency tuning in A1 of this species. These experiments are currently ongoing in our lab.

3.3.8 Frequency tuning in the ferret auditory cortex

Targeting A1 in ferrets is facilitated, compared to mice, by the gyrification of the cortical surface, which delineates reliable boarders between cortical regions. Specifically, the primary auditory cortical areas (A1 and AAF) of the ferret are located within the dorsal tip of the middle ectosylvian gyrus and extend ventrally for several millimeters (Bizley *et al.*, 2005; Shamma *et al.*, 1993). In these experiments, we focused on a region of about 1 mm^2 in area, in which we made 6 - 7 injections of GCaMP6m (Figure 3.10).

We imaged calcium transients from 311 neurons across 12 imaging fields in the two

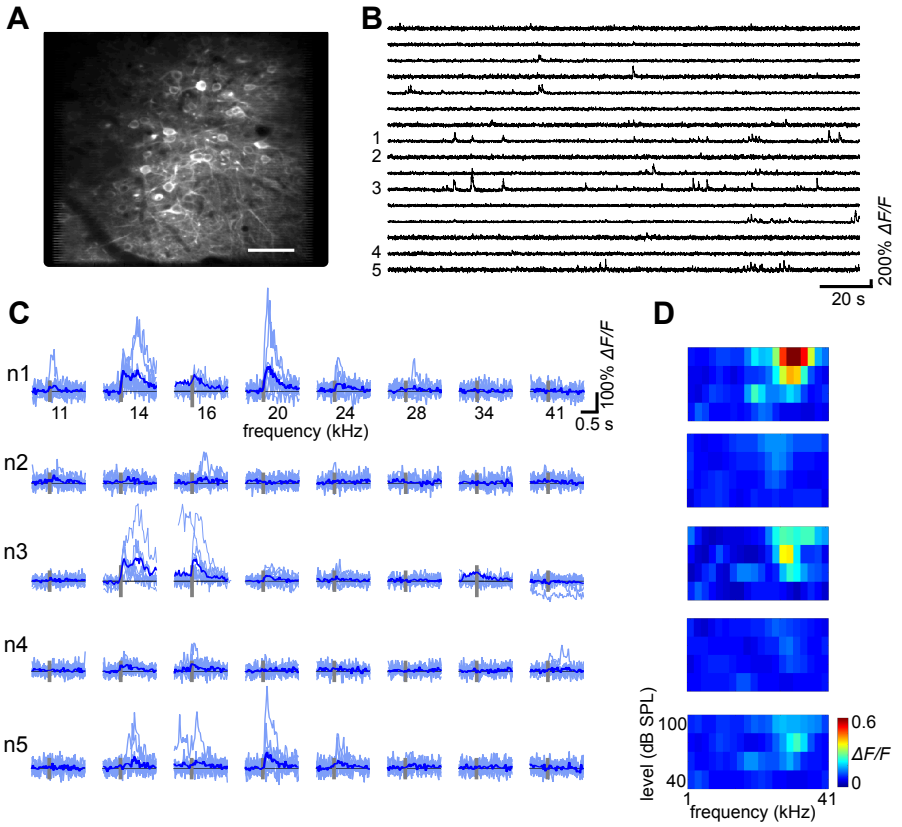

Figure 3.11: (A) An *in vivo* two-photon image of an optical plane at 190μm below the pial surface in the A1 of ferret F1606. Scale bar is 50μm. (B) Relative changes in fluorescence of 20 neurons from the field in A during presentation of pure tones. (C) Trial wise (light blue) and mean (dark blue) responses of 5 neurons indicated in B to tones of the 8 highest frequencies presented at 80 dB SPL. Grey bars indicate stimulus onset and duration. (D) Frequency Response Areas from five neurons in C. Colour scale is the same in all plots, so to better visualize differences in response levels between neurons.

animals. Each field had an area of 300 x 300 μm, and an example of one field is shown in Figure 3.11A, B. While imaging, we presented 10 repetitions of 20 pure tones with frequencies between 1.2 and 41 kHz at four intensity levels (40, 60, 80, 100 dB SPL). Figure 3.11C shows responses from five neurons in the same imaging field to 80 dB SPL pure tones presented at the eight highest frequencies used.

The majority of sensory evoked calcium transients were well aligned with the stimulus onset, and some neurons showed clear preferences for certain frequencies (e.g. neurons 1, 3 and 5 in Figure 3.11D), although the amplitude of their transients fluctuated considerably across individual presentations of the same tone.

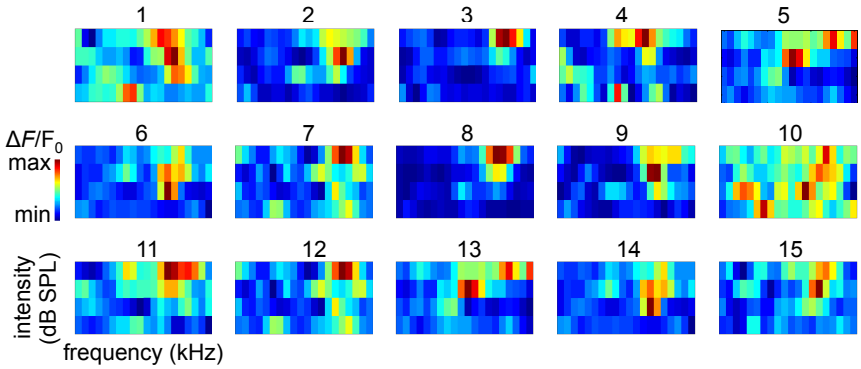

Figure 3.12: Frequency Response Area plots from 15 neurons imaged in A1. Neurons were selected from both ferrets.

Most of the sampled neurons had V-shaped (neurons 1 and 3 in Figure 3.11D and neurons 2, 3, 6, 8, 9, 14 in Figure 3.12) or I-shaped (neurons 1 and 12 in Figure 3.12) FRAs. Theses FRAs are similar to those already described in mice, and are consistent with those measured using electrophysiological recordings in ferret primary auditory regions (Bizley *et al.*, 2005).

Out of the 311 neurons imaged, 103 were responsive to pure tone stimulation (33.1%; paired t-test; $p < 0.01$) and, of these, 50 showed sensitivity to sound frequency (48.5% of responsive cells; two-way ANOVA; $p < 0.05$). Table 3.1 reports the number of sound responsive and frequency sensitive cells for each of the two ferrets.

As with my analysis of mouse imaging data (Figure 3.6), I examined the spatial organization of frequency preferences in the ferret auditory cortex through 2D maps that

	All imaged	Sound responsive	Frequency sensitive
F1606	134	35	12
F1605	171	68	38

Table 3.1: Number of imaged, sound responsive and frequency sensitive neurons in the two ferrets.

plot neurons according to their position within the cortical surface (Figure 3.13). Performing multiple GCaMP6 injections in each ferret allowed us to sample up to ∼1.5 mm of cortical space in one animal, although some regions within this space were not imaged due to the presence of blood vessels and gaps between injection sites. Only a small minority of neurons were tuned in ferret F1606 (Figure 3.13A left), making it difficult to recognize a topographic organization of frequency preferences. There was, accordingly, no significant correlation between the BFs of frequency-sensitive neurons and their position along the best tonotopic axis, which anyway was calculated basing on very few frequency preferences (Figure 3.13B left). On the other hand, the map from ferret F1605 contained more frequency-tuned neurons and clearly showed a region of high frequency tuning in the most frontal and dorsal of the imaged areas, as well as neurons tuned to lower frequencies more ventrally and caudally (Figure 3.13A right).

We confirmed this tonotopic organization statistically by demonstrating that the BFs of the imaged neurons correlated with their positions on the tonotopic gradient ($r = 0.66$; $p \ll 0.01$; Figure 3.13B right). The orientation of this tonotopic axis is in agreement with results from electrophysiological studies of A1 of the ferret (e.g. Bizley *et al.* (2005)). The bootstrapped analysis confirmed the presence of clusters of neurons with similar BFs in ferret F1605 ($p < 0.05$), but was not calculated in F1606, given the scarcity of frequency sensitive neurons. The standard deviation of the distribution of BFs within the eight imaging fields in F1605 was 0.56 ± 0.16 (mean $\pm$ se).

Finally, I calculated signal and noise correlations for pairs of neurons that were responsive to pure tone stimulation. Signal correlation values were significantly higher than noise correlations (Kruskal Wallis test; $p \ll 0.01$), with mean values of 0.33 ± 0.21 and 0.18 ± 0.15, respectively (74 pairs) (Figure 3.14A).

As found in mice, these two measures were highly correlated ($r = 0.69$; $p \ll 0.01$. Figure 3.14B), indicating that proximal neurons exhibiting a similar basal activity (represented by the noise correlation) are also likely to be responding similarly to sensory stimulation (represented by the signal correlation). This relationship between signal and noise correlations may result from anatomically closer neurons not only sharing similar inputs, but also computing incoming signals in similar ways, building up local functional subnetworks of cells. In light of this possibility, I further examined whether the distance

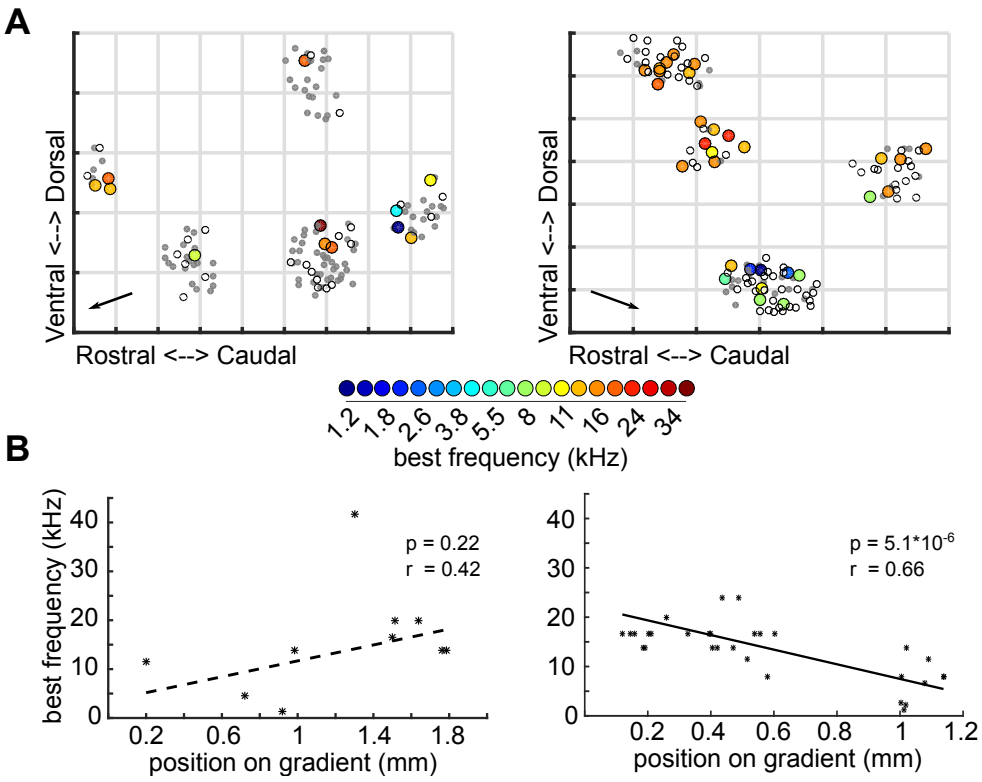

Figure 3.13: (A) 2D maps of BFs visualized as in Figures 3.5 and 3.7, but obtained from ferret F1606 (left) and F1605 (right). Dotted grids indicate areas of 200 x 200μm. (B) Best frequencies are plotted against distance on the tonotopic axis, separately for the two ferrets. The corresponding lines of best fit are shown.

between pairs of neurons influences their correlation more strongly when considered along the tonotopic gradient (the dorsoventral one in the ferret) compared to the orthogonal direction. I plotted signal and noise correlations separately as a function of the distance between neurons along the dorsoventral (Figure 3.14C and D left) and rostrocaudal (Figure 3.14C and D right) axes. However, distance did not significantly modulate signal or noise correlations on either of the two axes, a result which may depend on the very limited sample size. These results will therefore need to be confirmed by further measurements of frequency sensitivity in the ferret auditory cortex in future experiments.

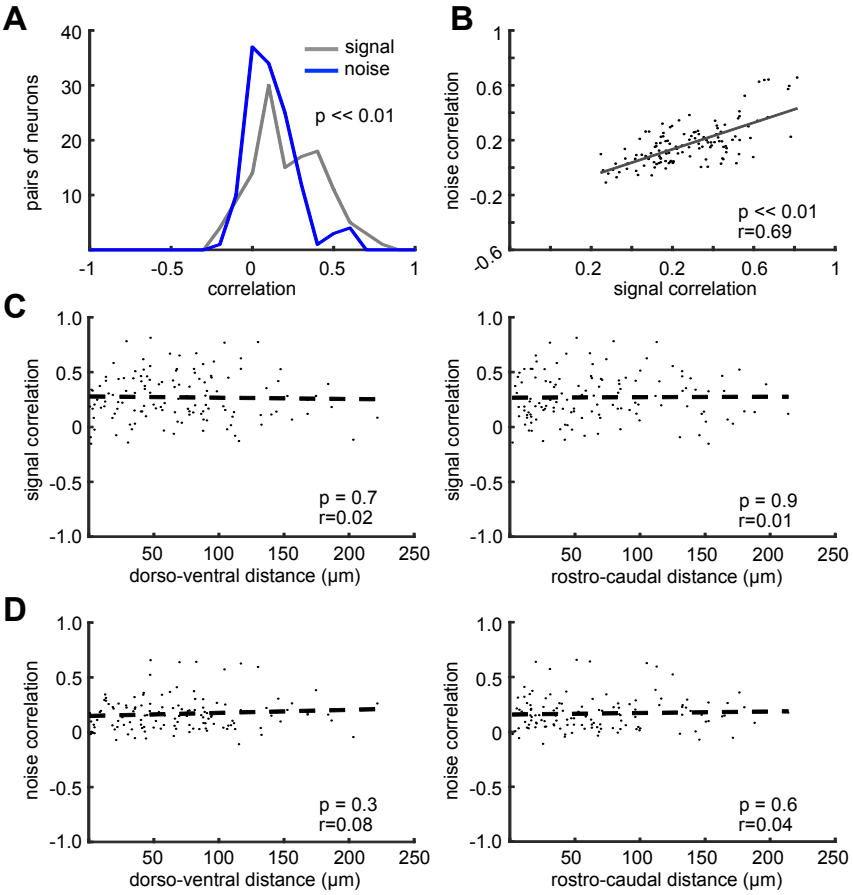

Figure 3.14: (A) Distribution of the signal (grey) and noise correlations (blue) between pairs of simultaneously recorded neurons responsive to pure tone presentation in the two ferrets. (B) Scatter plot of noise correlations plotted as a function of signal correlations in the same neuronal pairs. (C) The same signal correlations are plotted as function of the distance between pairs of simultaneously imaged frequency-responsive neurons. Distances along the dorsoventral (lef) and rostrocaudal planes (right) are plotted separately. (D) Data shown as in C, but indicating noise correlations. Lines in B, C and D indicate the best linear fit to the data and are continuous in case of significant correlation (alpha = 0.05). The correlation values for these fits are displayed as text.

3.4 Discussion

3.4.1 Results overview

In this Chapter, I have analysed how frequency preferences are distributed within small (within 200 μm) and larger areas (up to 1 mm) in the A1 of the mouse, taking advantage of the high spatial sampling resolution of two-photon calcium imaging. I have furthermore investigated, for the first time with this technique, the representation of sound frequency in another mammalian species, the ferret.

The fine scale organization of BFs was revealed in experiments in which the calcium indicator GCaMP6m was injected in layers II-III. In mice, although some BF variability was present, the majority of neurons within local cortical regions were tuned to a common frequency range, and BFs were spatially clustered in half of the animals in my dataset.

A wider scale picture of the representation of frequency tuning was provided by a reporter mouse line expressing GCaMP6f across the entire cortical surface. In this case, the presence of a high-to-low, rostral-to-caudal tonotopic progression of preferences was observed in all three animals used. Such evidence strongly suggests that the imaged neurons were principally located in A1. In the neighbouring AAF, the tonotopic gradient has a mirrored orientation, while secondary fields either contain neurons with much higher BFs or are less clearly tuned to sound frequency (Guo *et al.*, 2012; Hackett *et al.*, 2011; Issa *et al.*, 2014; Stiebler *et al.*, 1997; Tsukano *et al.*, 2015). Although my GCaMP6m injections may have encroached on neighbouring cortical fields, they were performed following the same stereotaxic coordinates used for the craniotomy in transgenic animals, suggesting that I should have also successfully targeted primary auditory cortex in the injected mice.

3.4.2 Contrasting results from low and high spatial resolution techniques

My findings suggest that tonotopy is present in the primary auditory cortex, but with some fine-grained variability in the BFs within areas of 200 x 200 μm. These results are in line with Rothschild *et al.* (2010) who, in one of the first two-photon reports of frequency organization in mouse A1, reported maps of frequency tuning very similar to mine, in

which neighbouring neurons were tuned to a common range of frequencies. A second two-photon study published in the same issue of Nature Neuroscience further confirmed these findings (Bandyopadhyay *et al.*, 2010). Nevertheless, the BF variability found in these papers and in my study is exclusively local, while tonotopy on the large scale is clear. Two-photon calcium imaging thus introduced a new level of spatial resolution in the investigation of cortical activity and was able to describe features that most of microelectrode recordings overlooked. Why is this?

Two-photon imaging has two fundamental features that may favour the observation of a fragmented local organization of cortical responses. First, this technique can record the responses of dozens of neighbouring neurons simultaneously, at a single-cell resolution. Second, it is not biased towards sampling the most active cells. In contrast, mircoelectrode recordings, which provide the bulk of the previous evidence on cortical tonotopy, sample predominantly the activity of neurons with high firing rates.

Another possible limitation of some electrophysiological techniques is that they average the activity of multiple neurons present in a given cortical area. In this respect, however, some distinctions are necessary. Such bias is typical of multi-unit recordings, which return a single signal obtained by measuring the activity of dozens of neurons within an area. As expected, studies using this methodology have generally reported smooth tonotopic maps, across several species (monkey: Recanzone *et al.* (1999); cat: Imaizumi *et al.* (2004); Reale and Imig (1980); rat: Polley *et al.* (2007); mouse: Stiebler *et al.* (1997)).

On the other hand, high-impedance, fine-tipped tungsten electrodes, usually employed in early studies, can reliably reach single-cell resolution. These investigations still reported smooth tonotopy, possibly because of the sparse sampling of the cortical surface (monkeys: Merzenich *et al.* (1973); cat: Merzenich *et al.* (1975); ferrets: Kelly *et al.* (1986); rat: Kilgard and Merzenich (1999)).

A clear tonotopy also emerged from studies using low resolution imaging techniques, like intrinsic imaging, which measures hemodynamic changes as neural correlates, averaging their signal over hundreds of micrometers (ferrets: Mrsic-Flogel *et al.* (2006); Nelken *et al.* (2004); rats: Bakin *et al.* (1996); mice: Tsukano *et al.* (2015)). On the other hand, single-unit electrophysiological measurements have been more varied in their

results. Bendor and Wang (2008) reported a smooth tonotopy by very densely sampling the three auditory core regions of the marmoset, while Schreiner and Sutter (1992) found a less precise spatial arrangement of sharpness of frequency tuning when recording the activity of single units (see also Goldstein Jr and Abeles (1975)).

An interesting indication of the biases of microelectrode recordings comes from an electrophysiological study itself. In 2012, Guo and colleagues carried out an extensive functional investigation of the A1 of the mouse, testing the presence of tonotopy across different experimental conditions (e.g. different anaesthetic states, types of microelectrode recording, and cortical layers). The frequency gradient was reported as robust and consistent. However, the authors stated that if units that were sound responsive, but with irregular tuning profiles, were included in their analysis, then tonotopy would have resulted in being more noisy in layers II-III. Units lacking a clear frequency tuning (i.e. a BF) are rarely reported in the results of electrophysiological experiments (Merzenich *et al.*, 1975; Reale and Imig, 1980), while I presented them in my results.

Nonetheless, Guo and colleagues also reported that pooling weakly and strongly tuned neurons when analysing recordings from layer IV did not disrupt the precision of the tonotopic order. The tendency of local tonotopy to become less pronounced in superficial layers, which do not receive ordered topographic inputs directly from the MGBv, has been also described in a calcium imaging study (Winkowski and Kanold, 2013) and in an experiment using voltage sensitive dyes (Hackett *et al.*, 2011). This may definitely be part of the reason why the local distribution of BFs in my experiments, performed in layers II-III, was not perfectly homogeneous. In fact, microelectrode recording studies have traditionally been carried out in infragranular layers of the auditory cortex. Neurons located at this level receive inputs directly from the thalamus, while horizontal cortico-cortical connections are not frequent, and thus neuronal receptive fields are less complex than in more superficial layers (Atencio and Schreiner, 2010; Barbour and Callaway, 2008). As a result, tonotopy is likely to be better conserved than in layers II-III.

3.4.3 Contrasting results across two-photon imaging studies

Discrepancies not only exist between imaging and electrophysiological results. While a "salt and pepper" tonotopy emerged in my work as well as in some of the published two-

photon imaging studies (Bandyopadhyay *et al.*, 2010; Rothschild *et al.*, 2010), another study outlined a different scenario, in which neighbouring A1 neurons exhibit strikingly similar, if not identical, tonal preferences (Issa *et al.*, 2014). How, then, can these contrasting results be reconciled?

Differences in the data analysis and experimental procedures may greatly influence the outcomes of two-photon calcium imaging investigations. Despite the rapid increase in the use of this technique in the last 10 years, a coherent framework of analytical methods is still lacking, and the continuous introduction of faster and more sensitive indicators makes it difficult to compare results across studies.

In fact, a difference in image analysis may partly explain why Issa and colleagues (2014) reported a surprisingly consistent tonotopic map. In their report, the authors did not apply any correction for eliminating neuropil contamination of somatic calcium signals. This contamination results from the diffuse activation of peri-somatic structures (mainly dendrites). Because it is diffuse, it is also synchronous across the entire imaging field and thus, when added to signals from cell bodies, it makes the sensory responses (i.e. frequency preferences in our case) appear more similar across neurons. This effect is comparable to that seen when artefacts along the z-axis, usually caused by breathing movements, contaminate two-photon acquisitions.

Estimating the time-varying neuropil signal and subtracting it from the somatic one is a measure often carried out in two-photon imaging studies to remove such artefacts (Barnstedt *et al.*, 2015; Chen *et al.*, 2013; Dombeck *et al.*, 2007; Kerlin *et al.*, 2010; Peron *et al.*, 2015). The failure to apply a neuropil correction may have led to the appearance of the tight local tonotopy described in Issa et al. (2014). Although Bandyopadhyday and colleagues (2010) did not carry out a conventional neuropil subtraction either, they performed a time-average of the imaging frames, to similarly tackle the issue of z-fluctuations which would have also removed neuropil artefacts.

A second difference in the study by Issa et al. (2014) is that their recordings were performed in awake mice, in contrast to my experiments and those of both Bandyopadhyay et al. (2010) and Rothschild et al. (2010). Previous electrophysiological studies in A1 have highlighted several differences between neuronal responses in anaesthetized and awake mammals. In the former condition, acoustic stimuli usually elicit transient

responses decaying shortly after the onset of the stimulus regardless of its duration, and defined by the presence of one or few action potentials (DeWeese *et al.*, 2003; Heil, 1997; Schnupp *et al.*, 2001). Moreover, these responses have been described as more often linear than those found in awake recordings (Kowalski *et al.*, 1996; Schnupp *et al.*, 2001). On the other hand, auditory responses in the awake cortex are usually sustained (Barbour and Wang, 2003; Gaese and Ostwald, 2003; Lu *et al.*, 2001), especially when driven by the neuron's preferred stimulus, as reported by Wang *et al.* (2005). Interestingly, this study revealed the great heterogeneity of awake responses, which is not a prominent feature of the anaesthetized cortex. A state of wakefulness favours a desynchronization of cortical neurons and a sharpening of sensory responses (Harris and Thiele, 2011; Poulet *et al.*, 2012), possibly highlighting differences even between neighbouring cells. Arguably, these evidence makes the local homogeneity of frequency tuning found by Issa and colleagues an even more surprising finding. If a precise tonotopy exists locally, this should emerge more easily under anaesthesia than in the awake state, as indicated by previous reports (Hackett *et al.*, 2011). It is worth noting that Issa and colleagues were not able to detect any stimulus-driven calcium transients when, occasionally, isofluorane was used in their animals (see Supplementary Information). Bandyopadhyay and colleagues used low doses of isofluorane during their imaging sessions (0.5% to 1%) and, as expected, obtained considerably heterogeneous local BFs maps. For my experiments, I used a mix of ketamine and medetomidine, similarly to Rothschild et al. (2010) who also reported maps characterized by an intermediate degree of BF variability. Studies in which tonotopy was tighter were instead generally conducted under barbiturate anaesthesia (Hackett et al, 2011, Polley et al, 2007).

In the light of this evidence, it may be interesting to repeat my experiments in awake mice, which may highlight the plastic nature of frequency tuning, by possibly revealing a higher degree of local variability.

3.4.4 Rodents and carnivores: possible species differences

High resolution imaging techniques have helped so far revealing the fine grained functional architecture of A1 in rodents, but to ultimately measure the validity of the "salt and pepper" structure proposed, it is vital to test this in the higher mammals from which

most of the evidence of smooth tonotopy has been derived.

In this dissertation, I have presented the first two-photon data obtained to date in the A1 of adult ferrets. In at least one animal, I found a dorsal-to-ventral decrease in BFs, in line with the orientation of the tonotopic gradient extending through the core auditory region previously reported in this species (Kelly et al, 1986; Nelken et al, 2004; Bizley et al, 2005). This high-to-low progression was also oriented slightly caudally, indicating that our imaging sites were located in A1 rather than AAF (Bizley et al, 2005). Analytical measures of local tonotopy (signal correlations and cotuning calculations) in these data should be considered carefully, since they were certainly affected by the limited size of the dataset. This is also the reason why I will not compare them to those obtained in my mice in this dissertation.

However, when inspecting the 2D map from the ferret yielding the greatest amount of data (F1605), a result comparable to the one I consistently found in mice emerged, with neighbouring neurons having similar, but not identical preferences. Interestingly, recent microelectrode recordings that densely sampled the whole ectosylvyan gyrus reported a consistent, but locally less homogeneous tonotopic organization (Bizley *et al.*, 2005, 2009) compared to earlier studies that examined the cortical surface more sparsely (Kelly et al, 1986). This perhaps suggests that the A1 of rodents and carnivores is organized according to similar functional principles.

The above hypothesis, however, needs to be reconciled with two reports from the early days of two-photon microscopy (Ohki *et al.*, 2005, 2006). Here, the authors highlighted species differences in visual cortex, finding that orientation selectivity is finely organized in the V1 of the cat (Ohki *et al.*, 2006), but not in the rat (Ohki *et al.*, 2005). One possibility still valid today is that, for the small, constrained cortex of the rodents, a precise organization of response properties is neither an evolutionally sustainable option, nor particularly necessary. For example, the tonotopic gradient contains the representation of a $\sim$40 kHz range of frequencies in both the mouse and the ferret (A1 in the mouse should represent frequencies up to $\sim$35 - 40 kHz; Linden *et al.* (2003); Stiebler *et al.* (1997)). However, it extends less than 1 mm in the rodent, but about 4 mm in the ferret. In this scenario, neurons tuned to all frequencies within the hearing range of the mouse are remarkably close in space, and wiring cells with similar BFs is not as

costly energetically as in larger mammals. To test this hypothesis it is vital to obtain evidence of the fine-scale organization of mammals larger than mice: this is among the main objectives of the future experiments in our lab.

It is also true that the map of V1 orientation selectivity reported by Ohki and colleagues appears substantially more heterogeneous than that of A1 frequency selectivity in my experiments. This may reflect differences between the organization of auditory and visual cortex, or may simply be a reflection of methodological differences. Ohki used OGB-1, a synthetic calcium indicator, while I used a recently developed genetically encoded sensor, GCaMP6. These two indicators have different degree of sensitivity for calcium ions and were expressed in cortical neurons through two different modalities (bulk loading and viral transfection). Therefore, they may give different readouts of neuronal activity: for example, OGB-1, but not GCaMP6, should detect neuronal subthreshold calcium transients. In fact, GCaMP6 was used in a recent calcium imaging study performed in the V1 of the tree shrew (Lee *et al.*, 2016), a small mammal with a well developed, primate-like visual system (Cao *et al.*, 2003). Here, the orientation tuning maps showed a smooth progression of preferences over an area of about 1 mm x 1 mm, but local variations of tuning were much higher than described in the cat for the same stimulus feature, and more similar to those I found when examining sound frequency in A1. It is interesting to note that Lee et al. (2016) used the same anaesthetic regime as my study (namely, ketamine and medetomidine).

In the V1 of the ferret, direction selectivity has been studied extensively by means of imaging techniques, and a spatial segregation of cortical areas with different preferences has been described, although this was more pronounced in imaging experiments based on more global intrinsic signals (Li *et al.*, 2006; Weliky *et al.*, 1996) than in those using the single-cell resolution provided by calcium transients (Li *et al.*, 2008; Van Hooser *et al.*, 2012). Examples of two-photon studies in the visual system have been used in the past to speculate about the species-specificity of tonotopic organization because auditory cortical studies have not yet been carried out in animals other than rodents (Kanold *et al.*, 2014; Rothschild *et al.*, 2010). However, comparisons across sensory modalities should be considered carefully. It could be argued that the direction of moving bars, for example, is a visual stimulus that finds its auditory counterpart in FM sweeps, rather than in

pure tones (i.e. a stimulus that moves continuously across the surface of the sensory epithelium). Thus, verification of how both tone frequency and FM sweep properties are organized within a common species is required. In view of this, in Chapter 5, I will examine the organization of FM sweep responses in the mouse.

3.4.5 Conclusions

How is sound frequency tuning really organized in A1? Is tonotopy smooth and tight, or is it fractured and sparse? I would argue that local tonotopy is more or less robust depending on the approach that researchers use to study it.

To summarize what has been discussed above, major factors which should be taken into consideration when examining tonotopy arise from technical differences between published reports, including:

- the cortical layers examined,
- the degree of spatial resolution achieved by the technique used,
- the species under study, and
- the anaesthetic state of the animal.

In addition, there are issues specifically related to two-photon calcium imaging, such as:

- biophysical properties of the calcium indicator, and
- differences in data analysis.

Contrasting results do not imply that some are more correct than others, but they may all just be highlighting different aspects of frequency tuning, which is a plastic feature of A1. Individual best frequencies can change according to the level of wakefulness (Hackett *et al.*, 2011), attentional state (Fritz *et al.*, 2003), or with experience (Dahmen *et al.*, 2008; Dorrn *et al.*, 2010; Polley *et al.*, 2006). In this respect, my experiments have revealed the presence of a moderate response variability under anaesthesia in layers II-III.

Several synapses and major processing steps separate the auditory cortex from the cochlea, and the cortex is the structure dedicated to accomplish a variety of complex

auditory functions (Nelken and Bar-Yosef, 2008; Nelken *et al.*, 2003). Therefore, further sound features should be studied with two-photon calcium imaging in order to unravel the functional properties of this area of the brain. This would help us understand whether the organization of responses in A1 follows a more "anatomical" or a more "functional" principle. In the first case, frequency responses should be the most rigorously organized feature, as tonotopy is the main property of the cochlea and is maintained through spatially ordered projections all the way up to the thalamus. On the other hand, given the complexity of the auditory cortex's roles, we also need to consider the organization of more behaviourally relevant sound features than pure tone frequency.

In the next Chapters, I will analyse the spatial distributions of two other sound features in auditory cortex: interaural intensity differences and frequency modulations. Although they are just two basic ones among the many properties building up the fascinating structure of natural sounds, these features are more complex (i.e. interaural intensity differences require a comparison of signals from both ears) and dynamic (frequency modulations are events that occur over time) than sound frequency. Studying the cortical representation of these three sound features individually and drawing comparisons between them is fundamental to understand the overall cortical processing of natural sounds.

Chapter 4

The representation of ILDs in A1

4.1 Introduction

Disparities in sound level between the two ears, known as Interaural Level Differences (ILDs), provide an important sound localization cue, and are the principal basis by which animals with small heads and high-frequency hearing, such as rats and mice, localize sounds in the horizontal plane (Chen *et al.*, 1995; Lauer *et al.*, 2011; Wesolek *et al.*, 2010). Extracellular unit recordings have been used to explore the sensitivity of neurons to ILDs in the primary auditory cortex (A1) of a variety of species. Nevertheless, fundamental questions remain unanswered.

One important and long-standing issue relates to the spatial organization of binaural responses in A1. Early investigations assigned discrete categories to describe cortical neurons' responses to stimuli characterized by interaural differences. Goldberg and Brown (1969) introduced a two-letter code to indicate these categories, in which binaural properties were defined by comparing the neuron's responses to monaural stimuli in each ear. According to this system, EI cells, showing monaural contralateral excitation (E) and ipsilateral inhibition (I), prevailed in A1 together with EE neurons, excited by monaural stimuli in either ear.

Intriguingly, these binaural classes were found to be organized into bands in A1 of cats (Imig *et al.*, 1977; Middlebrooks *et al.*, 1980) and ferrets (Kelly and Judge, 1994). Binaural bands alternated perpendicular to the tonotopic gradient and extended throughout the cortical depth (Abeles and Goldstein Jr, 1970).

Later studies employed a greater range of species and more diverse response categories. In particular, neurons sensitive to binaural stimuli were further classified according to the precise type of binaural interaction displayed, determined by comparing the magnitude of the neuron's binaural response to the summed magnitude of its monaural responses. For example, neurons showing "binaural facilitation" exhibited responses to binaural sounds higher than the summed responses to two monaural stimuli of the same intensity. This response profile is opposite to "binaural suppression". As a consequence of this increased complexity, the spatial organization of binaural properties within A1 became less clear. Rather than distinct bands, some studies reported less well organized clusters of neurons with similar binaural properties (Kelly and Sally, 1988; Nakamoto *et al.*, 2004; Reale and Kettner, 1986; Recanzone *et al.*, 1999; Rutkowski *et al.*, 2000), others found organization only in thalamo-recipent layers (Phillips and Irvine, 1983; Reser *et al.*, 2000), whereas the pallid bat seems to possess two separate regions in A1 with distinct binaural properties, although this species stands apart for its peculiar use of binaural cues for echolocation, beyond passive sound localization (Razak, 2011; Razak and Fuzessery, 2000, 2002). How neurons in A1 are organized according to their binaural properties remains therefore an open question.

In 2006, a thorough study by Campbell and colleagues described binaural properties in the A1 of the ferret, ignoring the traditional response categorization and basing this analysis exclusively on the shape of the neurons' binaural response functions. The authors found a continuous distribution of binaural responses, so that a segregation into discrete "binaural classes" was not appropriate (Campbell *et al.*, 2006). Such a finding, then, casts doubt on the presence of a discrete spatial organization of binaural response categories across the cortical surface and brings us to the second outstanding issue I will deal with in this Chapter, which concerns the diversity of spatial tuning profiles in A1.

Microelectrode recording studies in several species agree that half of A1 neurons are responsive to stimuli with varying ILDs, but lack any selectivity for sound location. In other words, these neurons are omnidirectional in the way they respond. Among the other neurons, selectivity for contralateral stimuli prevails, although a minority of cells tuned to ipsilateral or midline locations have been consistently described in carnivores (Irvine *et al.*, 1996; Middlebrooks and Pettigrew, 1981; Rajan *et al.*, 1990; Zhang *et al.*,

2004) and in bats (Razak, 2011). Interestingly, the rat seems to represent an exception. Multi-unit recordings (Yao *et al.*, 2013) and low resolution optical imaging (Higgins *et al.*, 2010) in this species found that almost all neurons in A1 and secondary auditory cortical fields prefer contralateral hemifield stimulation. However, neurons tuned to ILDs of 0 dB or favouring the ipsilateral ear have been detected in this species using single-unit (Kyweriga *et al.*, 2014) and whole-cell recordings (Chadderton *et al.*, 2009).

In the only published study investigating ILD sensitivity in the mouse in A1, Polley *et al.* (2013) found that ipsilateral tuning gradually increased during the critical developmental window for hearing, reaching adult-like levels at around post-natal day 16.

All the aforementioned studies examined the spatial response properties of cortical neurons using microelectrodes, which sparsely sample the cortex, favour the most active neurons, and potentially pool responses from several neurons. *In vivo* two-photon calcium imaging, on the other hand, can be used to simultaneously measure the responses of the majority of neurons located within a few hundred micrometers with single-cell resolution.

4.1.1 Aims

In the present Chapter, I used the genetically encoded calcium indicator GCaMP6 and two-photon calcium imaging to measure the responses to ILD noise bursts of A1 neurons.

My first aim was to characterize such responses in order to understand whether the representation of ILDs in the mouse is more similar to that sometimes described in rats, or resembles that found in the auditory cortex of higher mammals. Moreover, I aimed to describe the microscopic spatial representation of ILD preferences in the cortex. If A1 neurons are indeed arranged into binaural bands or clusters, as emerged in microelectrode recordings, then neighbouring cells within this region should have more similar binaural preferences than distant ones.

By sampling local neurons regardless of their size or level of activity, two-photon imaging may shed light on the potential local variability of binaural responses, similarly to what has been seen for frequency preferences. Indeed, a further aim of my experiments was to compare the local organizations of responses to these two sound features: sound frequency and ILDs. For this reason, I presented both ILD stimuli and pure tones to most neurons in my recordings.

4.2 Methods

Surgical procedures and image analysis are described in sections 2.1 and 2.2.1. Details about the coordinates of the viral vector injections and evidence that imaging was carried out in the core region of auditory cortex are also reported in sections 3.3.2 and 3.3.3.

4.2.1 ILD noise burst presentation

Broadband noise bursts (2 - 60 kHz), 100 ms long (∼3 imaging frames) with 5 ms cosine onset and offset ramps were presented binaurally at a rate of 0.65 Hz.

Noise bursts and pure tones have generally been used to investigate the binaural properties of cortical neurons. However, in this case, noise bursts were a more appropriate stimulus than tones, as it was not necessary to adapt them to the BFs of the units recorded. This is a vital advantage when using techniques like two-photon imaging, where many neurons of unknown frequency preferences are recorded at the same time.

Interaural level differences ranged from -30 dB to +30 dB, in 10 dB steps, where negative ILDs indicate that the sound level was greater in the contralateral ear (see Figure 4.1A). The same broadband noise bursts were also presented monaurally to each ear. I presented these stimuli at an average binaural levels (ABL) of 60 and 80 dB sound pressure level (SPL) for six mice, and 40, 60 and 80 dB SPL for 12 mice (including three mice from the reporter line).

As mentioned in section 1.2.1, the shadowing effect of the head and the external ears changes according to the frequency of the waves they interact with. High frequency sounds are particularly affected, and ILDs generated by them change more rapidly with azimuth, compared to those occurring at low frequencies. Based on the head-related transfer function of mice, the maximum ILDs generated by the interaction between sound waves and the external ears are between 30 and 40 dB. Indeed, Lauer and colleagues (2011) reported that ILDs as large as 40 dB can be reached for frequencies at ∼30 kHz, when the sound source is located 90° lateral from the midline. However Chen et al. (1995) reported a maximum ILD of 30 dB in mice, reached only by lateralized high frequency sounds, between 70 and 80 kHz (see Figure 1.1). Thus, the range of ILDs I have used in my experiments crosses the whole range of ILDs experienced by mice, and it corresponds to that used in previous studies of ILD sensitivity in the auditory system of this species

(Xiong *et al.*, 2013).

4.2.2 Identifying responsive neurons

Paired t-tests (one-tailed, alpha = 0.01) were carried out on the maximum $\Delta F/F_0$ values in the pre and post-stimulus windows across repeated presentations of any one sound, for each ILD. Neurons that showed a significant response at any ILD value were considered to be driven by binaural noise bursts.

4.2.3 Determining ILD sensitivity in responsive neurons

A neuron's trial-averaged response to each ILD and ABL combination, defined as the difference between the neuron's maximum $\Delta F/F_0$ in the stimulation and pre-stimulation periods (see section 2.2.2), was visualized as an ILD-response area plot (see Figure 4.1C). To test if a neuron was sensitive to ILDs, I compared the responses to binaural noise bursts across the seven ILDs using a one-way ANOVA (alpha = 0.05). Sensitivity to ILDs was assessed separately for each ABL. If a neuron was found to be sensitive at a given ABL, its preferred ILD was determined as the stimulus eliciting the highest average response. Taking the peak of the response curve as the neuron's stimulus preference has also been used in previous studies of ILD (Polley *et al.*, 2013) and ITD (Belliveau *et al.*, 2014) sensitivity in rodent auditory cortex.

Furthermore, I calculated the slopes of the ILD response functions as the difference between the average neuronal responses to two contiguous ILD values. These slopes were calculated between all pairs of contiguous ILD values, and were derived separately for each ABL.

4.2.4 Categorizing the binaural properties of neurons

To facilitate comparisons with earlier papers describing binaural organization in A1 (e.g. Imig *et al.* (1977); Middlebrooks *et al.* (1980); Nakamoto *et al.* (2004); Zhang *et al.* (2004), I discretely categorized the binaural properties of neurons based on their responses to noise bursts presented monaurally to either ear and diotically (i.e. with an ILD of 0 dB). Paired t-tests (one-tailed, alpha = 0.01) were used to compare the maximum $\Delta F/F_0$

values during the pre-stimulation and stimulation periods in order to determine if the neuron was responsive to each of the above monaural or diotic noise stimulus conditions.

The results of these t-tests were then used to classify each neuron into one of four binaural categories, following the categorization used by Zhang *et al.* (2004). Neurons were categorized separately for each ABL. A neuron was classified as: (1) "EO" if it significantly responded (i.e. passed the t-test) to monaural noise in the contralateral ear but not the ipsilateral ear; (2) "OE" if it was driven by monaural noise in the ipsilateral ear but not the contralateral ear; (3) "EE" if it was driven by monaural stimulation in both ears; (4) "OO/F" if it responded only to the binaural stimulus, but not to either monaural stimulus, thus showing binaural facilitation (termed "PB" or predominantly binaural in Zhang *et al.* (2004)). Thus, this last category of neurons (OO/F, or PB) includes, by definition, neurons sensitive to binaural stimulation (i.e. not monaural).

For the other three categories, I went on to investigate whether they showed binaural interactions by computing, for each EO, OE and EE neuron, a binaural interaction index (BII), which compares the response elicited by a binaural stimulus configuration to the sum of responses to the two monaural stimuli delivered at the same intensity in each ear (Goldberg and Brown, 1969; Higgins *et al.*, 2010; Zhang *et al.*, 2004). For example, for binaural stimuli at 60 dB ABL, the BII was calculated as follows:

$$BII = \frac{(\Delta F/F)_{60ipsi,60contra}}{(\Delta F/F)_{60ipsi} + (\Delta F/F)_{60contra}} \tag{4.1}$$

Where $(\Delta F/F)_{60ipsi,60contra}$ is the maximum response to binaural noise bursts of 0 ILD at 60 dB ABL, while $(\Delta F/F)_{60ipsi}$ and $(\Delta F/F)_{60contra}$ indicate responses to monaural bursts at 60 dB SPL in the ipsilateral and contralateral ear, respectively. Neuronal BII values were obtained separately for the three overall sound levels used.
A neuronal BII above 1.2 (i.e. a binaural response 20% higher than the sum of the two monaural responses, as in Zhang *et al.* (2004)) was considered as "binaural facilitation", and neurons were categorized as EO/F, OE/F or EE/F, according to the "monaural category" they belonged to. To the contrary, a BII below 0.8 was considered to represent "binaural inhibition", and neurons categorized as EO/I or OE/I. When BII were between 0.8 and 1.2, the binaural interaction was very weak, possibly resulting from random fluctuations. In these cases, neurons were categorized as EO/N, OE/N or EE/N, where

N stands for "null", indicating, in fact, monaural cells. For EE neurons, a binaural response <80% of the sum of the monaural responses and >80% of the response to monaural stimulation of the dominant ear was considered as "binaural occlusion", and the neurons classified as EE/O.

4.2.5 Aural Dominance Index

If the BII indicates which specific type of interaction characterizes a neuron's binaural response, a more general indication of the degree of "binaurality" of a neuron can be obtained through the Aural Dominance Index (ADI) (Xiong *et al.*, 2013). I have defined this as the difference between monaural contralateral and ipsilateral responses summed across the three overall sound levels (40, 60, 80 dB SPL), divided by their sum.

$$ADI = \frac{Contra_{(40+60+80)} - Ipsi_{(40+60+80)}}{Contra_{(40+60+80)} + Ipsi_{(40+60+80)}} \tag{4.2}$$

The ADI was calculated for all neurons responsive to noise bursts (t-test; p <0.01). According to this calculation, monaural neurons should present an ADI of ±1, with positive values indicating contralateral dominance and *vice versa*. I used a stricter criterion and considered monaural ipsilateral to be neurons with an ADI between -1.1 and -0.9, and monaural contralateral neurons as those with an ADI between 0.9 and 1.1. I have made this choice because calcium fluctuations are rarely exactly zero, which would have increased the risk of undersampling monaural neurons.

4.2.6 Principal components analysis

I used principal components analysis to identify common patterns in response to noise bursts with different ILDs across the population of neurons imaged in the mice to which noise bursts at all three ABLs were presented (n = 9). For all neurons that were responsive to noise bursts at any ABL, a principal components analysis was carried out on the response matrix consisting of the averaged responses to the 21 stimuli (7 ILDs x 3 ABLs). This produced 21 principal components, ordered according to the amount of neural response variance they explained.

4.3 Results

To investigate the micro-organization of spatial tuning in layers II-III of mouse auditory cortex, I performed *in vivo* two-photon calcium imaging in 15 animals in which the calcium indicator GCaMP6m had been expressed by AAV injection. All mice were presented with pure tones as well, and in 13 animals both types of stimuli were presented whilst imaging from the same fields.

4.3.1 Calcium transients in response to binaural noise bursts

I imaged calcium transients from 1913 neurons in 61 imaging fields with an area of 250 x 250 μm. Examples of the responses of five neurons to noise bursts presented at the 7 ILDs used are shown in Figure 4.1B.

The majority of calcium transients were aligned with the onset of sound stimulation. Some neurons showed a clear preference for one of the stimuli presented, exhibiting consistent responses across repetitions of the same stimulus (e.g. neurons 3-5, Figure 4.1B). For other neurons, the magnitude of the calcium transients in response to ILD stimuli varied considerably across repetitions of the same stimulus (e.g. neuron 2, Figure 4.1B), while still other neurons did not respond to the stimuli (e.g. neuron 1, Figure 4.1B).

For each neuron, I represented the average response to the noise bursts at each ILD and ABL in ILD-response area plots (Figure 4.1C). Most responsive neurons showed V-shaped responses, indicating monotonic intensity sensitivity, tuning to a particular ILD, and sharper ILD sensitivity at lower sound levels (e.g. neurons 2, 3 and 5; Figure 4.1C). A smaller subset of neurons showed different tuning characteristics, such as suppression by louder sounds (e.g. neuron 4; Figure 4.1B).

The calcium transients elicited by broadband noise bursts were significantly lower in amplitude compared to those in response to pure tones (noise bursts mean: 0.21 a.u.; pure tones mean: 0.58 a.u.; t-test on 700 neurons; $p << 0.01$). This finding is in agreement with what reported in several other mammalian species, from rodents to primates (Barbour and Wang, 2003; Lakatos *et al.*, 2005; Pandya *et al.*, 2008; Phillips and Cynader, 1985), and it may suggest that neurons narrowly tuned for sound frequency, like those in the core regions of the auditory cortex, are better driven by pure tones rather than noise bursts.

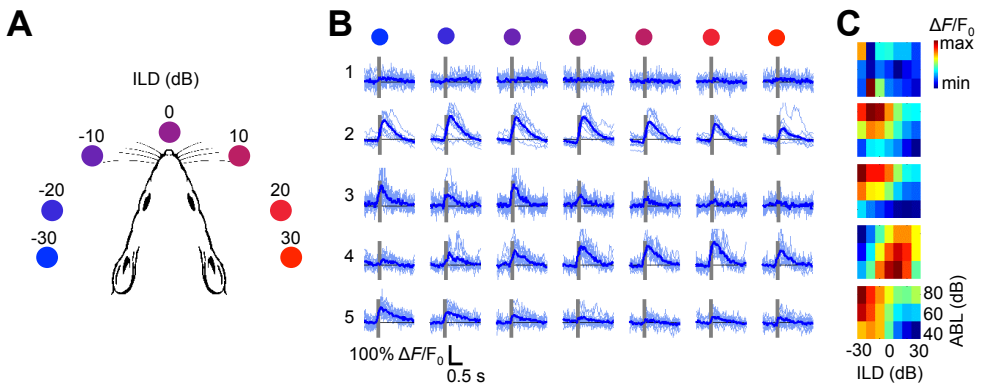

Figure 4.1: Panel A is a representation of auditory stimuli: seven ILDs ranging from -30 to 30 dB ILD in 10 dB steps were presented to the mouse during the imaging session. The position of the coloured dots indicates the corresponding azimuthal angle relative to the mouse head based on acoustical measurements by Chen et al. (1995). Monaural stimuli were also presented to each ear (not shown). B shows the individual (light blue) and mean (dark blue) responses of five neurons to each of the seven ILD values for noise bursts presented at 60 dB ABL. Grey bars indicate stimulus onset and duration. Panel C indicates ILD response area plots of each neuron.

To rule out the possibility that my ILD tuning results were biased by the presence of sub-threshold signals in the analysis, and to test the reliability of calcium signals in my dataset, I inferred firing rates from the intracellular calcium transients, using a compressive sensing algorithm (Dyer *et al.*, 2010) (see section 2.2.4). In Figure 4.2, I show the fluorescent traces and the corresponding spikes obtained in two neurons labelled with GCaMP6m (A) and two others expressing GCaMP6f (C).

When extracted spikes were used to compute neuronal ILD response curves (Figure 4.2B and D), these were found to be similar to those obtained from the calcium transients. I therefore used the normalized magnitude of the calcium signals to quantify neuronal stimulus selectivity.

4.3.2 Testing the neuronal sensitivity to binaural stimuli

I found that noise bursts presented at 40 dB ABL elicited responses from the lowest percentage of neurons (47.3 ± 3.6%; mean ± se across mice) (Figure 4.3A). The majority of imaged neurons responded to 80 dB ABL stimuli (62.5 ± 4.8%), indicating a larger recruitment of neurons for higher sound intensities over the 40 - 80 dB range used.

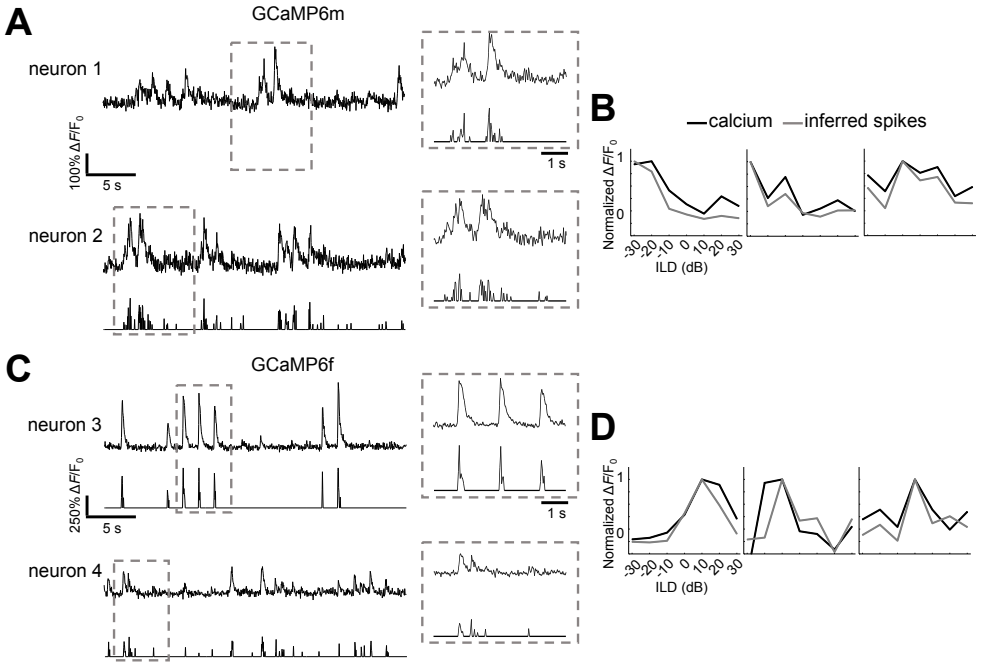

Figure 4.2: Calcium traces and inferred spike trains from four example neurons expressing GCaMP6m via injection (A) and GCaMP6f constitutively (C). Insets (right) show 5 second fragments from the traces in A and C. ILD response curves from three neurons expressing GCaMP6m (B) and three expressing GCaMP6f (D) were obtained using calcium signals (black lines) and inferred spikes (grey lines).

Overall, 76.6 ± 1.8% of neurons were noise-responsive for at least one of the three ABLs.

Before exploring the sensitivity of cortical neurons to ILDs, it is important to verify how many neurons were modulated by binaural stimulation, that is, were not monaural. With this purpose, I calculated the ADI for all neurons significantly responding to noise bursts (t-test; $p < 0.01$) in all mice tested with stimuli at three ABLs (nine injected and three transgenic mice, for a total of 866 neurons) (Figure 4.3B). Among these, 6.12% of cells had an ADI between 0.9 and 1.1, indicating monaural responses to contralateral stimuli only, while 2.08% neurons were monaural ipsilateral, with ADIs between -1.1 and -0.9. Therefore, the vast majority of my neurons (91.8%) exhibited some degree of binaural interactions, consistent with what has been reported previously in rodents (Higgins *et al.*, 2010; Polley *et al.*, 2013), as well as in higher mammals (Campbell *et al.*, 2006; Kitzes, 2008; Zhang *et al.*, 2004).

The mean ADI value was 0.48 (median value was 0.31). As can be seen in Figure 4.3B,

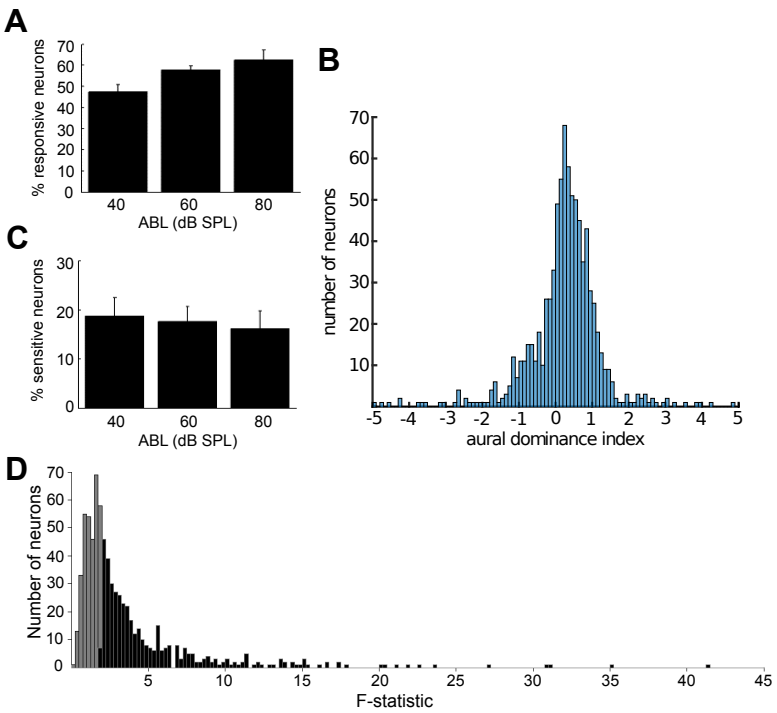

Figure 4.3: Panel A reports the mean percentages of neurons responsive to sound stimulation across mice at each of the ABLs tested. B represents the distribution of ADI values for all neurons responsive to ILD noise bursts across mice. In C are shown the mean percentages of ILD sensitive neurons, again across mice and for each of the three ABLs. D reports the distribution of the F statistic values for the main effect of ILD on the neuroal responses (two-way ANOVA). Grey bins indicate values below statistical significance ($p < 0.05$).

ADIs were occasionally <-1 or >1. These values occurred when neuronal responses were negative, as a consequence of $\Delta F/F$ fluctuations below zero. Negative responses to a monaural ipsilateral noise burst, for example, can produce both ADIs >1 and <-1, possibly indicating a particularly robust inhibition for ipsilateral sounds.

I then went on to test the ILD sensitivity of my binaural neurons. The proportion of these neurons fell slightly as the ABL was increased from 40 dB (18.7 ± 3.7% of all the imaged cells; 37.3 ± 5.6% of noise-responsive cells) to 80 dB SPL (16.1 ± 3.7% of all imaged cells; 25.7 ± 4.9% of noise-responsive cells) (Figure 4.3C). This is to be expected from the V-shaped ILD response area plots of most neurons.

As indicated from the results above, I have used a traditional binary segregation of sensitive and insensitive neurons to analyse my neuronal responses, based on the results

of a statistical test. However, to explore whether the neurons actually fell into two such populations, I examined the proportion of their response variance that was explained by the ILD. For all the injected mice in which all three ABLs were presented (n = 9), a two-way ANOVA was carried out on the responses from each neuron, with ILD and ABL as predictor variables. Plotting the F-statistic distribution for the main effect of ILD on neural response, across all neurons, revealed that their ILD sensitivity formed a continuous distribution across neurons that were significantly sensitive (black bins; $p < 0.05$) or insensitive (grey bins) to ILD (Figure 4.3D). There is no clear bimodal distribution of F values, as interpretations of statistical tests with hard boundaries can imply. This is an important point to keep in mind throughout the following analyses where, according to conventional practice, I segregated neurons into discrete categories according to their preferred ILD combination, or their binaural interactions.

For the noise-responsive neurons that showed significant ILD sensitivity, I next determined the preferred ILD at each ABL. Figure 4.4A shows the percentage of neurons preferring each ILD, averaged across mice. Most neurons preferred ILDs corresponding to contralateral positions at all ABLs tested, although a minority preferred sounds that were higher in level in the ipsilateral ear (23.3% of neurons at 60 dB ABL).

In order to determine the region of ILD "space" within which neuronal responses were most informative, I calculated the slope of the response curve between contiguous ILD values. This slope is steepest around ILDs for which the neuron is most sensitive. At 40 and 60 dB ABL, the majority of neurons showed higher acuity around midline ILDs than for the most lateralized values (Figure 4.4B). The distribution was flatter at 80 dB ABL, perhaps due to the reduced spatial sensitivity at this high sound intensity.

4.3.3 Sharpness of ILD sensitivity

I next measured the sharpness of ILD sensitivity. For brevity, I focus here on the data obtained at the intermediate sound level (60 dB ABL), but I obtained similar results for the lowest and highest (40 dB and 80 dB) ABLs.

The ILD bandwidth of a neuron was defined as the range of consecutive ILDs around the preferred ILD to which the neuron also responded significantly (paired t-test; $p < 0.01$). Therefore, if the neuron only responded to noise bursts presented at the preferred ILD,

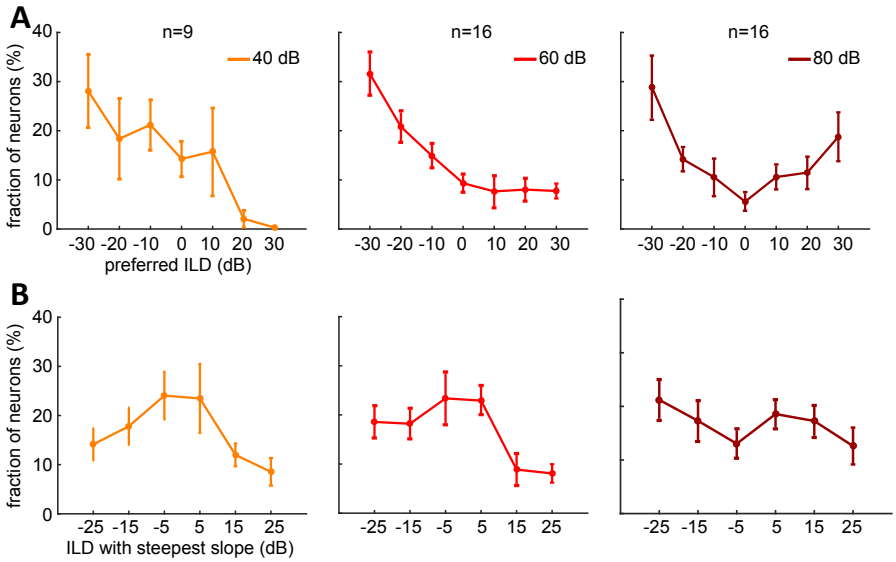

Figure 4.4: Panel A indicates the mean percentages of ILD preferences across mice. Data are presented separately for the three ABLs: 40 (left plot; yellow), 60 (center plot; light red), 80 dB (right plot; dark red). B contains data presented as in A, but indicating the mean position of the steepest ILD slopes across mice. All error-bars in this Figure indicate standard errors.

the bandwidth was <10 dB (as ILD stimuli were presented in 10 dB steps). I found that neurons often responded only to sounds within 40 dB of their preferred ILD (Figure 4.5A), irrespective of whether they responded best to contralateral, midline or ipsilateral ILDs.

Although many neurons responded monotonically as a function of ILD or were clearly tuned to a particular ILD value, some exhibited additional peaks in their ILD response areas. I defined these peaks empirically as the number of significant responses to an ILD that was outside the boundaries of the ILD bandwidth for a given neuron. Therefore, a neuron could have a minimum value of "2", indicating that it had only a single continuous range of significant responses, and a maximum possible value of "5", indicating that it responded to all five sounds that are non-continuous with its preferred ILD. I found that 63.9% of ILD-sensitive neurons exhibited single peaked ILD responses, and no neurons responded to more than three ILDs outside their main ILD bandwidth (Figure 4.5B).

Next, to visualize the typical ILD response curve more explicitly, I normalized the responses of each neuron across all ILDs and then averaged these normalized responses across neurons with the same preferred ILD. Figure 4.5C shows these normalized ILD response curves averaged across all neurons with a preferred ILD of -30 dB (blue), 0 dB

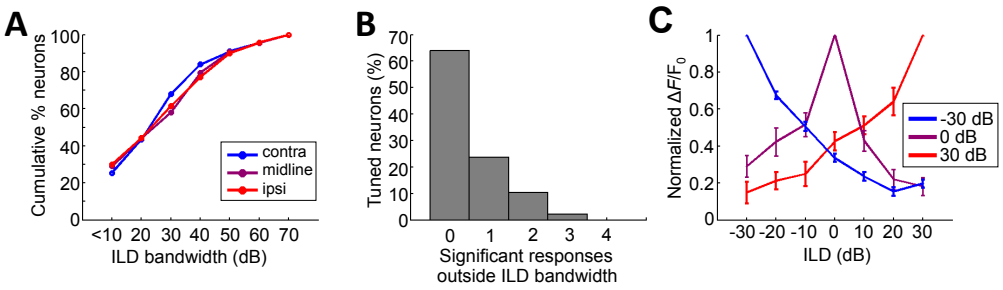

Figure 4.5: Panel A shows the cumulative distribution of ILD bandwidths for all ILD sensitive neurons. Distributions are shown separately for cells with contralateral ($\leq$ 10 dB), ipsilateral ($\geq$ 10 dB), and midline (between -10 and 10 dB) preferences. B contains the histogram of the number of ILD stimuli eliciting a significant response outside the ILD bandwidth. In panel C, the average normalized ILD response curves for all neurons preferring ilds of -30 (blue), 0 (purple) or 30 dB (red) are shown.

(purple) or 30 dB (red). The ILD functions for neurons preferring -30 and 30 dB ILDs had steep monotonic slopes and were almost symmetrical to one another around the midline. Neurons preferring 0 ILD were sharply tuned, but this response curve was asymmetrical around the midline, favouring responses to contralateral stimuli. Together, Figure 4.5A and C indicate that auditory cortical neurons can respond maximally to ILDs corresponding to a range of azimuthal locations, and are often responsive to ILDs in only one lateral hemifield.

4.3.4 Looking for common response patterns: PCA

As discussed in section 4.1, when analysing binaural sensitivity in auditory cortex, neurons have been generally classified according to the stimulus eliciting the highest response. For example, neurons responding maximally to sounds louder in the contralateral ear have been reported as contralaterally tuned. Such categorization does not explain how each neuron responds to a combination of ILDs and ABLs.

Taking advantage of the large number of neurons recorded in my two-photon imaging experiments, I used PCA to visualise the main response patterns emerging in my population of sound responsive cells. By projecting the 21-dimensional response matrix (3 ABLs x 7 ILDs) into an orthogonal system of axes, PCA defines the major response patterns in the dataset, each described by a principal component (PC). In this section, I report the shape of the first 4 PCs (similarly to Eskandar *et al.* (1992)). These accounted

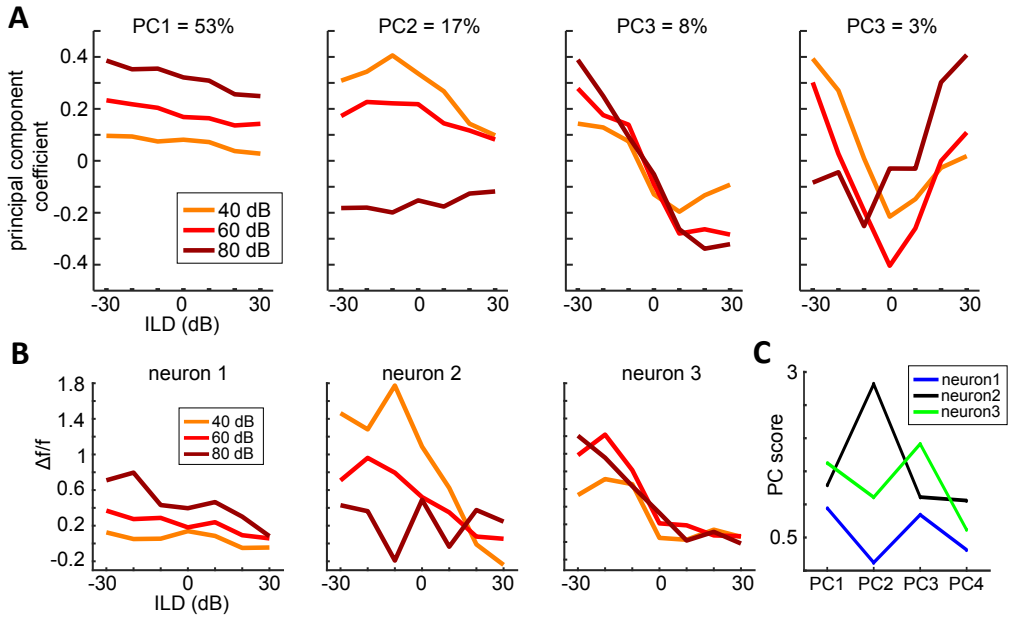

Figure 4.6: In panel A, the eigenvectors of the first four principal components resulting from a PCA are plotted. Panel B shows the response curves of three example neurons resembling the patterns defined by the first three PCs found. Panel C reports the scores obtained for each PC, in each of the three neurons.

for a total of 81.4% of the variance in the neural responses (53.4%, 16.9%, 7.9% and 3.2% each). My approach does not aim to investigate whether separate clusters of neurons exist, whose response profiles can be segregated according to the scores obtained in each neuron, for each PC (Campbell *et al.*, 2006). Rather, it aims to show the most common patterns in response to my combination of ILDs and ABLs.

The coefficients of the first four PCs are plotted in Figure 4.6A. This visualization of the first principal component illustrates that a monotonic increase in the neural response with ABL accounts for the most variance in my data. An example neuron showing a response profile resembling the one described by PC1 is reported in Figure 4.6B (left). However, if I normalized the ILD responses across neurons (so that each neuron had the same maximum amplitude), this first PC did not emerge, suggesting that it is likely to explain the variability in overall response strength across neurons, rather than their tuning to ILDs or ABLs.

The second component in the figure describes the behaviour of neurons that respond to sounds in only one hemifield of space at lower sound levels, and omnidirectionally at higher levels. The corresponding response profile of an example neuron is shown in

Figure 4.6B (middle).

The third principal component represents response functions in which neurons are activated primarily to sounds in one hemifield in a level-independent manner. The corresponding response profile of an example neuron is visualized in Figure 4.6B (right).

Finally, the fourth PC, describes the properties of few neurons with particularly steep ILD response functions, characterized by a notch at values around the midline. Figure 4.6C shows the scores obtained for each PC, for each of the three example neurons.

4.3.5 Local arrangement of binaural preferences

I examined the cortical location of neurons with different spatial preferences by producing two-dimensional (2D) maps of ILD preferences in which neurons are plotted according to their positions along the rostrocaudal and dorsoventral axes (Figure 4.7). As mentioned before, I tested the responses of most neurons by presenting both ILD noise bursts and pure tones, so that the maps in this Figure can be compared with those in Figure 3.7.

Despite the overall prevalence of contralateral preferences, the 2D maps illustrate that even neurons in the same imaging field (250 x 250 μm) could respond best to contralateral (blue) or ipsilateral (red) ILDs. In some mice (3 and 10), I observed occasional patches of more homogeneous ILD preferences, while the upper-left area in mouse 5 seemed to contain two groups of neurons tuned to the most ipsilateral (30 dB) and most contralateral ILDs (-30 dB). However, no systematic spatial organization of ILD preferences was apparent in these maps across the 15 mice I investigated.

I used a bootstrapping approach to empirically test if neurons with similar ILD preferences were spatially clustered in each mouse (see section 2.2.7). The ILD preferences of proximal cells were found to be significantly more similar than those of distant ones in only one animal (mouse 1) when ILDs at 60 dB ABL were considered. At 80 dB ABL the result was the same, while ILD preferences at 40 dB ABL clustered in two out of the eight animals in which stimuli at the lowest sound level were presented. Together, these results suggest that there is no overall organization of ILD preferences in layer II-III of mouse A1.

In addition to measuring ILD sensitivity, I categorized each neuron based on the binaural interaction emerging when comparing its responses to noise bursts presented

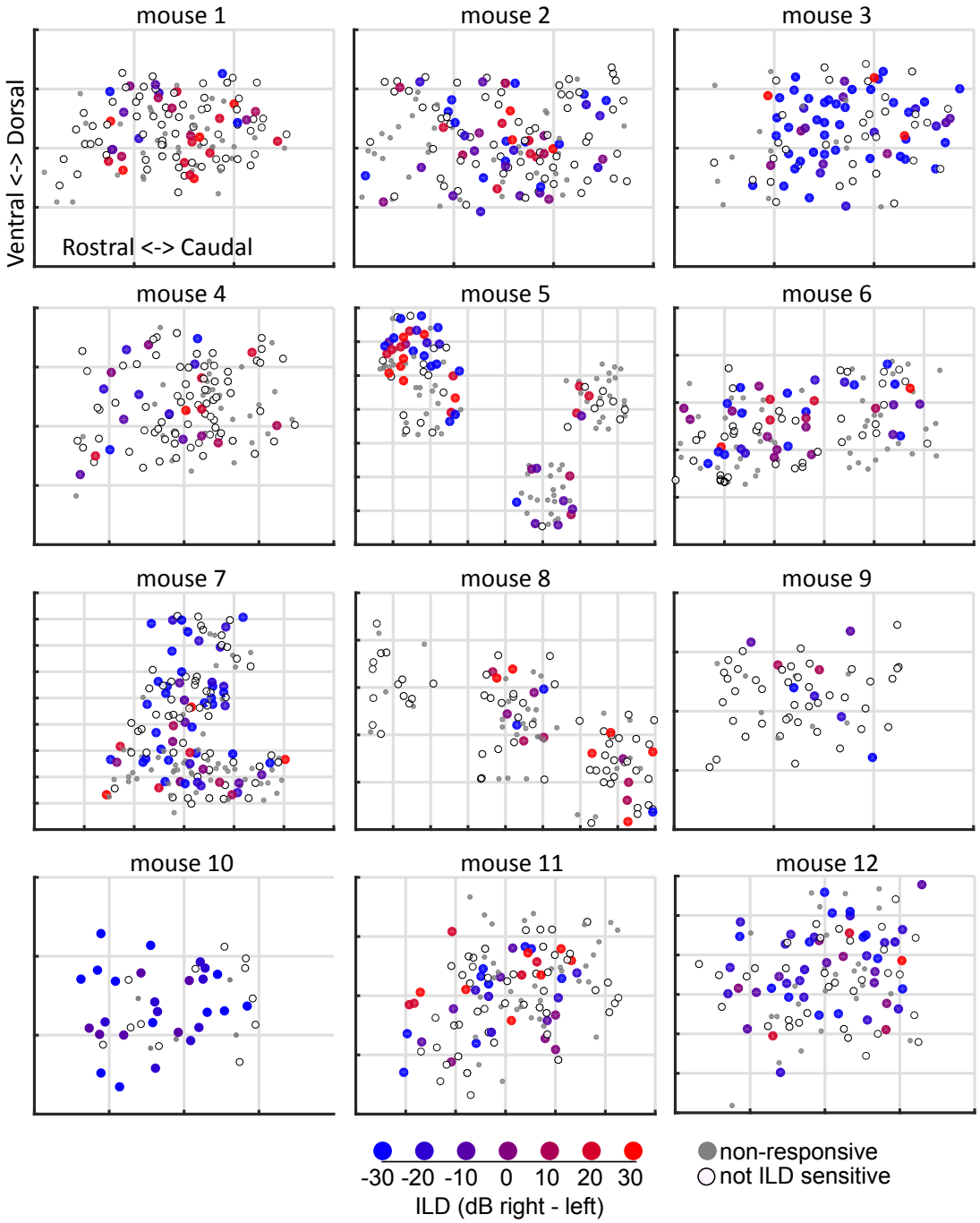

Figure 4.7: Neurons from 12 mice injected with GCaMP6m are plotted according to their position along the rostrocaudal and dorsoventral axes, with z-dimension collapsed. Non-responsive neurons are grey dots, while responsive neurons that are not sensitive to ILDs are white dots. ILD sensitive neurons are colour coded according to their preferred ILD. In the plots, this was derived for each neuron from the lowest ABL at which significant ILD sensitivity was measured. Dotted grids represent areas of 100 x 100 μm.

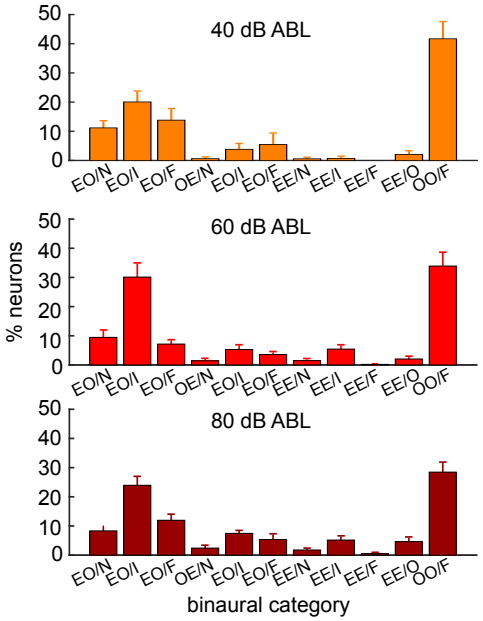

Figure 4.8: Distributions of responsive neurons in each binaural category, averaged across 15 mice (mean ± sem) and shown separately for each ABL.

monaurally in the ipsilateral ear and monaurally in the contralateral ear, with the responses to diotic stimuli at 0 dB ILD (see section 4.2.4).

As expected from the distribution of the ADI values in my population, most neurons were sensitive to binaural modulations at all three ABLs tested (Figure 4.8).

The vast majority of cells showed either binaural activation with no monaural responses (OO/F neurons; 33.9 ± 4.7% at 60 dB SPL), or contralateral responses (EO neurons; about 47% of neurons at 60 dB SPL). Of the neurons classified as EO, the majority showed binaural inhibition (30.1% ± 4.5% of all binaural interaction classes for sounds at 60 dB SPL). Similarly, the majority of OE neurons showed binaural inhibition (OE/I were 5.3 ± 1.4% of all classes at 60 dB ABL), although these were just a minority of the whole neuronal population. Overall, around 12% of neurons belong to the EO/N, OE/N or EE/N categories, which indicate absence of significant binaural interactions (i.e. monaural neurons).

The local spatial distribution of these binaural categories within the cortex is plotted in Figure 4.9, and can be compared to the preferred ILD distribution of the same neurons

in Figure 4.7. As with the ILD preferences, the binaural categories were often heterogeneously distributed within a local region of the cortex. However, in most imaging fields there was a disproportionally large number of EO/I, EO/F, or OO/F neurons.

The bootstrapping cluster analysis for responses at 60 dB ABL showed that neurons belonging to one of these three binaural classes were likely to be located near each other (within 150 μm) in four out of 15 mice (mice 2, 4, 6, 12). When neurons of all binaural categories where included, the bootstrapped analysis resulted in five mice with significant clustering (all the previous animals and mouse 7). In two of these five mice, BFs were also found to be clustered (mice 2 in Figure 3.6 and Figure 4.7; mouse 12 in Figure 4.7. Note that the map of BFs in this last mouse is not present in Figure 3.6). Clustering of binaural preferences was found in three out of eight mice when tested at 40 dB ABL, and in six out of 15 when tested at 80 dB ABL.

4.3.6 The generation of ILDs at low sound frequencies

Determining the frequency tuning of neurons tested for their binaural preferences not only provides a useful benchmark for my current investigation of the spatial organization of ILD preference distribution, but it is also necessary given the influence that sound frequency has on the generation of ILDs. I find it important to explain this point here, before presenting further results, although this involves a little digression.

Because of the small size of the mouse's head, ILDs produced by low frequency sounds in this species are very small. In particular, the sound pressure transformation at the pinna was estimated to be no larger than 5 dB for 10 kHz pure tones (Chen *et al.*, 1995). Moreover, in a study using prepulse inhibition of the acoustic startle reflex as an indicator of stimulus detection, mice seemed to be unable to recognize changes in azimuth location of bandpass noise containing frequencies up to 8 kHz (Allen and Ison, 2010). Nonetheless, a subsequent investigation involving more classical sound discrimination behavioural tasks reported similar discrimination performance for lowpass and highpass noise (Lauer *et al.*, 2011).

Based on these lines of evidence, it might seem pointless for me to measure the ILD sensitivity of neurons with BFs lower than 10 kHz, because, naturally, these cells are preferentially activated by tones generating negligible interaural level differences.

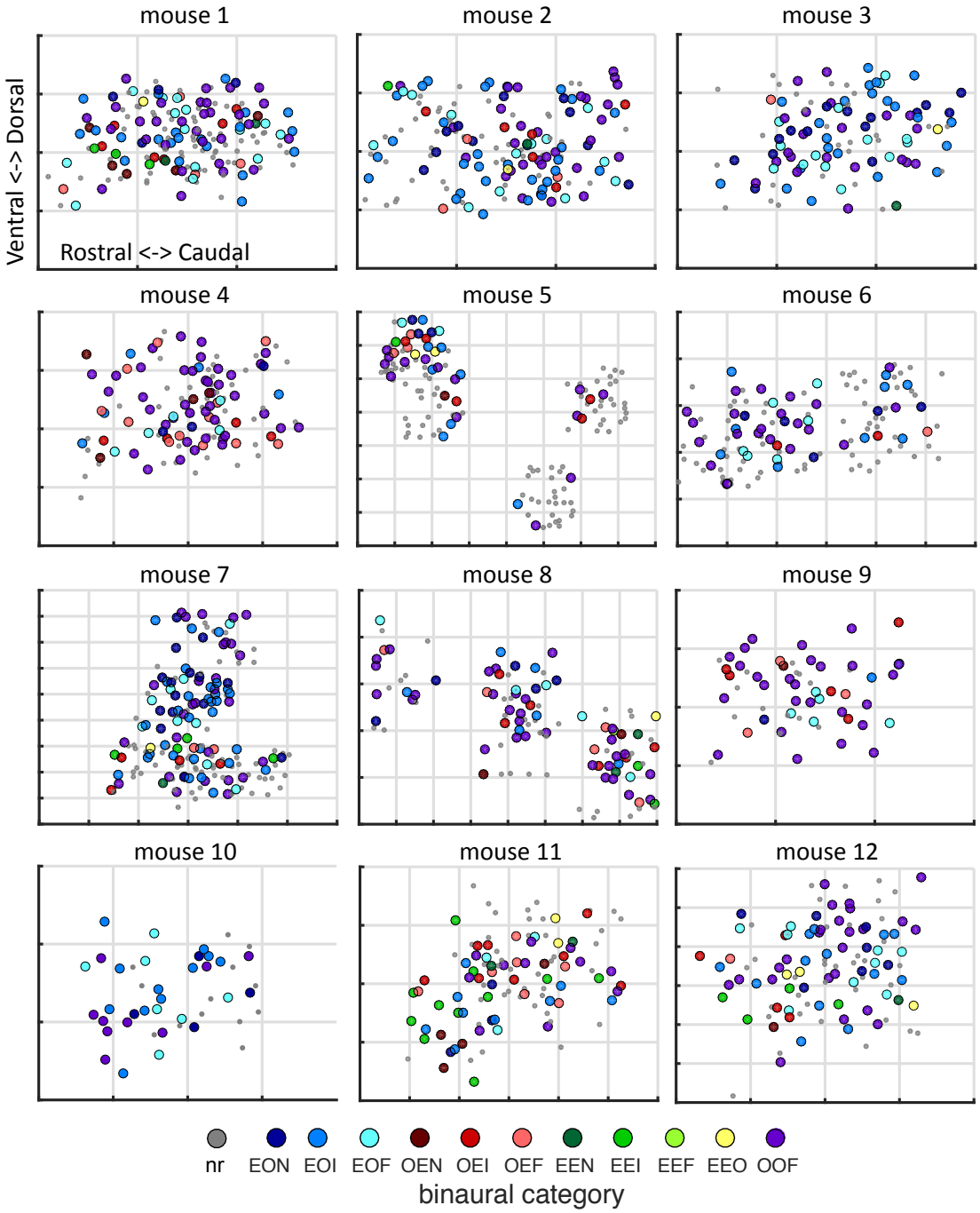

Figure 4.9: Neurons from 12 mice are plotted as in Figure 4.7 and colour coded according to their binaural category. Neurons depicted in grey did not respond to noise stimulation. In these plots, the binaural class of each neurons was derived from the lowest ABL elliciting a response.

However, some important aspects of the generation of ILDs should be considered before excluding these neurons.

Studies quantifying the head related transfer function (HRTF; see section 1.2.1) of laboratory animals, including those mentioned in mice, are generally performed in anechoic environments using free field stimuli. In a paper performing binaural recordings in echoic environments in humans, the size of the ILDs produced was only weakly affected by changes in sound frequency (Młynarski and Jost, 2014), suggesting that low frequency ILDs may be ecologically valid.

Moreover, ILDs generated in far-field conditions are generally smaller than those produced by near-field sounds. For example, ILDs become informative in humans at frequencies above around 4 kHz for tones placed >1 m from the listener's head, while they can be robust and useful for localization even below 1.5 kHz if sounds are located close to the head (Shinn-Cunningham *et al.*, 2000). Consequently, nearby low-frequency sounds in more natural echoic environments may generate larger ILDs in mice than those described by traditional free-field studies in this species. Furthermore, it has been shown that low BF neurons in the brainstem of the cat exhibit sensitivity for ILDs (Tollin and Yin, 2005).

4.3.7 ILD tuning in low BF neurons

To determine whether including neurons tuned to frequencies below 10 kHz (about 30% of my recordings) may have influenced the presence of local clusters of binaural responses, I repeated the bootstrapping procedure after excluding these neurons from my dataset.

ILD preferences did not cluster in any of the mice tested with both binaural noise bursts and pure tones in the same areas (13 mice; 60 dB ABL). Neurons of similar binaural classes formed local groups in three animals. This is therefore very similar to the results obtained with the full dataset.

I then went on to test the prediction that high frequency neurons may be more sensitive to ILDs, compared to low frequency neurons. A comparison of the steepest ILD slope values (from Figure 4.4B) and BFs of all neurons that were responsive and sensitive to both sound parameters (n = 496 neurons at 60dB ABL) revealed no correlation between these two measures ($r = 0.023$, $p = 0.75$) (Figure 4.10).

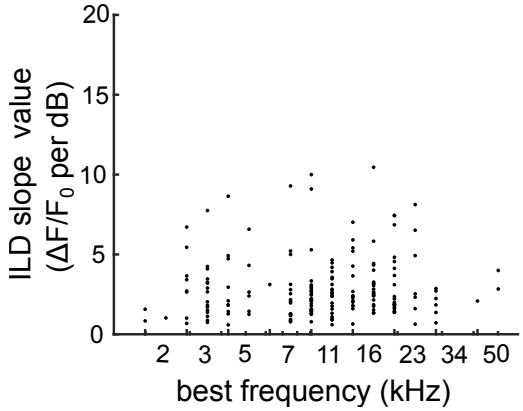

Figure 4.10: A scatter plot displaying the steepest ILD slope of neurons as a function of their BF, for all neurons sensitive to both ILD and tone frequency.

A similar finding has been reported in rat A1 using free-field stimuli (Yao *et al.*, 2013). In this configuration the HRTF of the animals tested would have played a role in shaping ILD generation and sensitivity. Since the filtering effects of the external ear should sharpen spatial receptive fields at high frequencies only, it is striking that cortical spatial sensitivity in rats is frequency independent. This evidence further convinced me to keep low BF neurons in my dataset, together with the evidence that over 90% of the noise-responsive cells were indeed modulated by the ILD, including those with low BFs. Nonetheless, I will discuss this issue more later on in this Chapter.

4.3.8 Evidence for subcortical networks: pairwise correlations

Similarities in the sensory responses of neurons may arise because they are connected together in a local network in which cells fire together. I therefore examined the degree of similarity in ILD sensitivity ("signal" correlations, SCs) and in stimulus-independent activity ("noise" correlations, NCs) between simultaneously imaged pairs of neurons, spaced up to 250 μm apart. The correlations were carried out only on those neurons whose responses were significantly modulated by ILDs.

As the distribution in Figure 4.11A shows, the mean signal correlation in my dataset, after removing the effects of trial-to-trial noise correlations, was 0.3 $\pm$ 0.35 (mean $\pm$ sd; n = 4,255 neuron pairs). Noise correlations were less variable than signal correlations, and mainly ranged from 0 to 0.4, with a mean value of 0.18 $\pm$ 0.16 (Figure 4.11B). Shuffling

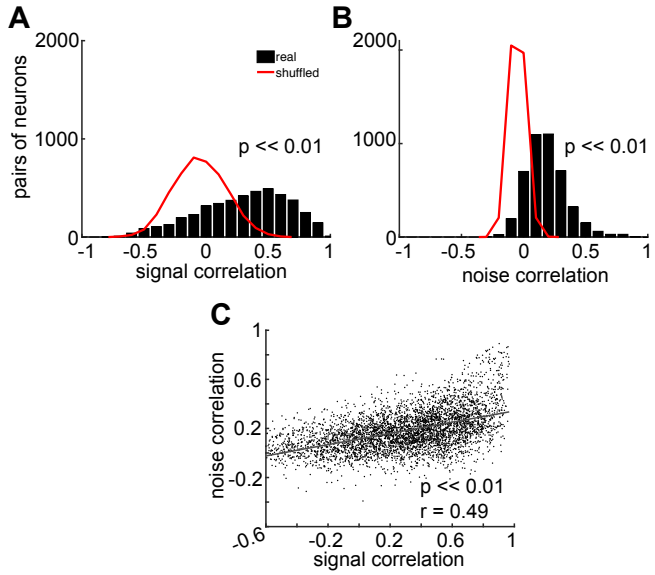

Figure 4.11: In panel A the distributions of pairwise signal correlations during ILD stimuli presentation are shown for real (black bars) and shuffled (red line) data. Panel B, presents data as in A, but for noise correlations. (C) Scatter plot of noise correlations as a function of signal correlations in the same neuronal pairs. The line indicates the best linear fit to the data. The Pearson correlation values for these fits are displayed as text.

the data in a bootstrapping analysis (red lines in the panels), demonstrated that the signal and noise correlations I observed were significantly larger than chance ($p \ll 0.01$). Signal and noise correlations were strongly correlated with each other ($r = 0.49$) (Figure 4.11C).

4.3.9 Binaural and frequency preferences within the local microcircuit

In order to compare the local spatial organization of frequency and ILD sensitivity, I also computed the signal correlations and noise correlations during pure tone stimulation for pairs of simultaneously imaged neurons, responsive to both frequency and noise bursts. Since only a subset of the neurons used for signal correlation and noise correlation calculations in the previous Chapter (section 3.3.5) were used here, the resulting values may be slightly different.

Signal (Figure 4.12A) and noise (Figure 4.12B) correlations were then plotted for both tones (red) and broadband noise (black) stimuli as a function of the distance between neuronal pairs along the dorsoventral (left) and rostrocaudal axes (right), in order to investigate whether cells positioned more proximally in cortical space showed more similar

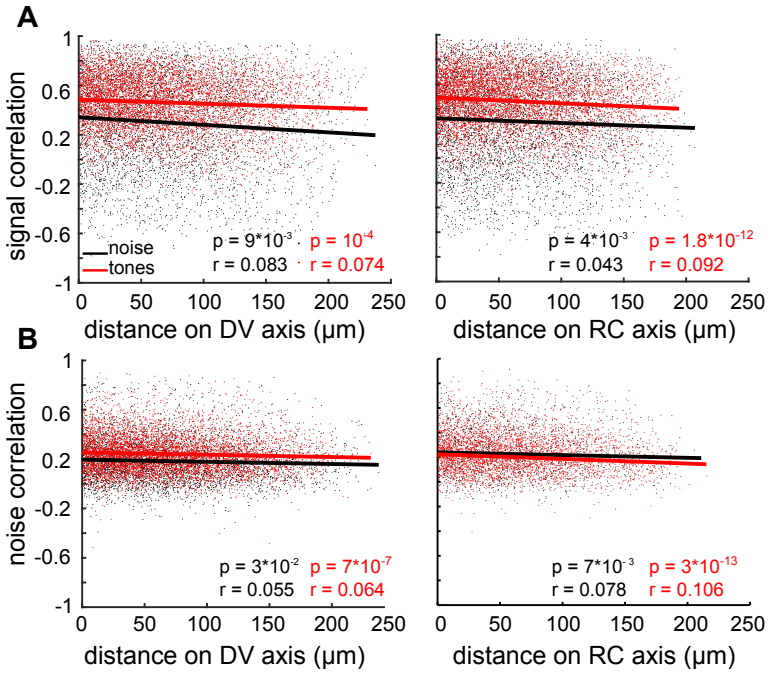

Figure 4.12: A shows the signal correlations calculated during presentation of ILD stimuli (black dots and line) and pure tones (red) as a funciton of dorsoventral (left) and rostrocaudal (right) distance between pairs of simultaneously imaged neurons. B contains data presented as in A, but for noise correlations. In A and B, lines indicate the best linear fit to the data.

responses than distant neurons. I decided to examine the distribution of correlation values on the two anatomical axes separately because the binaural bands described in early studies of cortical binaural sensitivity were found to alternate perpendicularly to the tonotopic gradient (which runs rostrocaudally in the mouse).

The signal correlations (0.46 ± 0.22) for tone responses were much higher than those measured in the responses to ILD stimuli (t-test, $p \ll 0.01$), possibly reflecting the more homogeneous distribution of BFs relative to the preferred ILDs within local regions of the cortex. The noise correlations for pure tone responses (0.24 ± 0.15) were similar to those exhibited by pairs of neurons during presentation of the ILD noise stimuli. A tail of higher correlation values (up to 0.8) was present among proximal neurons, both during ILD stimuli and pure tones presentation, suggesting that nearby neurons were more likely to be active on the same trials. Noise and signal correlations decreased only modestly, although significantly, with distance along the rostrocaudal and dorsoventral axes, as indicated by the r and p values in Figure 4.12.

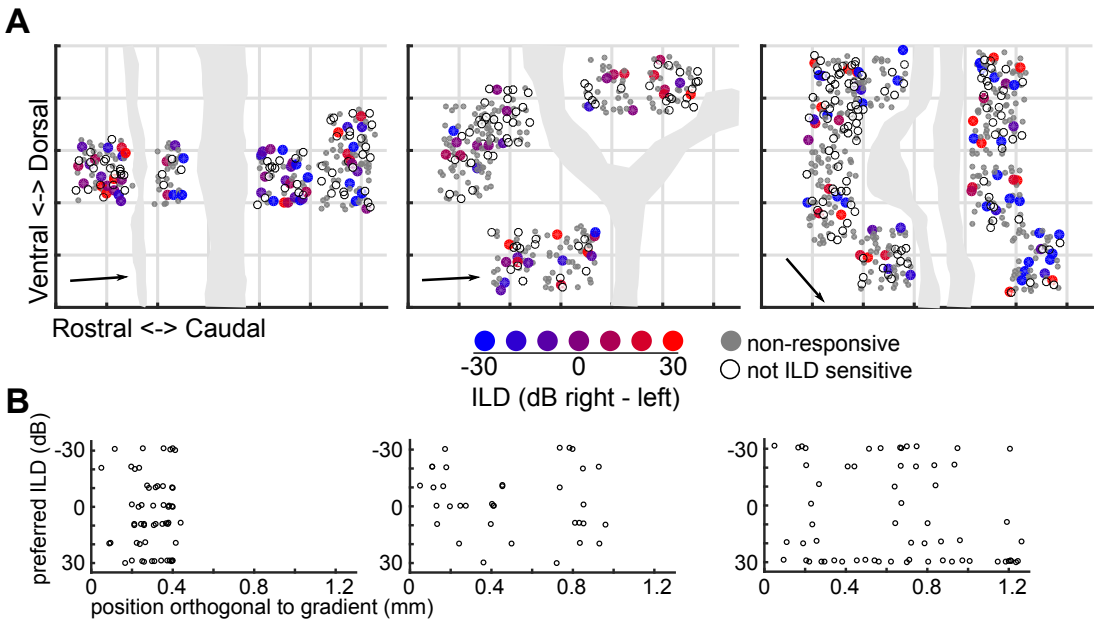

Figure 4.13: Dotted grids indicate 200 μm. Grey areas areas illustrate the position of blood vessels. The arrows indicate the orientation of the tonotopic gradient, calculated according to the BFs of the neurons in each mouse (also displayed in Figure 3.8). In B, preferred ILDs are plotted against distance on the axis orthogonal to the tonotopic gradient. To improve visibility data points have been randomly jittered.

4.3.10 Global arrangement of ILD preferences

I have so far focused on the distribution of binaural sensitivity within local areas (250 x 250 μm) of auditory cortex. As explained in Chapter 3, the availability of a reporter mouse line expressing GCaMP6f in cortical excitatory neurons allowed me to examine the representation of binaural preferences over a much larger area (up to 1.2 x 1.2 mm) in three mice, the same used for pure tone presentation (section 3.3.6).

Out of a total of 992 imaged cells in the three transgenic mice, 40.9% were found to be responsive to noise bursts across the three ABLs and of these, 32% were ILD sensitive. For each mouse, I produced 2D maps similar to those shown so far, reporting the preferred ILDs (Figure 4.13) and binaural classes (Figure 4.14) of the neurons imaged in the three mice. These maps can be compared with those of BFs from the same animals, illustrated in Figure 3.9.

In contrast to the topographic order in the sound frequency representation, visual

inspection of maps of ILD sensitivity suggested that this parameter did not change systematically across the cortical surface (Figure 4.13A). To quantitatively look for trends in the large-scale spatial organization of these responses, I plotted the distribution of preferred ILDs along the axis that was orthogonal to the BF gradient in each mouse (Figure 4.13B). This plot revealed no systematic relationship between preferred ILD and cortical position.

A previous study in bats found that the medial boundary value, corresponding to the ILD at which the neuronal response declines to 50% of maximum, changes systematically across auditory cortex (Razak, 2011). For this reason, I have computed this measure for neurons that monotonically preferred the contralateral space (EO/I and EO/F following the present classification) in the three transgenic mice. However, I did not observe an equivalent shift. This boundary did not regress perpendicular to the tonotopic gradient or with either of the two anatomical axes (data not shown).

For a complete investigation, besides examining the global arrangement of binaural responses, I have as well assessed their local organization in the transgenic mice. The bootstrapped cluster analysis found evidence of ILD clusters in one of the three mice regardless of the sound level at which the preferences were tested (in none of them when excluding BFs <10 kHz).

4.3.11 Global arrangement of binaural categories

Binaural categories also appeared to be heterogeneously distributed overall, although a prevalence of EO/I, EO/F and OO/F neurons was again clear (Figure 4.14A).

I then plotted the number of OO/F and EO/I neurons within 100 μm bins along the isofrequency gradient, as these are the categories usually described as being systematically distributed along this spatial axis.

These neuron types often overlapped, and a clear segregation in clusters was not apparent (Figure 4.14B). The bootstrapped analysis also provided no evidence of clustering of binaural categories in these three mice, not even when only EO/I, EO/F and OO/F neurons were considered (this result was obtained at 40 and 60 dB ABL, while binaural classes clustered in one mouse at 80 dB ABL). Together, these results suggest that on the global scale, if a clear tonotopy is evident in mouse A1, no segregation of neu-

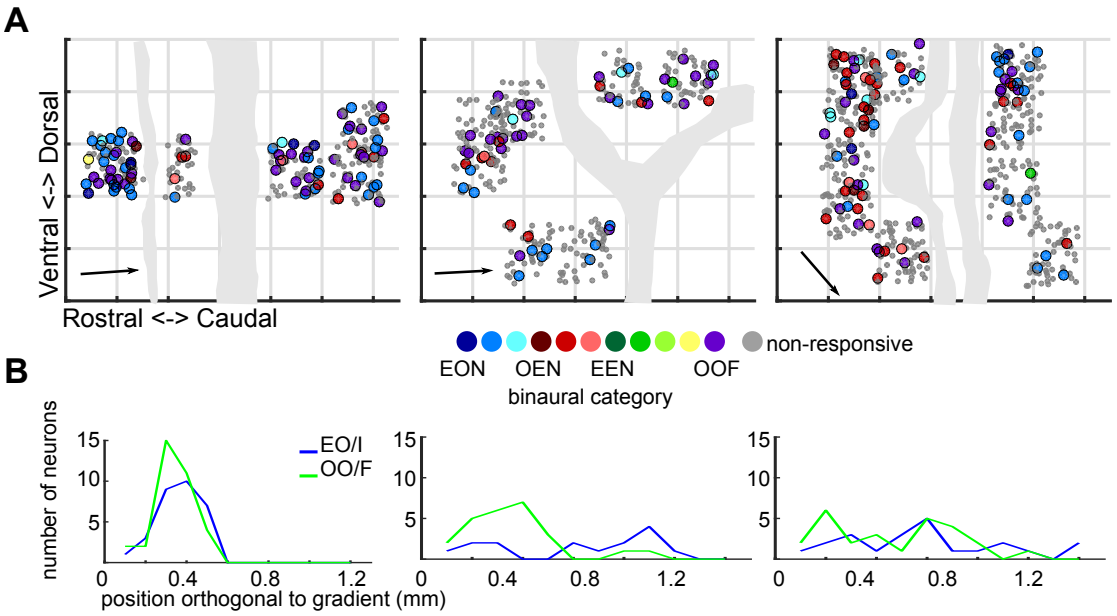

Figure 4.14: 2D plots similar to those in Figure 4.12, but indicating the binaural category of the neurons displayed. In B, the number of EO/I and OO/F cells along the axis orthogonal to the tonotopic gradient is shown separately for each mouse.

rons with different binaural properties is present beyond occasional clustering of binaural properties.

4.4 Discussion

4.4.1 Results overview

In this Chapter, I used *in vivo* two-photon calcium imaging to investigate the local and global organization of ILD sensitivity of layer II-III neurons in the mouse auditory cortex.

The responses of over 90% of the acoustically-driven neurons in my dataset were modulated by binaural interactions. Most of the ILD sensitive cells responded best to values corresponding to contralateral free-field sound sources. Nevertheless, ILD sensitivity varied considerably, and included peaked ILD functions corresponding to midline locations and neurons with a preference for ipsilateral ear stimulation.

Despite this diversity, I found virtually no clustering of neurons with similar ILD sensitivity and occasional anatomical groups of cells of the same binaural category. These results were accompanied by the absence of a systematic variation in binaural properties

across the cortex in most of the mice.

Together with the spectral cues generated by the head and external ears, ILD properties determine the spatial selectivity of cortical neurons in the mouse and therefore indicate that, as demonstrated in other mammals (Middlebrooks, 2002), there is no map of space in the auditory cortex of this species.

4.4.2 ILD sensitivity

My analysis of ILD sensitivity at different ABLs is consistent with the presence of a continuum of binaural sensitivity, ranging from a majority of neurons that are contralateral-dominant (about 65%) to those preferring stimuli that are more intense in the ipsilateral ear. A similar range of ILD sensitivity has been reported in extracellular recording studies in adult mice (Polley *et al.*, 2013), cats (Irvine *et al.*, 1996; Zhang *et al.*, 2004), ferrets (Campbell *et al.*, 2006), and pallid bats (Razak, 2011), which in turn underpins the heterogeneous spatial receptive fields of A1 neurons reported in most of these species (Imig *et al.*, 1990; Mickey and Middlebrooks, 2003; Middlebrooks and Pettigrew, 1981; Rajan *et al.*, 1990; Recanzone *et al.*, 2000; Stecker *et al.*, 2005).

A further common finding between mine and the aforementioned studies is the presence of large numbers of omnidirectional neurons, responding to binaural noise bursts but lacking preference for a particular location.

Together, these results indicate that ILD sensitivity in the auditory cortex of mice is typical of that found in other mammalian species making use of this cue for localization purposes, and that my calcium imaging data are consistent with the results from electrophysiological recordings. As mentioned earlier, rats seemed to provide an exception in this respect, based on the results of multi-unit recordings (Yao *et al.*, 2013) and low-resolution optical imaging studies (Higgins *et al.*, 2010). The authors of these works suggested that the absence of ipsilateral and midline tuning may be the physiological signature of the peculiar inability of these rodents to discriminate sounds within the lateral hemifield (Kavanagh and Kelly, 1987), which is nonetheless a piece of evidence that would benefit from further investigations. However, by recording single-unit activity in response to closed-field stimuli (i.e. directly into the ear canal, like I did), Kyweriga *et al.* (2014) reported proportions of contralateral, ipsilateral and midline preferences

very similar to mine (and to those in larger mammals).

It may then be the case that multi-unit recordings may have favoured the proportion of contralaterally tuned neurons in Yao *et al.* (2013). Indeed, if these are the vast majority in the rat A1, and the recorded signal from a cortical area is averaged across multiple neurons, then all the recorded sites are likely to appear as contralaterally tuned. Another source of discrepancy lies in the fact that Yao and colleagues used free-field stimuli: therefore the reported cortical responses may result from the integration of several spatial cues compared to the closed-field condition (but see Chadderton *et al.* (2009)).

The contribution of different sets of neurons with heterogeneous spatial tuning has recently proven essential in a computational study testing the sound localization performance of various decoders of neural responses (Goodman *et al.*, 2013). The authors obtained only poor predictions when the pooled activity of all cells in one hemisphere was used to estimate spatial location, whereas estimations improved substantially when taking into account the heterogeneity of spatial tuning in these neurons. Interestingly, pooling neuronal responses was found to be particularly suboptimal when the decoders were trained on more realistic acoustic environments, for example, when adding background noise to the binaural signals.

The implications of such findings are threefold. They suggest that the auditory system may require the presence of a continuum of spatial preferences, like the one found in my experiments, to accurately locate sound sources (see also Campbell *et al.* (2006)). They confirm the importance of studying neuronal spatial sensitivity at the single cell level and with high density sampling techniques, such as two-photon calcium imaging. Finally, they could be more directly tested by comparing the sound localization abilities of mice with the decoded ILD responses of large populations of cortical neurons, which in vivo calcium imaging uniquely allows us to obtain.

4.4.3 The ethological relevance of tuning to large ILDs

As in ferrets (Campbell *et al.*, 2006) and cats (Stecker *et al.*, 2005), I found that the slopes of the ILD response functions were sharpest around the midline. This supports the evidence from several species that sound localization accuracy is greatest frontally

(Mills, 1958; Parsons *et al.*, 1999; Recanzone and Beckerman, 2004).

Behavioural studies of sound localization in mice are so far limited (Allen and Ison, 2010; Ehret and Dreyer, 1984; Heffner *et al.*, 2001; Lauer *et al.*, 2011), and it is unknown whether their acuity varies with stimulus eccentricity in the manner predicted by the ILD sensitivity of cortical neurons.

What is clear, however, is that a species should code with maximal accuracy the natural binaural cues that it experiences. In a computational study, it has been proposed that gerbils, rodents with small heads and low frequency hearing, rely on two sub-populations of neurons to accomplish this aim (Harper and McAlpine, 2004). These are preferentially activated by ITDs at the limits or beyond the physiological range. A similar distribution was also found experimentally in the midbrain of the guinea pig (McAlpine *et al.*, 2001). This finding may help interpreting the presence in my experiments of contralateral neurons often responding maximally to the largest ILD presented (-30 dB). Harper and McAlpine explained the necessity of neurons tuned to very large ITDs by finding that the information they convey is maximal around the midline (i.e. for physiological ITDs), and not at the peak of their ITD response curves. Similarly, my neurons exhibited steepest slopes for ILDs corresponding to frontal azimuth locations. This model may explain the presence in my recordings of cells activated by "extreme" ILDs, generated more rarely than narrower values in mice.

Although HRTF measurements in mice indicated that ILDs are very small at low frequencies (Chen *et al.*, 1995; Lauer *et al.*, 2011), this does not take into account the fact that they can become much larger as the source approaches the head (Duda and Martens, 1998). This may be especially relevant in a species evolved to burrow, live in narrow spaces and deal continuously with nearby sounds.

It is important to say at this point that I can rule out the possible criticism that $\pm$30 dB ILD preferences may be an artefact and correspond to simple tuning to monaural stimuli, because over 90% of my acoustically-responsive cells were modulated binaurally (mainly as EO/I and EO/F, plus OO/F).

4.4.4 Spatial organization of binaural preferences

The unique one-dimensional arrangement of the cochlea contrasts with the two-dimensional organization of somatosensory and visual peripheral receptors. As a result, neurons tuned to the same frequency form isofrequency regions within which a systematic variation of sensitivity to stimulus features other than frequency could be found (Ehret and Schreiner, 1997). Among the sound parameters that may be arranged in this fashion, bands of cells with similar binaural properties elongated approximately orthogonal to the isofrequency axis have been described in A1 (Imig *et al.*, 1977; Middlebrooks *et al.*, 1980) and the secondary auditory cortical area (Schreiner and Cynader, 1984) in cats. Later studies described cortical neurons with the same binaural properties as arranged in spatially discrete clusters (Kelly and Judge, 1994; Nakamoto *et al.*, 2004; Recanzone *et al.*, 1999; Rutkowski *et al.*, 2000)).

In order to facilitate comparisons, I have used in this Chapter a categorization scheme of binaural properties already adopted in several previous studies (Kyweriga *et al.*, 2014; Nakamoto *et al.*, 2004; Zhang *et al.*, 2004).

Binaural classes were typically distributed evenly throughout the cortex, with rare OE and EE cells intermingled among the majority of EO/I, EO/F and OO/F neurons. A statistically significant clustering of binaural categories was observed in a minority of the animals. However, this was based on occasional clusters reminiscent of the non-random spatial distribution of binaural cell types described in rats (Kelly and Sally, 1988), ferrets (Kelly and Judge, 1994), and monkeys (Recanzone *et al.*, 1999), but rather different from the anatomically segregated EO and PB areas described in the pallid bat (Razak and Fuzessery, 2002).

My cellular imaging experiments also showed that preferred ILDs are heterogeneous within the local microarchitecture of mouse auditory cortex, and are not spatially organized on a more global scale. Furthermore, my quantitative analysis of ILD-ABL response areas supports the notion that the binaural responses of cortical neurons form a continuum, rather than a number of discrete classes (Campbell *et al.*, 2006). It is therefore perhaps not surprising that clearly segregated patches of neurons with distinct binaural properties were not a prominent feature of A1 in my experiments.

Binaural cues go through an extensive subcortical processing in mammals. Special-

ized ILD regions appear very early in the auditory pathway (the lateral superior olive, see section 1.3.3), and a "point-to-point" map of the space exists in the superior colliculus (see section 1.3.5). This may partly explain the "disorder" in the cortical ILD representation. However, sound frequency is processed subcortically as well, but nonetheless systematically represented in A1. One key difference between these two sound features is that while frequency sensitivity is arranged sistematically within each subcortical nucleus, ILD sensitivity is not. Therefore, the non-systematic arrangement of binaural values in the cortex may simply reflect that of subcortical regions (all, except the superior colliculus). This may even be a necessary solution in the mouse where, given the constrained size of the cortex, wiring neurons with similar spatial properties would happen anyway over short distances (as I already suggested when commenting on the spatial organization of frequency preferences, in section 3.4.4).

Two-photon imaging is optimally suited for shedding light on these possible microscopic peculiarities. Indeed, this method has already highlighted discrepancies in the functional micro-architecture of primary cortical areas of rodents and larger animals, for example, in the organization of orientation tuning in V1 (Ohki and Reid, 2007).

High-resolution calcium imaging in non-rodent species is needed to confirm whether the functional organization of binaural properties is preserved across mammals. To address this issue, two-photon experiments in ferret A1 are ongoing in our research group. So far, a study using low-resolution microscopy techniques (optical imaging of intrinsic signals) in A1 of this species found no evidence for topographic arrangement of ILD sensitivity (Nelken *et al.*, 2008), so I would predict that the heterogeneous organization across A1 of neuronal sensitivity to this binaural cue is likely to be found in other species too.

4.4.5 Methodological considerations

Cortical depth

Another potential source of variability in the organization of frequency preferences comes from the fact that my imaging experiments were restricted to cortical layers II-III.

Some authors have reported that binaural properties vary with depth and that a systematic organization of EI and EE responses may be present in layer IV only (Phillips

and Irvine, 1983; Reser *et al.*, 2000). Similarly, as discussed in section 3.4.2, tonotopy is more pronounced in layers that receive direct inputs from the thalamus (Guo *et al.*, 2012; Winkowski and Kanold, 2013). Moreover, neurons in the superficial layers of rat A1 seem to often show only broadly tuned, subthreshold modulations in response to binaural stimuli, although their spiking spatial receptive fields are narrower than the counterparts from granular layers (Chadderton *et al.*, 2009).

Indeed, a full characterization of cortical spatial response properties needs to take into account the laminar location of cortical neurons and the anatomical origin of the inputs reaching them. In this respect, calcium imaging experiments in cortical layer IV, or simultaneous imaging at multiple cortical depths through multiplexed two-photon imaging may be particularly useful.

Temporal coding

Several electrophysiological studies have demonstrated that the timing of the action potentials generated by auditory cortical neurons can sharpen the spatial tuning provided by a firing rate code (Nelken *et al.*, 2005; Stecker and Middlebrooks, 2003). For example, first-spike latency of cortical neurons in the cat increases along the horizontal axis, with contralateral sounds generally evoking spikes earlier than ipsilateral ones (Eggermont and Mossop, 1998; Mickey and Middlebrooks, 2003; Stecker and Middlebrooks, 2003). Similar evidence emerged later on in ferrets (Mrsic-Flogel *et al.*, 2005) and rats (Chadderton *et al.*, 2009). Although current calcium imaging methods do not provide sufficient temporal resolution to examine these fine temporal spike patterns, their functional relevance remains unclear. Both spike rate and first-spike latencies of responses are informative about a neuron's spatial tuning (Mickey and Middlebrooks, 2003; Mrsic-Flogel *et al.*, 2005; Nelken *et al.*, 2005). However, sound localization accuracy in ferrets can be fully accounted for by a population code that compares the firing rate of A1 neurons with different ILD preferences (Keating *et al.*, 2015). This suggests that the heterogeneous ILD responses revealed through my calcium transients may be sufficient to explain cortical ILD sensitivity and are likely to be behaviourally relevant.

Anaesthesia

My experiments were carried out under anaesthesia so that precisely-calibrated binaural stimuli could be delivered to the ears, to maximize head stability during imaging,

and to facilitate comparison with previous studies of ILD processing.

Although I cannot rule out the possibility that anaesthesia may have played a role in defining ILD sensitivity in my experiments, the spatial tuning of auditory cortical neurons in awake cats and non-human primates has been found to be more level invariant and less influenced by spike timing, but otherwise largely unchanged relative to anaesthetized animals (Mickey and Middlebrooks, 2003; Miller and Recanzone, 2009; Zhou and Wang, 2012). Therefore, it seems unlikely that the use of anaesthesia can account for the imprecise organization of binaural response properties in the cortex. Rather, it appears that the ILD preferences of A1 neurons are more varied within imaging fields than their BFs, as indicated by the marked differences in signal correlations. Thus, the cortical representations of ILDs and binaural response categories are considerably more heterogeneous than BF representations on both a local and global scale.

In the next Chapter, I will add further evidence to the description of the fine-scale organization of sensory responses in the mouse A1, by investigating sensitivity to FM sweeps.

Chapter 5

The representation of FM sweeps in A1

5.1 Introduction

Frequency modulated (FM) sweeps are continuous, monotonic spectral changes in the structure of a sound, and represent a common feature of the vocal calls of many animals, including mice and humans (see section 1.2.2). They are defined by parameters such as bandwidth, duration, rate and direction. These features are extracted from the incoming sounds and encoded in the responses of neurons throughout the subcortical auditory pathway and the auditory cortex (see sections 1.3 and 1.4.2).

Electrophysiological recording techniques have been used in rodents to study the sensitivity of cortical neurons to the rate and direction of FM sweeps, primarily in rats (Gaese and Ostwald, 1995; Ricketts *et al.*, 1998; Zhang *et al.*, 2003) and more recently in mice (Honma *et al.*, 2013; Trujillo *et al.*, 2011). However, the results emerging from these reports are not always consistent across studies and, in addition, show differences with the outcomes of experiments in higher mammals.

An early study in the A1 of the rat, found that 75% of the neurons sensitive to FM sweep direction preferred upward stimuli (Ricketts *et al.*, 1998). In contrast, one of the most recent investigations on FM sensitivity in the mouse described very poor selectivity for the direction of FM sweeps in the same region, with less than 20% neurons showing a direction preference (Trujillo *et al.*, 2011). This later study also investigated

the relationships between the FM direction preference of single cortical neurons and their best frequency, which should emerge as an effect of the "inhibitory sideband" mechanism described in section 1.3.4. However, Trujillo *et al.* (2011) did not find any correlation between the two measures. A different result has been found when the rat A1 was investigated (Zhang *et al.*, 2003). Here, the authors found that the FM sweep direction to which neurons were most responsive correlated strongly with the position of the recorded unit along the tonotopic gradient, with preferences progressing smoothly from upward to downward sweeps as the BFs increased. Given these differences across studies, it seems difficult to outline common principles of FM tuning organization even in two closely related species such as the rat and the mouse. Contrasting results have emerged in primates as well: a correlation between direction selectivity and BFs was found in A1 neurons of the squirrel monkey, but not the owl monkey, in two studies from the same research group (Atencio *et al.*, 2007; Godey *et al.*, 2005).

Such different results may of course arise from methodological differences between these studies. Indeed, similar discrepancies emerged from research in ferrets. Here, the use of logarithmically modulated, as opposed to linearly modulated FM sweeps, did not influence the spatial distribution of preferred rates across the auditory cortical surface: in both cases a coarse organization was found, with spots of preferences to fast FM rates alternating with groups of neurons showing tuning to slow FM sweeps (Mendelson *et al.*, 1993; Nelken and Versnel, 2000). On the other hand, the organization of direction preferences was more influenced by the trajectory of the frequency modulation (either linear or logarithmic). In this case, some clustering of preferences was also described in one study comparing the two types of FM sweeps (Nelken and Versnel, 2000), but spots of opposing direction selectivity were found in the same cortical locations, depending on the paradigm used. Nonetheless, a study focusing on processing of linear FM sweeps in the cat A1 described direction preferences as being "randomly organized" (Heil *et al.*, 1992).

Another open question relates to the relationship between the range of neuronal rate preferences and that of FM rates characterizing species-specific calls. In this respect, several species differences have already emerged. A preference for FM rates which are faster than those occurring in conspecific communication sounds was found in the cat A1

(Heil *et al.*, 1992; Mendelson *et al.*, 1993; Tian and Rauschecker, 1994). To the contrary, FM rate tuning in ferrets and owl monkeys seems to better correspond to the natural FM velocities of vocal calls in these species (Atencio *et al.*, 2007; Nelken and Versnel, 2000). Similarly, A1 neurons in mice have been found to be tuned to FM rates between 0.5 and 3 kHz/ms, which are found in adult mouse calls. On the other hand, an experiment by Honma *et al.* (2013) focusing specifically on slow rate FM processing in the mouse cortex, found that the dorsal posterior and the ultrasound fields encode slower sweeps (typically 0.003 - 0.06 kHz/ms) than A1.

5.1.1 Aims

Irrespective of the specific questions addressed in the previous investigations of cortical responses to FM sweeps, all the studies mentioned above utilized microelectrode recordings (or, in one case, transcranial flavoprotein fluorescence imaging: Honma *et al.* (2013)). None of them carried out a high density sampling of individual cortical neurons, which to date can only be achieved by using high resolution microscopy techniques, like two-photon calcium imaging.

The strength and novelty of my study therefore come from the fact that I have analysed FM responses in an unprecedented number of individual neurons simultaneously. To establish a relationship between FM cortical sensitivity and frequency modulation present in mouse vocalizations, I have presented FM sweeps of both directions, at rates mostly overlapping with those present in species-specific calls, and with bandwidths spanning ultrasonic as well as lower frequencies.

With these experiments, I will try to answer the following questions:

- What are the parameters of frequency modulated sweeps eliciting most of the sensitivity in auditory cortical neurons?
- What is the fine scale spatial organization of the responses to these parameters?
- How does tuning to FM sweeps parameters relate to that to pure tones frequency in individual neurons?

Bandwidth (kHz)	Duration (ms) 25	50	100	500
20	0.8	0.4	0.2	0.04
40	1.6	0.8	0.4	0.08
60	2.4	1.2	0.6	0.12

Table 5.1: FM rates in mice expressing GCaMP6m. Rates in kHz/ms of the FM sweeps presented to the mice expressing GCaMP6m delivered though viral vector injection. The rates resulted from the ratio between bandwidths and durations of the sweeps.

5.2 Methods

Surgical procedures and image analysis are described in sections 2.1 and 2.2.1. Details about the coordinates of the viral vector injections and evidence that imaging was carried out in the core region of auditory cortex are also reported in sections 3.3.2 and 3.3.3.

5.2.1 FM sweep presentation

Twenty-four linear FM sweeps were delivered binaurally at a sound intensity of 70 dB SPL to 11 mice injected with an AAV expressing GCaMP6m in A1. The starting frequency of all sweeps was 2 kHz. Each stimulus was repeated 10 times, in pseudorandom order. As detailed in Table 5.1, three *bandwidths* and four *durations* were used. The ratios between them determined the *rate* of the sweeps, which ranged between 0.04 and 2.4 kHz/ms. The combination of bandwidths and durations presented meant that two rates (0.4 and 0.8 kHz/ms) were presented twice as many times as the remaining eight (i.e. for 20 instead of 10 repetitions). Every sweep was presented in both *directions*: upward (from low to high frequencies) and downward (from high to low frequencies). The inter-stimulus interval was 2 s.

Three mice from the same GCaMP6f reporter line described previously (sections 3.3.6 and 4.3.10) were also used in these experiments. I presented FM sweeps at the same bandwidths used for the injected animals, but at a larger range of durations, which allowed FM sensitivity to be tested at all 10 rates in Table 5.1 plus a further five rates

Bandwidth (kHz)	Duration (ms)					
	5	10	25	50	100	500
20	4	2	0.8	0.4	0.2	0.04
40	8	4	1.6	0.8	0.4	0.08
60	12	6	2.4	1.2	0.6	0.12

Table 5.2: FM rates in mice expressing GCaMP6f. FM sweeps of 15 rates between 0.04 and 12 kHz/ms presented in the experiments on transgenic mice constitutively expressing GCaMP6f.

(Table 5.2).

It is worth noting here that sweeps of particularly short durations may be perceived as clicks to human listeners. However, Trujillo *et al.* (2011) reported that neurons in A1 of the mouse can discriminate between bandwidths of sweeps as short as 3 ms.

Typically, in electrophysiological experiments investigating neuronal sensitivity to FM sounds, the bandwidths of the sweeps are centred on the neuron's BF. This was not feasible in my experiments, given the large number of neurons simultaneously recorded in each imaging field. To address this issue, I used three different FM bandwidths and, in the experiments on GCaMP6f transgenic mice, I varied the starting frequency of the sweeps (2, 22 or 42 kHz). This allowed me to test whether neuronal sensitivity to rates depended on the range of frequencies included in the sweep.

5.2.2 Identifying responsive neurons

As described in section 2.2.2, the response to each presentation of a sweep was examined in two time windows. Here, the pre-stimulation period was comprised of eight frames immediately prior to stimulus onset (∼250 ms), while the stimulation period included 30 frames from the onset of the stimulus (∼1 s). The stimulation period was longer than that used for the analysis of pure tone and ILD responses because of the longer duration of some of the FM sweeps: the 500 ms long sweeps sometimes elicited large calcium transients returning to baseline ∼1 s after stimulus onset, as can be seen in Figure 5.1. For the same reason, I also chose to use a shorter pre-stimulation period for FM sweeps,

starting 1.75 s after the preceding stimulus, in order to avoid including the previous sound-driven calcium transient.

A main aim of my experiments was to determine neuronal preferences for each of the four FM parameters separately: bandwidth, duration, rate, and direction. In order to do so, it is first important to take into consideration that the rate of each FM stimulus is not independent of its bandwidth and duration, as it is in fact the result of the ratio between these two parameters. Thus, to dentify neurons that were responsive to FM stimuli, I performed two separate t-tests (1-tailed, alpha = 0.01): one comparing the average $\Delta F/F_0$ values in the pre and post-stimulus windows across repeated presentations of any sweep of different bandwidth and duration, and the other across repeated presentations of sweeps with different rate and direction.

5.2.3 Determining FM preferences of responsive neurons

To assess the FM sensitivity of responsive neurons, I represented the response of each neuron to each stimulus as the difference between the neuron's average $\Delta F/F_0$ in the stimulation and pre-stimulation periods. I then assessed neuronal sensitivity to each of the four FM parameters by performing ANOVAs on each neuron's responses.

Because FM rate is not independent of bandwidth and duration, the effects of these parameters had to be assessed in two separate ANOVA tests (alpha = 0.05): one using duration, bandwidth and direction as grouping variables, and the other one using direction and rate. If, for instance, a given neuron showed a significant effect of FM rate on its response, then its preferred rate was identified as the one eliciting the highest mean response. A similar procedure was applied to determine the preferred duration, bandwidth and direction of each neuron.

The direction of the frequency modulation may influence neuronal sensitivity to other FM parameters. To verify whether bandwidth, duration and rate preferences remained consistent across directions, I identified them not only by pooling upward and downward sweeps trials together as described above, but also by splitting the dataset into upward and downward trials and analysing them separately. For example, two separate ANOVA tests were carried out on the responses of each neuron to find its preferred FM rate for upward and downward sweeps.

5.2.4 Principal components analysis

The PCA was carried out on a matrix of the mean responses of all responsive neurons (rows), to each stimulus type (columns). For example, to identify common patterns in responses to FM rates and bandwidths, this response matrix consisted of the averaged responses to 12 stimuli (4 rates x 3 bandwidths), producing 12 principal components, ordered according to the amount of neural response variance they explained.

To similarly examine patterns of FM rate and direction tuning, the 20-column response matrix (10 rates x 2 directions) produced 20 principal components.

The same procedure was followed to identify common patterns in response to different durations of the FM sweeps, organized according to bandwidth (4 durations x 3 bandwidths; note that this is the same matrix used to examine rate and bandwidth tuning) or direction (4 durations x 2 directions).

5.2.5 Direction selectivity index

Previous reports had often used a Direction Selectivity Index (DSI) as measure of neural sensitivity to FM sweep direction (Razak and Fuzessery, 2006). This is calculated as follows:

$$DSI = \frac{(up - down)}{(down + up)} \tag{5.1}$$

Where *down* and *up* are the average neuronal responses to downward and upward sweeps, respectively. DSI is a value indicating neuronal preference for upward sweeps when positive, downward sweeps when negative, and no direction preference when near 0.

5.3 Results

I performed *in vivo* two-photon calcium imaging in 11 mice in which the calcium indicator GCaMP6m had been expressed in A1 by AAV injection.

Ten of these mice were also tested with pure tones and ILD noise bursts (Chapters 3 and 4), while one mouse received FM sweep and pure tone stimulation only.

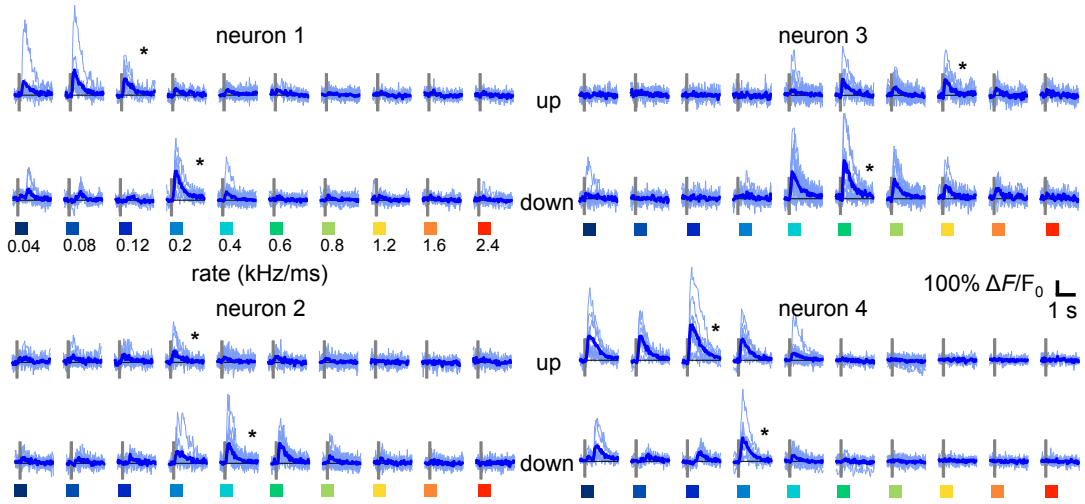

Figure 5.1: Trial wise (light blue) and mean (dark blue) responses of four neurons to sweeps of 10 different rates (columns; see coloured squares below) and 2 directions (rows; upward and downward). Grey bars indicate stimulus onset. Stars indicate preferred rates.

5.3.1 Neuronal sensitivity to FM sweeps

I imaged calcium transients from 1358 neurons in 43 imaging fields with an area of 250 x 250 μm.

While imaging, I presented 10 repetitions of 24 linear FM sweeps, at a sound level of 70 dB SPL. Figure 5.1 shows the responses of four neurons, sorted according to the 10 rates and 2 directions (upward and downward) of the FM sweeps. From these examples, it is evident that cells imaged in the same local area can prefer different rates, as neurons 1 and 4 respond preferentially to lower rates than neurons 2 and 3. These data also illustrate that FM rate tuning often remains similar between up and down sweep directions.

I found that 42.1 $\pm$ 6.9% of imaged neurons (mean $\pm$ se across mice; 572 cells in total) were responsive to at least one of the FM stimuli (paired t-test; $p < 0.01$).

Neurons were often found to be sensitive to the duration and rate of the FM sweeps (Figure 5.2A; respectively 53.4 $\pm$ 2.6% and 42.7 $\pm$ 4.9% of the cells responsive to each of this two parameters; 27 $\pm$ 3.5% and 23.7 $\pm$ 3.5% of all imaged cells), with sensitivity to bandwidth observed less commonly (17.4 $\pm$ 3% of bandwidth responsive cells; 9.8 $\pm$ 1.8% of imaged cells). Only 13.2 $\pm$ 2.9% of the direction responsive cells were found to be

sensitive to FM sweep direction (9.5% of total imaged, 129 cells). Of these, 65.9 ± 8% (85 neurons) preferred upward sweeps and 34.1 ± 8% (44 neurons) responded preferentially to downward sweeps (Figure 5.2B).

The direction of the frequency modulation may influence the sensitivity of cortical neurons for other parameters, such as rate. For this reason, although only few neurons showed direction selectivity, I initially calculated the preferred bandwidth, duration and rate of the FM sensitive neurons separately for upward and downward stimuli. When assessing rate tuning, the majority of sensitive neurons had preferences for slow modulations (Figure 5.2C), with 61.8% of neurons responding preferentially to rates between 0.04 and 0.12 kHz/ms when tested with upward stimuli, and 52.1% when tested with downward sweeps.

When the distributions of rate preferences for up and downward FM sweeps were compared in a χ^2 test, they were found to be significantly different ($p = 1.6 \times 10^{-4}$). *Post hoc* calculation of the adjusted residuals was then carried out to determine which specific rates in the observed distributions significantly differed between upward and downward sweep conditions. It emerged that the overall effect of sweep direction on rate preference resulted from a difference between the direction distributions at only two out of the 10 rates tested: 0.12 and 0.4 kHz/ms ($p = 4.0 \times 10^{-4}$ and $p = 2.0 \times 10^{-4}$; alpha = 0.005 with Bonferroni correction). The two distributions of duration preferences were also found to differ between upward and downward sweeps ($p = 0.0012$), while those of bandwidth preferences did not ($p = 0.056$). Overall, the vast majority of tested neurons preferred short bandwidths (Figure 5.2D) and long durations (Figure 5.2E) both for upward and downward sweep directions, which is in line with the observed consistent sensitivity for slow rates.

5.3.2 Rate sensitivity is invariant to FM bandwidth

The rates of frequency-modulated sweeps are the result of the ratio between their bandwidth and their duration, so it is unclear from the above analysis if neurons are sensitive to the rate of FM sweeps or simply to their duration. One way to examine this question is to compare the rate and duration sensitivty of a neuron across stimuli with different bandwidths. If a neuron is truly rate tuned, its rate response curve should be consistent

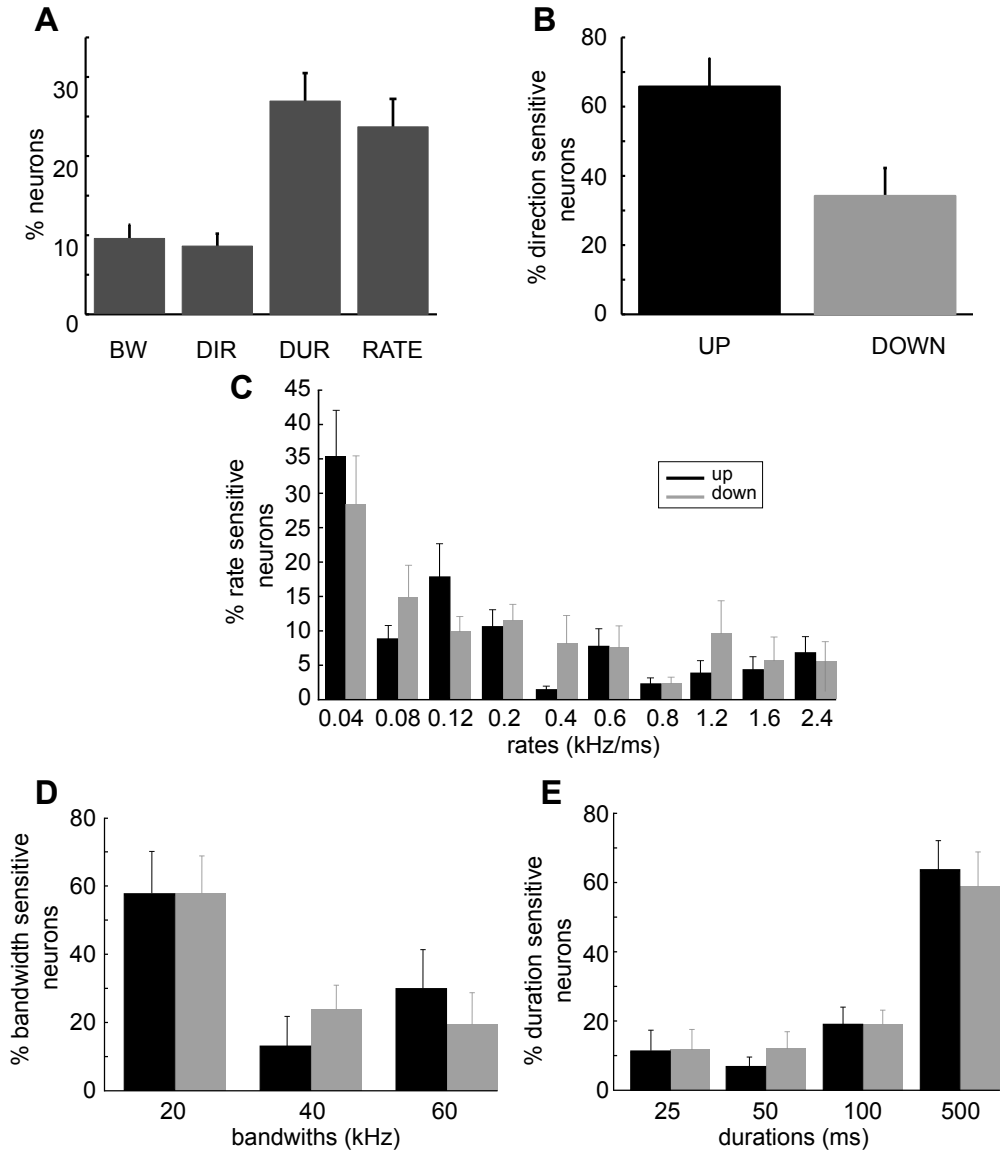

Figure 5.2: Panel A shows the percentages of neurons sensitive to eah of the FM parameters considered, over the total of neurons imaged (bandwidth: BW; direction: DIR; duration: DUR; rate). In B are displayed the percentages of neurons selective to upward and downward sweeps, among those sensitive to the sweeps' direction. (C) Distribution of rate preferences for upward (black) and downward (grey) sweeps. Distributions of bandwidth (D) and duration preferences (E) are shown as in C. All bars indicate means across mice (n = 11); error bars indicate standard errors.

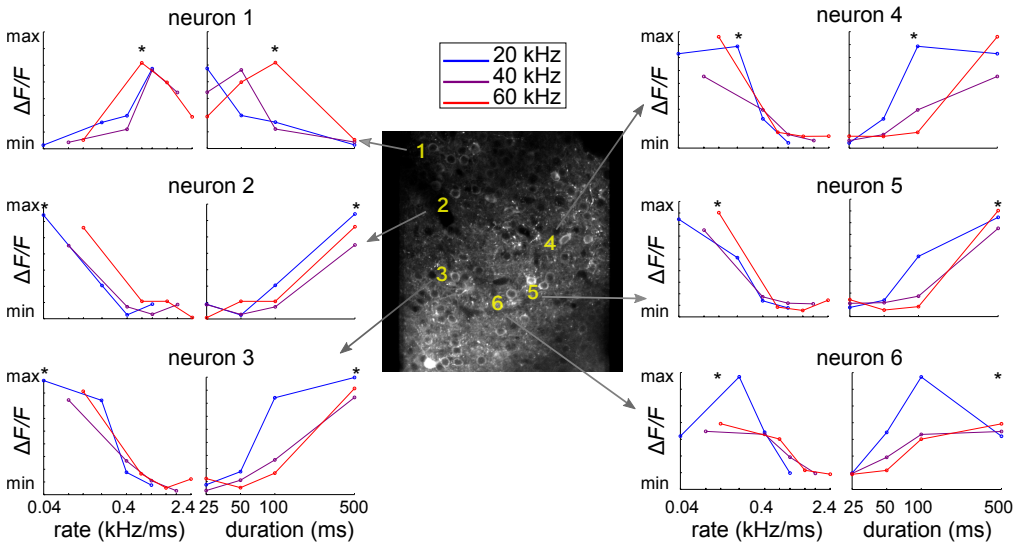

Figure 5.3: Average normalized response curves for six neurons indicated in yellow in the two-photon image in the centre (200 x 200 μm). For each neuron, the rate response curves (left) and direction response curves (right) shown were calculated from trial-averaged responses, and separately for the three bandwidths (see legend). Asterisks indicate neuronal preferred rate and preferred direction calculated across bandwidths. Note that for each bandwidth, only four rates were tested.

and continuous across the three different bandwidths. On the other hand, if the neuron is tuned to duration rather than rate, the duration response curve will be more invariant to bandwidth.

Figure 5.3 shows the rate response (first and third columns of plots) and duration response (second and fourth columns of plots) curves from six neurons in one imaging field, plotted separately for the three bandwidths. The overall preferred rate and duration of the neurons are also indicated in the plots (see asterisks). For all but one of the neurons shown, the duration response curves differ substantially with FM bandwidth. However, when the neuronal responses were plotted against FM rate, selectivity was less affected by bandwidth. The three rate response curves delineated a continuum of responses across the three bandwidths in at least four neurons (neurons 1, 2, 3, and 5).

These findings are representative of the population of neurons imaged in this study, and may indicate that these neurons are tuned to FM sweep rate more consistently than to duration. The same result was also reported by Trujillo *et al.* (2011), who, however, only presented the rate response curves of three example neurons as evidence

for this finding. A more comprehensive examination of cortical rate and duration tuning is necessary in order to firmly conclude that neurons across the entire population are predominantly rate-tuned.

The large number of neurons recorded in two-photon imaging experiments makes PCA a useful tool to capture common patterns in neuronal responses to FM sweeps in a way that is independent from any preconceived expectations. Here, I used PCA to examine the variance in the responses of all FM-driven neurons in my dataset, pooled across all 11 mice. The responses to stimuli presented at each duration and bandwidth combination were averaged across trials.

Figure 5.4 visualizes the coefficients of the first four principal components plotted as a function of FM duration (A) and rate (B). The first of the principal components visualized in 5.4A and 5.4B explains almost half (44%) of the variance, and the consistency of this principal component across bandwidths in the top plot suggests that it represents a preference for an intermediate duration (100 ms). Interestingly, when I repeated the PCA after normalizing responses across neurons (so that the response of each neuron has the same maximum amplitude), this first principal component did not emerge, while the subsequent three principal components were preserved. This suggests that principal component one shown in Figure 5.4 explains the variability in overall response strength across neurons, rather than tuning to FM parameters themselves.

Most of the stimulus-specific response variance in my dataset (29%) was therefore explained by the second principal component shown in Figure 5.4A and B. Visual inspection of the second plot in 5.4A suggests that this component describes a bandwidth-dependent duration tuning. It highlights the tendency for neurons to respond more strongly to longer durations and shorter bandwidths (i.e. faster FM rates). The corresponding plot in Figure 5.4B confirms that this tuning to shorter rates is consistent across all FM bandwidths tested. This result confirms that most of the stimulus sensitivity observed in the responses of neurons to FM sweep stimuli reflects tuning to the rate of the sweeps, rather than to the sweep duration.

The third principal component visualized in Figure 5.4A and B explains only 8% of the response variance. It describes the behaviour of neurons showing a change in response strength when sweeps of intermediate durations and intermediate rates were presented,

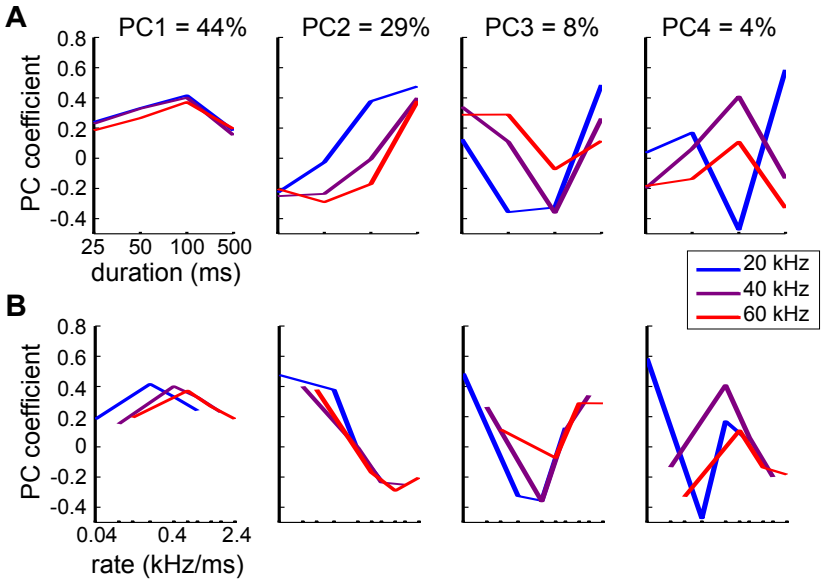

Figure 5.4: Principal components analysis was conducted and the eigenvectors of the first (left), second (centre-left), third (centre-right) and fourth (right) principal components are plotted to illustrate the effects of bandwidth and duration (A) and of bandwidth and rate (B) on neural response variance.

particularly at the narrow and intermediate bandwidths. The fourth principal component explains just 4% of the response variance, and describes a different (almost mirrored) duration tuning between the shortest bandwidth and the two wider bandwidths.

5.3.3 Rate sensitivity is invariant to FM direction

Tuning to FM duration and rate may change not only according to the bandwidth of a sweep, but also to its direction. PCA provides an unbiased way to visualize patterns in these direction-dependent changes in responses across my population of neurons.

I computed the PCA on the same responses analysed above, but here I calculated the trial-averaged responses for each duration and direction combination (i.e. eight stimulus conditions), pooling across bandwidths. In a separate PCA, trial-averaged responses were computed for each of the 20 rate and direction conditions.

The coefficients of the first four principal components are plotted in Figure 5.5, for the duration (A) and rate (B) analysis. Again, the first principal component explained a large amount of variance in neural responses (45% for duration, and 37% for rate), but repeating the PCAs with normalized responses showed that these first components

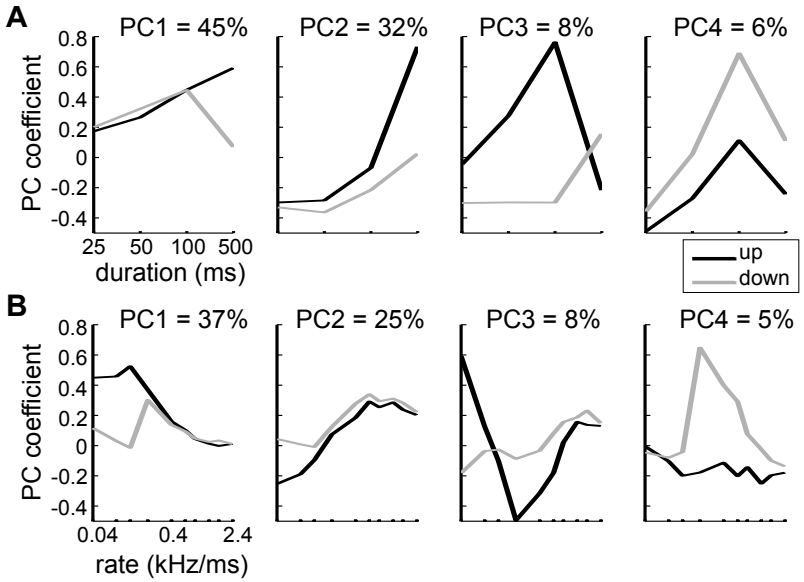

Figure 5.5: The first four principal components resulting from the PCA are visualized here as in Figure 5.4, but illustrating the effects of direction and duration (A) and of direction and rate (B) on neural response variance.

returned the differences in overall response strength across neurons.

The second principal component therefore explained the majority of the stimulus-specific variance in Figure 5.5 (32% for duration, and 25% for rate), as observed in Figure 5.4. Here, the second component described a monotonic sensitivity that is similar between upsweeps and downsweeps across most rates tested. The duration tuning, however, is more direction-dependent.

The third and fourth principal components in both the direction and rate analyses explained relatively little variance. Overall, the most direction independent response described is principal component two for the rate analysis, in which neurons responded similarly in the two directions to sweeps of all rates, except the two slowest ones.

5.3.4 The effect of starting frequency on FM sensitivity

To investigate whether neural sensitivity to FM sweep parameters was influenced by the range of frequencies crossed by the sweep, rather than by FM features such as rate and direction, I presented FM sweeps of 20 kHz bandwidth starting at three different frequencies (2, 22, and 42 kHz) to three transgenic mice expressing GCaMP6f in cortical

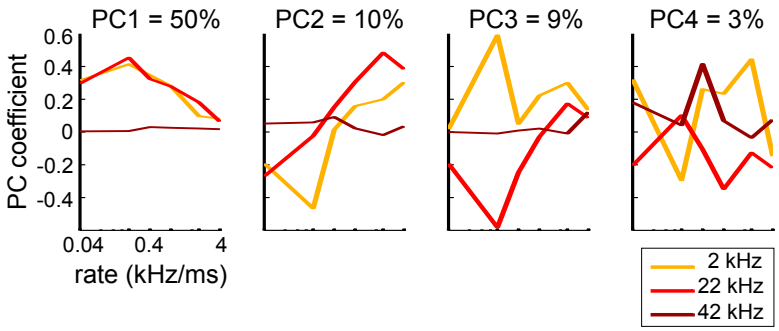

Figure 5.6: Starting frequencies were 2 (yellow), 22 (red) and 42 kHz (dark red). The eigenvectors of the first four principal components resulting from the PCA are plotted as in Figure 5.4 and Figure 5.5, but as a function of FM rate.

excitatory neurons.

Once again, I took advantage of the unbiased nature of PCA to answer this question. The most striking result of this analysis (Figure 5.6) is the lack of rate tuning for sweeps starting at 42 kHz in all of the first three principal components. Indeed, the coefficients of the principal components for the sweeps starting at 42 kHz are all near zero, indicating a failure of the neuron to deviate from its average response. This is expected because such upsweeps would end when reaching a frequency of 62 kHz, crossing a spectral range that is well outside the excitatory tuning curve of most of the neurons in my recordings. The same is also true for downward sweeps starting at this frequency, which would end at 42 kHz, a frequency higher than most neuronal best frequencies in A1 (Figure 3.2 and 3.8) (Tsukano *et al.*, 2016).

For sweeps starting at lower frequencies (2 and 22 kHz), neural response variance is mostly explained in the peaked responses of highly active neurons. The second principal component represents the variability introduced by neurons showing monotonic sensitivity to FM rates, particularly for sweeps starting at 22 kHz. These results may suggest that the FM starting frequency has little influence on FM responses as long as the sweep crosses the excitatory area around the best frequency in the neuron's FRA. Nonetheless, this hypothesis should be tested on a larger dataset, as these conclusions are drawn from a relatively small number of responsive neurons in only three mice.

5.3.5 Local organization of rate preferences

The rate of an FM sweep is possibly its most relevant parameter, because it ultimately contains information about the spectro-temporal complexity of the sweep, indicating the speed at which frequency changes.

As I just showed, FM rate is the parameter, together with duration, which most of the FM responsive neurons imaged in my study are sensitive for. Furthermore, neuronal tuning to rate is invariant to the bandwidth of the sweep, while tuning to duration is not. Thus, I will examine the spatial organization of preferences for FM rate and FM duration through 2D maps obtained in the 11 mice imaged. Because only a minority of neurons were found to be sensitive to the direction of FM sweeps (Figure 5.2A), the responses to up and downward sweeps were pooled to determine the overall rate and duration preferences for neurons in these maps.

Mice 1 to 9 in Figure 5.7 and 5.8 are the same animals shown in Figure 3.6 and 4.7, where the spatial organization of frequency preferences and binaural preferences was analysed, respectively. Mouse 12 is reported in Figure 3.6, but not in Figure 4.7. Note that the imaging fields displayed here for FM stimuli in mice 3, 4, 5, and 9 were at different cortical depths within layers II-III, but at similar rostrocaudal and dorsoventral positions, to those shown in Figure 3.6 and 4.7. Thus, they show responses from different neurons.

Best FM rate maps

By visually inspecting Figure 5.7, we see that mice 2, 3, 4, 6 and 9 were all characterized by tuning to slow rates. This may have been a consequence of the fact that viral vector injections were carried out using the same coordinates in all mice, and thus a progression of rate preferences may have been apparent only in those animals in which the labelling covered a larger cortical area (mice 5, 7, 8, 12). Interestingly, the spatial organization of rate sensitivity seemed to be correlated to that of frequency sensitivity, with areas that are tuned to low frequency tones (Figure 3.6) emerging here as tuned to slow rates and *vice versa*, in a rostrocaudal gradient of preferences. This was most clear in mouse 5, but perhaps also present in mice 1, 8 and 12 as well. In contrast, no systematic organization of rate preferences, nor of frequency preferences, was apparent in mouse 7, despite the large cortical area sampled.

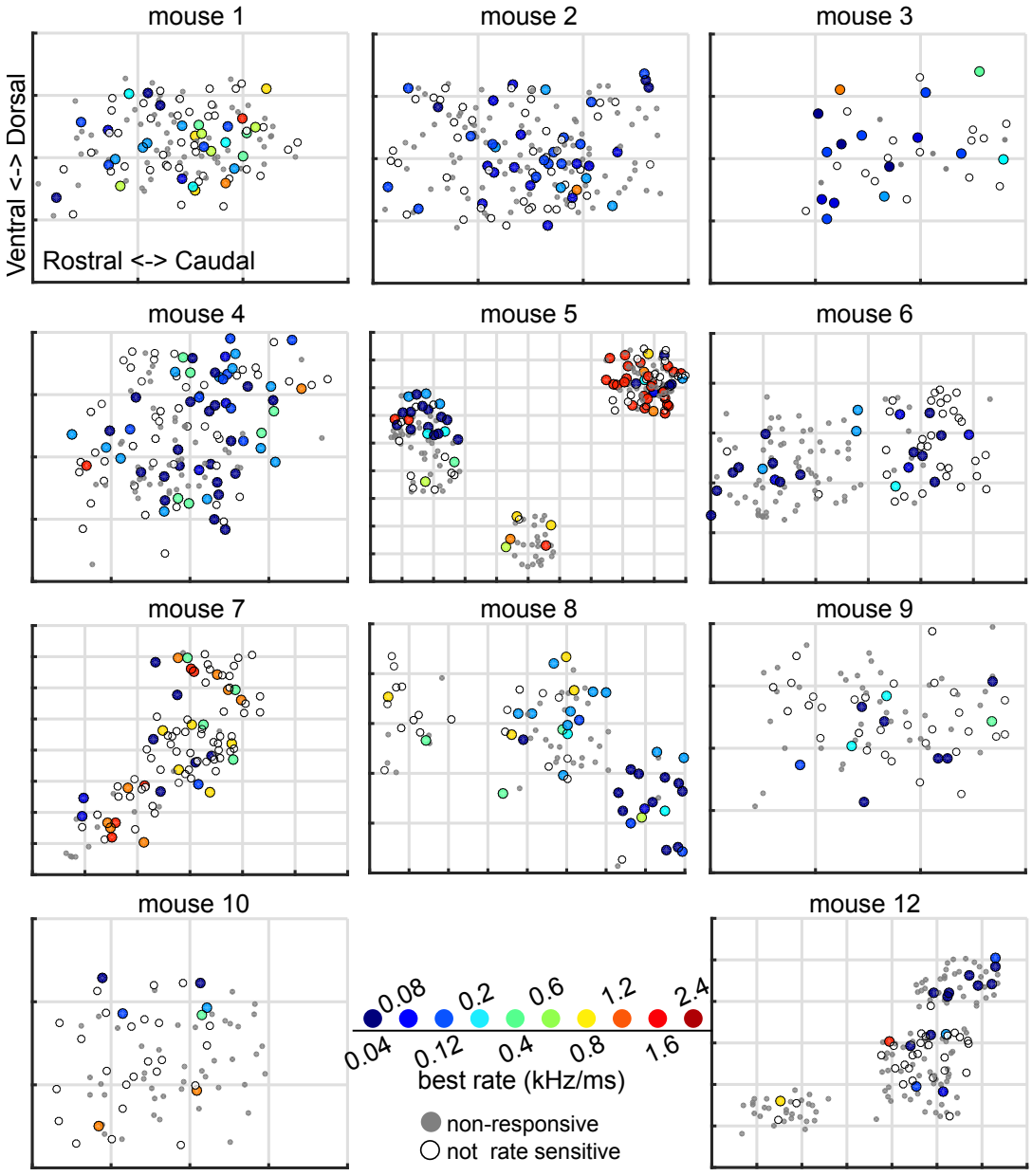

Figure 5.7: Neurons in 11 mice are plotted according to their position on the rostrocaudal and dorsoventral axes. Non-responsive neurons are represented by grey dots, while responsive neurons that are not sensitive to FM rates are represented by white dots. Sensitive neurons are colour coded according to their best FM rate. Each dotted square in the maps delineates an area of 100 x 100 μm.

A bootstrapped analysis (see 2.2.7) revealed that the rate preferences of neurons located within 150 μm in 3D cortex space were more similar than those of more distant neurons in five out of 11 mice. Three of these five mice also showed local clustering of sound frequency preferences.

Best FM duration maps

Perhaps unsurprisingly, duration preferences (Figure 5.8) showed a similar arrangement to that observed for rate responses.

There is a particularly clear segregation of tuning visible in mouse 5, in which there are two distinct areas: one tuned to short durations and another to long durations. Furthermore, there is a progression of preferences from short, to mid, to long durations present in mouse 8.

The bootstrapped analysis identified significant clustering of duration preferences in four out of the 11 mice. Three of these four mice showed clustering of frequency preferences and of rate tuning as well. Table 5.3 summarizes the results of the bootstrapped analysis run on preferences to pure tone frequency, FM rate and FM duration.

When the bootstrapped cluster analysis was run on responses to upward and downward sweeps separately, the same number of mice and in fact the same mice, reported a positive result both for rate (five mice) and for duration (four mice) when tested for upward sweeps, as found when both directions were pooled. There was modestly more neuronal clustering for downward sweeps, where the cluster analysis was significant in six mice both for FM duration and rate. These are the same mice described above, plus mouse 9.

5.3.6 Global organization of rate preferences

With the aim of studying the global organization of responses to FM parameters, I imaged calcium transients in three transgenic mice expressing GCaMP6f in cortical excitatory neurons.

Unfortunately, I was able to sample a region extending ~500 μm rostrocaudally in one mouse and less than that in the other two. The reasons for the limited amount of data I was able to collect in these animals are not clear. However, I believe it could be due to a drop in the expression of the transgene (GCaMP6f) in litters born after several

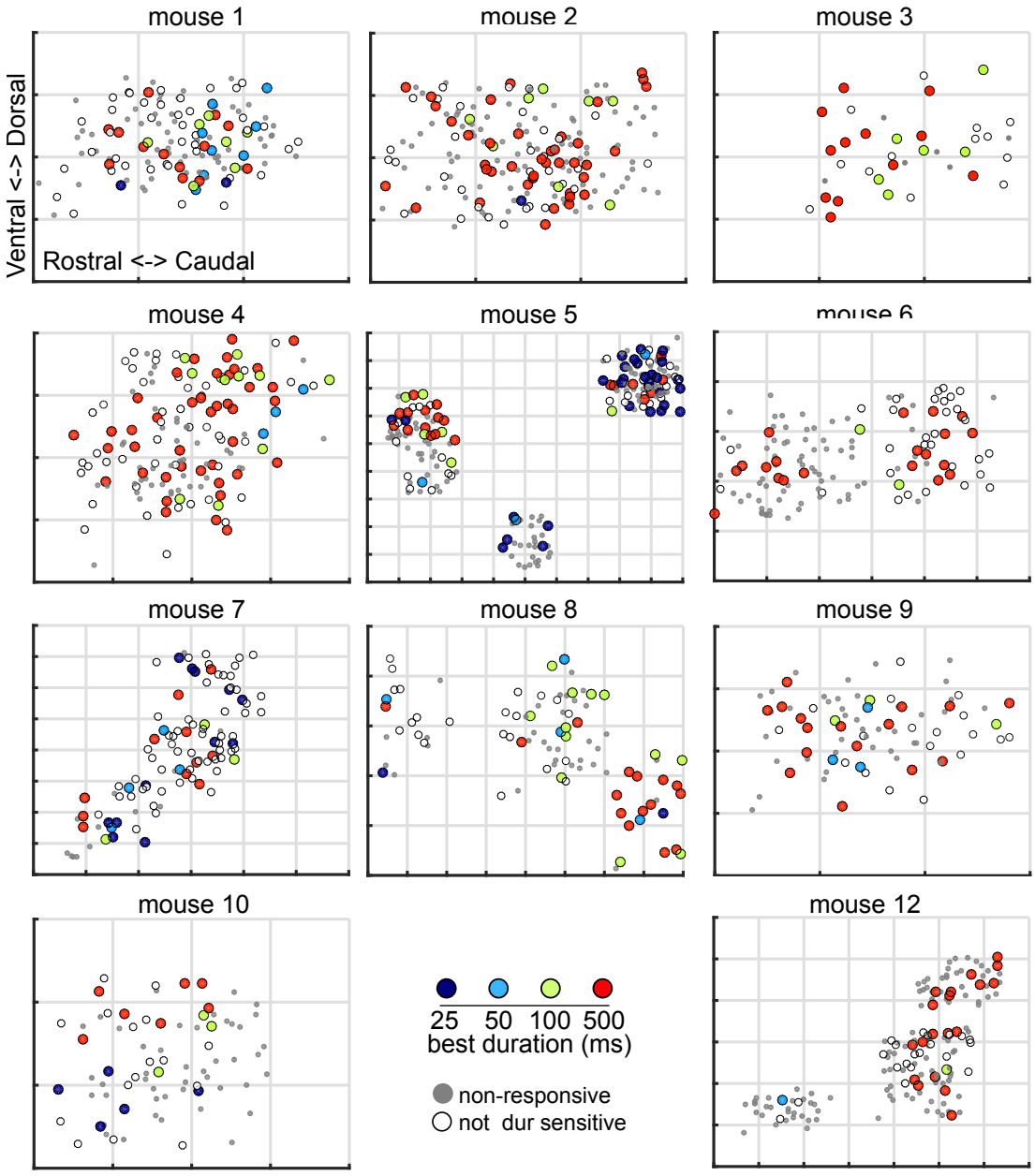

Figure 5.8: Spatial plots of neurons in the same 11 mice shown in Figure 5.7. Neurons are colour coded according to their best FM duration. Each dotted square in the maps delineates an area of 100 x 100 μm.

	Frequency	FM rate	FM duration
Mouse 1		✓	✓
Mouse 2	✓	✓	✓
Mouse 3		✓	
Mouse 5	✓	✓	✓
Mouse 8	✓	✓	✓

Table 5.3: Summary of mice in which best frequencies, preferred FM rates and preferred FM durations clustered in neurons located up to 150 μm apart in 3D cortical space.

crossings of the same line.

A total of 533 neurons were imaged in the three mice, and 32.4% of these were responsive to FM sweep stimulation (t-test, $p = 0.01$). The lower proportion of neurons responsive to FM sweeps was likely due to the lower sensitivity of GCaMP6f compared to GCaMP6m (Chen *et al.*, 2013). Sixty cells (11.2% of total imaged) were found to be sensitive to FM sweep duration, and 51 cells were significantly modulated by rate (two-way ANOVA, $p < 0.05$).

Similarly to my results in GCaMP6m injected animals, smaller proportions of neurons were sensitive to FM sweep direction (12 cells; seven preferring upward sweeps, and five preferring downward sweeps) and bandwidth (17 cells). Again confirming the data from the injected animals, 58.5% of sensitive neurons responded preferentially to the longest FM duration, and 73.6% preferred the three slowest rates presented.

Two-dimensional maps of frequency (left), FM rate (centre) and FM duration preferences (right) from the mouse with the most extensive imaging are shown in Figure 5.9.

5.3.7 Evidence for local subnetworks: signal correlations

The maps of best FM rate and durations, together with the results of the cluster analysis in this Chapter, suggest that the fine-scale organization of preferences for FM parameters may be more homogeneous than that of binaural responses, and thus more similar to that of frequency tuning.

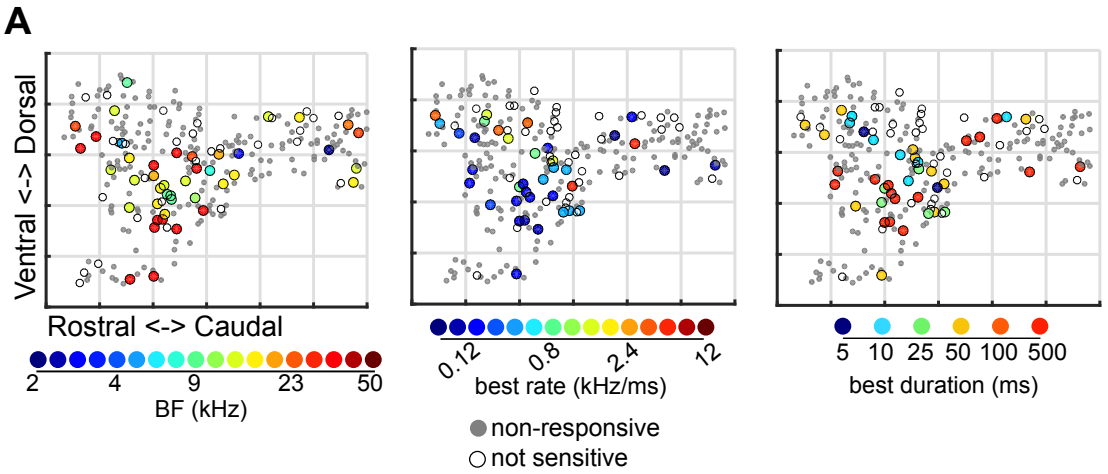

Figure 5.9: 2D maps obtained from one transgenic mouse expressing GCaMP6f. Neurons are colour coded according to their BF (left), best FM rate (centre), and best FM duration (right). Note that the durations of the sweeps, and thus the rates, are different from those used in the mice previously presented in this Chapter. Each dotted square delineates an area of 100 x 100 μm.

To test this claim more directly, I computed the signal correlation between pairs of neurons recorded in the same imaging field during FM sweep and pure tone stimulation, for neurons distant up to 250 μm. This measure has already highlighted differences in the local organization of binaural and frequency preferences (section 4.3.8).

The mean signal correlation for FM sweeps, after removing the effects of trial-to-trial noise correlations, was 0.40 $\pm$ 0.36 (mean $\pm$ sd; n = 1451 neuron pairs) (Figure 5.10A, grey line).

To examine if neighbouring neurons are more likely to be active together during FM sweep or pure tone presentation, I have then plotted signal (Figure 5.10B) and noise (Figure 5.10C) correlations for both FM sweeps (black) and tones (red) as a function of the distance between neuronal pairs along the dorsoventral (left) and rostrocaudal (right) axes. It is useful to compare this figure with Figure 5.11, to verify the hypothesis that signal correlations during FM sweep and pure tone stimulation are more similar to those during FM sweep and binaural noise burst presentation.

Note that the correlation values during tone (Figure 5.10) and binaural noise stimulation (Figure 5.11) may be slightly different from those reported in sections 3.3.5 and

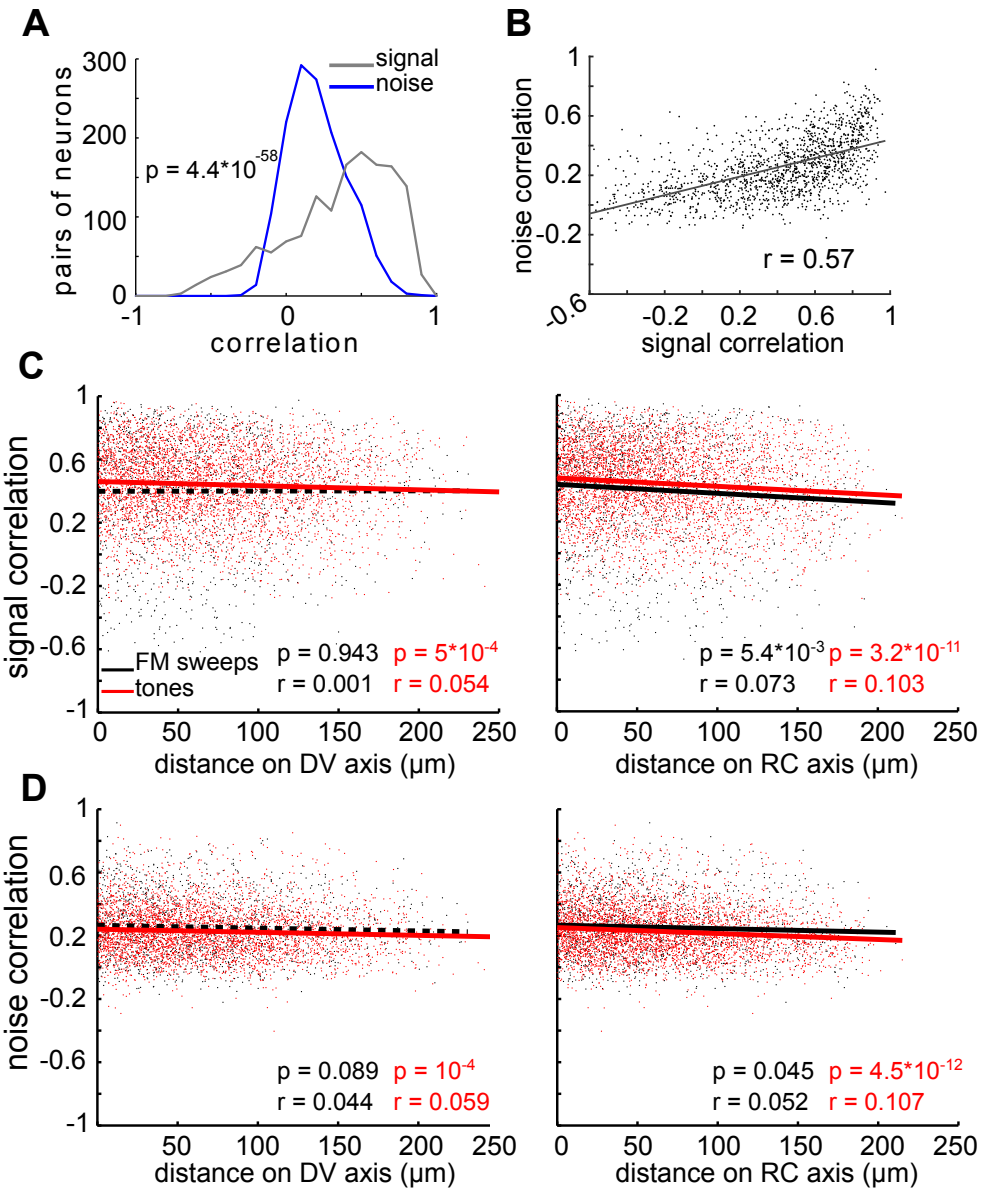

Figure 5.10: Panel A shows the distribution of the signal (grey) and noise correlations (blue) between pairs of neurons responsive to FM sweeps. (B) NCs are plotted as a function of SCs for all the neuronal pairs tested. (C) The same SCs are plotted as a function of neuronal distance for pairs of neurons responsive to FM sweeps (black) and pure tones (red). Lines indicate the best linear fit to the data and are continuous in case of significant correlations (alpha = 0.05). The Pearson correlation values for the fits are displayed as text. In D data are shown as in C, but indicating NCs.

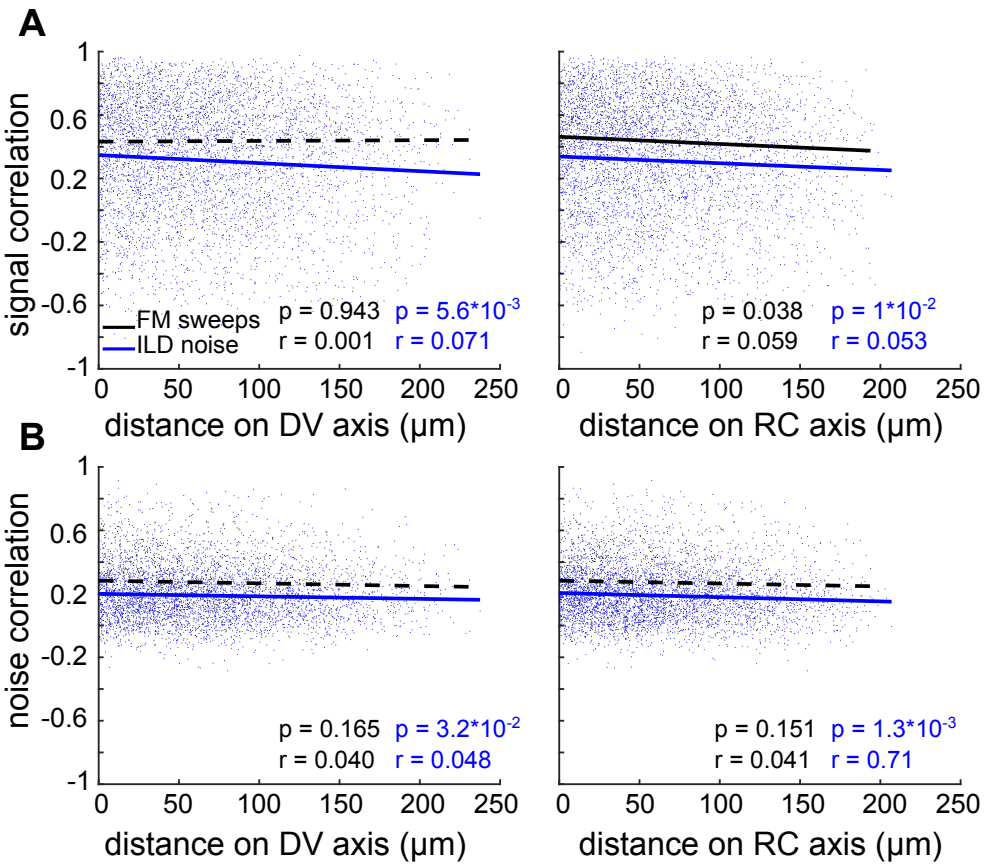

Figure 5.11: Plots of signal (A) and noise (B) correlations, visualized as in Figure 5.10, but calculated during presentation of FM sweeps (black) and ILD stimuli (blue). Lines indicate the best linear fit to the data and are continuous in case of significant correlation (alpha = 0.05). The Pearson correlation values for these fits are displayed as text.

4.3.8, as only a subset of neurons was tested here, namely those that had received FM stimulation as well.

Signal correlations for FM sweeps were marginally lower than those for pure tones, both when measured along the dorsoventral and the rostrocaudal axis. However, this small difference between the overall signal correlations for FM sweeps and tones was statistically significant (t-test; $p = 3.25 \times 10^{-7}$): this result may have been influenced by the particularly large size of the samples. In contrast, the signal correlations for FM responses were much higher than those measured in the responses to ILD stimuli (t-test; $p = 2.11 \times 10^{-25}$). The weak decrease in FM signal correlation with increasing distance between neurons was only significant along the rostrocaudal axis (Figure 5.10B

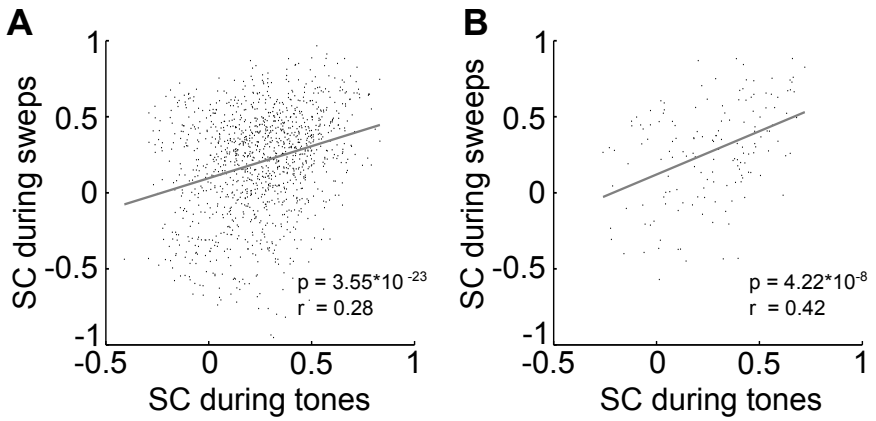

Figure 5.12: Signal correlations during presentation of FM sweeps are plotted as a function of the signal correlations obtained during pure tone presentation. Pairs of neurons selective for FM rate (A) or FM direction (B) are used. The continuous lines indicate a significant correlation between the two measures (alpha = 0.05).

and 5.11A) (r = 0.073; p = 0.0054), the same axis along which the tonotopic organization of frequency responses extends, and on which the pairwise SCs during pure tone presentation are more influenced by neuronal distance. This result further emphasizes the possible presence of common principles underlying the spatial organization of responses to these two tonal sounds.

To further test this hypothesis, I explored whether cells showing similar FRAs were also responding similarly to frequency modulation. I compared the SCs in response to pure tones and FM sweeps for pairs of neurons that were sensitive to both these types of stimuli.

When neurons significantly modulated by sound frequency and by FM rate were taken into account, their signal correlations calculated during FM sweep and tone presentation showed a positive correlation (Figure 5.12A; r = 0.28; p = 3.55x10^{-23}). In addition, when neurons sensitive to pure tones and direction of the FM sweeps were tested, their signal correlations were even more strongly correlated (Figure 5.12B; r = 0.422; p = 4.22x10^{-8}). Note that a smaller number of cells were included in this latter comparison, given the weak direction selectivity in my recordings.

Together, these results indicate that neurons tending to be active together during pure tone presentation, and thus having similar frequency tuning, are also more similarly

modulated by the rate and direction of frequency modulated sweeps.

5.3.8 Evidence for local subnetworks: noise correlations

Together with signal correlations, also pairwise noise correlations may be used to assess the presence of local subnetworks in my recordings.

During FM sweep stimulation, these were significantly lower than signal correlations, with a mean value of 0.25 ± 0.19 ($p = 4.4 \times 10^{-58}$; Figure 5.10A, blue line). When the NCs of each neuronal pair were compared to their SCs these were found to be highly correlated (Figure 5.10B; $r = 0.57$; $p \ll 0.001$), indicating that neurons active together may have similar FM preferences.

Noise correlations decreased significantly along the rostrocaudal (Figure 5.10C; $r = 0.052$; $p = 0.04$), but not the dorsovetral axis ($r = 0.044$; $p = 0.09$). However, this trend was twice as steep as the one detected for noise correlation during pure tones presentation (rostrocaudal axis: $r = 0.107$; $p = 4.5 \times 10^{-12}$). Finally, noise correlations during FM sweep presentation were significantly higher than those during binaural noise stimulation (Figure 5.11B; t-test; $p = 6.39 \times 10^{-46}$).

Noise correlations are not informative about neuronal sensory receptive fields but, reflecting the trial-to-trial variability in neuronal responses, they give an indication about the general state of the network that the imaged neurons are part of. For this reason, I expected noise correlations measured during the three stimulus types to be fairly similar. I would than argue that the difference emerging when noise bursts as opposed to FM sweeps were delivered may be a consequence of slightly different physiological state of the animals (e.g. in the level of anaesthesia).

5.3.9 Correlation between FM direction sensitivity and BFs

If sensitivity to the direction of FM sweeps is defined by sideband inhibition (see section 1.3.4), a correlation between BF and FM direction tuning should exist in cortical neurons. Specifically, neurons tuned to low frequencies should respond preferentially to upward sweeps and vice versa.

A well-established measure of direction selectivity relies on the calculation of the Direction Selectivity Index (DSI; see section 5.2.5 for details). It is common practice to

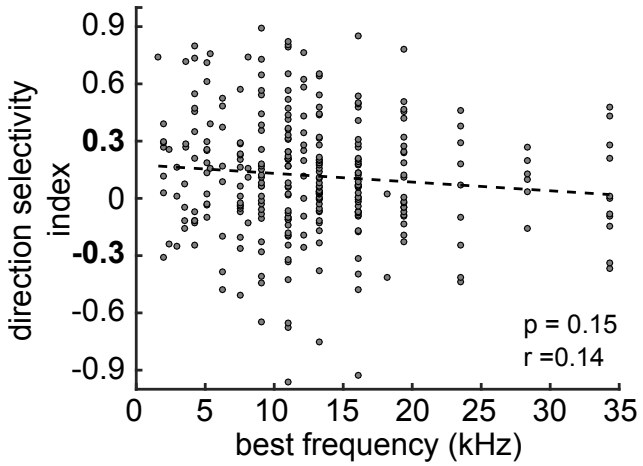

Figure 5.13: DSI values of neurons plotted as a function of their BFs. The dotted line indicates the absence of significant correlation between the two measures when only neurons with -0.3 > DSI > 0.3 were considered (alpha = 0.05).

define a neuron as significantly modulated by FM direction when its DSI is below -0.33 (downward tuning) or above +0.33 (upward tuning) (Hage and Ehret, 2003; Zhang *et al.*, 2003).

I calculated the DSI of all neurons imaged during both pure tone and FM sweep stimulation (1543 neurons, across eight GCaMP6m injected mice and three transgenic mice). Of these, neurons found to be sensitive to FM sweep direction (ANOVA; $p < 0.05$) often had a weak DSI (0.2 ± 2.1; mean $\pm$ sd). Figure 5.13 shows neuronal DSI plotted as a function of the BFs of the same neurons. Only 99 neurons were significantly modulated by sound frequency and characterized by a significant DSI. A comparison between these two measures in these neurons revealed no correlation, ($r = 0.09$; $p = 0.12$). Note that only neurons with BFs up to 35 kHz were considered: these are 98.3% of the frequency-sensitive neurons in my dataset, and this frequency is the upper limit of the range of best frequencies described in the mouse A1 (Linden *et al.*, 2003; Stiebler *et al.*, 1997).

5.3.10 Correlation between best FM rates and BFs

To test whether the frequency preference of a neuron is informative about its tuning to the rate of FM sweeps, I compared the BFs and best FM rates of all neurons significantly modulated by both these parameters.

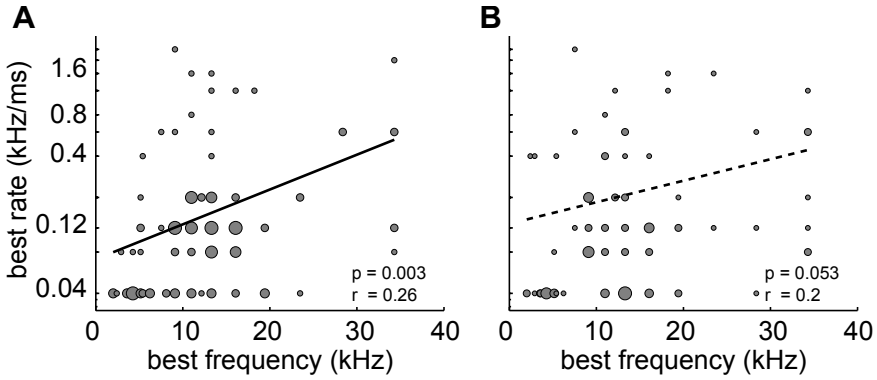

Figure 5.14: Bubble plots showing neuronal best rates as a function of BF. Rate preferences are shown separately for upward (A) and downward (B) sweeps. The size of each data-point is proportional to the number of neurons with the corresponding best rate and frequency combination. Continuous line indicates significant correlations between the two measures (alpha = 0.05).

Here, best rates were calculated separately for upward (120 neurons) and downward stimuli (93 neurons) (Figure 5.14). There was a significant correlation with BFs when best rates were computed for upward sweeps (A; r = 0.26; p = 0.003; 120 neurons) but not for downward sweeps (B; r = 0.20; p = 0.053; 93 neurons).

5.4 Discussion

5.4.1 Results overview

I used two-photon calcium imaging in cortical layers II-III of anaesthetised mice to characterize the responses to linear FM sweep stimuli of an unprecedented number of neurons in the same animal, and to unravel the fine-scale organization of these responses.

I found that neurons were preferentially activated by slow FM sweeps, regardless of sweep direction. An examination of neural response curves and PCA revealed that rate tuning was more invariant to the bandwidth of the frequency modulation than duration tuning. FM rate preferences and pure tone frequency preferences showed similar signal correlation values for neuronal pairs and these were higher than those found during binaural noise stimulation. Furthermore, I described a similar degree of local spatial organization in the tuning to pure tone frequencies and to a higher order feature of the sound, (namely, the rate of frequency modulation). However, BFs of individual neurons

correlated with the rate of upward, but not downward sweeps.

5.4.2 FM Rate sensitivity: main features

In my experiments, neuronal tuning to FM rates was largely invariant across FM bandwidths and starting frequencies. This was confirmed by PCA. In particular, the invariance across the lower two of the starting frequencies, although tested in only three mice, was important to confirm that neurons were indeed responding to the speed of the frequency modulation, and not simply to the integrated spectrum of frequencies covered by the sweeps.

More than half of rate-sensitive neurons in layers II-III of the A1 of the mouse preferred rates between 0.04 and 0.12 kHz/ms, which were the three slowest speeds among the 10 presented (up to 2.4 kHz). In order to help comparing my results to published ones, Figure 5.15 shows the range of rates preferred by the majority of sensitive neurons in mine and other studies investigating rate preferences in the auditory cortex of mice, rats, chinchillas, ferrets and cats, using linear FM sweeps. I shall focus on the results in mice first (dark blue lines).

It is worth mentioning that Trujillo and colleagues (2011) categorized neurons according to their rate selectivity into four classes (fast, slow, all, and band-pass), and only band-pass cells were included in their analysis of rate preferences (and showed in Figure 5.15, second line from bottom), although slow-pass rate responses were most common in A1 (as in my present data). However, the authors themselves stated that, if the rate preferences of slow-pass FM rate neurons were included in their analysis, the overall tuning would have shifted toward rates slower than the range 1 - 3 kHz/ms reported. Thus, although the ranges of FM rates tested do not overlap completely across studies, tuning to linear FM sweeps of slow rates in the A1 of the mouse is consistently reported, as confirmed also by the fact that the only study analysing responses to very high rates (up tp 20 kHz/ms; Trujillo *et al.* (2011)) found very sparse, if any preferences above 7 kHz/ms. In line with this finding, mouse auditory cortex has been shown to be involved in the discrimination of FM sweeps as slow as 0.02 kHz/ms in a study testing the acquisition of fear memories associated to FM sweeps before and after pharmacological and optogenetic inactivation of cortical pyramidal neurons (Letzkus *et al.*, 2011). This value

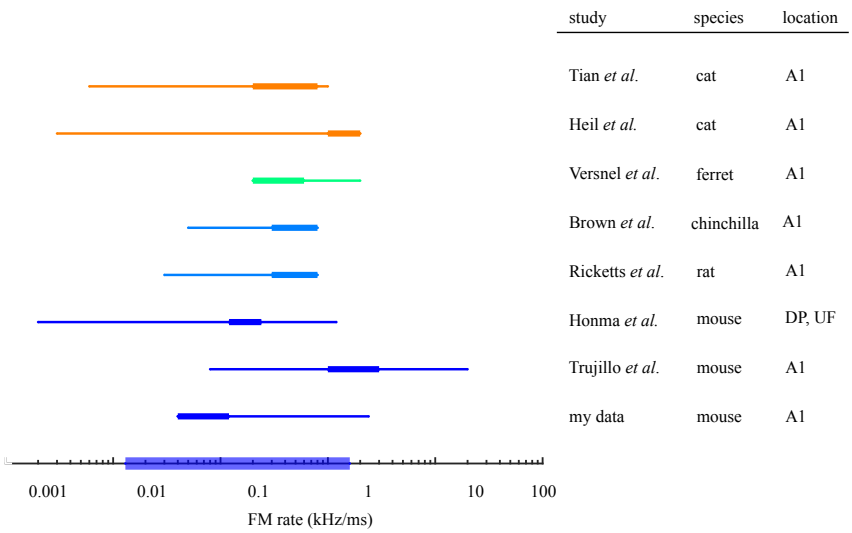

Figure 5.15: Schematic plot indicating the range of FM rates used to study FM sensitivity in several experiments from different species. Lines are colour coded according to the species. The narrower part of each line indicates the range of FM rates used in the study, while the thicker part is the range of best FM rates found. The blue line on the horizontal axis indicates the range of rates found in mice species-specific calls. The table on the right contains a reference to each study and indicates the species and the region of auditory cortex investigated.

is just below that of the slowest rate I have presented, and it is possible that it could have elicited good tuning if I used it.

5.4.3 FM Rate sensitivity: comparison with rates of species-specific calls

It is interesting to understand whether the rates preferred by the neurons I have imaged correspond to those typical of mice vocalizations. For this reason, Figure 5.15 also indicates the range of rates of FM components described in mice calls (blue line on x-axis).

Visual examination of most published spectrograms reveal the presence of FM components with rates between 0.15 - 1.6 kHz/ms, (Grimsley *et al.*, 2011; Hage and Ehret, 2003; Holy and Guo, 2005; Liu *et al.*, 2003). The slowest among the rates described (0.15 kHz/ms) was found in vocalizations from CBA/CaJ adult pairs (Liu *et al.*, 2003). FM components as slow as 0.013 kHz/ms were recorded in adult mice of another strain (BxD: a first generation obtained by crossing the C57B6/J and DBA2/J strains), during

courtship (Arriaga *et al.*, 2012). However, adult males of the same strain emitted FM sweeps generally around 1 kHz/ms in a further study (Holy and Guo, 2005). Such large range may be explained by the fact that reports analysing the production of species-specific communication calls in mice have used animals of both sexes, from different strains, and living in different social contests.

The preferred rates I have found fall within the overall range of natural FM sweeps I identified when examining published studies. Nonetheless, it would be interesting to repeat my experiments under similar conditions (same age, same sex), but in mice of different strains. Also, tuning to FM rate may be plastic in the auditory cortex, and change according to life stage, and to the exposure to different types of experiences. Experience-dependent functional plasticity is an established feature of auditory cortical neurons (Bakin and Weinberger, 1990; Weinberger, 2004) and repeating my experiments, for instance, in young subjects or in mice who underwent exposure to sweeps of a certain range, may highlight the presence of neurons tuned to different FM speeds.

Tuning to the speed of linear FM sweeps has been studied also in A1 of carnivores, in particular in cats and ferrets. Interestingly, in this last species, preferred rates were not dissimilar from those found in mice, as shown in Figure 5.15. The most common best rates found here were also close to the range of FM sweeps in ferret vocalizations (Nelken and Versnel, 2000). Tuning to FM rates matching those used for communication was also found in primates (Atencio *et al.*, 2007; Godey *et al.*, 2005). The cat, instead, seems to make an exception, as the best rates of cortical neurons in this species are generally > 1 kHz/ms (Heil *et al.*, 1992; Mendelson and Cynader, 1985; Mendelson *et al.*, 1993; Tian and Rauschecker, 1994), while species-specific calls can be as slow as 0.003 kHz/ms (Yeon *et al.*, 2011). Thus, it has been proposed that A1 may be dedicated to the detection of preys' calls, since the best rates observed were close to frequency transitions occurring in mouse vocalizations. On the other hand, as it emerges from Figure 5.15, neurons in the A1 of the chinchilla respond preferentially to FM rates > 0.3 khz/ms, although their vocalizations contain FM modulation lower by one order of magnitude (Brown and Harrison, 2009).

The reception of species-specific sounds in mice, as in all other mammals, is crucial primarily for social interaction and reproductive success. Thus, I would argue that,

if cortical neurons are tuned to FM rates occurring in nature, and if cortical tuning to sound features changes with experiences (Weinberger, 2004), they should certainly detect species-specific FM rates, rather than rates from predators calls, especially in laboratory strains, which have never been exposed to other animals vocalizations. This corresponds to what I found in mice and to what was previously described in ferrets and monkeys, and it remains to be clarified why cortical neurons in the A1 of cats and chinchilla respond preferentially to sweeps of different rates.

5.4.4 FM Rate sensitivity: relationship with frequency tuning

Another evidence emerging when looking at FM rates preferences in my experiments is that this correlates with neuronal BFs in response to upwards, but not downwards sweeps. This difference may depend on the range of BFs found in my recordings, on the starting frequency of the FM sweeps presented, and on the effect of sideband inhibition. Upward sounds, starting at 2 kHz, first cross frequencies that are relatively close to the BFs of most neurons, eliciting a response in these cells. On the other hand, downward sounds, starting at 62 kHz, extend first through frequencies that, especially at 70 dB SPL (the intensity of my FM sweeps), are inhibitory for most of my neurons, being much higher than their BF. In fact, downward sweeps of 20 and 40 kHz bandwidths stop at frequencies higher than most of neuronal BFs, whatever their rate is. For this reason, a correlation between BFs and preferred rate may not exist when accounting for the particular downward sweeps I have presented.

5.4.5 Direction selectivity: relationship with frequency tuning

Given the tonotopic organization of A1 and given that, according to the asymmetry of inhibitory sidebands in cortical FRAs (see section 1.3.4), FM direction selectivity depends on the neuron's best frequency (Razak and Fuzessery, 2006, 2007; Ye *et al.*, 2010), it is reasonable to expect ordered maps of FM direction selectivity to be a pronounced feature of A1. In my recordings it was not possible to examine the spatial arrangement of upward and downward preferring neurons because of the very sparse direction sensitivity observed, with average DSI around 0.2, and only 9.6% of the imaged neurons showing a preferred direction. A prevalence of neuronal DSIs fluctuating around 0 has been already

described in the A1 of the mouse (Trujillo *et al.*, 2011), as well as in that of other species: rat (Orduña *et al.*, 2001; Pandya *et al.*, 2008) , ferret (Shamma *et al.* (1993); Kowalski *et al.* (1995); but see Nelken and Versnel (2000), in which upward FM preferences in response to logarithmic sweeps prevailed, but direction selectivity in response to linear sweeps was not reported), cat (Mendelson *et al.*, 1993), squirrel moneky (Godey *et al.*, 2005), owl monkey (Atencio *et al.*, 2007). Thus, it seems that relatively low direction selectivity is a common feature of A1 of many mammals.

However, this evidence may depend on the BFs of the neurons recorded. In works that attempted to map FM sweep and pure tone sensitivity across the whole extent of A1, it is clear that only cells with very high or very low frequency tuning were also strongly sensitive for FM direction: this can be easily seen by inspecting the BFs and DSIs maps reported by Godey *et al.* (2005) and by Zhang *et al.* (2003). In particular, Zhang described this in the A1 of the rat, a rodent with a range of audible frequencies similar to that of the mouse. Here, only neurons with BF lower than 4 kHz or higher than 30 kHz had DSI < -0.3 or DSI > 0.3. My recordings were instead characterized by an overrepresentation of BFs between 9 - 23 kHz (Figure 3.2 and 3.6), which may explain the poor direction selectivity. As mentioned, the FM direction selectivity of neurons tuned to low or high frequencies within the audible range of a species is shaped by the so-called "asymmetric inhibitory sidebands" in the FRAs of such neurons. For example, low-frequency neurons are generally inhibited by frequencies that are higher and not lower than their BF. In this case, an upward FM sweep would first cross low (excitatory) frequencies, likely eliciting a response in the tested neuron. To the contrary, a downward sweep (depending on its bandwidth and starting frequency) will first inhibit the cell. This mechanism would determine the neuron's preference for upward sweeps. Such asymmetry is naturally absent in neurons that are tuned to intermediate frequencies (as those in my dataset), which thus may be equally excited by sweeps of same rate and starting frequency, but opposite direction. Weak direction selectivity was also found in the A1 of the ferret in neurons with "symmetric FRAs" (Shamma *et al.*, 1993).

Similarly, the fact that the DSI in my recordings was around 0, and the BFs in an intermediate range, may explain the absence of significant correlation between DSI and BFs (Figure 5.13). If a larger gamma of BFs, and consequently stronger DSIs were

present, the mentioned correlation could have possibly been stronger as well.

5.4.6 Prevalence of tuning to upward sweeps

Of the few neurons expressing direction selectivity in my dataset, almost 70% preferred upward sweeps. This may be explained by the prevalence of upsweeps in the communication calls of this species. A study on CBA/CaJ mice, one of the most common strains in auditory research, showed that the presence of upsweeps in vocalizations increases with the age of the mouse (Grimsley *et al.*, 2011). In fact upsweeps become the most represented components of communication calls in the adult, while downsweeps decrease substantially with age.

5.4.7 Spatial distribution of FM rate preferences

The prevalence of tuning to low FM sweep rates in my experiments does not imply a lack of tuning to higher rates in A1, within the range of those used by mice for communication. Another possible reason explaining the prevalence of slow best rates in my study is that I have recorded neuronal activity from an area of A1 specifically tuned to slow FM rates. Indeed, when GCaMP6m labelling extended across regions larger than ∼300 x 300 μm, populations of neurons tuned to faster rates emerged. This is particularly true in mouse 5 in Figure 5.7, where a substantial distance separates the two imaged areas. Spatial changes in rate preferences are also visible, although less pronounced, in mouse 8, where a more spatially continuous population of neurons was analysed.

The above results may indicate two principles of FM sweep organization. First, neurons located within local areas of A1 (within 200 μm) are tuned to similar rates, as confirmed analytically using cluster analysis (section 5.3.2) and signal correlations (Figure 5.10). Second, such responses may be organized in a topographic fashion across the more global ($>$ 500 μm) surface of A1. This latter hypothesis could not be fully tested here because of the lack of data from the GCaMP6f reporter line, which would have been the ideal tool for a large scale cortical examination. In a microelectrode recording study in the A1 of the cat, an interesting concentric organization of FM rate preferences has been observed (Mendelson *et al.*, 1993), possibly inherited from the organization of rate tuning in the central nucleus of the IC. In this subcortical structure, best rates progress

gradually from fast, to intermediate, to slow, and then back to intermediate and fast along the dorso-ventral axis (Hage and Ehret, 2003). A rough topography, although based on clusters of similar tuning rather than an ordered progression of responses, was also described in the A1 of the ferret (Nelken and Versnel, 2000). In a multi-unit investigation in the A1 of the mouse, Trujillo *et al.* (2011), found clusters of neighbouring neurons with similar FM rate preferences, despite a considerable interindividual variability in the large scale spatial organization of this responses.

As mentioned above, to assess the fine scale organization of A1, I have calculated the signal corelations between pairs of simultaneously recorded cells. The relatively high values found during FM stimulation suggest the possible presence of local sub-networks of neurons with similar receptive fields, confirming the homogeneous FM tuning revealed through the maps and the cluster analysis in some, although not all, mice. In addition, the average signal correlation during FM stimulation (0.4) was higher than observed during binaural noise stimulation of the same cells (0.3) and similar to that obtained during pure tones presentation (0.46). This result possibly indicates that neurons that are closely spaced may be engaged in similar computations when FM sounds or pure tones are presented, more than during presentation of broadband noises. The correlation between signal correlations during FM sweep and pure tone presentation further confirmed this hypothesis (Figure 5.12). However, the strength of this correlation was much lower than that found by Geis and Borst (2012) in the mouse IC ($r = 0.77$). This is not surprising, because cortical neurons have to integrate across a larger variety of synaptic inputs and decode a higher number of complex sound features than collicular neurons.

5.4.8 Methodological considerations

Differences in stimulation paradigms, anaesthetic regimes, recording techniques and data analysis can influence the outcome of studies on neuronal sensitivity to similar sensory stimuli, with contrasting results often emerging in the same species.

Use of linear sweeps

In 2000, Nelken and Versnel used both linearly and exponentially modulated frequency sweeps in ferret A1 to test whether the inconsistencies in the spatial organization of FM responses found in literature were imputable to methodological biases or reflected

actual species differences. They found that the spatial distribution of rate, but not that of direction sensitivity, was invariant to the linearity of frequency modulation.

Due to the tonotopic organization of the auditory system, logarithmic FM sweeps elicit equal stimulation across all the included frequencies. Consequentially, they should result in the perception of a constant rate of frequency modulation. Here, I decided to instead use linear FM sweeps for two main reasons. First, to facilitate comparison with the existing literature, as previous published studies on FM sweeps sensitivity in the mouse auditory cortex (Honma *et al.*, 2013; Trujillo *et al.*, 2011) and IC (Hage and Ehret, 2003) have used linear FM sounds. My second reason lies in the prevalence of linear FM sweep components in mouse communication calls. In 2005, Holy and Guo reported spectrograms of calls from adult male BxD mice containing marked linear upward FM components (see Figure 1.2 for spectrograms). The same shape of frequency modulation was described in the calls of BxD, C57BL6 (Arriaga *et al.*, 2012), and CBA/CaJ adult mice involved in several contexts, including: male-male interactions; female-female; female-male; male with female bedding; and females isolated from their pups (Grimsley *et al.*, 2011; Portfors, 2007). These examples do not demonstrate the absence of logarithmic modulations in mouse calls, which were recorded in C57Bl6 pups by Scattoni *et al.* (2008), but are a strong indication of the large use of linear FM sweeps for communication purposes in laboratory strains of mice. Linear FM sweeps were therefore an appropriate choice for my investigations, as studying the processing of FM sweeps in auditory cortex ultimately finds its value in the fact that cortical encoding of such sounds is necessary for communication in all mammals.

Anaesthesia and cortical depth

To the best of my knowledge, all studies specifically dedicated to mapping FM responses across the surface of A1 have been carried out in anaesthetised animals. This facilitates comparisons between studies, but clearly does not rule out the possibility that neuronal response profiles and spatial distribution of FM preferences may be different in awake, and likely even more so in animals engaged in behavioural tasks. For instance, both early and recent studies have consistently reported lower proportions of tone-responsive neurons in the A1 of awake animals (Evans and Whitfield, 1964; Hromádka *et al.*, 2008). In 2009, Sadagopan and Wang discovered, in awake marmosets, that neu-

rons which were unresponsive to pure tones were instead "features detectors", involved in encoding high-order sound features, including FM sweeps. In my anesthetised recordings, 50% of neurons were responsive to tones (934 cells), and only around 100 cells were sensitive both to tone frequency and FM parameters (sections 5.3.9 and 5.3.10). According to the results just mentioned, these numbers may be even lower if I imaged calcium transients in cortical neurons of awake mice, while cells responsive or sensitive to FM sweeps, but not to pure tones, may possibly increase. A particularly interesting facet of tone-unresponsive neurons is that their high selectivity, together with their low spontaneous firing rates, has made electrophysiological isolation and recording from them particularly difficult. This issue can be overcome by two-photon calcium imaging, which samples neurons in a way that is unbiased for their level of activity, making it a powerful tool to shed light on how the awake auditory cortex can encode complex acoustic features.

Moreover, the tone-unresponsive neurons in Sadagopan and Wang (2009) were found mostly in supragranular layers. A two-photon calcium imaging study has already described a progressive decrease in frequency tuning going from thalamo-recipient layers (layer IV) to shallower cortical depths in the mouse A1 (Winkowski and Kanold, 2013). These evidences may suggest that layers II-III are in fact the ones in which it is more likely to find neurons specifically activated by the spectro-temporal changes of a sound rather than by static features. For this reason, studying responses to frequency modulated sweeps in superficial layers may have given me a better insight into understanding the cortical processing of this type of sound, while I would expect a weaker degree of FM sensitivity if imaging in layer IV.

Temporal coding

Neurons have been shown to use their firing patterns, firing rate, or the latency of their responses to transmit information about sensory stimuli (Panzeri *et al.*, 2010). Because of the lower temporal resolution of calcium imaging compared to electrophysiological techniques, the responses to FM sweeps reported in my study are the read out of the spiking activity averaged in large time bins ($\sim$1s). Fine temporal profiles of neuronal responses were therefore not considered.

Previous electrophysiological studies have shown that temporal spiking patterns of

auditory cortical neurons can carry information about FM sweep sounds (Brown and Harrison, 2009; Fuzessery *et al.*, 2011; Gaese and Ostwald, 1995; Gordon and O'Neill, 1998). For example, "onset" responses to FM sweeps were found to be selective for FM direction in the A1 of a rodent, the chinchilla. Two-photon calcium imaging cannot resolve such short-latency responses, due to the intrinsic temporal limits of calcium indicators, and this may be a further reason why I was unable to detect sensitivity to this FM parameter. On the other hand, both FM rate and direction are encoded by "late" responses, occurring during the sweep (Brown and Harrison, 2009). How much of the FM sensitivity is determined by rate rather than temporal coding still needs to be clarified. The primary aim of my experiments was to examine, for the first time, the fine scale spatial organization of FM responses. Intracellular recordings, although providing optimal temporal resolution, simply cannot offer the neural sampling density to answer this question. Extracellular recordings, on the other hand, measure the integrated local voltage fluctuations, and so we cannot be certain if this activity arises from single neurons, nor where these neurons are precisely located. In this respect, two-photon calcium imaging is the only technique to date allowing a single-cell resolution high-density sampling of neurons in areas as small as $\sim$200 x 200 μm. This property makes it a suitable tool for constructing fine scale maps of cortical sensory responses.

Chapter 6

General Discussion

6.1 Summary of findings

My thesis was characterized by the use of one technique, *in vivo* two-photon calcium imaging, to answer several questions about the response properties of the auditory cortex of the mouse. Only a few auditory studies have so far conjugated this animal model and this technique. However, the mouse is a genetically malleable species, and its employment as an auditory model will surely continue to increase in the years to come, in parallel with the use of neuroscience techniques that take advantage of genetic interventions, such as optogenetics and two photon-microscopy.

The aims of my work in mice were threefold: (1) to reveal, for the first time, how sound features other than frequency are represented at the local scale in A1; (2) to improve our understanding of some important and long-standing questions (for example, that of the presence of tuning to ipsilateral and midline ILDs in the A1 of rodents); (3) to create a benchmark for future fine-scale mapping studies of the mouse auditory cortex. Finally, I also aimed to set the groundwork for two-photon studies of the auditory cortex of the ferret: a long-established and important auditory model.

My key findings and conclusions are as follows.

1. Most neurons in local auditory cortical regions (within ∼200 μm) are tuned to a common narrow frequency range. In more than half of the animals in my dataset neurons with similar BFs are significantly closer in space than cells with different frequency tuning. Therefore, sound frequency is systematically represented at the

fine-scale level in the mouse A1.

2. On the global scale (up to 1 mm) the presence of a tonotopic progression of frequency preferences is recognizable in the mouse auditory cortex, indicating the location of primary regions.

3. Over 90% of the A1 neurons responsive to noise bursts are sensitive to binaural modulations. In particular, the large portion of binaurally facilitated neurons suggests that the mouse may be a good model for the study of auditory processing in noisy environments.

4. Although most neurons show a preference for ILDs corresponding to contralateral positions, neurons preferentially activated by ipsilateral and midline positions are present too, similarly to what found in larger mammals.

5. Preferred ILDs do not form local clusters and, consequently, are not systematically represented on the larger scale.

6. The two most frequent binaural categories, (namely, EO/I and OO/F), do not alternate along the anatomical axis perpendicular to the tonotopic one. They form scattered clusters in about one fourth of the animals, indicating a weaker large-scale organization compared to frequency responses.

7. Among the FM sweep parameters considered (bandwidth, duration, rate, direction), A1 neurons are most sensitive to the rate of the sweeps, and prefer slow speeds regardless of FM bandwidth. These speeds fall within the range of those used by mice in communication calls.

8. A weak sensitivity to FM direction is present in A1, although this result may have been biased by the BFs of the imaged neurons, generally tuned to intermediate frequencies among those represented in A1.

9. Preferred FM rates cluster in almost half on the mice, indicating a level of local organization more similar to that of frequency tuning than to that of ILD responses.

10. Pairwise signal correlations during FM sweep stimulation are significantly higher than those measured when binaural noise bursts were presented, but are instead

more similar to signal correlations obtained during pure tone presentation. This result confirms that local neurons are less likely to be involved in similar computations when encoding intensity cues for spatial location, compared to sound frequency and its changes over time.

6.2 Evidence for local networks in auditory cortex

The main insight that two-photon imaging experiments allowed me to provide relates to the functional micro-architecture of A1. My findings indicate that neuronal ensembles covering 150 - 200 μm of cortical space may form local computational units. This indication, which was particularly strong when testing neurons with pure tones and FM sweeps, emerged from two measurements.

First, in the bootstrapped cluster analysis, the highest number of clusters in my mice was found when using a bin size of 150 μm (see section 2.2.7). Second, the pairwise signal correlations, calculated for neurons within single imaging fields ($\sim$200 x 200 μm), decreased weakly, but significantly, with increasing neuronal distance along the anatomical axes (the only exception is that of signal correlations along the dorsoventral axis, during FM sweep presentation).

Moreover, my pairwise noise correlations for local neurons were on average $\sim$0.2. Notably, Rothschild *et al.* (2010) found a very similar value (0.18) for noise correlations of simultaneously imaged neuronal pairs during pure tone stimulation in the mouse A1 (layers II-III). Interestingly, it has been previously demonstrated that noise correlations of this order can be sufficient for a local network to reliably process a given sensory stimulus, without the need to involve a larger neuronal population (Schneidman *et al.*, 2006; Sompolinsky *et al.*, 2001). This indication is therefore in favour of the presence of small subnetworks of neurons involved in independent local computations.

Basing on the above observations, there must be something unique about the organization of the $\sim$200 μm spatial scale. The columnar arrangement of sensory cortices is a long-established principle according to which neurons are organized in parallel columns with a diameter of 300 - 600 μm, extending through the cortical layers (Mountcastle *et al.*, 1957). Within these structures, mini-columns with a diameter as narrow as 50 - 100 μm have been described, grouping neurons activated by very similar values of a certain sen-

sory feature (e.g. similar sound frequencies) (Mountcastle, 1997, 2003). My groups of neurons showing comparable responses may correspond to the layer II-III representation of these cortical mini-columns, and define small functional units encoding acoustic stimuli in A1. Multiplexed two-photon calcium imaging consists in the quasi-simultaneous imaging of neuronal populations separated by tens of micrometers in depth. Therefore, this technique would be ideally suited to test the presence of functional mini-columns by revealing, in one animal, to what extent individual neurons located at different cortical depths within one anatomical column have similar sensory preferences.

The homogeneity of response profiles is an identifying property of cortical mini-columns, yet my 2D maps of neural responses have revealed that best frequency and preferred FM sweep rate, the two most strongly organized sound features in my experiments, are locally similar, but not identical. However, the "preference" of a sensory neuron is a discrete value that cannot fully account for its overall response profiles. For this reason, more comprehensive measures, such as signal and noise correlations, are better suited to indicate the possible presence of local subnetworks. Furthermore, we should not forget that the homogeneity within mini-columns was defined in electrophysiological studies of the cortex using extracellular techniques that sample the cortical surface sparsely and tend to favour big and highly active neurons (Mountcastle *et al.*, 1957). Still today, these techniques offer the highest temporal resolution among neurophysiological methodologies, and will continue being key in the study of cortical functions. Nonetheless, calcium imaging has represented in the last decade a way to access a superior level of spatial detail, and therefore it allowed to highlight some microscopic features of the cortex that can aid the comprehension of some of its organizational principles.

6.3 What is the functional relevance of local heterogeneity?

Local variability also emerged in visual and somatosensory cortex in the mouse, when mapping ocular dominance scores (Mrsic-Flogel *et al.*, 2007) and whisker selectivity (Sato *et al.*, 2007).

In 2011, Ko and colleagues performed paired intracellular recordings in layers II-III of the mouse V1 on blocks of cerebral tissue previously imaged *in vivo*. These experiments indicated that local cortical areas containing neurons with mixed orientation preferences

are characterized by mixed levels of synaptic connectivity. In particular, local neurons with similar tuning are twice as likely to be monosynaptically connected as local neurons with different orientation preferences. Previous *in vitro* paired recordings highlighted the presence of heterogeneous local connections also in the V1 of the rat, although without clarifying their functional implications (Yoshimura and Callaway, 2005; Yoshimura *et al.*, 2005). Similar organizing principles may be common across sensory cortices and thereby characterize auditory cortex, too.

Directly testing this possibility was not among the main aims of my experiments. However, indirect support of this hypothesis comes from the results of my examination of signal correlations as a function of noise correlations. The correlation between these measures is high, especially when computed on responses to pure tones and FM sweeps ($r = 0.57$ in both cases, while $r = 0.49$ during ILD noise bursts). In addition, the plots representing these measures (Figures 3.7C and 5.10B) show a majority of cells with relatively similar receptive fields (medium to high signal correlation values) but weakly connected (low noise correlation), and then a small tail of similarly tuned (high signal correlation) and strongly connected (high noise correlation) neurons, suggesting that both strongly and weakly correlated neurons may coexist in local cortical areas presenting similar but not identical tuning to a given sensory feature (pure tones and rate of FM sweeps, in this case).

To understand the implications that synaptic connectivity has on the functional properties of local groups of neurons in auditory cortex, future investigations should pair *in vivo* two-photon imaging with *in vitro* intracellular recordings from two or more neurons simultaneously. The imaging experiments would reveal the sensory properties of the many individual neurons recorded in a given cortical area. Following these, synaptic connectivity may be assessed *in vitro* for some of the neurons analysed *in vivo*, in an approach similar to that of Ko *et al.* (2011): by inducing spiking activity in each neuron in turn, and at the same time recording membrane potentials from the others.

Finally, some local variability would allow neighbouring neurons to encode several sensory features. This process may start at early levels in the auditory cortex (e.g. A1), given (a) the remarkable amount of sound processing performed already by subcortical nuclei (see section 1.3 1.3), and (b) the important role that A1 has in making associations

among acoustic features to form auditory objects (Nelken and Bar-Yosef, 2008).

6.4 The spatial variability of ILD responses

The lack of a systematic arrangement of ILD responses in the subcortical nuclei involved in their processing (except for the superior colliculus, see section 1.3.5) may play an important role in determining their lack of spatial organization in A1. This is the most weakly organized neuronal property among those I have tested, and despite the signal correlations in the responses to binaural noise bursts decrease (weakly, but significantly) with neuronal distance, their values are considerably lower on average than those calculated for pure tone and FM sweep responses.

Previous electrophysiological recordings have highlighted the absence of a topographic order in the cortical representation of binaural location cues in carnivores and primates (Nakamoto *et al.*, 2004; Recanzone *et al.*, 1999; Rutkowski *et al.*, 2000). However, possible differences in the cortical representation of sensory features between rodents and larger mammals are a currently debated topic, as we have seen several times in this dissertation. Therefore, two-photon imaging experiments in different species would be useful to ultimately confirm whether the same fine-scale principles are shared by animals using different binaural cues. This comparison is particularly important given that the auditory cortex may not be necessary for sound localization in rats, a rodent species with a similar level of cortical complexity to the mouse (Kelly, 1980; Kelly and Kavanagh, 1986), while it is instead crucial in higher mammals (Jenkins and Merzenich, 1984; Malhotra and Lomber, 2007; Nodal *et al.*, 2010) (see section 1.4.1).

My work indicates that primary auditory cortical neurons in the mouse generally prefer sounds favouring the contralateral ear, although some tuning to ipsilateral and midline positions exists as well. These findings are similar to those from the A1 of primates and carnivores (Irvine *et al.*, 1996; Middlebrooks and Pettigrew, 1981; Rajan *et al.*, 1990; Zhang *et al.*, 2004), and different from that reported sometimes in rats, where all neurons were described as contralaterally tuned (Yao *et al.*, 2013). However, this similarity alone is not sufficient to demonstrate that auditory cortex is actively involved in binaural processing in mice. To test this hypothesis, mice should be trained on sound localization tasks, and their performance should be tested before and after

cortical lesion or inactivation. Two important points should be taken into consideration when planning these experiments.

Firstly, training mice for sound localization tasks may help solve the controversies about the localization abilities of rodent species. To my knowledge, only four studies exist to date on this matter (Allen and Ison, 2010; Ehret and Dreyer, 1984; Heffner and Heffner, 1988; Heffner *et al.*, 2001). Each of these works used different training protocols and different data analysis methods, employed a low number of experimental animals, and obtained conflicting results. For example, while Ehret and Dreyer (1984) found a minimum audible angle (MAA) of 7° using eight mice, Heffner and Heffner (1988) reported results from only three mice, and a MAA of 19°. Three animals were used also in Heffner *et al.* (2001). Given these discrepancies, an insight into the localization abilities of the mouse would be interesting in itself, even before determining the involvement of A1.

Moreover, it has been reported that rodents have good sound discrimination performance only for frontal locations near the midline, while are unable to discriminate sound sources within lateral hemifields, differently from higher mammals (ferrets: Nodal *et al.* (2008); cats: Malhotra *et al.* (2004); monkeys: Recanzone and Beckerman (2004); humans: Middlebrooks and Onsan (2012)). In the light of my findings, which highlight the similarities in cortical binaural tuning between mice and carnivores, it is particularly interesting to clarify the sound localization abilities of mice before and after inactivation of A1. Pilot behavioral experiments on mice with intact auditory cortex have started over the summer in our lab, with the specific aim to determine whether mice are able to discriminate two sound sources within one hemifiled.

The second point of consideration is the specificity of the technique to use to investigate the role of mouse A1 in sound localization. In higher mammals, this has been determined through lesion (Heffner and Heffner, 1990; Jenkins and Merzenich, 1984; Kavanagh and Kelly, 1987)) and inactivation experiments (Bizley *et al.*, 2007; Malhotra *et al.*, 2004; Malhotra and Lomber, 2007; Smith *et al.*, 2004). However, these types of procedures impair activity not only in the target region, but also in all other areas that depend on its output to perform properly. Therefore, more modern techniques, such as optogenetic inactivation of specific neuronal populations, may be a more appropri-

ate solution for tackling this issue. For example, two-photon calcium imaging in A1 of head-restricted mice performing a sound-source discrimination task may be carried out while optically suppressing the activity of local excitatory neurons, which represent the majority of neocortical cells (∼80%) (White, 1989). Targeted inactivation may be accomplished by using murine reporter lines expressing archaerhodopsin, a chloride pump (Weible *et al.*, 2014), or by injecting the protein in A1 through a viral vector (Nomura *et al.*, 2015).

6.5 Unresponsive neurons and the search for the optimal auditory stimulus

In each of my three experiments, I found that at least half of the imaged neurons were unresponsive to the sound presented. This result was partly determined by the presence of some poorly labeled cells in GCaMP6m injected mice. Nonetheless, it is in line with the sparse spiking activity characteristic of auditory cortex (Hromádka *et al.*, 2008; Sakata and Harris, 2009) as well as of visual (Vinje and Gallant, 2000), motor (Brecht *et al.*, 2004) and somatosensory (Margrie *et al.*, 2002) areas.

Experimental and theoretical work has recognized that sparse coding can be an efficient way of processing sensory inputs, as first proposed by Barlow (1961), and more recently reviewed by Olshausen and Field (2004). Having few neurons active in response to a given stimulus may improve the information storage capacity of neural networks, and it may help the cortex save energy (Willshaw *et al.*, 1969). Moreover, few highly-informative neurons, that is, neurons exhibiting temporally precise responses to natural stimuli, can carry all the information present within a larger neuronal population in the primate auditory cortex (Ince *et al.*, 2013).

Microelectrode recordings, together with computational approaches, have been key in revealing sparse cortical coding, thanks to their superior temporal resolution, as extensively reviewd in Panzeri *et al.* (2015). While two-photon calcium imaging cannot match this temporal precision, it may provide complementary insights in investigating the principles at the basis of population coding in the cortex. First, it would allow us to directly measure the degree of sparseness within a cortical region, because the activity

of a large number of individual neurons can be measured simultaneously. In contrast, previous microelectrode recordings have sparsely sampled a smaller number of individual neurons, or have pooled the activity of many cells across different recording sessions in order to subsequently infer population dynamics offline.

Secondly, two-photon imaging can help us design the "optimal acoustic stimulus" for auditory cortical neurons. This is a stimulus that is able to drive large populations of neurons and elicit sustained, high-amplitude responses (Hromádka *et al.*, 2008). This search is more complicated in the auditory cortex compared to, for example, the visual cortex. In the latter, the properties of local neurons have been defined clearly since the earliest investigations (Hubel and Wiesel, 1962), and the limited amount of subcortical processing in this pathway, compared to the auditory one, has certainly helped us to more fully characterize the receptive fields of visual cortical neurons. Auditory neuroscientists have usually tried to define the optimal stimulus by adapting their stimuli to the response profiles of individual neurons recorded separately (deCharms *et al.*, 1998; Wang *et al.*, 2005). Thus, these studies have focused on understanding what the best stimulus is for one or few neurons in one experiment. To the contrary, two-photon imaging would rather analyze the stimulus responses of many neurons at the same time, at a single-cell level. Thus, through methods able to quantify the amount of information carried by large groups of individual neurons about a given sensory stimulus (traditionally Shannon information and Fisher information), it may help understanding whether an ideal stimulus for entire populations of auditory cortical neurons exists.

Finally, decoding algorithms carried out on large sets of two-photon imaging data would ultimately serve to elucidate how cortical processing shapes perception (Bathellier *et al.*, 2012). For example, one could measure how accurately one neuron encodes ILDs (or rates of FM sweeps) and compare its performance to that of the total of neurons imaged simultaneously in the same cortical field. The results obtained can be then compared to the performance of the animal engaged in a sound-source localization task (or in a task involving the identification of a FM sweep). This way we could assess how much of the perceptual abilities of the mouse can be predicted by the responses of a cortical neuronal population of a given size.

6.6 General methodological considerations

6.6.1 The use of anaesthesia

The use of anaesthesia in my experiments must be taken into account when interpreting and generalizing my results. Given that I have already discussed its potential influence specifically for each experiment (see sections 3.4.3, 4.4.5, and 5.4.8), I will now briefly comment on the general effects that the use of anaesthetics may have on studies of auditory cortical functions.

Several studies have demonstrated that population processing in auditory cortex changes according to the patterns of spontaneous activity of the network, commonly referred to as "cortical states" (Hubel *et al.*, 1959; Issa and Wang, 2008; Marguet and Harris, 2011; Otazu *et al.*, 2009). Under anaesthesia, and generally during slow wave sleep, the cortical state is defined as "synchronized", because cortical neurons undergo together slow fluctuations between phases of spiking and silence. In contrast, during active wakefulness, these slow, synchronous oscillations are replaced by a "desynchronized", neuronal activity at higher frequencies. Nonetheless, cortical states are not bimodal, and rather include a range of possible patterns of activity, as reviewed by Harris and Thiele (2011).

Recently, Sakata and Harris (2012) have examined how cortical states influence the activity of specific classes of neurons in the rat A1. They found that the spiking activity of pyramidal neurons in superficial layers, the same cells I have studied, is enhanced during synchronized states (similar to anaesthetized conditions), and suppressed in desynchronized ones (similar to wakefulness). Changes in cortical state were continuously monitored and could occur spontaneously or be induced. In support of this evidence, (Haider *et al.*, 2013) demonstrated that "inhibition dominates sensory responses in the awake cortex" by directly measuring synaptic conductances to layers II-III neurons in the V1 of both anaesthetized and awake mice.

An increase in cortical inhibition in awake, passive listening animals,resulting in a sharper selectivity of A1 neurons, has been described in the past (Sadagopan and Wang, 2010). On the other hand, the effects that active listening during an auditory task can have on the response properties of A1 neurons are more complicated. For example, a

study in behaving cats found that the spatial receptive fields of cortical units sharpen during a localization task, compared to a periodicity discrimination task (Lee and Middlebrooks, 2011). On the other hand, Fritz *et al.* (2003) detected a facilitatory effect in the A1 of ferrets attending a pure tone detection task. This was represented by changes in the spectro-temporal receptive fields of cortical neurons consisting in either a decrease of sideband inhibition or an enhancement of the excitatory area around the target frequency. Regardless of the specific mechanism, a change in the cortical balance between excitation and inhibition should be at the basis of these plastic changes in cortical receptve fields. According to Lee and Middlebrooks (2011), I would expect to find sharper tuning to binaural location cues, if repeating my experiments in awake behaving mice. To test whether this effect is accompained by a stronger activation of the local inhibitory neurons, calcium imaging experiments should be performed in layers II-III to record the activity of both inhibitory and excitatory populations by means of an indicator able to label both cell types. The two populations could then be distinguished by labelling the interneurons with a second fluorophore, excited by light of a different wavelength compared to the calcium indicator.

Experiments in awake animals would be an important next step from this thesis, as they are generally the ideal condition for neurophysiological investigations of sensory encoding, because anaesthesia inevitably shapes neural response profiles according to the molecular targets and mechanisms of action of the drugs used. However, it was essential to start off by using anaesthesia in order to provide better stimulus control and a more stable preparation.

6.6.2 The choice of the calcium indicator

When performing two-photon calcium imaging experiments, it is important to take into consideration the biophysical properties of the indicator used. These include the dynamic range (the ratio between its minimum and maximum fluorescence intensities), the time necessary for the indicator to reach peak fluorescence and return to baseline values (rise and decay times), and the sensitivity for calcium ions, commonly defined as the intracellular concentration of calcium at which half of the indicator's molecules are bound to the ion at equilibrium (Kd) (Grienberger and Konnerth, 2012). In particular, the indicator's

sensitivity can greatly influence the outcome of calcium imaging experiments.

When frequency tuning in the A1 of the mouse was studied for the first time using two-photon calcium imaging, the authors of those studies used Fluo-4, a low affinity synthetic indicator (Kd = 350 nM) (Bandyopadhyay *et al.*, 2010; Rothschild *et al.*, 2010). This probe is likely to reflect only supra-threshold calcium changes in response to sensory stimulation. However, Bandyopadhyay and colleagues also utilized OGB-1, a high-affinity indicator (Kd = 170 nM), which may report subthreshold calcium fluctuations and that, according to the authors, led to finding a more homogeneous organization of frequency preferences compared to Fluo-4.

One reason for this latter result may be that subthreshold receptive fields are broader than their counterparts based on action potentials. This property, often referred to as the "iceberg effect", has been described in visual (Carandini and Ferster, 2000), somatosensory (Margrie *et al.*, 2002) and auditory cortex. In the auditory cortex, Chadderton *et al.* (2009) described the iceberg effect on spatial receptive fields, while Wehr and Zador (2003) revealed its contribution in shaping spectral tuning. However, I argue that the contribution of the iceberg effect should have resulted in a high percentage of neurons that are responsive, but non-selective for sound frequency, rather than in a more variable representation of best frequencies, as Bandyopadhyay *et al.* (2010) suggested.

Like Bandyopadhyay *et al.* (2010), I used two probes of different sensitivities in my experiments: GCaMP6m (Kd = 167 nM) and GCaMP6f (Kd = 375 nM). Nonetheless, unlike Bandyopadhyay *et al.* (2010), I found almost identical levels of neuronal cotuning for pure tone responses in the two cases (0.78 $\sim$ 0.04 octaves for GCaMP6m and 0.79 $\sim$ 0.1 octaves for GCaMP6f), although, as expected, I obtained a larger fraction of sound responsive neurons with the more sensitive indicator, GCaMP6m. The differences between our studies may occur because probes of the GCaMP6 family, (even the most sensitive one, GCaMP6s), are not able to reflect the relatively weak calcium fluctuations caused by EPSPs, and instead should only reflect supra-threshold activity, as reported by Chen *et al.* (2013).

The field of two-photon microscopy is evolving at an incredibly fast pace. Many different calcium indicators and reporter mouse lines are released every year. For this reason, and due to the different analytical approaches used across research groups, it is

sometimes complicated to compare results across studies. In this thesis, I have used principally GCaMP6m to answer my three main research questions, and the same indicator will be used in future to continue our experiments in the auditory cortex of the ferret. This consistency is an important point, as it will facilitate the comparison of frequency, binaural, and FM sensitivity in two different models, by excluding potential biases due to the biophysical properties of the indicator.

6.7 In conclusion

In this thesis, I have described the cortical tuning to pure tones, binaural noises, and FM sweeps in the mouse by sampling an unprecedented number of local neurons simultaneously, at a single-cell level.

I have shown that the spatial organization of neuronal best frequencies follows a tonotopic organization, with some local variations. Furthermore, while binaural responses are poorly organized on both the local and the global spatial scale, local neurons have often similar preferences to the rate of FM sweeps.

Therefore, my experiments have contributed to advancing our knowledge of the auditory cortex of an animal model, the mouse, whose use is quickly spreading in auditory research.

The main focus of my story has been two-photon calcium imaging. This technique is characterized by superior spatial-sampling rates, and research groups using it take advantage of a continuous flow of improvements, both experimental (e.g. higher temporal resolution, possibility of quasi-simultaneous imaging in different cortical layers) and analytical (e.g. automated ROI detection, algorithms for extraction of spike trains). Therefore, in parallel with microelectrode recordings, two-photon imaging will certainly play a critical role in the future, in helping neuroscientists understand the functional organization of mammalian cortical circuits.

References

Abeles, M. and Goldstein Jr, M. (1970). Functional architecture in cat primary auditory cortex: columnar organization and organization according to depth. *Journal of neurophysiology*, 33(1):172–187.

Ahrens, M. B., Linden, J. F., and Sahani, M. (2008). Nonlinearities and contextual influences in auditory cortical responses modeled with multilinear spectrotemporal methods. *The Journal of Neuroscience*, 28(8):1929–1942.

Aitkin, L. M. and Martin, R. L. (1987). The representation of stimulus azimuth by high best-frequency azimuth-selective neurons in the central nucleus of the inferior colliculus of the cat. *Journal of neurophysiology*, 57(4):1185–1200.

Allen, P. D. and Ison, J. R. (2010). Sensitivity of the mouse to changes in azimuthal sound location: angular separation, spectral composition, and sound level. *Behavioral neuroscience*, 124(2):265.

Andermann, M. L., Gilfoy, N. B., Goldey, G. J., Sachdev, R. N., Wölfel, M., McCormick, D. A., Reid, R. C., and Levene, M. J. (2013). Chronic cellular imaging of entire cortical columns in awake mice using microprisms. *Neuron*, 80(4):900–913.

Andoni, S., Li, N., and Pollak, G. D. (2007). Spectrotemporal receptive fields in the inferior colliculus revealing selectivity for spectral motion in conspecific vocalizations. *The Journal of neuroscience*, 27(18):4882–4893.

Arriaga, G., Zhou, E. P., and Jarvis, E. D. (2012). Of mice, birds, and men: the mouse ultrasonic song system has some features similar to humans and song-learning birds. *PLoS One*, 7(10):e46610.

Atencio, C. A., Blake, D. T., Strata, F., Cheung, S. W., Merzenich, M. M., and Schreiner, C. E. (2007). Frequency-modulation encoding in the primary auditory cortex of the awake owl monkey. *Journal of Neurophysiology*, 98(4):2182–2195.

Atencio, C. A. and Schreiner, C. E. (2010). Columnar connectivity and laminar processing in cat primary auditory cortex. *PLoS One*, 5(3):e9521.

Bajo, V. M., Nodal, F. R., Moore, D. R., and King, A. J. (2010). The descending corticocollicular pathway mediates learning-induced auditory plasticity. *Nature neuroscience*, 13(2):253–260.

Bakin, J. S., Kwon, M. C., Masino, S. A., Weinberger, N. M., and Frostig, R. D. (1996). Suprathreshold auditory cortex activation visualized by intrinsic signal optical imaging. *Cerebral Cortex*, 6(2):120–130.

Bakin, J. S. and Weinberger, N. M. (1990). Classical conditioning induces cs-specific receptive field plasticity in the auditory cortex of the guinea pig. *Brain research*, 536(1-2):271–286.

Bandyopadhyay, S., Shamma, S. A., and Kanold, P. O. (2010). Dichotomy of functional organization in the mouse auditory cortex. *Nature neuroscience*, 13(3):361–368.

Bao, S., Chan, V. T., and Merzenich, M. M. (2001). Cortical remodelling induced by activity of ventral tegmental dopamine neurons. *Nature*, 412(6842):79–83.

Bar-Yosef, O., Rotman, Y., and Nelken, I. (2002). Responses of neurons in cat primary auditory cortex to bird chirps: effects of temporal and spectral context. *The Journal of neuroscience*, 22(19):8619–8632.

Barbour, D. L. and Callaway, E. M. (2008). Excitatory local connections of superficial neurons in rat auditory cortex. *The Journal of Neuroscience*, 28(44):11174–11185.

Barbour, D. L. and Wang, X. (2003). Auditory cortical responses elicited in awake primates by random spectrum stimuli. *Journal of Neuroscience*, 23(18):7194–7206.

Barlow, H. B. (1961). Possible principles underlying the transformations of sensory messages.

Barnstedt, O., Keating, P., Weissenberger, Y., King, A. J., and Dahmen, J. C. (2015). Functional microarchitecture of the mouse dorsal inferior colliculus revealed through in vivo two-photon calcium imaging. *The Journal of Neuroscience*, 35(31):10927–10939.

Bartlett, E. L. (2013). The organization and physiology of the auditory thalamus and its role in processing acoustic features important for speech perception. *Brain and language*, 126(1):29–48.

Bathellier, B., Ushakova, L., and Rumpel, S. (2012). Discrete neocortical dynamics predict behavioral categorization of sounds. *Neuron*, 76(2):435–449.

Belliveau, L. A., Lyamzin, D. R., and Lesica, N. A. (2014). The neural representation of interaural time differences in gerbils is transformed from midbrain to cortex. *The Journal of Neuroscience*, 34(50):16796–16808.

Bendor, D. and Wang, X. (2005). The neuronal representation of pitch in primate auditory cortex. *Nature*, 436(7054):1161–1165.

Bendor, D. and Wang, X. (2008). Neural response properties of primary, rostral, and rostrotemporal core fields in the auditory cortex of marmoset monkeys. *Journal of neurophysiology*, 100(2):888–906.

Binns, K., Grant, S., Withington, D., and Keating, M. (1992). A topographic representation of auditory space in the external nucleus of the inferior colliculus of the guinea-pig. *Brain research*, 589(2):231–242.

Bizley, J. K., Nodal, F. R., Nelken, I., and King, A. J. (2005). Functional organization of ferret auditory cortex. *Cerebral Cortex*, 15(10):1637–1653.

Bizley, J. K., Nodal, F. R., Parsons, C. H., and King, A. J. (2007). Role of auditory cortex in sound localization in the midsagittal plane. *Journal of neurophysiology*, 98(3):1763–1774.

Bizley, J. K., Walker, K. M., Silverman, B. W., King, A. J., and Schnupp, J. W. (2009). Interdependent encoding of pitch, timbre, and spatial location in auditory cortex. *The Journal of Neuroscience*, 29(7):2064–2075.

Bonhoeffer, T., Grinvald, A., *et al.* (1991). Iso-orientation domains in cat visual cortex are arranged in pinwheel-like patterns. *Nature*, 353(6343):429–431.

Bonin, V., Histed, M. H., Yurgenson, S., and Reid, R. C. (2011). Local diversity and fine-scale organization of receptive fields in mouse visual cortex. *The Journal of neuroscience*, 31(50):18506–18521.

Boudreau, J. C. and Tsuchitani, C. (1968). Binaural interaction in the cat superior olive s segment. *Journal of Neurophysiology*, 31(3):442–454.

Braitenberg, V. and Braitenberg, C. (1979). Geometry of orientation columns in the visual cortex. *Biological cybernetics*, 33(3):179–186.

Brecht, M., Schneider, M., Sakmann, B., and Margrie, T. W. (2004). Whisker movements evoked by stimulation of single pyramidal cells in rat motor cortex. *Nature*, 427(6976):704–710.

Britt, R. and Starr, A. (1976). Synaptic events and discharge patterns of cochlear nucleus cells. ii. frequency-modulated tones. *Journal of Neurophysiology*, 39(1):179–194.

Brosch, M. and Schreiner, C. E. (1999). Correlations between neural discharges are related to receptive field properties in cat primary auditory cortex. *European Journal of Neuroscience*, 11(10):3517–3530.

Brown, T. A. and Harrison, R. V. (2009). Responses of neurons in chinchilla auditory cortex to frequency-modulated tones. *Journal of neurophysiology*, 101(4):2017–2029.

Brugge, J. F., Reale, R. A., Hind, J. E., Chan, J. C., Musicant, A. D., and Poon, P. W. (1994). Simulation of free-field sound sources and its application to studies of cortical mechanisms of sound localization in the cat. *Hearing research*, 73(1):67–84.

Budinger, E. and Scheich, H. (2009). Anatomical connections suitable for the direct processing of neuronal information of different modalities via the rodent primary auditory cortex. *Hearing research*, 258(1):16–27.

Calford, M. B., Moore, D. R., and Hutchings, M. E. (1986). Central and peripheral contributions to coding of acoustic space by neurons in inferior colliculus of cat. *Journal of neurophysiology*, 55(3):587–603.

Campbell, R. A., Doubell, T. P., Nodal, F. R., Schnupp, J. W., and King, A. J. (2006). Interaural timing cues do not contribute to the map of space in the ferret superior colliculus: a virtual acoustic space study. *Journal of neurophysiology*, 95(1):242–254.

Cao, J., Yang, E.-B., Su, J.-J., Li, Y., and Chow, P. (2003). The tree shrews: adjuncts and alternatives to primates as models for biomedical research. *Journal of medical primatology*, 32(3):123–130.

Carandini, M. and Ferster, D. (2000). Membrane potential and firing rate in cat primary visual cortex. *The Journal of Neuroscience*, 20(1):470–484.

Cariani, P. (1999). Temporal coding of periodicity pitch in the auditory system: an overview. *Neural plasticity*, 6(4):147–172.

Caviness, V. S. and Frost, D. O. (1980). Tangential organization of thalamic projections to the neocortex in the mouse. *Journal of Comparative Neurology*, 194(2):335–367.

Chadderton, P., Agapiou, J. P., McAlpine, D., and Margrie, T. W. (2009). The synaptic representation of sound source location in auditory cortex. *The Journal of Neuroscience*, 29(45):14127–14135.

Chase, S. M. and Young, E. D. (2005). Limited segregation of different types of sound localization information among classes of units in the inferior colliculus. *The Journal of neuroscience*, 25(33):7575–7585.

Chase, S. M. and Young, E. D. (2006). Spike-timing codes enhance the representation of multiple simultaneous sound-localization cues in the inferior colliculus. *The Journal of neuroscience*, 26(15):3889–3898.

Chechik, G., Anderson, M. J., Bar-Yosef, O., Young, E. D., Tishby, N., and Nelken, I. (2006). Reduction of information redundancy in the ascending auditory pathway. *Neuron*, 51(3):359–368.

Chen, Q., Cain, D., and Jen, P. (1995). Sound pressure transformation at the pinna of mus domesticus. *Journal of Experimental Biology*, 198(9):2007–2023.

Chen, T.-W., Wardill, T. J., Sun, Y., Pulver, S. R., Renninger, S. L., Baohan, A., Schreiter, E. R., Kerr, R. A., Orger, M. B., Jayaraman, V., *et al.* (2013). Ultrasensitive fluorescent proteins for imaging neuronal activity. *Nature*, 499(7458):295–300.

Chen, X., Leischner, U., Rochefort, N. L., Nelken, I., and Konnerth, A. (2011). Functional mapping of single spines in cortical neurons in vivo. *Nature*, 475(7357):501–505.

Cheung, S. W., Bedenbaugh, P. H., Nagarajan, S. S., and Schreiner, C. E. (2001). Functional organization of squirrel monkey primary auditory cortex: responses to pure tones. *Journal of Neurophysiology*, 85(4):1732–1749.

Chklovskii, D. B. and Koulakov, A. A. (2004). Maps in the brain: what can we learn from them? *Annu. Rev. Neurosci.*, 27:369–392.

Creutzfeldt, O., Hellweg, F.-C., and Schreiner, C. (1980). Thalamocortical transformation of responses to complex auditory stimuli. *Experimental Brain Research*, 39(1):87–104.

Dahmen, J. C., Hartley, D. E., and King, A. J. (2008). Stimulus-timing-dependent plasticity of cortical frequency representation. *The Journal of Neuroscience*, 28(50):13629–13639.

deCharms, C. R., Blake, D. T., and Merzenich, M. M. (1998). Optimizing sound features for cortical neurons. *science*, 280(5368):1439–1444.

Denk, W., Strickler, J. H., Webb, W. W., *et al.* (1990). Two-photon laser scanning fluorescence microscopy. *Science*, 248(4951):73–76.

DeWeese, M. R., Wehr, M., and Zador, A. M. (2003). Binary spiking in auditory cortex. *The Journal of Neuroscience*.

Dombeck, D. A., Graziano, M. S., and Tank, D. W. (2009). Functional clustering of neurons in motor cortex determined by cellular resolution imaging in awake behaving mice. *The Journal of Neuroscience*, 29(44):13751–13760.

Dombeck, D. A., Khabbaz, A. N., Collman, F., Adelman, T. L., and Tank, D. W. (2007). Imaging large-scale neural activity with cellular resolution in awake, mobile mice. *Neuron*, 56(1):43–57.

Dorrn, A. L., Yuan, K., Barker, A. J., Schreiner, C. E., and Froemke, R. C. (2010). Developmental sensory experience balances cortical excitation and inhibition. *Nature*, 465(7300):932–936.

Drager, U. and Hubel, D. H. (1975). Responses to visual stimulation and relationship between visual, auditory, and somatosensory inputs in mouse superior colliculus. *Journal of Neurophysiology*, 38(3):690–713.

Drullman, R., Festen, J. M., and Plomp, R. (1994). Effect of reducing slow temporal modulations on speech reception. *The Journal of the Acoustical Society of America*, 95(5):2670–2680.

Duda, R. O. and Martens, W. L. (1998). Range dependence of the response of a spherical head model. *The Journal of the Acoustical Society of America*, 104(5):3048–3058.

Dyer, E. L., Duarte, M. F., Johnson, D. H., and Baraniuk, R. G. (2010). Recovering spikes from noisy neuronal calcium signals via structured sparse approximation. In *International Conference on Latent Variable Analysis and Signal Separation*, pages 604–611. Springer.

Eggermont, J. J. and Mossop, J. E. (1998). Azimuth coding in primary auditory cortex of the cat. i. spike synchrony versus spike count representations. *Journal of neurophysiology*, 80(4):2133–2150.

Ehret, G. (1974). Age-dependent hearing loss in normal hearing mice. *Naturwissenschaften*, 61(11):506–507.

Ehret, G. and Dreyer, A. (1984). Localization of tones and noise in the horizontal plane by unrestrained house mice (mus musculus). *Journal of experimental biology*, 109(1):163–174.

Ehret, G. and Schreiner, C. (1997). Frequency resolution and spectral integration (critical band analysis) in single units of the cat primary auditory cortex. *Journal of Comparative Physiology A*, 181(6):635–650.

Elliott, T. M. and Theunissen, F. E. (2009). The modulation transfer function for speech intelligibility. *PLoS comput biol*, 5(3):e1000302.

Eramudugolla, R., McAnally, K. I., Martin, R. L., Irvine, D. R., and Mattingley, J. B. (2008). The role of spatial location in auditory search. *Hearing research*, 238(1):139–146.

Erulkar, S., Butler, R., and Gerstein, G. (1968). Excitation and inhibition in cochlear nucleus. ii. frequency-modulated tones. *Journal of Neurophysiology*, 31(4):537–548.

Eskandar, E. N., Richmond, B. J., and Optican, L. M. (1992). Role of inferior temporal neurons in visual memory. i. temporal encoding of information about visual images, recalled images, and behavioral context. *Journal of neurophysiology*, 68(4):1277–1295.

Evans, E. and Whitfield, I. (1964). Classification of unit responses in the auditory cortex of the unanaesthetized and unrestrained cat. *The Journal of physiology*, 171(3):476.

Fitzpatrick, D. C., Batra, R., Stanford, T. R., and Kuwada, S. (1997). A neuronal population code for sound localization. *Nature*, 388(6645):871–874.

Fritz, J., Shamma, S., Elhilali, M., and Klein, D. (2003). Rapid task-related plasticity of spectrotemporal receptive fields in primary auditory cortex. *Nature neuroscience*, 6(11):1216–1223.

Froemke, R. C. and Martins, A. R. O. (2011). Spectrotemporal dynamics of auditory cortical synaptic receptive field plasticity. *Hearing research*, 279(1):149–161.

Furukawa, S., Xu, L., and Middlebrooks, J. C. (2000). Coding of sound-source location by ensembles of cortical neurons. *The Journal of Neuroscience*, 20(3):1216–1228.

Fuzessery, Z. and Hall, J. (1996). Role of gaba in shaping frequency tuning and creating fm sweep selectivity in the inferior colliculus. *Journal of Neurophysiology*, 76(2):1059–1073.

Fuzessery, Z. M. (1994). Response selectivity for multiple dimensions of frequency sweeps in the pallid bat inferior colliculus. *Journal of neurophysiology*, 72(3):1061–1079.

Fuzessery, Z. M., Razak, K. A., and Williams, A. J. (2011). Multiple mechanisms shape selectivity for fm sweep rate and direction in the pallid bat inferior colliculus and auditory cortex. *Journal of Comparative Physiology A*, 197(5):615–623.

Fuzessery, Z. M., Richardson, M. D., and Coburn, M. S. (2006). Neural mechanisms underlying selectivity for the rate and direction of frequency-modulated sweeps in the inferior colliculus of the pallid bat. *Journal of neurophysiology*, 96(3):1320–1336.

Gaese, B. H. and Ostwald, J. (1995). Temporal coding of amplitude and frequency modulation in the rat auditory cortex. *European Journal of Neuroscience*, 7(3):438–450.

Gaese, B. H. and Ostwald, J. (2003). Complexity and temporal dynamics of frequency coding in the awake rat auditory cortex. *European Journal of Neuroscience*, 18(9):2638–2652.

Geis, H. and Borst, J. (2012). Intracellular responses to frequency modulated tones in the dorsal cortex of the mouse inferior colliculus. *Frontiers in neural circuits*, 7:7–7.

Gittelman, J. X., Li, N., and Pollak, G. D. (2009). Mechanisms underlying directional selectivity for frequency-modulated sweeps in the inferior colliculus revealed by in vivo whole-cell recordings. *The Journal of Neuroscience*, 29(41):13030–13041.

Godey, B., Atencio, C. A., Bonham, B. H., Schreiner, C. E., and Cheung, S. W. (2005). Functional organization of squirrel monkey primary auditory cortex: responses to frequency-modulation sweeps. *Journal of Neurophysiology*, 94(2):1299–1311.

Goldberg, J. M. and Brown, P. B. (1969). Response of binaural neurons of dog superior olivary complex to dichotic tonal stimuli: some physiological mechanisms of sound localization. *Journal of neurophysiology*, 32(4):613–636.

Goldstein Jr, M. H. and Abeles, M. (1975). Single unit activity of the auditory cortex. In *Auditory System*, pages 199–218. Springer.

Goodman, D. F., Benichoux, V., and Brette, R. (2013). Decoding neural responses to temporal cues for sound localization. *Elife*, 2:e01312.

Gordon, M. and O'Neill, W. E. (1998). Temporal processing across frequency channels by fm selective auditory neurons can account for fm rate selectivity. *Hearing research*, 122(1):97–108.

Grienberger, C. and Konnerth, A. (2012). Imaging calcium in neurons. *Neuron*, 73(5):862–885.

Grimsley, J. M., Monaghan, J. J., and Wenstrup, J. J. (2011). Development of social vocalizations in mice. *PloS one*, 6(3):e17460.

Grothe, B., Pecka, M., and McAlpine, D. (2010). Mechanisms of sound localization in mammals. *Physiological Reviews*, 90(3):983–1012.

Guizar-Sicairos, M., Thurman, S. T., and Fienup, J. R. (2008). Efficient subpixel image registration algorithms. *Optics letters*, 33(2):156–158.

Guo, W., Chambers, A. R., Darrow, K. N., Hancock, K. E., Shinn-Cunningham, B. G., and Polley, D. B. (2012). Robustness of cortical topography across fields, laminae, anesthetic states, and neurophysiological signal types. *The Journal of neuroscience*, 32(27):9159–9172.

Hackett, T. A., Barkat, T. R., O'Brien, B. M., Hensch, T. K., and Polley, D. B. (2011). Linking topography to tonotopy in the mouse auditory thalamocortical circuit. *The Journal of Neuroscience*, 31(8):2983–2995.

Hage, S. R. and Ehret, G. (2003). Mapping responses to frequency sweeps and tones in the inferior colliculus of house mice. *European Journal of Neuroscience*, 18(8):2301–2312.

Haider, B., Häusser, M., and Carandini, M. (2013). Inhibition dominates sensory responses in the awake cortex. *Nature*, 493(7430):97–100.

Harper, N. S. and McAlpine, D. (2004). Optimal neural population coding of an auditory spatial cue. *Nature*, 430(7000):682–686.

Harris, K. D. and Shepherd, G. M. (2015). The neocortical circuit: themes and variations. *Nature neuroscience*, 18(2):170–181.

Harris, K. D. and Thiele, A. (2011). Cortical state and attention. *Nature reviews neuroscience*, 12(9):509–523.

Heffner, H. E. and Heffner, R. S. (1990). Effect of bilateral auditory cortex lesions on sound localization in japanese macaques. *Journal of Neurophysiology*, 64(3):915–931.

Heffner, H. E. and Heffner, R. S. (2007). Hearing ranges of laboratory animals. *Journal of the American Association for Laboratory Animal Science*, 46(1):20–22.

Heffner, R. S. and Heffner, H. E. (1988). Sound localization in a predatory rodent, the northern grasshopper mouse (onychomys leucogaster). *Journal of Comparative Psychology*, 102(1):66.

Heffner, R. S., Koay, G., and Heffner, H. E. (2001). Sound-localization acuity changes with age in c57/bl6j mice. In Willott, J., editor, *Handbook of mouse auditory research: From behavior to molecular biology*, chapter 3, pages 31–35. CRC Press, Boca Raton, FL.

Heil, P. (1997). Auditory cortical onset responses revisited. ii. response strength. *Journal of Neurophysiology*, 77(5):2642–2660.

Heil, P., Rajan, R., and Irvine, D. R. (1992). Sensitivity of neurons in cat primary auditory cortex to tones and frequency-modulated stimuli. ii: Organization of response properties along the isofrequency dimension. *Hearing research*, 63(1):135–156.

Hellweg, F., Koch, R., and Vollrath, M. (1977). Representation of the cochlea in the neocortex of guinea pigs. *Experimental brain research*, 29(3-4):467–474.

Higgins, N. C., Storace, D. A., Escabí, M. A., and Read, H. L. (2010). Specialization of binaural responses in ventral auditory cortices. *The Journal of Neuroscience*, 30(43):14522–14532.

Hind, J. E. (1953). An electrophysiological determination of tonotopic organization in auditory cortex of cat. *Journal of neurophysiology*.

Holy, T. E. and Guo, Z. (2005). Ultrasonic songs of male mice. *PLoS Biol*, 3(12):e386.

Honma, Y., Tsukano, H., Horie, M., Ohshima, S., Tohmi, M., Kubota, Y., Takahashi, K., Hishida, R., Takahashi, S., and Shibuki, K. (2013). Auditory cortical areas activated by slow frequency-modulated sounds in mice. *PloS one*, 8(7):e68113.

Horie, M., Tsukano, H., Hishida, R., Takebayashi, H., and Shibuki, K. (2013). Dual compartments of the ventral division of the medial geniculate body projecting to the core region of the auditory cortex in c57bl/6 mice. *Neuroscience research*, 76(4):207–212.

Hromádka, T., DeWeese, M. R., and Zador, A. M. (2008). Sparse representation of sounds in the unanesthetized auditory cortex. *PLoS Biol*, 6(1):e16.

Hubel, D. and Wiesel, T. (1963). Shape and arrangement of columns in cat's striate cortex. *The Journal of physiology*, 165(3):559.

Hubel, D. H., Henson, C. O., Rupert, A., and Galambos, R. (1959). "Attention" units in the auditory cortex. *Science*, 129(3358):1279–1280.

Hubel, D. H. and Wiesel, T. N. (1962). Receptive fields, binocular interaction and functional architecture in the cat's visual cortex. *The Journal of physiology*, 160(1):106–154.

Hübener, M., Shoham, D., Grinvald, A., and Bonhoeffer, T. (1997). Spatial relationships among three columnar systems in cat area 17. *The journal of neuroscience*, 17(23):9270–9284.

Imaizumi, K., Priebe, N. J., Crum, P. A., Bedenbaugh, P. H., Cheung, S. W., and Schreiner, C. E. (2004). Modular functional organization of cat anterior auditory field. *Journal of neurophysiology*, 92(1):444–457.

Imaizumi, K. and Schreiner, C. E. (2007). Spatial interaction between spectral integration and frequency gradient in primary auditory cortex. *Journal of neurophysiology*, 98(5):2933–2942.

Imig, T., Adria, H., *et al.* (1977). Binaural columns in the primary field (A1) of cat auditory cortex. *Brain research*, 138(2):241–257.

Imig, T. J., Irons, W. A., and Samson, F. R. (1990). Single-unit selectivity to azimuthal direction and sound pressure level of noise bursts in cat high-frequency primary auditory cortex. *Journal of Neurophysiology*, 63(6):1448–1466.

Ince, R. A., Panzeri, S., and Kayser, C. (2013). Neural codes formed by small and temporally precise populations in auditory cortex. *The Journal of Neuroscience*, 33(46):18277–18287.

Irvine, D., Rajan, R., and Aitkin, L. (1996). Sensitivity to interaural intensity differences of neurons in primary auditory cortex of the cat. i. types of sensitivity and effects of variations in sound pressure level. *Journal of neurophysiology*, 75(1):75–96.

Irving, R. and Harrison, J. (1967). The superior olivary complex and audition: a comparative study. *Journal of Comparative Neurology*, 130(1):77–86.

Ison, J. R., Allen, P. D., and O'Neill, W. E. (2007). Age-related hearing loss in c57bl/6j mice has both frequency-specific and non-frequency-specific components that produce a hyperacusis-like exaggeration of the acoustic startle reflex. *Journal of the Association for Research in Otolaryngology*, 8(4):539–550.

Issa, E. B. and Wang, X. (2008). Sensory responses during sleep in primate primary and secondary auditory cortex. *The Journal of Neuroscience*, 28(53):14467–14480.

Issa, J., Heffele, B., Zhang, M., Young, E., and Yue, D. (2016). Spatiotemporal response properties across auditory cortical fields under widefield imaging. ARO Abstr PS 507.

Issa, J. B., Haeffele, B. D., Agarwal, A., Bergles, D. E., Young, E. D., and Yue, D. T. (2014). Multiscale optical calcium imaging of tonal organization in mouse auditory cortex. *Neuron*, 83(4):944–959.

Ito, T. and Oliver, D. L. (2014). Local and commissural ic neurons make axosomatic inputs on large gabaergic tectothalamic neurons. *Journal of Comparative Neurology*, 522(15):3539–3554.

Jenkins, W. M. and Merzenich, M. M. (1984). Role of cat primary auditory cortex for sound-localization behavior. *Journal of Neurophysiology*, 52(5):819–847.

Joachimsthaler, B., Uhlmann, M., Miller, F., Ehret, G., and Kurt, S. (2014). Quantitative analysis of neuronal response properties in primary and higher-order auditory cortical fields of awake house mice (mus musculus). *European Journal of Neuroscience*, 39(6):904–918.

Kaas, J. H. (1997). Topographic maps are fundamental to sensory processing. *Brain research bulletin*, 44(2):107–112.

Kanold, P. O., Nelken, I., and Polley, D. B. (2014). Local versus global scales of organization in auditory cortex. *Trends in neurosciences*, 37(9):502–510.

Kanwal, J. S., Matsumura, S., Ohlemiller, K., and Suga, N. (1994). Analysis of acoustic elements and syntax in communication sounds emitted by mustached bats. *The Journal of the Acoustical Society of America*, 96(3):1229–1254.

Kavanagh, G. L. and Kelly, J. B. (1987). Contribution of auditory cortex to sound localization by the ferret (mustela putorius). *Journal of Neurophysiology*, 57(6):1746–1766.

Keating, P., Dahmen, J. C., and King, A. J. (2015). Complementary adaptive processes contribute to the developmental plasticity of spatial hearing. *Nature neuroscience*, 18(2):185–187.

Keating, P., Rosenior-Patten, O., Dahmen, J. C., Bell, O., and King, A. J. (2016). Behavioral training promotes multiple adaptive processes following acute hearing loss. *eLife*, 5:e12264.

Kelly, J. B. (1980). Effects of auditory cortical lesions on sound localization by the rat. *Journal of Neurophysiology*, 44(6):1161–1174.

Kelly, J. B. and Judge, P. W. (1994). Binaural organization of primary auditory cortex in the ferret (mustela putorius). *Journal of neurophysiology*, 71(3):904–913.

Kelly, J. B. and Kavanagh, G. L. (1986). Effects of auditory cortical lesions on pure-tone sound localization by the albino rat. *Behavioral neuroscience*, 100(4):569.

Kelly, J. B., Kavanagh, G. L., and Dalton, J. C. (1986). Hearing in the ferret (mustela putorius): thresholds for pure tone detection. *Hearing research*, 24(3):269–275.

Kelly, J. B. and Sally, S. L. (1988). Organization of auditory cortex in the albino rat: binaural response properties. *Journal of neurophysiology*, 59(6):1756–1769.

Kerlin, A. M., Andermann, M. L., Berezovskii, V. K., and Reid, R. C. (2010). Broadly tuned response properties of diverse inhibitory neuron subtypes in mouse visual cortex. *Neuron*, 67(5):858–871.

Kettner, R. E., Feng, J., and Brugge, J. F. (1985). Postnatal development of the phase-locked response to low frequency tones of auditory nerve fibers in the cat. *The Journal of neuroscience*, 5(2):275–283.

Kilgard, M. P. and Merzenich, M. M. (1999). Distributed representation of spectral and temporal information in rat primary auditory cortex. *Hearing research*, 134(1):16–28.

King, A., Moore, D., and Hutchings, M. (1994). Topographic representation of auditory space in the superior colliculus of adult ferrets after monaural deafening in infancy. *Journal of neurophysiology*, 71(1):182–194.

King, A. and Palmer, A. (1983). Cells responsive to free-field auditory stimuli in guinea-pig superior colliculus: distribution and response properties. *The Journal of Physiology*, 342:361.

King, A. J. (2004). The superior colliculus. *Current Biology*, 14(9):R335–R338.

King, A. J., Kacelnik, O., Mrsic-Flogel, T. D., Schnupp, J. W., Parsons, C. H., and Moore, D. R. (2001). How plastic is spatial hearing? *Audiology and Neurotology*, 6(4):182–186.

King, A. J. and Nelken, I. (2009). Unraveling the principles of auditory cortical processing: can we learn from the visual system? *Nature neuroscience*, 12(6):698–701.

King, A. J., Schnupp, J. W., and Thompson, I. D. (1998). Signals from the superficial layers of the superior colliculus enable the development of the auditory space map in the deeper layers. *The Journal of neuroscience*, 18(22):9394–9408.

Kisley, M. A. and Gerstein, G. L. (1999). Trial-to-trial variability and state-dependent modulation of auditory-evoked responses in cortex. *Journal of Neuroscience*, 19(23):10451–10460.

Kitzes, L. (2008). Binaural interactions shape binaural response structures and frequency response functions in primary auditory cortex. *Hearing research*, 238(1):68–76.

Knudsen, E. I., Lac, S. d., and Esterly, S. D. (1987). Computational maps in the brain. *Annual review of neuroscience*, 10(1):41–65.

Ko, H., Hofer, S. B., Pichler, B., Buchanan, K. A., Sjöström, P. J., and Mrsic-Flogel, T. D. (2011). Functional specificity of local synaptic connections in neocortical networks. *Nature*, 473(7345):87–91.

Koch, U. and Grothe, B. (1998). Gabaergic and glycinergic inhibition sharpens tuning for frequency modulations in the inferior colliculus of the big brown bat. *Journal of Neurophysiology*, 80(1):71–82.

Kohn, A. and Smith, M. A. (2005). Stimulus dependence of neuronal correlation in primary visual cortex of the macaque. *The Journal of neuroscience*, 25(14):3661–3673.

Köppl, C. (1997). Phase locking to high frequencies in the auditory nerve and cochlear nucleus magnocellularis of the barn owl, tyto alba. *The Journal of neuroscience: the official journal of the Society for Neuroscience*, 17(9):3312.

Kowalski, N., Depireux, D. A., and Shamma, S. A. (1996). Analysis of dynamic spectra in ferret primary auditory cortex. i. characteristics of single-unit responses to moving ripple spectra. *Journal of neurophysiology*, 76(5):3503–3523.

Kowalski, N., Versnel, H., and Shamma, S. A. (1995). Comparison of responses in the anterior and primary auditory fields of the ferret cortex. *Journal of Neurophysiology*, 73(4):1513–1523.

Kubota, Y., Kamatani, D., Tsukano, H., Ohshima, S., Takahashi, K., Hishida, R., Kudoh, M., Takahashi, S., and Shibuki, K. (2008). Transcranial photo-inactivation of neural activities in the mouse auditory cortex. *Neuroscience research*, 60(4):422–430.

Kumar, T. R., Larson, M., Wang, H., McDermott, J., and Bronshteyn, I. (2009). Transgenic mouse technology: principles and methods. *Molecular Endocrinology: Methods and Protocols*, pages 335–362.

Kumpik, D. P., Kacelnik, O., and King, A. J. (2010). Adaptive reweighting of auditory localization cues in response to chronic unilateral earplugging in humans. *The Journal of Neuroscience*, 30(14):4883–4894.

Kuo, R. I. and Wu, G. K. (2012). The generation of direction selectivity in the auditory system. *Neuron*, 73(5):1016–1027.

Kyweriga, M., Stewart, W., Cahill, C., and Wehr, M. (2014). Synaptic mechanisms underlying interaural level difference selectivity in rat auditory cortex. *Journal of neurophysiology*, 112(10):2561–2571.

Lakatos, P., Pincze, Z., Fu, K.-M. G., Javitt, D. C., Karmos, G., and Schroeder, C. E. (2005). Timing of pure tone and noise-evoked responses in macaque auditory cortex. *Neuroreport*, 16(9):933–937.

Lauer, A. M., Slee, S. J., and May, B. J. (2011). Acoustic basis of directional acuity in laboratory mice. *Journal of the Association for Research in Otolaryngology*, 12(5):633–645.

Lee, C., Schreiner, C., Imaizumi, K., and Winer, J. (2004). Tonotopic and heterotopic projection systems in physiologically defined auditory cortex. *Neuroscience*, 128(4):871–887.

Lee, C.-C. and Middlebrooks, J. C. (2011). Auditory cortex spatial sensitivity sharpens during task performance. *Nature neuroscience*, 14(1):108–114.

Lee, H., Wallani, T., and Mendelson, J. (2002). Temporal processing speed in the inferior colliculus of young and aged rats. *Hearing research*, 174(1):64–74.

Lee, K.-S., Huang, X., and Fitzpatrick, D. (2016). Topology of on and off inputs in visual cortex enables an invariant columnar architecture. *Nature*, 533(7601):90–94.

Letzkus, J. J., Wolff, S. B., Meyer, E. M., Tovote, P., Courtin, J., Herry, C., and Lüthi, A. (2011). A disinhibitory microcircuit for associative fear learning in the auditory cortex. *Nature*, 480(7377):331–335.

Li, Y., Fitzpatrick, D., and White, L. E. (2006). The development of direction selectivity in ferret visual cortex requires early visual experience. *Nature neuroscience*, 9(5):676–681.

Li, Y., Van Hooser, S. D., Mazurek, M., White, L. E., and Fitzpatrick, D. (2008). Experience with moving visual stimuli drives the early development of cortical direction selectivity. *Nature*, 456(7224):952–956.

Linden, J. F., Liu, R. C., Sahani, M., Schreiner, C. E., and Merzenich, M. M. (2003). Spectrotemporal structure of receptive fields in areas ai and aaf of mouse auditory cortex. *Journal of Neurophysiology*, 90(4):2660–2675.

Linden, J. F. and Schreiner, C. E. (2003). Columnar transformations in auditory cortex? a comparison to visual and somatosensory cortices. *Cerebral Cortex*, 13(1):83–89.

Liu, R. C., Miller, K. D., Merzenich, M. M., and Schreiner, C. E. (2003). Acoustic variability and distinguishability among mouse ultrasound vocalizations. *The Journal of the Acoustical Society of America*, 114(6):3412–3422.

Loftus, W. C., Bishop, D. C., and Oliver, D. L. (2010). Differential patterns of inputs create functional zones in central nucleus of inferior colliculus. *The Journal of neuroscience*, 30(40):13396–13408.

Loftus, W. C., Bishop, D. C., Saint Marie, R. L., and Oliver, D. L. (2004). Organization of binaural excitatory and inhibitory inputs to the inferior colliculus from the superior olive. *Journal of Comparative Neurology*, 472(3):330–344.

Lomber, S. G. and Malhotra, S. (2008). Double dissociation of "what" and "where" processing in auditory cortex. *Nature neuroscience*, 11(5):609–616.

Lu, T., Liang, L., and Wang, X. (2001). Temporal and rate representations of time-varying signals in the auditory cortex of awake primates. *Nature neuroscience*, 4(11):1131–1138.

Lui, B. and Mendelson, J. (2003). Frequency modulated sweep responses in the medial geniculate nucleus. *Experimental brain research*, 153(4):550–553.

Maldonado, P. E., Gödecke, I., Gray, C. M., and Bonhoeffer, T. (1997). Orientation selectivity in pinwheel centers in cat striate cortex. *Science*, 276(5318):1551–1555.

Malhotra, S., Hall, A. J., and Lomber, S. G. (2004). Cortical control of sound localization in the cat: unilateral cooling deactivation of 19 cerebral areas. *Journal of Neurophysiology*, 92(3):1625–1643.

Malhotra, S. and Lomber, S. G. (2007). Sound localization during homotopic and heterotopic bilateral cooling deactivation of primary and nonprimary auditory cortical areas in the cat. *Journal of neurophysiology*, 97(1):26–43.

Margrie, T. W., Brecht, M., and Sakmann, B. (2002). In vivo, low-resistance, whole-cell recordings from neurons in the anaesthetized and awake mammalian brain. *Pflügers Archiv*, 444(4):491–498.

Marguet, S. L. and Harris, K. D. (2011). State-dependent representation of amplitude-modulated noise stimuli in rat auditory cortex. *The Journal of neuroscience*, 31(17):6414–6420.

McAlpine, D. (2005). Creating a sense of auditory space. *The Journal of physiology*, 566(1):21–28.

McAlpine, D., Jiang, D., and Palmer, A. R. (2001). A neural code for low-frequency sound localization in mammals. *Nature neuroscience*, 4(4):396–401.

Mendelson, J. and Cynader, M. (1985). Sensitivity of cat primary auditory cortex (al) neurons to the direction and rate of frequency modulation. *Brain research*, 327(1):331–335.

Mendelson, J. and Ricketts, C. (2001). Age-related temporal processing speed deterioration in auditory cortex. *Hearing research*, 158(1):84–94.

Mendelson, J., Schreiner, C., and Sutter, M. (1997). Functional topography of cat primary auditory cortex: response latencies. *Journal of Comparative Physiology A*, 181(6):615–633.

Mendelson, J. R., Schreiner, C. E., Sutter, M. L., and Grasse, K. L. (1993). Functional topography of cat primary auditory cortex: responses to frequency-modulated sweeps. *Experimental Brain Research*, 94(1):65–87.

Merzenich, M. M., Jenkins, W. M., Johnston, P., Schreiner, C., *et al.* (1996). Temporal processing deficits of language-learning impaired children ameliorated by training. *Science*, 271(5245):77.

Merzenich, M. M., Knight, P. L., and Roth, G. L. (1973). Cochleotopic organization of primary auditory cortex in the cat. *Brain research*, 63:343–346.

Merzenich, M. M., Knight, P. L., and Roth, G. L. (1975). Representation of cochlea within primary auditory cortex in the cat. *Journal of neurophysiology*, 38(2):231–249.

Merzenich, M. M. and Reid, M. D. (1974). Representation of the cochlea within the inferior colliculus of the cat. *Brain research*, 77(3):397–415.

Mickey, B. J. and Middlebrooks, J. C. (2003). Representation of auditory space by cortical neurons in awake cats. *The Journal of neuroscience*, 23(25):8649–8663.

Middlebrooks, J. C. (1987). Binaural mechanisms of spatial tuning in the cat's superior colliculus distinguished using monaural occlusion. *Journal of neurophysiology*, 57(3):688–701.

Middlebrooks, J. C. (1999). Individual differences in external-ear transfer functions reduced by scaling in frequency. *The Journal of the Acoustical Society of America*, 106(3):1480–1492.

Middlebrooks, J. C. (2002). Auditory space processing: here, there or everywhere? *Nature neuroscience*, 5(9):824–826.

Middlebrooks, J. C., Dykes, R. W., and Merzenich, M. M. (1980). Binaural response-specific bands in primary auditory cortex (ai) of the cat: topographical organization orthogonal to isofrequency contours. *Brain research*, 181(1):31–48.

Middlebrooks, J. C. and Onsan, Z. A. (2012). Stream segregation with high spatial acuity. *The Journal of the Acoustical Society of America*, 132(6):3896–3911.

Middlebrooks, J. C. and Pettigrew, J. D. (1981). Functional classes of neurons in primary auditory cortex of the cat distinguished by sensitivity to sound location. *J Neurosci*, 1(1):107–120.

Miller, L. M. and Recanzone, G. H. (2009). Populations of auditory cortical neurons can accurately encode acoustic space across stimulus intensity. *Proceedings of the National Academy of Sciences*, 106(14):5931–5935.

Mills, A. W. (1958). On the minimum audible angle. *The Journal of the Acoustical Society of America*, 30(4):237–246.

Mitani, A., Itoh, K., and Mizuno, N. (1987). Distrubution and size of thalamic neurons projecting to layer i of the auditory cortical fields of the cat compared to those projecting to layer iv. *Journal of Comparative Neurology*, 257(1):105–121.

Młynarski, W. and Jost, J. (2014). Statistics of natural binaural sounds. *PloS one*, 9(10):e108968.

Moller, A. (1969). Unit responses in the cochlear nucleus of the rat to sweep tones. *Acta Physiologica Scandinavica*, 76(4):503–512.

Moshitch, D., Las, L., Ulanovsky, N., Bar-Yosef, O., and Nelken, I. (2006). Responses of neurons in primary auditory cortex (A1) to pure tones in the halothane-anesthetized cat. *Journal of neurophysiology*, 95(6):3756–3769.

Mountcastle, V. B. (1997). The columnar organization of the neocortex. *Brain*, 120(4):701–722.

Mountcastle, V. B. (2003). Introduction. *Cerebral Cortex*, 13(1):2–4.

Mountcastle, V. B. *et al.* (1957). Modality and topographic properties of single neurons of cat's somatic sensory cortex. *Journal of Physiology*, 20(4):408–434.

Mrsic-Flogel, T. D., Hofer, S. B., Ohki, K., Reid, R. C., Bonhoeffer, T., and Hübener, M. (2007). Homeostatic regulation of eye-specific responses in visual cortex during ocular dominance plasticity. *Neuron*, 54(6):961–972.

Mrsic-Flogel, T. D., King, A. J., Jenison, R. L., and Schnupp, J. W. (2001). Listening through different ears alters spatial response fields in ferret primary auditory cortex. *Journal of Neurophysiology*, 86(2):1043–1046.

Mrsic-Flogel, T. D., King, A. J., and Schnupp, J. W. (2005). Encoding of virtual acoustic space stimuli by neurons in ferret primary auditory cortex. *Journal of neurophysiology*, 93(6):3489–3503.

Mrsic-Flogel, T. D., Versnel, H., and King, A. J. (2006). Development of contralateral and ipsilateral frequency representations in ferret primary auditory cortex. *European Journal of Neuroscience*, 23(3):780–792.

Nakamoto, K. T., Zhang, J., and Kitzes, L. M. (2004). Response patterns along an isofrequency contour in cat primary auditory cortex (ai) to stimuli varying in average and interaural levels. *Journal of neurophysiology*, 91(1):118–135.

Nelken, I. (2008). Processing of complex sounds in the auditory system. *Current opinion in neurobiology*, 18(4):413–417.

Nelken, I. and Bar-Yosef, O. (2008). Neurons and objects: the case of auditory cortex. *Frontiers in neuroscience*, 2(1):107.

Nelken, I., Bizley, J. K., Nodal, F. R., Ahmed, B., King, A. J., and Schnupp, J. W. (2008). Responses of auditory cortex to complex stimuli: functional organization revealed using intrinsic optical signals. *Journal of neurophysiology*, 99(4):1928–1941.

Nelken, I., Bizley, J. K., Nodal, F. R., Ahmed, B., Schnupp, J. W., and King, A. J. (2004). Large-scale organization of ferret auditory cortex revealed using continuous acquisition of intrinsic optical signals. *Journal of neurophysiology*, 92(4):2574–2588.

Nelken, I., Chechik, G., Mrsic-Flogel, T. D., King, A. J., and Schnupp, J. W. (2005). Encoding stimulus information by spike numbers and mean response time in primary auditory cortex. *Journal of computational neuroscience*, 19(2):199–221.

Nelken, I., Fishbach, A., Las, L., Ulanovsky, N., and Farkas, D. (2003). Primary auditory cortex of cats: feature detection or something else? *Biological cybernetics*, 89(5):397–406.

Nelken, I. and Versnel, H. (2000). Responses to linear and logarithmic frequency-modulated sweeps in ferret primary auditory cortex. *European Journal of Neuroscience*, 12(2):549–562.

Nodal, F., Bajo, V., Parsons, C., Schnupp, J., and King, A. (2008). Sound localization behavior in ferrets: comparison of acoustic orientation and approach-to-target responses. *Neuroscience*, 154(1):397–408.

Nodal, F. R., Kacelnik, O., Bajo, V. M., Bizley, J. K., Moore, D. R., and King, A. J. (2010). Lesions of the auditory cortex impair azimuthal sound localization and its recalibration in ferrets. *Journal of neurophysiology*, 103(3):1209–1225.

Nomura, H., Hara, K., Abe, R., Hitora-Imamura, N., Nakayama, R., Sasaki, T., Matsuki, N., and Ikegaya, Y. (2015). Memory formation and retrieval of neuronal silencing in the auditory cortex. *Proceedings of the National Academy of Sciences*, 112(31):9740–9744.

Nyby, J. (2001). Auditory communication among adults. *Handbook of mouse auditory research: from behavior to molecular biology*, pages 3–18.

O'Connor, K. N. and Sutter, M. L. (2000). Global spectral and location effects in auditory perceptual grouping. *Journal of Cognitive Neuroscience*, 12(2):342–354.

Ohki, K., Chung, S., Ch'ng, Y. H., Kara, P., and Reid, R. C. (2005). Functional imaging with cellular resolution reveals precise micro-architecture in visual cortex. *Nature*, 433(7026):597–603.

Ohki, K., Chung, S., Kara, P., Hübener, M., Bonhoeffer, T., and Reid, R. C. (2006). Highly ordered arrangement of single neurons in orientation pinwheels. *Nature*, 442(7105):925–928.

Ohki, K. and Reid, R. C. (2007). Specificity and randomness in the visual cortex. *Current opinion in neurobiology*, 17(4):401–407.

Ohl, F. W., Wetzel, W., Wagner, T., Rech, A., and Scheich, H. (1999). Bilateral ablation of auditory cortex in mongolian gerbil affects discrimination of frequency modulated tones but not of pure tones. *Learning & Memory*, 6(4):347–362.

Olshausen, B. A. and Field, D. J. (2004). Sparse coding of sensory inputs. *Current opinion in neurobiology*, 14(4):481–487.

Orduña, I., Mercado, E., Gluck, M. A., and Merzenich, M. M. (2001). Spectrotemporal sensitivities in rat auditory cortical neurons. *Hearing research*, 160(1):47–57.

Osanai, H. and Tateno, T. (2016). Neural response differences in the rat primary auditory cortex under anesthesia with ketamine versus the mixture of medetomidine, midazolam and butorphanol. *Hearing research*, 339:69–79.

Otazu, G. H., Tai, L.-H., Yang, Y., and Zador, A. M. (2009). Engaging in an auditory task suppresses responses in auditory cortex. *Nature neuroscience*, 12(5):646–654.

Palmer, A. and King, A. (1985). A monaural space map in the guinea-pig superior colliculus. *Hearing research*, 17(3):267–280.

Palmer, A. and Russell, I. (1986). Phase-locking in the cochlear nerve of the guinea-pig and its relation to the receptor potential of inner hair-cells. *Hearing research*, 24(1):1–15.

Pandya, P. K., Rathbun, D. L., Moucha, R., Engineer, N. D., and Kilgard, M. P. (2008). Spectral and temporal processing in rat posterior auditory cortex. *Cerebral Cortex*, 18(2):301–314.

Panzeri, S., Brunel, N., Logothetis, N. K., and Kayser, C. (2010). Sensory neural codes using multiplexed temporal scales. *Trends in neurosciences*, 33(3):111–120.

Panzeri, S., Macke, J. H., Gross, J., and Kayser, C. (2015). Neural population coding: combining insights from microscopic and mass signals. *Trends in cognitive sciences*, 19(3):162–172.

Panzeri, S., Petroni, F., Petersen, R. S., and Diamond, M. E. (2003). Decoding neuronal population activity in rat somatosensory cortex: role of columnar organization. *Cerebral Cortex*, 13(1):45–52.

Park, T. J., Klug, A., Holinstat, M., and Grothe, B. (2004). Interaural level difference processing in the lateral superior olive and the inferior colliculus. *Journal of neurophysiology*, 92(1):289–301.

Parsons, C. H., Lanyon, R. G., Schnupp, J. W., and King, A. J. (1999). Effects of altering spectral cues in infancy on horizontal and vertical sound localization by adult ferrets. *Journal of neurophysiology*, 82(5):2294–2309.

Peron, S. P., Freeman, J., Iyer, V., Guo, C., and Svoboda, K. (2015). A cellular resolution map of barrel cortex activity during tactile behavior. *Neuron*, 86(3):783–799.

Philibert, B., Beitel, R. E., Nagarajan, S. S., Bonham, B. H., Schreiner, C. E., and Cheung, S. W. (2005). Functional organization and hemispheric comparison of primary auditory cortex in the common marmoset (callithrix jacchus). *Journal of Comparative Neurology*, 487(4):391–406.

Phillips, D. and Cynader, M. (1985). Some neural mechanisms in the cat's auditory cortex underlying sensitivity to combined tone and wide-spectrum noise stimuli. *Hearing research*, 18(1):87–102.

Phillips, D. and Irvine, D. (1983). Some features of binaural input to single neurons in physiologically defined area ai of cat cerebral cortex. *Journal of Neurophysiology*, 49(2):383–395.

Phillips, D., Judge, P., and Kelly, J. (1988). Primary auditory cortex in the ferret (mustela putorius): neural response properties and topographic organization. *Brain research*, 443(1-2):281–294.

Pick, G. (1979). A study of frequency transitions in cat vocalizations. *The Journal of the Acoustical Society of America*, 66(2):594–597.

Polley, D. B., Read, H. L., Storace, D. A., and Merzenich, M. M. (2007). Multiparametric auditory receptive field organization across five cortical fields in the albino rat. *Journal of Neurophysiology*, 97(5):3621–3638.

Polley, D. B., Steinberg, E. E., and Merzenich, M. M. (2006). Perceptual learning directs auditory cortical map reorganization through top-down influences. *The journal of neuroscience*, 26(18):4970–4982.

Polley, D. B., Thompson, J. H., and Guo, W. (2013). Brief hearing loss disrupts binaural integration during two early critical periods of auditory cortex development. *Nature communications*, 4.

Poon, P. W., Chen, X., and Cheung, Y. (1992). Differences in fm response correlate

with morphology of neurons in the rat inferior colliculus. *Experimental brain research*, 91(1):94–104.

Popescu, M. V. and Polley, D. B. (2010). Monaural deprivation disrupts development of binaural selectivity in auditory midbrain and cortex. *Neuron*, 65(5):718–731.

Portfors, C., Mayko, Z., Jonson, K., Cha, G., and Roberts, P. (2011). Spatial organization of receptive fields in the auditory midbrain of awake mouse. *Neuroscience*, 193:429–439.

Portfors, C. V. (2007). Types and functions of ultrasonic vocalizations in laboratory rats and mice. *Journal of the American Association for Laboratory Animal Science*, 46(1):28–34.

Poulet, J. F., Fernandez, L. M., Crochet, S., and Petersen, C. C. (2012). Thalamic control of cortical states. *Nature neuroscience*, 15(3):370–372.

Radziwon, K. E., June, K. M., Stolzberg, D. J., Xu-Friedman, M. A., Salvi, R. J., and Dent, M. L. (2009). Behaviorally measured audiograms and gap detection thresholds in cba/caj mice. *Journal of Comparative Physiology A*, 195(10):961–969.

Rajan, R., Aitkin, L., Irvine, D., and McKay, J. (1990). Azimuthal sensitivity of neurons in primary auditory cortex of cats. i. types of sensitivity and the effects of variations in stimulus parameters. *Journal of Neurophysiology*, 64(3):872–887.

Rauschecker, J. P. (1998). Parallel processing in the auditory cortex of primates. *Audiology and Neurotology*, 3(2-3):86–103.

Razak, K. A. (2011). Systematic representation of sound locations in the primary auditory cortex. *The Journal of Neuroscience*, 31(39):13848–13859.

Razak, K. A. and Fuzessery, Z. M. (2000). A systematic representation of interaural intensity differences in the auditory cortex of the pallid bat. *Neuroreport*, 11(13):2919–2924.

Razak, K. A. and Fuzessery, Z. M. (2002). Functional organization of the pallid bat auditory cortex: emphasis on binaural organization. *Journal of neurophysiology*, 87(1):72–86.

Razak, K. A. and Fuzessery, Z. M. (2006). Neural mechanisms underlying selectivity for the rate and direction of frequency-modulated sweeps in the auditory cortex of the pallid bat. *Journal of neurophysiology*, 96(3):1303–1319.

Razak, K. A. and Fuzessery, Z. M. (2007). Development of inhibitory mechanisms underlying selectivity for the rate and direction of frequency-modulated sweeps in the auditory cortex. *The Journal of neuroscience*, 27(7):1769–1781.

Razak, K. A. and Fuzessery, Z. M. (2008). Facilitatory mechanisms underlying selectivity for the direction and rate of frequency modulated sweeps in the auditory cortex. *The Journal of Neuroscience*, 28(39):9806–9816.

Razak, K. A. and Fuzessery, Z. M. (2009). Gaba shapes selectivity for the rate and direction of frequency-modulated sweeps in the auditory cortex. *Journal of neurophysiology*, 102(3):1366–1378.

Reale, R. A. and Imig, T. J. (1980). Tonotopic organization in auditory cortex of the cat. *Journal of Comparative Neurology*, 192(2):265–291.

Reale, R. A. and Kettner, R. E. (1986). Topography of binaural organization in primary auditory cortex of the cat: effects of changing interaural intensity. *Journal of neurophysiology*, 56(3):663–682.

Recanzone, G. a., Schreiner, C., and Merzenich, M. M. (1993). Plasticity in the frequency representation of primary auditory cortex following discrimination training in adult owl monkeys. *The Journal of Neuroscience*, 13(1):87–103.

Recanzone, G. H. (2008). Representation of con-specific vocalizations in the core and belt areas of the auditory cortex in the alert macaque monkey. *The Journal of neuroscience*, 28(49):13184–13193.

Recanzone, G. H. and Beckerman, N. S. (2004). Effects of intensity and location on sound location discrimination in macaque monkeys. *Hearing research*, 198(1):116–124.

Recanzone, G. H. and Cohen, Y. E. (2010). Serial and parallel processing in the primate auditory cortex revisited. *Behavioural brain research*, 206(1):1–7.

Recanzone, G. H., Guard, D. C., Phan, M. L., and Su, T.-I. K. (2000). Correlation between the activity of single auditory cortical neurons and sound-localization behavior in the macaque monkey. *Journal of neurophysiology*, 83(5):2723–2739.

Recanzone, G. H., Schreiner, C. E., Sutter, M. L., Beitel, R. E., and Merzenich, M. M. (1999). Functional organization of spectral receptive fields in the primary auditory cortex of the owl monkey. *The Journal of comparative neurology*, 415(4):460–481.

Reed, M. C. and Blum, J. J. (1990). A model for the computation and encoding of azimuthal information by the lateral superior olive. *The Journal of the Acoustical Society of America*, 88(3):1442–1453.

Rendall, D., Rodman, P. S., and Emond, R. E. (1996). Vocal recognition of individuals and kin in free-ranging rhesus monkeys. *Animal behaviour*, 51(5):1007–1015.

Reser, D., Fishman, Y. I., Arezzo, J. C., and Steinschneider, M. (2000). Binaural interactions in primary auditory cortex of the awake macaque. *Cerebral Cortex*, 10(6):574–584.

Ricketts, C., Mendelson, J., Anand, B., and English, R. (1998). Responses to time-varying stimuli in rat auditory cortex. *Hearing research*, 123(1):27–30.

Romanski, L. M., Tian, B., Fritz, J., Mishkin, M., Goldman-Rakic, P. S., and Rauschecker, J. P. (1999). Dual streams of auditory afferents target multiple domains in the primate prefrontal cortex. *Nature neuroscience*, 2(12):1131–1136.

Rothschild, G. and Mizrahi, A. (2015). Global order and local disorder in brain maps. *Neuroscience*, 38(1):247.

Rothschild, G., Nelken, I., and Mizrahi, A. (2010). Functional organization and population dynamics in the mouse primary auditory cortex. *Nature neuroscience*, 13(3):353–360.

Rutkowski, R. G., Wallace, M. N., Shackleton, T. M., and Palmer, A. R. (2000). Organisation of binaural interactions in the primary and dorsocaudal fields of the guinea pig auditory cortex. *Hearing research*, 145(1):177–189.

Ryan, A. F., Woolf, N. K., and Sharp, F. R. (1982). Tonotopic organization in the central auditory pathway of the mongolian gerbil: A 2-deoxyglucose study. *Journal of Comparative Neurology*, 207(4):369–380.

Rybalko, N., Šuta, D., Nwabueze-Ogbo, F., and Syka, J. (2006). Effect of auditory cortex lesions on the discrimination of frequency-modulated tones in rats. *European Journal of Neuroscience*, 23(6):1614–1622.

Sadagopan, S. and Wang, X. (2009). Nonlinear spectrotemporal interactions underlying selectivity for complex sounds in auditory cortex. *The Journal of neuroscience*, 29(36):11192–11202.

Sadagopan, S. and Wang, X. (2010). Contribution of inhibition to stimulus selectivity in primary auditory cortex of awake primates. *The Journal of Neuroscience*, 30(21):7314–7325.

Sakata, S. and Harris, K. D. (2009). Laminar structure of spontaneous and sensory-evoked population activity in auditory cortex. *Neuron*, 64(3):404–418.

Sakata, S. and Harris, K. D. (2012). Laminar-dependent effects of cortical state on auditory cortical spontaneous activity. *Frontiers in neural circuits*, 6:109.

Sally, S. L. and Kelly, J. B. (1988). Organization of auditory cortex in the albino rat: sound frequency. *Journal of Neurophysiology*, 59(5):1627–1638.

Sanes, D. H. (1990). An in vitro analysis of sound localization mechanisms in the gerbil lateral superior olive. *The Journal of neuroscience*, 10(11):3494–3506.

Sato, T. R., Gray, N. W., Mainen, Z. F., and Svoboda, K. (2007). The functional microarchitecture of the mouse barrel cortex. *PLoS Biol*, 5(7):e189.

Scattoni, M. L., Gandhy, S. U., Ricceri, L., and Crawley, J. N. (2008). Unusual repertoire of vocalizations in the btbr t+ tf/j mouse model of autism. *PloS one*, 3(8):e3067.

Schneidman, E., Berry, M. J., Segev, R., and Bialek, W. (2006). Weak pairwise correlations imply strongly correlated network states in a neural population. *Nature*, 440(7087):1007–1012.

Schnupp, J. W., Garcia-Lazaro, J. A., and Lesica, N. A. (2015). Periodotopy in the gerbil inferior colliculus: local clustering rather than a gradient map. *Frontiers in neural circuits*, 9.

Schnupp, J. W., Mrsic-Flogel, T. D., and King, A. J. (2001). Linear processing of spatial cues in primary auditory cortex. *Nature*, 414(6860):200–204.

Schofield, B. R., Mellott, J. G., and Motts, S. D. (2014). Subcollicular projections to the auditory thalamus and collateral projections to the inferior colliculus. *Frontiers in neuroanatomy*, 8:70.

Schreiner, C. E. and Cynader, M. S. (1984). Basic functional organization of second auditory cortical field (A2) of the cat. *Journal of Neurophysiology*, 51(6):1284–1305.

Schreiner, C. E. and Langner, G. (1988). Periodicity coding in the inferior colliculus of the cat. ii. topographical organization. *Journal of neurophysiology*, 60(6):1823–1840.

Schreiner, C. E. and Mendelson, J. R. (1990). Functional topography of cat primary auditory cortex: distribution of integrated excitation. *Journal of Neurophysiology*, 64(5):1442–1459.

Schreiner, C. E. and Sutter, M. L. (1992). Topography of excitatory bandwidth in cat primary auditory cortex: single-neuron versus multiple-neuron recordings. *Journal of Neurophysiology*, 68(5):1487–1502.

Schreiner, C. E. and Winer, J. A. (2007). Auditory cortex mapmaking: principles, projections, and plasticity. *Neuron*, 56(2):356–365.

Schulze, H., Hess, A., Ohl, F. W., and Scheich, H. (2002). Superposition of horseshoe-like periodicity and linear tonotopic maps in auditory cortex of the mongolian gerbil. *European Journal of Neuroscience*, 15(6):1077–1084.

Shamma, S. A., Fleshman, J. W., Wiser, P. R., and Versnel, H. (1993). Organization of response areas in ferret primary auditory cortex. *Journal of Neurophysiology*, 69(2):367–383.

Sherman, S. M. and Guillery, R. (2002). The role of the thalamus in the flow of information to the cortex. *Philosophical Transactions of the Royal Society of London B: Biological Sciences*, 357(1428):1695–1708.

Shinn-Cunningham, B. G., Santarelli, S., and Kopco, N. (2000). Tori of confusion: Binaural localization cues for sources within reach of a listener. *The Journal of the Acoustical Society of America*, 107(3):1627–1636.

Smith, A. L., Parsons, C. H., Lanyon, R. G., Bizley, J. K., Akerman, C. J., Baker, G. E., Dempster, A. C., Thompson, I. D., and King, A. J. (2004). An investigation of the role of auditory cortex in sound localization using muscimol-releasing elvax. *European Journal of Neuroscience*, 19(11):3059–3072.

Smith, S. L. and Häusser, M. (2010). Parallel processing of visual space by neighboring neurons in mouse visual cortex. *Nature neuroscience*, 13(9):1144–1149.

Sompolinsky, H., Yoon, H., Kang, K., and Shamir, M. (2001). Population coding in neuronal systems with correlated noise. *Physical Review E*, 64(5):051904.

Stecker, G. C., Harrington, I. A., and Middlebrooks, J. C. (2005). Location coding by opponent neural populations in the auditory cortex. *PLoS Biol*, 3(3):e78.

Stecker, G. C. and Middlebrooks, J. C. (2003). Distributed coding of sound locations in the auditory cortex. *Biological cybernetics*, 89(5):341–349.

Stiebler, I. (1987). *Frequenzrepräsentation und Schallempfindlichkeit im Colliculus inferior und auditorischen Cortex der Hausmaus (Mus musculus)*. Hartung-Gorre.

Stiebler, I. and Ehret, G. (1985). Inferior colliculus of the house mouse. i. a quantitative study of tonotopic organization, frequency representation, and tone-threshold distribution. *Journal of Comparative Neurology*, 238(1):65–76.

Stiebler, I., Neulist, R., Fichtel, I., and Ehret, G. (1997). The auditory cortex of the house mouse: left-right differences, tonotopic organization and quantitative analysis of frequency representation. *Journal of Comparative Physiology A*, 181(6):559–571.

Suga, N. (1965a). Analysis of frequency-modulated sounds by auditory neurones of echolocating bats. *The Journal of Physiology*, 179(1):26.

Suga, N. (1965b). Functional properties of auditory neurones in the cortex of echo-locating bats. *The Journal of physiology*, 181(4):671.

Sutter, M. and Schreiner, C. (1995). Topography of intensity tuning in cat primary auditory cortex: single-neuron versus multiple-neuron recordings. *Journal of Neurophysiology*, 73(1):190–204.

Svoboda, K., Denk, W., Kleinfeld, D., Tank, D. W., *et al.* (1997). In vivo dendritic calcium dynamics in neocortical pyramidal neurons. *Nature*, 385(6612):161–165.

Talavage, T. M., Ledden, P. J., Benson, R. R., Rosen, B. R., and Melcher, J. R. (2000). Frequency-dependent responses exhibited by multiple regions in human auditory cortex. *Hearing research*, 150(1):225–244.

Tallal, P. and Piercy, M. (1973). Defects of non-verbal auditory perception in children with developmental aphasia.

Thivierge, J.-P. and Marcus, G. F. (2007). The topographic brain: from neural connectivity to cognition. *Trends in neurosciences*, 30(6):251–259.

Tian, B. and Rauschecker, J. P. (1994). Processing of frequency-modulated sounds in the cat's anterior auditory field. *Journal of Neurophysiology*, 71(5):1959–1975.

Tian, B. and Rauschecker, J. P. (2004). Processing of frequency-modulated sounds in the lateral auditory belt cortex of the rhesus monkey. *Journal of Neurophysiology*, 92(5):2993–3013.

Tian, B., Reser, D., Durham, A., Kustov, A., and Rauschecker, J. P. (2001). Functional specialization in rhesus monkey auditory cortex. *Science*, 292(5515):290–293.

Tollin, D. J. and Yin, T. C. (2005). Interaural phase and level difference sensitivity in low-frequency neurons in the lateral superior olive. *The Journal of neuroscience*, 25(46):10648–10657.

Trujillo, M., Measor, K., Carrasco, M. M., and Razak, K. A. (2011). Selectivity for the rate of frequency-modulated sweeps in the mouse auditory cortex. *Journal of neurophysiology*, 106(6):2825–2837.

Trujillo, M. and Razak, K. A. (2013). Altered cortical spectrotemporal processing with age-related hearing loss. *Journal of neurophysiology*, 110(12):2873–2886.

Tsukano, H., Horie, M., Bo, T., Uchimura, A., Hishida, R., Kudoh, M., Takahashi, K., Takebayashi, H., and Shibuki, K. (2015). Delineation of a frequency-organized region isolated from the mouse primary auditory cortex. *Journal of neurophysiology*, 113(7):2900–2920.

Tsukano, H., Horie, M., Hishida, R., and Shibuki, K. (2013). New subarea in the rostrodorsal part of the primary auditory cortex in mice. In *Journal of Physiological Sciences*, volume 63, pages S205–S205.

Tsukano, H., Horie, M., Hishida, R., Takahashi, K., Takebayashi, H., and Shibuki, K. (2016). Quantitative map of multiple auditory cortical regions with a stereotaxic fine-scale atlas of the mouse brain. *Scientific reports*, 6.

Van Hooser, S. D., Heimel, J. A., Chung, S., and Nelson, S. B. (2006). Lack of patchy horizontal connectivity in primary visual cortex of a mammal without orientation maps. *The Journal of neuroscience*, 26(29):7680–7692.

Van Hooser, S. D., Li, Y., Christensson, M., Smith, G. B., White, L. E., and Fitzpatrick, D. (2012). Initial neighborhood biases and the quality of motion stimulation jointly influence the rapid emergence of direction preference in visual cortex. *The Journal of Neuroscience*, 32(21):7258–7266.

Vinje, W. E. and Gallant, J. L. (2000). Sparse coding and decorrelation in primary visual cortex during natural vision. *Science*, 287(5456):1273–1276.

Wang, X., Lu, T., Snider, R. K., and Liang, L. (2005). Sustained firing in auditory cortex evoked by preferred stimuli. *Nature*, 435(7040):341–346.

Wehr, M. and Zador, A. M. (2003). Balanced inhibition underlies tuning and sharpens spike timing in auditory cortex. *Nature*, 426(6965):442–446.

Weible, A. P., Moore, A. K., Liu, C., DeBlander, L., Wu, H., Kentros, C., and Wehr, M. (2014). Perceptual gap detection is mediated by gap termination responses in auditory cortex. *Current Biology*, 24(13):1447–1455.

Weinberger, N. M. (2004). Specific long-term memory traces in primary auditory cortex. *Nature Reviews Neuroscience*, 5(4):279–290.

Weiss, D. J., Garibaldi, B. T., and Hauser, M. D. (2001). The production and perception of long calls by cotton-top tamarins (saguinus oedipus): acoustic analyses and playback experiments. *Journal of Comparative Psychology*, 115(3):258.

Weliky, M., Bosking, W. H., and Fitzpatrick, D. (1996). A systematic map of direction preference in primary visual cortex.

Wesolek, C. M., Koay, G., Heffner, R. S., and Heffner, H. E. (2010). Laboratory rats (rattus norvegicus) do not use binaural phase differences to localize sound. *Hearing research*, 265(1):54–62.

Wetzel, W., Ohl, F. W., and Scheich, H. (2008). Global versus local processing of frequency-modulated tones in gerbils: an animal model of lateralized auditory cortex functions. *Proceedings of the National Academy of Sciences*, 105(18):6753–6758.

White, E. L. (1989). *Cortical circuits: synaptic organization of the cerebral cortex: structure, function, and theory*. Birkhauser.

Willshaw, D. J., Buneman, O. P., and Longuet-Higgins, H. C. (1969). Non-holographic associative memory. *Nature*.

Wilson, D. E., Whitney, D. E., Scholl, B., and Fitzpatrick, D. (2016). Orientation selectivity and the functional clustering of synaptic inputs in primary visual cortex. *Nature neuroscience*.

Winer, J. A., Larue, D. T., and Huang, C. L. (1999). Two systems of giant axon terminals in the cat medial geniculate body: convergence of cortical and gabaergic inputs. *The Journal of comparative neurology*, 413(2):181–197.

Winer, J. A. and Schreiner, C. E. (2005). The central auditory system: a functional analysis. In *The inferior colliculus*, pages 1–68. Springer.

Winkowski, D. E. and Kanold, P. O. (2013). Laminar transformation of frequency organization in auditory cortex. *The Journal of Neuroscience*, 33(4):1498–1508.

Wong, P., Gharbawie, O. A., Luethke, L. E., and Kaas, J. H. (2008). Thalamic connections of architectonic subdivisions of temporal cortex in grey squirrels (sciurus carolinensis). *Journal of Comparative Neurology*, 510(4):440–461.

Woods, T. M., Lopez, S. E., Long, J. H., Rahman, J. E., and Recanzone, G. H. (2006). Effects of stimulus azimuth and intensity on the single-neuron activity in the auditory cortex of the alert macaque monkey. *Journal of neurophysiology*, 96(6):3323–3337.

Woolsey, C. N. and Walzl, E. M. (1942). Topical projection of nerve fibers from local regions of the cochlea to the cerebral cortex of the cat. *Bull Johns Hopkins Hosp*, 71(315-344):127.

Xiong, X. R., Liang, F., Li, H., Mesik, L., Zhang, K. K., Polley, D. B., Tao, H. W., Xiao, Z., and Zhang, L. I. (2013). Interaural level difference-dependent gain control and synaptic scaling underlying binaural computation. *Neuron*, 79(4):738–753.

Yao, J. D., Bremen, P., and Middlebrooks, J. C. (2013). Rat primary auditory cortex is tuned exclusively to the contralateral hemifield. *Journal of neurophysiology*, 110(9):2140–2151.

Ye, C.-q., Poo, M.-m., Dan, Y., and Zhang, X.-h. (2010). Synaptic mechanisms of direction selectivity in primary auditory cortex. *The Journal of Neuroscience*, 30(5):1861–1868.

Yeon, S. C., Kim, Y. K., Park, S. J., Lee, S. S., Lee, S. Y., Suh, E. H., Houpt, K. A., Chang, H. H., Lee, H. C., Yang, B. G., *et al.* (2011). Differences between vocalization evoked by social stimuli in feral cats and house cats. *Behavioural processes*, 87(2):183–189.

Yoshimura, Y. and Callaway, E. M. (2005). Fine-scale specificity of cortical networks depends on inhibitory cell type and connectivity. *Nature neuroscience*, 8(11):1552–1559.

Yoshimura, Y., Dantzker, J. L., and Callaway, E. M. (2005). Excitatory cortical neurons form fine-scale functional networks. *Nature*, 433(7028):868–873.

Yu, H., Majewska, A. K., and Sur, M. (2011). Rapid experience-dependent plasticity of synapse function and structure in ferret visual cortex in vivo. *Proceedings of the National Academy of Sciences*, 108(52):21235–21240.

Zeng, F.-G., Nie, K., Stickney, G. S., Kong, Y.-Y., Vongphoe, M., Bhargave, A., Wei, C., and Cao, K. (2005). Speech recognition with amplitude and frequency modulations. *Proceedings of the National Academy of Sciences of the United States of America*, 102(7):2293–2298.

Zhang, J., Nakamoto, K. T., and Kitzes, L. M. (2004). Binaural interaction revisited in the cat primary auditory cortex. *Journal of neurophysiology*, 91(1):101–117.

Zhang, L. I., Tan, A. Y., Schreiner, C. E., and Merzenich, M. M. (2003). Topography and synaptic shaping of direction selectivity in primary auditory cortex. *Nature*, 424(6945):201–205.

Zhang, Y., Dyck, R. H., Hamilton, S. E., Nathanson, N. M., and Yan, J. (2005). Disrupted tonotopy of the auditory cortex in mice lacking m 1 muscarinic acetylcholine receptor. *Hearing research*, 201(1):145–155.

Zhou, Y. and Wang, X. (2012). Level dependence of spatial processing in the primate auditory cortex. *Journal of neurophysiology*, 108(3):810–826.

Zurita, P., Villa, A., De Ribaupierre, Y., De Ribaupierre, F., and Rouiller, E. (1994). Changes of single unit activity in the cat's auditory thalamus and cortex associated to different anesthetic conditions. *Neuroscience research*, 19(3):303–316.